

**ADVANCED TECHNIQUES IN RAMAN TWEEZERS  
MICROSPECTROSCOPY FOR APPLICATIONS IN BIOMEDICINE**

**by**

**Phillip Jess**

**A Thesis Submitted for the Degree of Ph.D.  
at the  
University of St. Andrews**



**2007**

**Full metadata for this item is available in the St Andrews  
Digital Research Repository  
at:**

**<https://research-repository.st-andrews.ac.uk/>**

**Please use this identifier to cite or link to this item:**

**<http://hdl.handle.net/10023/410>**

**This item is protected by original copyright**

**This item is licensed under a  
[Creative Commons License](#)**

# **Advanced Techniques in Raman Tweezers Microspectroscopy for applications in Biomedicine**

A thesis submitted to the University of  
St Andrews in the application for the  
Degree of Doctor of Philosophy

by

Phillip Ronald Thomas Jess

12<sup>th</sup> April 2007

# Abstract

---

This thesis investigates the use of Raman tweezers microspectroscopy to interrogate the biochemistry of single biological cells. Raman tweezers microspectroscopy is a powerful technique, which combines traditional Raman microspectroscopy and optical trapping, allowing the manipulation and environmental isolation of a biological cell of interest whilst simultaneously probing its biochemistry gleaned a wealth of pertinent information.

The studies carried out in this thesis can be split into two broad categories: firstly, the exploitation of Raman tweezers microspectroscopy to study biological cells and secondly developments to the Raman tweezers microspectroscopy technique that extend its capabilities and the range of samples that can be studied. In the application of Raman tweezers, the stacking and interrogation of multiple cells is reported allowing a rapid representative Raman signal to be recorded from a small cell population with improved signal to noise. Also demonstrated is the ability of Raman spectroscopy to identify and grade the development of Human Papillomavirus induced cervical neoplasia with sensitivities of up to 96 %. These studies demonstrate the potential of Raman spectroscopy to study biological cells but it was noted that the traditional Raman tweezers system struggled to manipulate large cells thus a decoupled Raman tweezers microspectroscopy system is presented where a dual beam fibre optical trap is used to perform the trapping function and a separate Raman probe is introduced to probe the biochemical nature of the trapped cell. This development allowed the trapping and examination of very large cells whilst opening up the possibility of crating Raman maps of trapped objects. Raman tweezers microspectroscopy could potentially become an important clinical diagnostic and biological monitoring tool but is held back by the long signal integration times required due to the weak nature of Raman scattering. The final study presented in this thesis examines the potential of wavelength modulated Raman spectroscopy to improve signal to noise ratios and reduce integration times.

All these studies aim to demonstrate the potential and extend the performance of Raman tweezers microspectroscopy.

---

Declarations

---

I, Phillip Ronald Thomas Jess, hereby certify that this thesis, which is approximately 60,000 words in length, has been written by me, that it is the record of work carried out by me and that it has not been submitted in any previous application for a higher degree.

date signature of candidate.....

I was admitted as a research student in September 2003 and as a candidate for the degree of Doctor of Philosophy in September 2004; the higher study for which this is a record was carried out in the University of St Andrews between 2003 and 2007.

date signature of candidate.....

I hereby certify that the candidate has fulfilled the conditions of the Resolution and Regulations appropriate for the degree of Doctor of Philosophy in the University of St Andrews and that the candidate is qualified to submit this thesis in application for that degree.

date signature of supervisor.....

In submitting this thesis to the University of St Andrews I understand that I am giving permission for it to be made available in accordance with the regulations of the University Library for the time being in force, subject to any copyright vested in the work not being affected thereby. I also understand that the title and abstract will be published, and that a copy of the work may be made and supplied to any bona fide library or research worker. I hereby certify that the candidate has fulfilled the conditions of the Resolution and Regulations appropriate for the degree of Doctor of Philosophy in the University of St Andrews and that the candidate is qualified to submit this thesis in application for that degree.

date signature of candidate.....

---

# Acknowledgements

---

I would like to begin by thanking my supervisor Professor Kishan Dholakia for the opportunity to work in his group and for the help and advice he has given me over the last three and a bit years. This has very much been an interdisciplinary project and I probably wouldn't have got very far without the help of Professor Andrew Riches and Professor Simon Herrington at the Bute medical school who I'd like to thank for their help and guidance including answering many of my daft biology questions.

Science is very much a team sport and there are several people who deserve a mention for their help in the lab. Thanks to Veneranda Garcés-Chávez who helped get the Raman project going, to Klaus Metzger for his help with fibre trapping, to Dan Smith and Lynn Paterson for their help with sample preparation and to Michael Mazilu for his help with the data processing and analysis.

As well as the lab I'd like to thank those who kept the office and bar such an entertaining place and to those who answered more of my daft biology questions you all know who you are.

On a more personal note I'd like to thank my parents, Alan and Elaine, for their support and encouragement without which I would have probably quit a long time ago. I would also like to thank Sarah for her support and enduring a lot of talk of random science over the years, the same goes for Robert.

---

# Publications

---

## Peer reviewed publications

Jess PRT, Garcés-Chávez V, Smith D, Mazilu M, Paterson L, Riches A, Herrington CS, Sibbett W and Dholakia K. **Dual beam fibre trap for Raman micro-spectroscopy of single cells.** Optics Express 2006; **14**: 5779-5791

Jess PRT, Garcés-Chávez V, Riches AC, Herrington CS and Dholakia K. **Simultaneous Raman micro-spectroscopy of optically trapped and stacked cells.** Journal of Raman Spectroscopy 2007; **38**: 1082-1088

Jess PRT, Smith DDW, Mazilu M, Dholakia K, Riches AC and Herrington CS. **Early detection of cervical neoplasia by Raman spectroscopy.** International Journal of Cancer 2007; Epub ahead of print: August 2007-09-03

## Non peer reviewed publications

Jess PRT, Garcés-Chávez V, Metzger NK, Paterson L, Riches AC and Dholakia K. **Dual Technique Decoupled Raman Micro Spectroscopy.** Proceedings of SPIE 2005; **5930**: 0A-1

Metzger NK, Jess PRT, Paterson L, Wright EM and Dholakia K. **Optical Binding of Chinese Hamster Ovary Cells.** Proceedings of SPIE 2005; **5930**: 0M-1

Jess PRT, Garcés-Chávez V, Smith D, Mazilu M, Paterson L, Riches A, Herrington CS, Sibbett W and Dholakia K. **Sub Cellular Raman Analysis using a Dual Beam Fibre Trap.** Centenary Meeting of the Pathological Society of Great Britain & Ireland (Poster) 2006

## Publicity

**Dual Beam fibre trap improves Raman microspectroscopy.** Biophotonics International 2006; **August**: 23

## Patents

Jess PRT, Mazilu M and Dholakia K. **Wavelength Encoded Raman Spectroscopy.** Patent Applied for 2006

---

---

# Contents

---

<b>1. Raman Tweezers Microspectroscopy: a powerful investigative tool for the biological and medical sciences.....</b>	<b>1</b>
1.1 Raman tweezers microspectroscopy: an introduction.....	1
1.2 Synopsis of thesis.....	3
1.3 References.....	6
<b>2. Investigating the World Through Light.....</b>	<b>8</b>
2.1 Life the Universe and Everything .....	8
2.2 Light in the Biological and Medical sciences.....	9
2.2.1 Absorption Spectroscopy.....	10
2.2.2 Emission Spectroscopy.....	11
2.2.3 Scattering based spectroscopy.....	12
2.3 Tools of the trade: Practical aspects of Spectroscopy.....	15
2.3.1 The Laser.....	16
2.3.2 Spectrographs.....	17
2.3.3 Detectors.....	18
2.3.4 Microscopy.....	20
2.4 The use of light based spectroscopy in the investigation of biological systems.....	21
2.4.1 Fluorescence imaging and spectroscopy.....	22
2.4.1.1 Fluorescence imaging.....	22
2.4.1.2 Flow Cytometry.....	23

---

---

2.4.1.3 Forster Resonance Energy Transfer (FRET).....	24
2.4.1.4 Total Internal Reflection Fluorescence Microscopy (TIRFM).....	25
2.4.2 Multiphoton spectroscopy.....	26
2.4.3 Elastic light scattering.....	27
2.4.4 Infra-red absorption spectroscopy.....	27
2.4.5 Raman Spectroscopy, Surface enhanced Raman Spectroscopy (SERS) and Coherent anti-stokes Raman Spectroscopy (CARS).....	29
2.4.5.1 Raman Spectroscopy.....	29
2.4.5.2 Surface Enhanced Raman Spectroscopy (SERS).....	30
2.4.5.3 Coherent Anti-Stokes Raman Spectroscopy (CARS)..	31
2.5 Outlooks for Raman spectroscopy and optical spectroscopy and imaging in the biological and medical sciences.....	32
2.6 References.....	33
<b>3. The Raman Effect: An Introduction and Theory.....</b>	<b>40</b>
3.1 A brief history of Raman Spectroscopy.....	40
3.2 Concepts and principles in Raman Spectroscopy.....	41
3.3 The Classical Theory of Raman Spectroscopy.....	53
3.4 References.....	58
<b>4. Optical Trapping: An Introduction and Theory.....</b>	<b>60</b>
4.1 Introduction to Optical Trapping.....	60
4.2 The Origins and Forces involved in Optical Trapping.....	62
4.2.1 Optical Trapping in the Mie Regime.....	64

---

---

4.2.2 Optical Trapping in the Rayleigh Regime.....	69
4.2.3 Optical trapping when particle diameter $\sim$ = to the trapping wavelength.....	72
4.3 The Basic Optical Tweezers Set-Up.....	73
4.4 Applications of Optical Traps in Biology.....	78
4.5 Dual Beam Optical Traps.....	79
4.5.1 The Fibre Optical Light Force Trap.....	79
4.5.2 Operation and Theory of the Fibre Trap.....	80
4.5.3 Applications of the Fibre Optical Trap.....	84
4.6 Conclusions.....	85
4.7 References.....	85
4.8 Bibliography.....	88
<b>5. Raman Tweezers Microspectroscopy: An Introduction and Research Perspective.....</b>	<b>89</b>
5.1 Introduction.....	89
5.2 Raman Tweezers Microspectroscopy.....	91
5.3 Raman Tweezers Microspectroscopy: A Research Review.....	93
5.4 Conclusions.....	99
5.5 References.....	100
5.6 Bibliography.....	104
<b>6. The Construction and Evolution of the Raman Tweezers System.....</b>	<b>105</b>
6.1 Considerations in the construction of a Raman Tweezers Experimental Setup.....	105

---

---

6.1.1 The choice of trapping and excitation wavelength.....	106
6.1.2 Microscope Objective.....	109
6.1.3 Confocal apertures.....	110
6.1.4 Introduction of the laser into the optical system and efficient collection optics.....	112
6.2 The Raman Tweezers spectroscopy system.....	113
6.3 Construction, Alignment, Calibration and Testing of the RTS system...	119
6.3.1 Construction, Alignment and Calibration.....	119
6.3.2 Testing the Raman Tweezers system and Data Treatment.....	124
6.4 Evolution of the Raman Tweezers Spectroscopy System.....	131
6.5 References.....	137

## **7. Simultaneous Raman Microspectroscopy of Optically Trapped and Stacked cells..... 139**

7.1 Introduction and Experimental Aims.....	139
7.2 Experimental Methods and Procedures.....	143
7.2.1 Experimental Setup.....	144
7.2.2 Samples and Preparation.....	146
7.2.3 Experimental Procedures.....	146
7.2.4 The experimental method for stacking microparticles.....	147
7.3 Experimental Results and Discussion.....	149
7.4 Conclusions.....	160
7.5 References.....	162

---

---

**8. Early Detection of Cervical Neoplasia by Raman Microspectroscopy.....164**

8.1 Motivations.....	164
8.2 Prospects for Raman spectroscopy in Cancer diagnostics.....	165
8.3 Cervical cancer and the Human Papillomavirus.....	167
8.4 Experimental Aims.....	170
8.5 Previous Studies on Cervical Neoplasia.....	171
8.6 Materials and Experimental Methods.....	172
8.6.1 Raman Tweezers experimental setup.....	172
8.6.2 Cell types, cell culture and sample preparation.....	173
8.6.3 Experimental Procedures.....	174
8.6.4 Spectral Analysis.....	176
8.7 Results.....	178
8.7.1 Spectral Interpretation and Discussion.....	178
8.7.2 Can Raman spectroscopy discriminate between healthy cells and those affected by HPV?.....	183
8.8 Conclusion.....	192
8.9 References.....	195

**9. A Dual Beam Fibre Trap for Raman Microspectroscopy of Single Cells.....200**

9.1 Introduction and Motivations.....	200
9.1.1 Introduction and issues in tweezing large cells for study with Raman tweezers microspectroscopy.....	200
9.1.2 Proposed systems to extend the functionality of Raman tweezers .....	203
9.1.3 The use of fibre optical traps to trap cells for Raman analysis.	207

---

---

9.2 Experimental apparatus and Procedures.....	208
9.2.1 Experimental apparatus and construction.....	208
9.2.1.1 Choice of Fibre optical cable.....	210
9.2.1.2 Fibre optic launch system.....	211
9.2.1.3 Constructing the fibre optical trap.....	214
9.2.2 Sample preparation.....	217
9.2.3 Fibre optical trap operation and evaluation.....	218
9.3 Experimental Results.....	221
9.4 Microfluidic Raman Tweezers spectroscopy.....	233
9.4.1 Introduction and motivations.....	233
9.4.2 Construction and operation of the microfluidic Raman system .....	234
9.4.3 Raman examination of particles in a microfluidic flow system .....	236
9.5 Conclusions.....	237
9.6 References.....	240
<b>10. Wavelength Modulated Raman Spectroscopy.....</b>	<b>244</b>
10.1 Introduction and Motivations.....	244
10.2 Experimental Aims.....	245
10.3 Current approaches to reducing Raman signal acquisition times.....	246
10.4 Wavelength modulation spectroscopy and its incorporation with Raman spectroscopy.....	250
10.5 Experimental Setup and procedures.....	253
10.5.1 Experimental Setup.....	253

---

---

10.5.2 Experimental samples.....	254
10.5.3 Experimental procedures.....	255
10.5.4 Spectral analysis.....	255
10.6 Results.....	256
10.6.1 Assessment of the inherent noise of the CCD camera .....	256
10.6.2 Wavelength modulation Raman spectroscopy applied to polystyrene microspheres.....	259
10.6.3 Wavelength modulation Raman spectroscopy applied to biological cells.....	265
10.7 Conclusions.....	271
10.8 References.....	274
<b>11. Thesis Conclusions.....</b>	<b>277</b>
11.1 Thesis Conclusions.....	277
11.2 The outlook for Raman tweezers microspectroscopy.....	285
<b>Appendix A. Optical and quasi-optical techniques in the biomedical sciences...AI</b>	
A.1 Introduction.....	AII
A.1.1 Optical Coherence Tomography (OCT).....	AIII
A.1.2 Nuclear Magnetic Resonance (NMR), Magnetic Resonance Imaging (MRI) and Electron Spin Resonance (ESR).....	AIV
A.1.3 X-Ray scattering.....	AVI
A.2 Summary.....	AVII
A.3 References.....	AVII

---

---

**Appendix B. The Quantum Theory of Raman Spectroscopy.....BI**

B.1 The Quantum Theory of Raman Spectroscopy.....BII

B.2 References.....BVIII

**Appendix C. A brief Introduction to the Eukaryotic Cell.....CI**

C.1 Introduction to Eukaryotic cells.....CII

C.2 A Tour of the Cell.....CIII

C.2.1 The Cellular Plasma Membrane.....CV

C.2.2 The Nucleus.....CVI

C.2.3 The Endomembrane system.....CIX

C.2.4 Mitochondria.....CXII

C.2.5 The Cytoskeleton.....CXII

C.2.6 The Extracellular Matrix.....CXIII

C.3 The cell cycle.....CXIV

C.4 Conclusion.....CXVII

C.5 References.....CXVII

**Appendix D. Principle Component Analysis.....DI**

D.1 Introduction to principle component analysis.....DII

D.2 Demonstration of the operation of Principle component analysis.....DIII

D.3 Conclusions.....DIX

---

---

# 1. Raman Tweezers Microspectroscopy: a powerful investigative tool for the biological and medical sciences

---

*Raman tweezers microspectroscopy is emerging as a powerful tool for investigating biological and medical samples, in particular single biological cells. In this discussion we introduce Raman tweezers microspectroscopy, the focus of this thesis, and summarise the results and discussions subsequently presented in this thesis.*

---

## 1.1 Raman tweezers microspectroscopy: an introduction

Raman tweezers microspectroscopy is the combination of traditional Raman spectroscopy and optical trapping. This technique is attracting a great deal of attention for the study of biomedical samples in particular single biological cells. Raman spectroscopy is a vibrational spectroscopy technique based on the inelastic scattering of light from molecular bonds and was first observed by Raman and Krishnan in 1923 [1]. With improvements in instrumentation, Raman spectroscopy has been recognised

---

---

as a potentially powerful technique in the study of biomedical samples as it is capable of building up a chemical fingerprint of the substance under study without the need for any molecular markers or tags. This effectively means Raman spectroscopy is able to probe an ensemble of many biochemicals simultaneously. However there are some drawbacks to using Raman spectroscopy that, for the most part, centre on the weak nature of the inelastic scattering process upon which Raman spectroscopy is based. The probability of a bond inelastically scattering a photon is only approximately one in thirty million which means it takes a relatively long time to build up an informative Raman spectrum. Furthermore this means the technique is extremely sensitive to any fluorescence interference. Such a background can swamp and mask the Raman signal, from the sample or surrounding environment. This can be a serious problem in the study of biological cells as they often have an inherent fluorescence and the fluorescence from glass coverslips, upon which the samples are placed for study, is extremely strong. Compounding this is the fact that the cells, especially those whose natural state is in suspension, can often drift out of the Raman probe beam before a good Raman spectrum can be acquired; all this means it is very difficult to acquire Raman signals from single biological cells. In order to be able obtain good quality Raman spectra from single cells we require a method to hold and manipulate our biological cell away from interfering fluorescent surfaces and other interfering objects.

Part of the solution is to use infrared laser beams, which reduce sample fluorescence. A key method for successfully overcoming these problems and making single cell Raman spectroscopy a practical reality is the incorporation of optical tweezers [2] into traditional Raman spectroscopy to form Raman tweezers microspectroscopy. Optical tweezers is a technique that uses a highly focussed single

---

---

laser beam to capture and manipulate micro objects such as biological cells. Through the transfer of momentum from the photons to the object being trapped, the object is drawn into the laser focus, the most intense region of the laser beam. The trapped object can then be manipulated in three dimensions and moved away from interfering objects or surfaces. This is exactly what we require to obtain good quality Raman signals from our cells and furthermore the focussed laser beam required for optical trapping is ideal to excite the Raman scattering in the sample. The technique was first demonstrated by Lankers *et al* in 1994 [3] and was subsequently first applied to study cells in 2002 by Xie *et al* [4]. By combining Raman spectroscopy with optical trapping we have a technique that can grab a biological cell, environmentally isolate it from any interfering surfaces or other cells and probe its biochemical nature and behaviour. By combining Raman spectroscopy with optical tweezers a powerful investigative technique has been formed for the study of biological cells and the potential of this technique has not gone unnoticed giving rise to an increasing body of work probing various aspects of cell behaviour from environmental responses [5] to neoplastic changes [6].

In this thesis we aim to develop a Raman tweezers microspectroscopy system to study single biological cells and probe their biochemical behaviour. Furthermore we also want to explore any opportunities to develop the experimental technique to extend the samples and applications that Raman tweezers microspectroscopy can interrogate.

## **1.2 Synopsis of thesis**

This thesis will chart the development of our Raman tweezers system and its application in the study of biological cells. Furthermore we will also see how the

---

---

experimental apparatus may be altered to extend the reach and ability of Raman tweezers spectroscopy.

This thesis is designed to reach as wide a disciplinary audience as possible and is therefore laid out in such a manner that an expert in the field may move straight to the independent experimental chapters that detail the results and conclusions acquired and reached during the course of the research undertaken for this thesis. However those readers wanting to extend their understanding of the subject will find detailed descriptions of the theory that underlies Raman tweezers spectroscopy and discussions on aspects of the construction of a basic Raman tweezers system and the current state of knowledge in the field.

In any discussion on a technology designed to probe biomedical samples we cannot ignore the host of technologies that currently exist. Chapter 2 gives an insight into the processes and instrumentation that underlie spectroscopy in general and goes onto to discuss current biological and medical imaging technologies in order to help us further understand the contribution that Raman tweezers microscopy can make to this research area.

Chapters 3 & 4 give grounding in the theory of Raman spectroscopy and optical trapping respectively for those who wish to understand in greater detail the underlying concepts that underpin the operation of Raman tweezers microspectroscopy.

Chapter 5 presents a more detailed discussion of the combination of Raman spectroscopy and optical tweezers to form the Raman tweezers technique which is followed by a review of the research currently presented in the field. Chapter 6 then details the experimental considerations in the construction of a Raman tweezers system. This is followed by a discussion describing the construction of our Raman

---

---

tweezers microspectroscopy system and charts its evolution throughout the course of the research carried out for this thesis.

Chapters 7, 8, 9 & 10 contain the main body of the research carried out during my PhD for this thesis. Chapter 7 describes how the simple technique of optical stacking, a phenomenon that occurs in optical traps where particles align vertically near the beam focus, may be used to help us acquire rapid representative Raman spectra of small cell populations. One of the most promising and exciting applications of Raman tweezers microspectroscopy is in cancer diagnostics and as such chapter 8 details a large study into how Raman tweezers microspectroscopy maybe used to identify and grade the development of cervical neoplasia. One point that became clear in the first two studies presented was that the single beam tweezers struggled to manipulate the large biological cells for Raman study, thus in chapter 9 we present a decoupled Raman tweezers system, where the trapping and Raman probe functions are fulfilled by separate laser beams, to improve the trapping and analysis of large biological cells. By decoupling the Raman probe and trapping functions we can maximise their individual performance for the trapping and analysis of large cells. Our decoupled Raman tweezers system uses a fibre optical light force trap as the primary trapping mechanism to allow the stable trapping and detailed study of large cells. Raman tweezers microspectroscopy has the potential to become a true clinical diagnostic technique however the major hurdle holding it back is the long signal integration times required, furthermore Raman tweezers microspectroscopy could better monitor biochemical reactions in cells if Raman spectra could be acquired in a much shorter time. In chapter 10 we investigate the possibility of using wavelength modulated Raman tweezers microspectroscopy to reduce integration times and further extend the ability and potential applications of the technique.

---

---

Finally in chapter 11 we sum up the conclusions reached in this thesis and pass brief comment on the outlook for Raman tweezers microspectroscopy.

Also included are four appendices aimed to aid the readers understanding of the theory and results presented in this thesis. Appendix A describes optical and quasi optical biomedical imaging technologies that do not necessarily compete directly with Raman spectroscopy but have had a large impact on the biomedical sciences. Knowledge of these important techniques will help us understand the role Raman spectroscopy may play in examining the biological and medical sciences. Appendix B contains a discussion on the quantum theory of Raman spectroscopy; although not required to understand the results presented in this thesis it is the most successful theory describing the origins of Raman spectra and is presented here for the interested reader. Appendix C gives a basic tour of the biological cell and the cell cycle. Many of the results presented in this thesis concern biological cells, thus a basic knowledge of the cell and its respiratory behaviour is useful in the interpretation of the results. Finally in Appendix D a fuller description of the operation of the statistical technique of principle component analysis, used to discriminate between the Raman spectra of different cell types, is presented. This is to aid the reader in their analysis of the results presented in chapter 8.

This thesis aims to demonstrate the potential of Raman tweezers spectroscopy by demonstrating how it may be applied to monitor complicated biological systems and their behaviour and how small changes in experimental design and analysis could extent the potential applications and use of this promising and exciting technique.

### 1.3 References

[1] Raman CV and Krishnan KS. **A new type of secondary radiation.** Nature 1928;

---

---

**121:** 501-502

- [2] Ashkin A, Dziedzic JM, Bjorkholm JE and Chu S. **Observation of a single-beam gradient force optical trap for dielectric particles.** Optics Letters 1986; **11:** 288-290
- [3] Lankers M, Popp J and Kiefer W. **Raman and Fluorescence Spectra of Single Optically Trapped Microdroplets in Emulsions.** Applied Spectroscopy 1994; **48:** 1166-1168
- [4] Xie C, Dinno M and Li YQ. **Near-infrared Raman spectroscopy of single optically trapped biological cells.** Optics Letters 2002; **27:** 249-251
- [5] Singh GP, Creely CM, Volpe G, Grotsch H and Petrov D. **Real-Time Detection of Hyperosmotic Stress Response in Optically Trapped Single Yeast Cells Using Raman Microspectroscopy.** Analytical Chemistry 2005; **77:** 2564-2568
- [6] Chan JW, Taylor DS, Zwerdling T, Lane SM, Ihara K and Huser T. **Micro-Raman Spectroscopy Detects Individual Neoplastic and Normal Haematopoietic Cells.** Biophysical Journal 2006; **90:** 648-656

---

# 2. Investigating the world through Light

---

*The use of light as an investigative tool has had a major impact in the biological and medical sciences increasing our understanding and even opening up new fields of study. Light can be employed in many guises to investigate matter and it is this that is addressed in the subsequent discussion, allowing us to set a background for and provide further understanding of the value of Raman spectroscopy for investigating biological and medical samples. This discussion covers the basic principles of light matter interactions that power the various techniques that are subsequently discussed with reference to their relative merits in the probing of biomedical samples.*

---

## 2.1 Life the Universe and Everything

Light, or more correctly electromagnetic radiation, is all around us and influences our lives on a daily basis. Light from the sun supports photosynthesis in plants and plankton, in our oceans, forming the base of the food chain that supports the majority of the life on earth. As humans we gain one fifth of our experience of the world through electromagnetic radiation, interpreted by our eyes. We communicate with each other via telephone, where the information is increasingly carried by light along fibre optics, cellular phones, where the information is carried by microwaves, and satellite communications, where electromagnetic waves are broadcasted around the world by space satellites. Much of our entertainment, such as radio and television, is brought to us via electromagnetic radiation broadcast from masts. Furthermore, much of what we know about the universe was gained by examining the light

---

---

collected from galaxies, the cosmic microwave background and we even listen to electromagnetic radiation to try to find extraterrestrial intelligence.

Information can be gleaned in many ways from the interaction of light with matter and an exciting opportunity exists for the study of biological systems, through light and more specifically by Raman tweezers spectroscopy, that can help us understand their behaviour better and make a contribution towards the biological and medical sciences. It is this opportunity which this thesis aims to explore.

## **2.2 Light in the Biological and Medical sciences**

The use of light in medicine is not a new concept but goes back as far as the ancient Egyptians, Greeks and Romans who believed that light could heal and revitalise the sick. However it was with the advent of the laser [1] that light truly began to make its impact in the biological and medical arena. Lasers can now be found in many biomedical applications from imaging through to diagnostics and therapies such as the treatment of glaucoma and diabetic retinopathy in the field of ophthalmology [2], Photodynamic therapy [3] and laser microsurgery [4] in oncology, and in many more areas. In biology lasers are impacting areas such as gene therapy [5], addressing fundamental questions in DNA properties and functionality [6] and cell sorting [7] to name but a few.

Lasers are opening up new areas in and revolutionising aspects of the biological and medical sciences. In this thesis the use of lasers to probe and interrogate biological systems will be explored and it is useful to understand how, through interactions with matter, light can tell us about the systems we examine.

Spectroscopy is the general term that describes the theory and interpretation of interactions between matter and electromagnetic radiation. The different types of

---

---

spectroscopies, which will be addressed later in this discussion, can be placed into three broad types: absorption, emission and scattering. The following descriptions assume the quantum nature of light

### 2.2.1 Absorption Spectroscopy

Absorption spectroscopy involves the passing of a range of frequencies, from a broadband source or a scanned laser source, through the sample under evaluation. The intensity of the collected light is recorded and normally represented graphically, as a function of wavelength or frequency so that any change, from the input intensity, can be easily observed. The graphical representation of this is normally referred to as an absorption spectrum. It is also common to record the absorbance vs. intensity where:

$$\text{absorbance} = \alpha l = -\ln\left(\frac{I}{I_0}\right) \quad (2.1)$$

where:  $I$  = measured intensity after sample

$I_0$  = input intensity

$\alpha$  = absorption coefficient

$l$  = path length

A simulated absorption spectrum, in order to illustrate the argument, can be seen in figure 2(a) accompanied by its corresponding absorbance spectra in figure 2(b). It must be noted that real absorption spectra are normally much more detailed but the principles remain the same.

Both the chemical composition and the concentration of the sample can be inferred from the wavelength, at which the absorption occurs, and amount of absorbance measured respectively. The wavelength at which photon absorption occurs directly correlates to a quantised energy transition within the atom or molecule, related to the photon wavelength via equation 1.2. This can be an electronic transition

---

---

between the various orbitals, which would manifest as an absorption in the visible to UV region of the electromagnetic spectrum, or an absorption creating vibrational, rotational or translational motion within the intra-molecular bonds that appear as absorptions in the infrared regions of the electromagnetic spectrum.

$$E = h \frac{c}{\lambda} \quad (2.2)$$

where:  $E$  = Photon energy/ transition energy  
 $h$  = Planck's constant  
 $c$  = speed of light  
 $\lambda$  = wavelength of absorbed photon

The concentration of substance present may be determined by comparing the value of the absorbance for an unknown concentration to that of a known concentration of the same substance under evaluation.

Typical applications of absorption spectroscopy normally include environmental monitoring for substances such as mercury [8] or in the monitoring of chemical reactions [9].

### 2.2.2 Emission Spectroscopy

Emission spectroscopy normally refers to the collection and examination of light emitted, by a sample under study, as it decays from some excited state to a lower one. The intensity of the collected light is often plotted as a function of wavelength and is commonly known as an emission spectrum. These spectra usually display a flat background with narrow, but not monochromatic, spikes at wavelengths corresponding to energy transitions within atoms or molecules described by equation 2.3.

---

$$E_i - E_f = h \frac{c}{\lambda} \quad (2.3)$$

where:  $E_i$  = Energy of the initial level  
 $E_f$  = Energy of the final level

The substance under study may be put into an excited state manually, by mechanisms such as optical, thermal or electrical stimulation. The object under study may also be naturally stimulated, such as the atoms and molecules in stars excited by the ongoing nuclear fusion or interstellar gas clouds stimulated by light from nearby stars. A schematic of this process can be seen in Figure 2(c). A molecule is excited in phase (i) to a higher level, as discussed before this excitation can take many forms. Often in phase (ii), although not necessary, the molecule will undergo some sort of non radiative decay such as transferring energy in collisions. Finally the molecule, in phase (iii), returns to its ground state releasing energy in the form of a photon giving information about its chemical composition.

The width of the emission spikes can be very narrow for low density gases but more often emission spectra contain broad lines, as a result of broadening mechanisms such as Doppler [10] or thermal broadening [11]. Often materials can be engineered to have broad emission spectra such as LED's or laser gain media.

Some typical applications of emission spectroscopy are the study of chemical compositions of materials such as galaxies [12] or for the study of advanced light emitting materials [13].

### 2.2.3 Scattering based spectroscopy

Scattering based spectroscopy refers to the examination of how scattered light interacts with the material it is propagating in. It falls into two main types: elastic and inelastic scattering.

---

---

In elastic scattering the photon interacting with the atom or molecule does not match a quantised energy transition so the atom is raised to a virtual energy level, as this is unstable the photon is immediately rejected and scattered unchanged in energy. Physically this corresponds to unstable deformation in the electron orbitals that can not be sustained hence the photon is rapidly rejected. This is commonly known as Rayleigh scattering. A schematic of Rayleigh scattering can be seen in figure 2(d i).

Molecules do not have distinct electronic energy levels; rather they are a close band of near degenerate energy states. These bands of energy states relate to the molecules bond stretching, rotational and translational energies that are commonly known as the molecules vibrational energy states. The energy of these vibrational states are small relative to electronic transitions and are involved in the process of inelastic scattering. As in elastic scattering the molecule absorbs a photon that does not match directly any quantised energy transition within it, thus the molecule is excited to an unstable virtual state. Inelastic scattering occurs if the molecule does not return to its original vibrational energy level. Thus a photon is scattered with a slightly smaller or larger energy depending on whether the molecule transferred energy to, or removed energy from the photon. This change in energy is manifested as a change in wavelength of the photon, via equation 2.4. If the photon loses energy this is known as a Stokes transition and if the photon gains energy it is referred to as an antistokes transition. A schematic of a stokes transition can be seen in figure 2(d ii) the collection and examination of these inelastically scattered photons is known as Raman spectroscopy [14]. Physically this inelastic scattering refers to an unstable deformation in the electron orbitals and an induction in nuclear movement which results in a transfer of energy so that when the photon is rejected it displays a change in frequency [15].

---

---

Common applications of scattering spectroscopies can range from cancer diagnosis [16] to the analysis of pigments in fine art [17].

$$E_{sc} = hc \left( \frac{1}{\lambda_{in}} \pm \frac{1}{\lambda_{vib}} \right) \quad (2.4)$$

Where:  $E_{sc}$  = Energy of the inelastically scattered photon  
 $\lambda_{in}$  = Wavelength of the incident photon  
 $\lambda_{vib}$  = Corresponding wavelength of the vibrational energy gap excited or de-excited during scattering process

These are the broad principles of these three main types of spectroscopy; they each have their individual sub techniques that can employed in a variety of situations as we have seen.

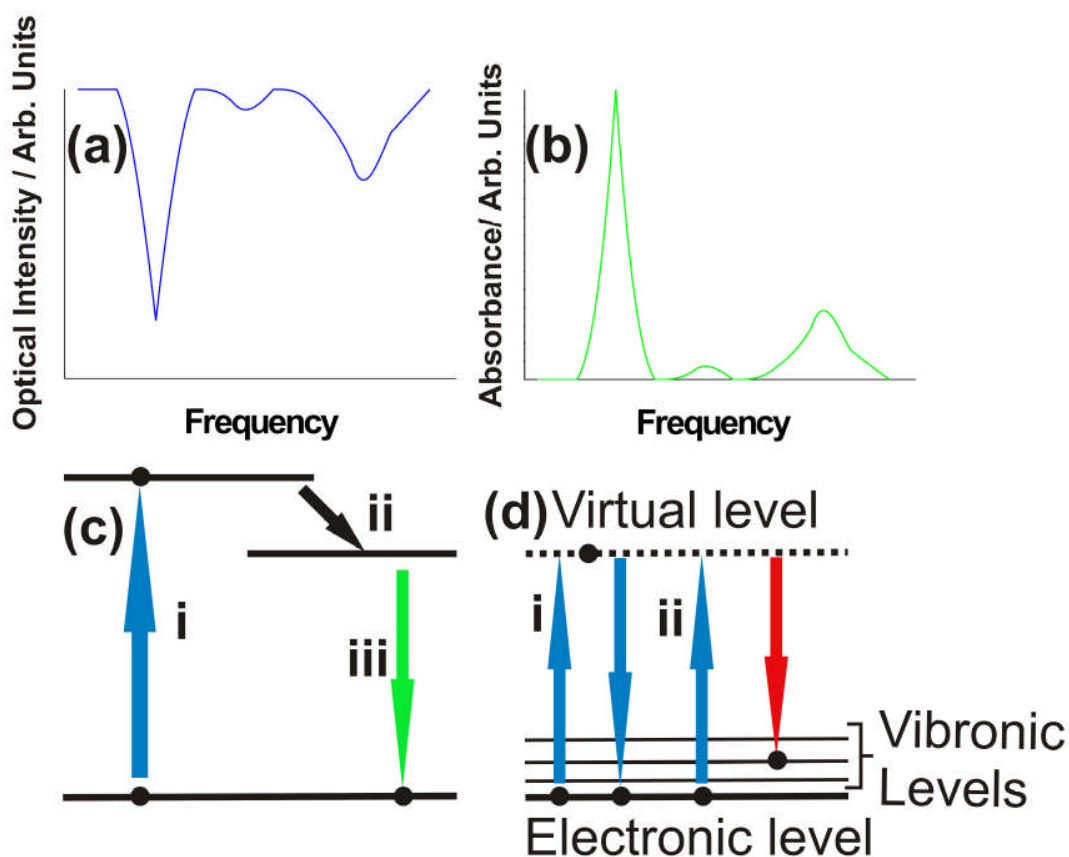


Figure 2. (a) Fabricated Absorption spectra and (b) its accompanying Absorbance spectra. (c) schematic of fluorescence emission process and (d) a schematic of both elastic and inelastic scattering events.

### 2.3 Tools of the trade: Practical aspects of Spectroscopy

The various spectroscopy based techniques, employing the previously discussed light matter interactions, often rely on some key equipment, such as lasers, and can often be combined with other non spectroscopic techniques, microscopy being the most notable, to further extend their applicability. A basic understanding of the central spectroscopic tools and non spectroscopic complimentary techniques will enhance the understanding of the techniques discussed in section 2.4. Although this discussion will not be exhaustive it will cover the basics of the important instruments

---

and techniques often employed in spectroscopy based studies and where required the references point to more detailed examinations.

### **2.3.1 The Laser**

Perhaps of all the recent advances in scientific instruments the advent of the laser [1] has had the largest impact on biomedical imaging. It has simplified instrumentation, increased the accuracy of results due to the nature of the light produced and even inspired new techniques. Laser is an acronym standing for **light amplification by stimulated emission of radiation**. A laser essentially consists of a gain medium, put into an excited state, enclosed within a cavity that reflects most of the emitted photons, from the gain medium, back into the gain medium. It is the interaction between the excited molecules, in the gain medium, and the photons contained within the cavity that gives the output of the laser its unique properties. If a photon in the cavity is to trigger one of the excited molecules in the gain medium to relax causing a stimulated emission the released photon will have an identical frequency to the interacting one. The remarkable feature of this process is that the emitted photon is in phase with, has the polarisation of, and propagates in the same direction as the stimulating radiation. It is these unique properties of the laser that allow precise delivery to samples, high resolution absorption and scattering spectroscopies and temporal experiments. With continuing advances in laser technologies a large variety of wavelengths are available from compact and affordable instruments allowing for the flexible and advanced study of biomedical samples.

---

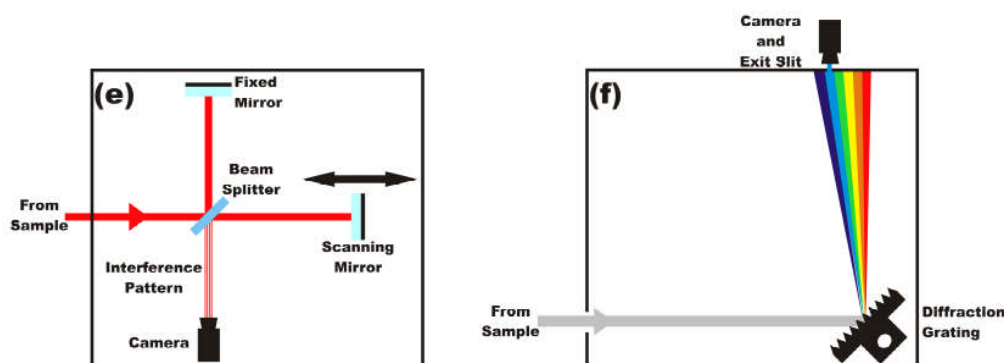
### 2.3.2. Spectrographs

Spectrographs are used in experiments where the information from the sample is related to wavelength and is received simultaneously; examples of such techniques are Raman spectroscopy and broadband absorption spectroscopy. The main function of the spectrograph is to allow the study of light intensity at each individual wavelength. There are two main types of spectrographs Fourier Transform spectrographs and dispersive spectrographs.

Fourier transform spectrographs are based on a Michelson interferometer [18] with a scanning mirror. The incoming light from the sample is split and then recombined with the use of a beam splitter. By scanning the mirror in the reference arm of the interferometer an interference pattern is produced that encodes the spectrum of the sample. In fact it turns out that the interference pattern is the Fourier transform [19] of the spectrum, thus the spectrum can be extracted. A schematic of a Fourier transform spectrograph can be seen in figure 2(e). Fourier transform spectrometers have a multiplex advantage meaning that the signals at each wavelength can be recorded simultaneously; conversely however this also leads to an increased noise potentially masking weak signals. Fourier transform spectrographs also allow an image to be recorded simultaneously but do not have the same resolving power achievable with dispersive spectrographs.

Dispersive spectrographs rely on gratings [20] to separate spatially the various wavelengths present. This is often used in combination with a slit to select the required wavelength interval for recording. The resolution of the spectrograph is a combination of the dispersive power of the graph, the focal length of the spectrograph and the size of the slit used to select the wavelength for examination. A schematic of a dispersive spectrograph can be seen in figure 2(f).

Fourier transform spectrographs are often used in situation where there are high light levels, where rapid recording of the signal is required and in spectral regions where suitable multi-channel detectors are not available. Dispersive spectrographs are normally used when high resolution is required, although with advent of high quality multi-channel detectors they can also record a number of wavelengths simultaneously and rapidly.



Figures 2(e & f). Figure 2(e) shows a schematic of Fourier transform spectrograph. Figure 2(f) shows a schematic of a dispersive spectrograph.

### 2.3.3 Detectors

There are many detectors used throughout various spectroscopic applications but perhaps those that have had the greatest impact and have found greatest use are the CCD camera and the photomultiplier tube (PMT).

Photomultiplier tubes [21] are used in the most demanding of low light applications and are capable of operating at single photon level. When a photon strikes the detector an electron is released according to the photoelectric effect. This electron is then drawn into an electron multiplier where it releases more electrons and the signal is detected as a small current proportional to the amount of light entering the detector. PMT's are extremely sensitive but are not known as 'fast' devices; where speed is important avalanche photodiodes (APD) [22] are often used. APD's are the semiconductor equivalent of a PMT and are much faster devices though perhaps not

---

quite as sensitive. PMT's remain however the most widely used as they are available to cover spectral regions from UV to the near infra-red. PMT's are single channel detectors and as such are only able to record one signal at a time, this remains their greatest disadvantage and are best employed when only one low light signal is required to be recorded.

Perhaps the most important detector in many spectroscopic and biomedical imaging applications is the CCD camera. This is silicon semiconductor based device that is divided into individual pixels allowing the recording of both intensity and spatial information simultaneously. The device operates on the principle of semiconductors [23]. If a photon, with enough energy, strikes a pixel it may elevate an electron, in the semiconductor valence band, into the conduction band. The electron is however confined in the area of the pixel and when signal acquisition is complete an electronic circuit 'counts' the electrons in each pixel giving the signal intensity. Many of these cameras are cooled, either with liquid nitrogen or thermoelectric coolers, to reduce thermal noise and allow the collection of good quality signals. Thermal noise, often referred to as the dark count, is the result of thermally released electrons, rather than photon released electrons, that contribute a random noise component to the signal. By cooling the cameras we can reduce the dark count. Liquid nitrogen is obviously the best coolant but there are practical disadvantages to this, such as having to refill the camera constantly, so many cameras are thermoelectrically cooled which reduces thermal noise to a satisfactory level but not to the same extent as possible with liquid nitrogen. These cameras are often used with dispersive spectrographs to allow the recording of entire spectra in one acquisition or they can be employed in imaging looking at fluorescence emissions for example recording simultaneously intensity and fluorophore position.

---

---

CCD cameras have the advantage of recording both intensity and position and are replacing PMT's in many applications although they do not have the same sensitivity as PMT's and can't really be employed in single photon use, thus are best utilised in low signal spatial imaging and spectroscopy.

### **2.3.4 Microscopy**

Much has been made of instruments and techniques that have impacted biology and medicine in this discussion but perhaps the technique that single handedly revolutionised our understanding of biology at cell level is the microscope [24]. A microscope is defined as a device that uses a lens or system of lenses to produce a greatly magnified image of an object not normally visible to the naked eye. Microscopy is thus the use of a microscope in an investigation, observation or experiment.

The main component of the classical microscope is the microscope objective which is a series of high quality lenses that are used to collect transmitted or reflected light from a sample and form a magnified image that can be recorded on a camera or, with use of another lens, be projected to the eye. The resolution that can be achieved by optical microscopes is approximately 200 nm. The most common form of optical microscopy is confocal microscopy [25]; this is a technique that allows images to be acquired from very well defined narrow areas in the samples under study with the use of an aperture placed at the image plane.

In order to achieve greater resolution and more detailed images of samples other forms of microscopy have been developed; these include electron microscopy [26], where the quantum nature of particles is exploited to obtain greater resolution and magnifications of up to 200 000, and atomic force microscopy [27] which

---

employs a fine tip that interacts with the electric field of individual molecules producing images on the near atomic scale.

Microscopy is a versatile technique and is easily combined with spectroscopic techniques for the study of tissues, cells and single molecules. Furthermore microscopes can be used 'in reverse' allowing the precise and targeted delivery of laser beams and other light sources to areas of tissue and even sub cellular components.

Each spectroscopic technique requires its own specialist equipment and optics but the aforementioned techniques and equipment are the major instruments employed in a great deal of experiments and should aid the understanding of the value and limitations of the following techniques in the interrogation of biological and medical samples.

## **2.4 The use of light based spectroscopy in the investigation of biological systems**

As this thesis deals with the use of Raman tweezers micro-spectroscopy to investigate biological systems it is useful to briefly discuss other light based spectroscopy techniques that can be used to study cells and small biological tissues to set a background for our evaluation and enable us to further understand the value of Raman spectroscopy and indeed its limitations in the investigation of biological and medical samples. There are many techniques that have been developed to investigate biomedical systems; however we will concentrate here only on those likely to be in direct competition with Raman spectroscopy. For the interested reader a brief overview of some of the important optical and quasi optical biomedical imaging

---

---

technologies, not likely to be in direct competition with Raman spectroscopy, can be found in Appendix A. All the following techniques are based the principles of light matter interactions discussed in section 2.2.

### **2.4.1 Fluorescence imaging and Spectroscopy**

Perhaps out of all the spectroscopy techniques used in the biological sciences fluorescence has had the greatest penetration finding many uses from molecular biology to cancer diagnosis.

#### **2.4.1.1 Fluorescence Imaging**

In molecular and cell biology fluorescence spectroscopy is often used in combination with fluorophores such as green fluorescent protein (GFP), the most widely used, that fluoresces green when exposed to an excitation in the blue region of the electromagnetic spectrum, from a laser source or a mercury discharge lamp. This fluorescent protein can be tagged onto certain molecules by incorporating the gene for GFP with the gene of the molecule of interest such that when the protein of interest is manufactured by the cell it will have the small GFP attached. This allows the influence of the tagged molecule to be charted in biomolecular processes or reactions through fluorescence imaging [28]. The unique way GFP is produced means it can also be used to investigate DNA replication or the success of transfection procedures [29].

Fluorescence spectroscopy has also been used in the diagnosis of certain cancers used in combination with a fluorescent drug. Patients ingest the drug, which fluoresces green when exposed to blue excitation, that clings preferentially to cancerous tumours. A fibre optic probe can then be used, in combination with an

---

---

excitation source, to image tissue and look for areas of high fluorescence indicating a tumour [30]. Furthermore the use of natural laser induced auto-fluorescence has also demonstrated the ability to discriminate between healthy and neoplastic tissues [31].

#### **2.4.1.2 Flow Cytometry**

An important use of fluorescence in the study of biological cells is in fluorescence activated cell sorting (FACS) [32]. FACS is a specialised form of flow cytometry [33] that is used to sort and analyse a fluorescently labelled cell population. Fluorescent markers can be used to target cells with a specific trait of interest within a general heterogeneous population. A solution of the cells is then placed into the flow cytometer where they are flowed past a bank of lasers and detectors to excite and detect any fluorescence emissions from the cells. According to their fluorescence the cells can be sorted into different chambers thus allowing the isolation and counting of the cell population of interest. This is a very high throughput technique that can sort analyse up to ten thousand samples per second. As well as sorting populations of cells FACS has been used in cancer diagnostics in a derivative technique known as DNA flow cytometry or DNA-FCM [34]. In this technique the nuclei of cells, taken from a biopsy, are stained with a fluorescent marker and passed through the flow cytometer which measures the level of fluorescence and hence the DNA content present in the sample. As cancer is often associated with an increase in cellular DNA content DNA-FCM can potentially give a diagnosis. However the technique requires a large amount of material to give an accurate diagnosis and may not be able to detect the onset of cancer at a very early stage.

---

### 2.4.1.3 Forster Resonance Energy Transfer (FRET)

FRET is a fluorescence based technique that allows the examination of protein-protein [35] or protein-DNA [36] interactions with resolutions of a few hundred angstroms. The process of FRET requires the two interacting molecules to be tagged with fluorescent proteins, a donor and an acceptor fluorophore, where the emission band of one fluorophore overlaps with the excitation band of the other. The technique operates by observing the transfer of energy between the two fluorescent molecules. The transfer of energy, from the donor in an excited state to the acceptor, is not mediated by photon emission and absorption, rather the energy is transferred via, as the name suggests, a non-radiative fashion through long range dipole interactions. The acceptor then manifests the occurrence of a transition by fluorescing at a different wavelength in comparison to the donor emission. Throughout an entire sample the interactions are manifested, when the sample is exposed to the exciting wavelength of the donor, as a drop in fluorescence from the donor molecule and an increase in fluorescence from the acceptor molecule. Furthermore FRET is extremely sensitive to separation of the interacting fluorophores thus can be used a molecular ruler [36].

FRET is a very sensitive technique that has opened up the study of molecule interactions in the cellular environment with unprecedented precision, however only one specific interaction can be studied at one particular time and is dependant on suitable fluorophores to tag the molecules of interest. FRET is best used in the study of individual protein interactions rather than ensembles.

---

#### **2.4.1.4 Total Internal Reflectance Fluorescence Microscopy (TIRFM)**

TIRFM is a microscopy based technique that allows the excitation of only a very fine layer close to a refractive index border, normally a microscope slide and the solution in which the sample under study is immersed, via an evanescent field caused by total internal reflection. The objects for study are normally tagged with fluorescent markers so that their presence or position within the solution or a cell may be observed. Normally a laser beam is introduced through a specialised microscope objective at an angle such as when the laser strikes the glass solution boundary it is totally internally reflected. This creates a short range evanescent field at the boundary that is capable of exciting the fluorophores close to the boundary. The use of this method to excite the fluorophores results in an increase of signal to noise ratio by a factor of approximately twentyfive. It should be noted that this technique can be performed with prisms rather than microscopes, however microscopy is the preferred option due to its added advantages. TIRFM can be used to study single biologically important molecules [37] all the way up to full cell imaging [38].

TIRFM is an extremely useful technique in studying cellular and single molecule function giving excellent signal to noise ratios; however it remains dependant on fluorophores to monitor its desired target thus cannot engage an entire ensemble, such as complete cell behaviour, simultaneously.

Fluorescence imaging has had a massive impact on the world of biology opening up many research aspects of molecular biology, it has also been investigated as a possible diagnostic technique for cancer with promising results. However fluorescence imaging using tags is molecule specific and finds difficulty engaging large ensembles such as whole cells and is best exploited to study the function of

---

---

single molecules in systems. When studying whole systems with natural fluorescence, such as tissues, the retrieved signal is an amalgamation of many molecules and contributions from individual groups of molecules is difficult to discern, thus it may be difficult to pick up subtle variations such as those involved in the earliest stages of neoplastic development.

#### **2.4.2 Multiphoton spectroscopy**

Multiphoton spectroscopy is probably the most common example of a nonlinear technique being used in medical imaging. Once again it is normally used in combination with fluorophores tagged to a molecule or component of interest. Excitation of the fluorophore is achieved by a two photon excitation; physically this means the fluorophore is excited to a virtual energy level, an unstable deformation of the electron cloud, but instantaneously absorbs another photon to raise the molecule into the excited state and stable reconfiguration of the electron cloud. The density of photons has to be very high to achieve this effect thus it can only occur at the focus of the excitation beam, this means a reasonable resolution image can be achieved along with an increased signal to noise ratio and, because the effect only occurs at the focus, photo bleaching in the surrounding area is avoided. Typical applications of multiphoton spectroscopy and imaging include high resolution non invasive in vivo imaging of blood flow and even brain imaging [39].

Multiphoton spectroscopy can aid in giving, if combined with confocal microscopy, high resolution and high signal to noise fluorescence images in vivo and in vitro. However this technique, as with many fluorescence techniques, normally relies on fluorescent labels, to reveal the molecule or substance of interest. This

---

technique is very useful for observing individual events in cells or even living animals however it cannot engage large ensembles of biochemicals simultaneously.

### **2.4.3 Elastic light scattering**

Elastic light scattering is a technique that examines how Rayleigh scattered light propagates through media. In the examination of medical and biological samples this often means studies of how light interacts with tissues and is often used in combination with Monte Carlo simulations to understand what is occurring. The main application of this technique is in the detection of neoplastic changes in tissues. The scattering is affected by physical changes associated with the onset of neoplasia and has the possibility of being able to detect phases in the development of cancer [16].

This technique has great potential in cancer diagnostics as it is sensitive to structural changes within the cells and tissues. As it examines structure, the technique is not capable of targeting molecular interactions as such and may not be totally sensitive to the biochemical changes associated with the very earliest stages of cancer development and cannot be used to monitor chemical reactions as it does not probe the propagating environments biochemistry.

### **2.4.4 Infra-red absorption spectroscopy**

Infra-red absorption spectroscopy, as the name might suggest, uses a broad infra-red source that probes the vibrational energy states of molecules. This technique is extremely well established and is used routinely for the determination of molecules and their structure. The technique works by comparing a reference arm with one that passes through the sample under study. The sample itself is placed in a holder or between two special windows normally constructed of high purity salt (sodium

---

chloride) as it does not absorb in the infrared region. When a spectrum is examined it will display a series of absorption minima that correspond directly to a unique vibration state of a unique bond. This essentially means that a chemical fingerprint of the substance under study can be built up, furthermore, due to its widespread use, extensive data bases exist to compare unknown compounds with.

Infrared spectroscopy has found wide use throughout the biological and medical sciences being used in such situations as the study of protein secondary structure [40], the study of arthritis [41] and also in diagnosis of cancer [42] to name but a few. Although infrared spectroscopy is traditionally a transmission technique there is a large effort in the development of reflectance infrared absorption spectroscopy for in vivo imaging to exploit this powerful technique further [43].

Infrared spectroscopy is widely used and powerful technique, capable of studying and engaging large ensembles simultaneously giving information on chemical composition and structure without the need for markers or fluorophores. This has become a popular technique in studying the many biological and medical systems. Although this technique is powerful it does have a few drawbacks, the samples require extensive preparation and require special substrates for analysis and the spectra do suffer from absorption interference caused by water that can make the study of some samples difficult, such as cells in solution, and some samples absorb the IR light completely making it impossible to obtain spectra.

---

## **2.4.5 Raman Spectroscopy, Surface enhanced Raman Spectroscopy (SERS) and Coherent anti-stokes Raman Spectroscopy (CARS)**

### **2.4.5.1 Raman Spectroscopy**

Raman spectroscopy is an inelastic scattering technique that probes the vibrational energy levels within molecules. Raman spectroscopy is an established technique and is regularly used in chemistry to investigate chemical substances and is often used in combination with infra-red absorption spectroscopy as the two techniques are mutually exclusive i.e. vibrational transitions that are Raman active are not IR active. The physical origin of the inelastic scattering lies in the scattering molecule retaining some of the energy of the scattered photon which results in nuclear movement in the intra molecular atoms. The scattered photon is then released with a slightly changed energy and hence wavelength. Each chemical bond requires a unique energy to vibrate, thus a fingerprint can be built up of the chemicals present in the sample under investigation by collecting the scattered photons with varying wavelengths.

Raman spectroscopy is not extensively used throughout the biological sciences probably due to its reputation for being quite difficult to implement. An inelastic scattering event has a very low probability, approximately one in thirty million, thus the signal is extremely weak can be obscured by fluorescence or the Rayleigh scattered light. However with modern spectrographs, CCD cameras and optics, this is no longer a problem and Raman is emerging as an exciting technique for probing whole biological systems. The main advantages of Raman spectroscopy, in the study of biological and medical systems, are the independence of the technique from exciting wavelength allowing the experimentalist to choose a wavelength suitable for the sample under study and the ability of the technique to engage simultaneously large

---

biochemical ensembles, such as cells or tissues, without the need for markers. Raman spectroscopy is an ideal tool for monitoring many biochemical changes simultaneously rather than single molecular interactions as the signal from a single molecule is too weak to register in a reasonable time, although it must be stated that Raman labels have been developed to tag molecules of interest and allow the imaging of their interactions within cells [44].

The most common applications of Raman spectroscopy, when applied to biological and medical sciences, is in the diagnosis of cancer for which the technique holds great potential [45]; although this is the main focus of much research Raman has also been used to study malaria [46] and the HIV virus [47] to name a few applications.

Raman spectroscopy is a versatile technique capable of engaging large ensembles of molecules however it can take a reasonable amount of time to record a good signal, on the order of minutes, and has difficulty recording signals from single molecules thus is best used for the study of single cells and tissues.

#### **2.4.5.2 Surface Enhanced Raman Spectroscopy (SERS)**

In order to increase the sensitivity and signal strength of Raman Spectroscopy the technique of SERS is often employed. This technique produces a Raman signal enhancement of up to  $10^{14}$ . This massively improves the sensitivity of the technique and opens up the possibility of rapid single molecule studies. The enhancement, of the Raman signal, occurs when a molecule is in close proximity to a metal nanoparticle or metallic surface, silver and gold providing the largest enhancement, due to a surface plasmon resonance [48]. There are two theories that attempt to explain the enhancement of the Raman signal: the first is the electromagnetic theory that

---

---

describes an interaction between the incoming radiation and the plasmon resonance causing an enhancement in the local electric field [49] and the second is a chemical enhancement where a bond is formed between the metallic surface and the molecule under examination that increases the molecular polarisability giving an enhancement in the signal [50]. It is widely now agreed that the enhancement is caused not by just one of these mechanisms but a combination of them.

SERS is a powerful technique in the study of single molecules and has been used in applications such as biohazard detection [51] through to the study of DNA [52]. Investigations have been made into examinations of whole cells with SERS however this gives only enhancement at the locations in the cell where the gold nanoparticles, uptaken by the cells, aggregate so only a few locations in the cell can be examined as there is no real control over where in cell this happens thus the technique is not ideal for the study of single cells [53].

SERS allows the extension of the advantages of Raman spectroscopy into the world of single molecule biophysics. However the enhancement provided is dependant on metallic surfaces or particles and the enhancement range is small, on the order of nanometres, thus is not very suitable for studying whole cells and tissues.

#### **2.4.5.3 Coherent Anti-Stokes Raman Spectroscopy (CARS)**

CARS is a non-linear technique closely related to the Raman effect that employs pulsed lasers to examine the vibrational levels in molecules. CARS is normally employed in the study of samples that suffer from high interference as it enhances and examines the anti-stokes transitions. Anti-stokes transitions occur when a photon interacts with an atom in motion, the energy of the motion can then be transferred to the scattered photon, and this process manifests itself in the release of a

---

---

photon with a shorter wavelength. CARS is a pump probe nonlinear technique that employs two pulsed lasers that have a wavelength difference corresponding to the energy of the Raman transition, related through equation 2.2, to be probed. The two beams combine to force the molecule into the excited state thus when it relaxes, due to interaction with the probe laser, the photon it scatters will have the molecular vibrational energy, for that transition, transferred to it. This technique results in an enhancement of the signal and the fact that the output is coherent means it is emerging as a popular technique for the study of traditionally difficult high noise samples and situations. CARS is a relatively new technique but has been applied successfully in the study of biological samples in applications such as three dimensional cell imaging [54] and has been shown to be endoscope compatible in principle [55].

CARS is emerging as an important technique for examining the vibrational structure of previously challenging samples. However the technique does require complex lasers and there is the concern of applying pulsed sources to biological samples as there is evidence that photon damage in biological matter is a two photon process [56].

## **2.5 Outlooks for Raman spectroscopy and optical spectroscopy and imaging in the biological and medical sciences**

Optical imaging has revolutionised some aspects of modern biology and medicine and opened up many more, including areas such as single molecule biophysics. The use of optical imaging techniques find such favour as, for the most part, they are non-invasive and normally relatively easy to implement. The use of optical imaging and spectroscopy is likely to become more widespread as new

---

techniques come to maturity and equipment continues to evolve and become better and more cost effective.

Raman spectroscopy, of all the techniques discussed in the previous section, is probably one of the most under utilised. The advent of modern holographic gratings and advanced optics coupled with advances in near infra-red laser sources has overcome the obstacles that previously stood in the way of the wide spread use of Raman as a diagnostic and monitoring tool. Raman spectroscopy is a useful tool for studying biomedical samples, especially in the study in the study of single cells, as it can engage many biochemicals simultaneously and give a good overview of the systems behaviour without the need for chemical markers. However it cannot study single molecules or single chemical reactions, in the way fluorescence can, as the signal integration times are relatively long. Thus it is best employed in the study of the behaviour of whole systems making the study of single cells an ideal application for Raman spectroscopy, which when combined with optical tweezers can form a powerful investigative technique. This is confirmed with the increase in published research articles demonstrating the value of Raman spectroscopy in many biomedical applications. Raman spectroscopy holds great promise for studying biological and medical systems, coupled with continuing advances and development of the technique itself as well as instrumentation Raman may be able to play a vital role in the progress of the biomedical sciences.

## 2.6 References

- [1] Svelto O. **Principles of Lasers 4<sup>th</sup> edition**. 1998; Plenum press, New York: pp 1-14
- [2] Sliney DH and Wolbarsht. **Future applications of lasers in surgery and**

- 
- medicine: a review.** Journal of the Royal Society of Medicine 1989; **82**: 293-296
- [3] Dougherty TJ, Gomer CJ, Henderson BW, Jori G, Kessel D, Korbelik M, Moan J and Peng Q. **Photodynamic Therapy.** Journal of the National Cancer Institute 1998; **90**: 889-905
- [4] Bandieramonte G, Chiesa F, Lupi M and Marchesini. **Laser microsurgery in Oncology: indications, techniques and results of a 5 year experience.** Lasers in Surgery and Medicine 1987; **7**: 478-486
- [5] Stevenson D, Agate B, Tsampoula X, Fischer P, Brown CTA, Sibbett W, Riches A, Gunn-Moore F and Dholakia K. **Femtosecond optical transfection of cells: viability and efficiency.** Optics Express 2006; **14**: 7125-7133
- [6] Long MJ, Fordyce PM, Engh AM, Neuman KC and Block SM. **Simultaneous coincident optical trapping and single molecule fluorescence.** Nature Methods 2004; **1**: 133-139
- [7] Paterson L, Papagiakoumou E, Milne G, Garcés-Chávez V, Tartakova, Sibbett W and Dholakia K. **Light induced cell separation in a tailored optical landscape.** Applied Physics Letters 2005; **87**: 123901-123903
- [8] Carruthers AE, Lake TK, Shah A, Allen JW, Sibbett W and Dholakia K. **Single – scan spectroscopy of mercury at 253.7 nm by sum frequency mixing of violet and red microlensed diode lasers.** Optics Communications 2005; **255**: 261-266
- [9] Gutierrez-Alejandre A, Larrubia MA, Ramirez J and Busca G. **FT-IR evidence of the interaction of benzothiophene with the hydroxyl groups of H-MFI and H-MOR Zeolites.** Vibrational Spectroscopy 2006; **41**: 42-47
- [10] Svelto O. **Principles of Lasers 4<sup>th</sup> edition.** 1998; Plenum press, New York: pp 44
-

- 
- [11] Svelto O. **Principles of Lasers 4<sup>th</sup> edition.** 1998; Plenum press, New York: pp 48
- [12] Massey P and Hunter DA. **Star formation in R136: A cluster of O3 stars revealed by Hubble space telescope spectroscopy.** The Astrophysical Journal 1998; **493**: 180-194
- [13] Richards GJ, Markham JPJ, Lo SC, Namdas EB, Sharma S, Burn PL and Samuel IDW. **A light-blue phosphorescent dendrimer for efficient solution-processed light emitting diodes.** Advanced Functional Materials 2005; **15**: 1451-1458
- [14] Raman CV and Krishnan KS. **A New Type of Secondary Radiation.** Nature 1928; **121**: 501
- [15] Smith E and Dent G. **Modern Raman Spectroscopy: A Practical Approach.** 2005; John Wiley & Sons Ltd: pp 1-20
- [16] Sokolov K, Drezek R, Gossage K, Kortum RR. **Reflectance spectroscopy with polarised light: is it sensitive to cellular and nuclear morphology.** Optics Express 1999; **5**: 302-317
- [17] Davey R, Gardener DJ, Singer BW and Spokes M. **Examples of analysis of pigments from fine art objects by Raman microscopy.** Journal of Raman Spectroscopy 2005; **25**: 53-57
- [18] Hecht E. **Optics 4<sup>th</sup> Edition.** 2002; Addison Wesley: pp 407-408
- [19] Hecht E. **Optics 4<sup>th</sup> Edition.** 2002; Addison Wesley: pp 316-320
- [20] Hecht E. **Optics 4<sup>th</sup> Edition.** 2002; Addison Wesley: pp 476-485
- [21] Wilson J and Hawkes J. **Optoelectronics: an introduction 3<sup>rd</sup> Edition.** 1998; Prentice Hall: pp 307-311
- [22] Wilson J and Hawkes J. **Optoelectronics: an introduction 3<sup>rd</sup> Edition.** 1998;
-

---

Prentice Hall: pp 337-340

- [23] Davies JH. **The Physics of Low-Dimensional Semiconductors**. 1998;  
Cambridge University Press: pp 45-111
- [24] Slayter EM and Slayter HS. **Light and Electron Microscopy**. 1992; Cambridge  
University Press: 131-146
- [25] Stevens JK, Mills LR and Trogadis JE. **Three Dimensional Confocal  
Microscopy: Volume Investigation of Biological Systems**. 1994; Academic  
Press: pp 3-24
- [26] Slayter EM and Slayter HS. **Light and Electron Microscopy**. 1992; Cambridge  
University Press: 192-210
- [27] Morris VJ, Kirby AR and Gunning AP. **Atomic Force Microscopy for  
Biologists**. 1999; Imperial College Press: pp 5-74
- [28] Westphal M, Jungbluth A, Heidecker M, Muhlbauer B, Heizer C, Schwartz J-M,  
Marriott G and Gerisch G. **Micro filament dynamics during cell movement  
and chemotaxis monitored using a GFP-actin fusion protein**. *Current Biology*  
1997; **7**: 176-183
- [29] Paterson L, Agate B, Comrie M, Ferguson R, Lake T, Morris J, Carruthers A,  
Brown CT, Sibbett W, Bryant P, Gunn-Moore F, Riches A and Dholakia K.  
**Photoporation and cell transfection using a violet diode laser**. *Optics Express*  
2005; **13**: 595-600
- [30] McKechnie T, Jahan A, Tait I, Cuschieri A, Sibbett W and Padgett M. **An  
Endoscopic system for the early detection of cancers of the GI tract**. *Review  
of Scientific Instruments* 1998; **69**: 2521-2523
- [31] Hung J, Lam S, LeRiche and Pakic B. **Autofluorescence of normal and  
malignant bronchial tissue**. *Lasers in Surgery and Medicine* 1991; **11**: 99-105
-

- 
- [32] Recklenwald D & Radbruch A. **Cell separation methods and applications.** 1998; Marcel Dekker inc: pp 237-270
- [33] Vo-Dinh T. **Biomedical Photonics handbook.** 2003; CRC Press LLC: pp 25-1-25-15
- [34] Dey P, Saikia and Vohra H. **DNA Flow-cytometry on fine needle aspiration cytology of lymph node: how helpful is it?** Indian Journal of Pathology and Microbiology 2000; **43**: 127-130
- [35] Sekar RB and Periasamy A. **Fluorescence Resonance Energy Transfer (FRET) microscopy imaging of live cell protein localisations.** Journal of Cell Biology 2003; **160**: 629-633
- [36] Didenko VV. **DNA probes using Fluorescence Resonance Energy Transfer (FRET): designs and applications.** Biotechniques 2001; **31**: 1106-1116
- [37] Tokunaga M, Kitamura K, Saito K, Iware AH and Yanagida T. **Single Molecule imaging of fluorophores and enzymatic reactions achieved by objective-type total internal reflection fluorescence microscopy.** Biochemical and Biophysical Research Communications 1997; **235**: 47-53
- [38] Olveczky BP, Periasamy N and Verkman AS. **Mapping fluorophore distributions in 3 dimensions by quantitative multiple angle total internal**
- [39] Zipfel WR, Williams RM and Webb WW. **Nonlinear magic: multiphoton microscopy in the biosciences.** Nature Biotechnology 2003; **21**: 1369-1377
- [40] Surewicz WK, Mantsch HM and Chapman D. **Determination of protein secondary structure by Fourier transform Infrared spectroscopy: A critical Assessment.** Biochemistry 1993; **32**: 389-394
- [41] Eysel HH, Jackson M, Nikulin A, Somorjai RL, Thomson GTD and Mantsch HH. **A novel diagnostic test for arthritis: Multivariant analysis of infrared**
-

- 
- spectra of synovial fluid.** *Biospectroscopy* 1997; **3**: 161-167
- [42] Wong PTT, Wong RK, Caputo TA, Godwin TA and Rigas B. **Infra-red Spectroscopy of Exfoliated Human Cervical cells: Evidence of extensive structural changes during carcinogenesis.** *Proceedings of the National Academy of Sciences* 1991; **88**: 10988-10992
- [43] Bommannon, Polts RO and Guy RH. **Examination of stratum corneum barrier function by Infrared Spectroscopy.** *Journal of Investigative Dermatology* 1990; **95**: 403-408
- [44] Feofanov AN, Grichine AI, Shitova LA, Karmakova TA, Yakubovskavya RI, Egret-Charlier M and Vigney P. **Confocal Raman Microspectroscopy and Imaging study of therahtal in living cancer cells.** *Biophysical Journal* 2000; **78**: 499-512
- [45] Stone N, Kendall C, Smith J, Crow P and Barr H. **Raman spectroscopy for identification of epithelial cancers.** *Faraday Discussions* 2004; **126**: 141-157
- [46] Wood BR, Langford SJ, Cooke BM, Glenister FK, Lim J and McNaughton D. **Raman imaging of hemozoin within the food vacuole of plasmodium falciparum trophozoites.** *FEBS Letters* 2003; **554**: 247-252
- [47] Yiming XU and Chuanazong LU. **Raman spectroscopic study on structure of human immunodeficiency Virus (HIV) and hypericin-induced photosensitive damage of HIV.** *Science in China series C: life sciences* 2005; **48**: 117-132
- [48] Aroca R. **Surface-Enhanced Vibrational Spectroscopy.** 2006; John Wiley & Sons: pp 35-69
- [49] Aroca R. **Surface-Enhanced Vibrational Spectroscopy.** 2006; John Wiley & Sons: pp 73-101
-

- 
- [50] Aroca R. **Surface-Enhanced Vibrational Spectroscopy**. 2006; John Wiley & Sons: pp 107-129
- [51] Papadakis SJ, Miragliotta JA, Gu Z and Gracias DH. **Scanning surface-enhanced Raman spectroscopy of silver nanowires**. Proceedings of SPIE 2005; **5927**: 1H1-1H8
- [52] Faulds K, Smith WE and Graham D. **Evaluation of surface-enhanced Resonance Raman scattering for Quantitative DNA analysis**. Analytical Chemistry 2004; **76**: 412-417
- [53] Kneipp K, Haka AS, Kneipp H, Badizadegan K, Yoshiza N, Boone C, Shafer-Peltier KE, Motz JT, Dasari RR and Feld MS. **Surface-Enhanced Raman Spectroscopy in Single Living Cells using Gold Nanoparticles**. Applied Spectroscopy 2002; **56**: 150-154
- [54] Zumbusch A, Holtom GR and Xie XS. **Three Dimensional Vibrational imaging by Coherent Anti-Stokes Raman scattering**. Physical Review Letters 1999; **82**: 4142-4145
- [55] Legare F, Evans CL, Ganikhanov F and Xie XS. **Towards CARS Endoscopy**. Optics Express 2006; **14**: 4427-4432
- [56] Konig K, Liang H, Berns MW and Tromberg BJ. **Cell damage in near infra-red multimode optical traps as a result of multiphoton absorption**. Optics Letters 1996; **21**: 1090-1092
-

---

# 3. The Raman Effect: An Introduction and Theory

---

*Raman spectroscopy is based on the inelastic scattering of light by molecules; with each molecular bond releasing slightly different inelastically scattered photons a chemical fingerprint can be built up of the substance under study making Raman spectroscopy a popular diagnostic tool. In this discussion we shall see the origins of the technique and gain a conceptual understanding of the underlying processes that result in the inelastically scattered light. The conceptual classical theory of Raman scattering is presented in order to appreciate further the operation, advantages and potential drawbacks of this exciting technique.*

---

## 3.1 A brief history of Raman Spectroscopy

The phenomenon of inelastic scattering of light from molecules was first predicted in 1923 by Smekal [1] and first observed experimentally in 1928 by Raman and Krishnan [2], then at Calcutta University. The collection and examination of inelastically scattered light has since become known as Raman spectroscopy. In the original experiment, that Raman used to first observe the effect, sunlight was collected and focussed by a telescope onto the sample that was normally a purified liquid or a dust free vapour. A lens was placed by the sample, at  $90^\circ$  to the input beam, to collect the scattered radiation which was then passed through a system of optical filters that was designed to demonstrate the presence of scattered radiation

---

with a different wavelength to that of the incident light. A schematic of Raman's original experiment can be seen in figure 3(a). For this work Raman received the Nobel Prize in physics in 1930. Despite this, Raman spectroscopy has not been in widespread use and normally confined to academic laboratories as the optics and sources required were complex and not robust. However with improvements in spectrographs, detectors and most notably the realisation of the laser, Raman spectroscopy has become the powerful and accessible technique known today.

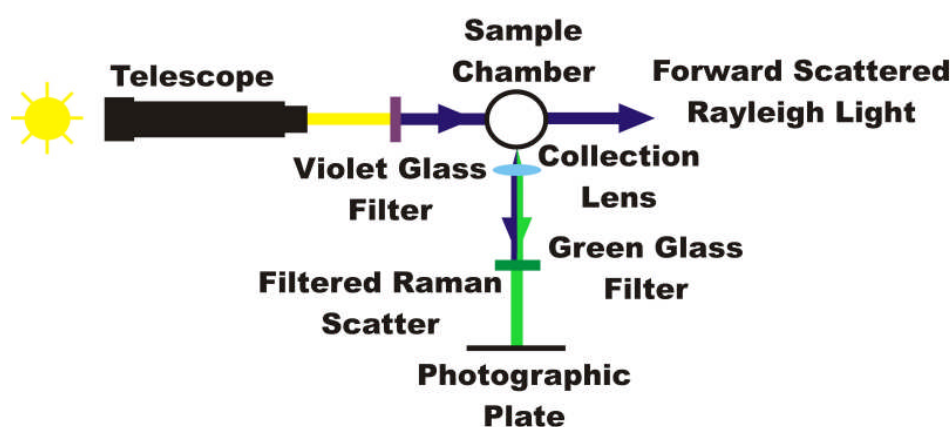


Figure 3(a). A schematic of Raman's original experiment. Sunlight was collected with a telescope and passed through a violet glass filter onto the sample. A lens was placed at  $90^\circ$  to the input beam to collect the inelastically scattered light. This was then passed through a green glass filter to remove the Rayleigh scattered light and a photographic plate was used to record the presence of any inelastically scattered light

### 3.2 Concepts and principles in Raman spectroscopy

Raman spectroscopy is a laser based spectroscopy technique that probes the vibrational energy levels within molecules through the examination of inelastically scattered light.

When light interacts with matter it may be absorbed, scattered or may pass through the sample without interaction. If a photon is incident upon molecules, and does not match a specific electronic transition, there is good possibility it will be scattered. The scattering process does not require that the photon be emitted back onto

---

the incident propagation vector rather, on average, scattered radiation is emitted into a  $4\pi$  sphere, this means scattered photons can be observed by collecting light at some angle to the incident radiation and barring absorption, due to the incident wavelength matching a transition between electronic states, the efficiency of the scattering process is inversely proportional to wavelength raised to the fourth power.

Conceptually the interaction between a photon and the scattering molecule can be considered as an unstable transitory complex between the distorted energy levels of the molecule and the photon [3]. If we consider the photon, whose wavelength is normally much larger than the molecules it is interacting with, as an oscillating dipole it can interact with the molecule and distort the electron cloud surrounding the nuclei. The interaction of the light and molecule causes the electron cloud to polarise and raises the molecule to a higher energy state. At that moment it can be said that the energy of the light is transferred to the molecule. This high energy state is a short lived complex between the light and the molecule in which there is no appreciable movement of the nuclei. This complex, often referred to as the virtual state of the molecule, is unstable and therefore very short lived releasing the energy rapidly in the form of scattered radiation. As the virtual state is so short lived the nucleus does not have time to respond and move to find a new equilibrium state with the distorted electron cloud. It should be noted that this higher energy state does not involve the promotion of an electron to any higher energy level, as in absorption; rather it is superposition of all the energy states of the static molecule forming a new unstable virtual state. The nature of this virtual state is a direct reflection of the properties of the exciting laser beam defining both the energy and the extent of the electron cloud distortion. The instantaneous release of energy from the virtual state without loss of energy is known as Rayleigh scatter and is the most common scattering effect.

---

---

Rayleigh scattering is the most dominant process but another rarer event is also observed; this is an inelastic scattering, known as Raman scattering, and only occurs once in every  $10^6$ - $10^8$  interactions. This occurs when the interacting photon again forms the transient complex causing a distortion in the electron cloud whilst simultaneously inducing nuclear motion. The motion of nucleus requires an appreciable amount of energy transferred from the complex to the molecule and this manifests itself as a reduction in the energy of the ejected photon. The reverse process is also possible, if a molecule is already in motion the energy can be transferred to the photon during the lifetime of the complex and manifests as a photon ejected with a higher energy.

If we think of the quantum picture of the molecule and photon we can understand further the process of inelastic scatter and understand the quantised nature of the energy variations in the inelastically scattered photons. Figures 3(a-c) show diagrams of the energy levels typical of a molecule undergoing the scattering process, this more commonly referred to as a Jablonski diagram or reduced Morse curve and describes the energy of the allowed quantum states of a static molecule. A Morse curve is a diagram that describes the energy of the allowed quantum states as the nuclear separation varies. In the scattering process however, even for inelastic scattering where nuclear movement is induced, the nuclei in the molecule do not have time to move appreciably thus we can describe the energy of the allowed quantum states for the molecule as if it was in a static state. Thus we use a Jablonski diagram to describe the energy levels of our molecule undergoing the scattering process instead of a full Morse curve. As well as the defined electronic energy levels, there is a collection of levels close to the electronic level with small energy gaps separating them. This collection of energy levels is the result of the vibrational states within a

---

---

molecule, and reflects the extra energy in the molecule when it is undergoing processes such as bond stretching or twisting. It should be noted that Jablonski diagrams are not to scale as the separation in energy between electronic levels is very large in comparison to the separation of the vibrational energy levels. These vibrational levels describe the energy required to power a specific vibration in a specific bond. Examination of figure 3(b) shows a photon causing the excitation of the molecule, from the ground electronic state, to a virtual state. As this is unstable the photon is ejected and the molecule returns to the ground state. This is the most common form of scattering and is, as previously mentioned, known as Rayleigh scattering. Figure 3(c) displays an inelastic scattering event, as before a photon interacts with a molecule in the ground state and raises it to an unstable virtual level. When the photon is ejected the molecule returns to one of the excited vibrational states. Physically the photon has induced nuclear movement and transferred energy to the molecule causing a bond vibration. This is manifested as the release of a photon with a slightly reduced energy, hence longer wavelength. This process is referred to as a Stokes transition. An alternative inelastic scattering event is the anti-Stokes transition as shown in Figure 3(d). This requires the molecule to be initially in a raised vibrational level. Again the photon causes the molecule to be raised to an unstable virtual energy level, when the photon is released the molecule transfers its vibrational energy to it and thus returns to the ground electronic state. This is manifested by the release of a photon with a higher energy and hence shorter wavelength.

---

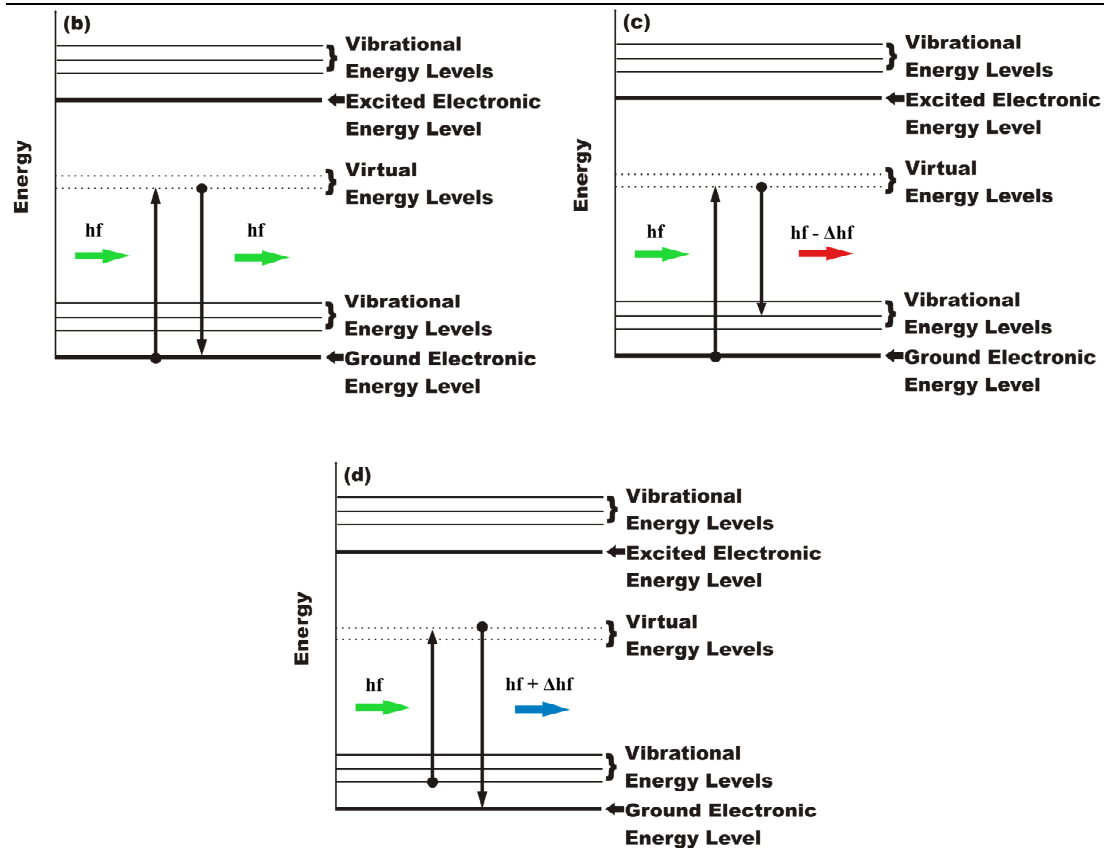


Figure 3. (b) Quantum depiction of an elastic Rayleigh scattering event. (c) Quantum depiction of inelastic Stokes scattering and (d) the alternative inelastic scattering process Anti-Stokes scattering.

If the scattered radiation is collected from the sample, a spectrum of the form of figure 3(e) will be observed. Figure 3(e) is a simulated spectrum and consists of an intense line attributed to the Rayleigh scattering surrounded, on each side, by small identical sets of sidebands at higher and lower energies due to the inelastic Stokes and anti-Stokes events. The sidebands are identical as the same set of vibrational energy levels are involved in both processes.

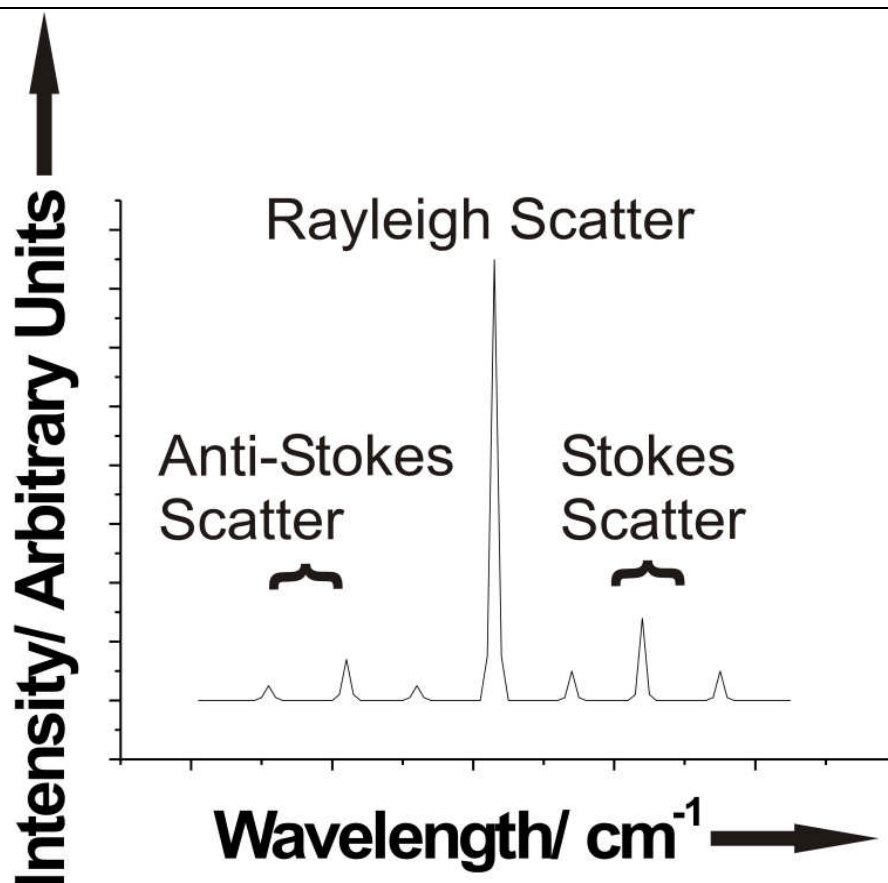


Figure 3(e). A simulated spectra of the collected scattered light from a medium represented by figures 3(a-c).

As represented in Figure 3(d) the Anti-Stokes process requires the molecule to be, at the time of interaction, in an excited vibrational state. It is thus a much rarer event as at room temperature most molecules are in the ground state. The ratio of Stokes to Anti-Stokes events can be calculated from the Boltzmann equation as shown in equation 3.1 [4].

$$R_s = \left( \frac{\lambda_s}{\lambda_a} \right)^4 \exp\left( -\frac{h\Delta\nu}{kT} \right) \quad (3.1)$$

Where:  $R_s$  = ratio of the intensity of stokes to anti-stokes  
 $\lambda_s$  &  $\lambda_a$  = Wavelengths at which the stokes and anti-stokes scattering occurs respectively  
 $\Delta\nu$  = the energy gap, in terms of frequency, between the exciting radiation and the anti-stokes line  
 $T$  = sample temperature

---

As the anti-Stokes transitions are very weak it is normal to only record and consider the Stokes scattering. This plot of Stokes scattering is commonly referred to as the Raman spectra of the sample.

The power of Raman spectroscopy lies in the multiple peaks produced by the inelastic scattering. Each peak, representing a vibrational energy state, correlates directly to a specific vibration of a specific chemical bond. Thus a chemical fingerprint of the substance under study can be built up and even the structure of the chemical compounds within the molecule may be eluded too. It should be noted however that Raman spectra from real samples are often much more complicated with multiple peaks that can occasionally overlap due to the many chemical compounds present that can produce near degenerate energy levels on the Jablonski diagram. Furthermore each bond may contribute more than one energy level as the extent of any particular vibration is also quantised. If this occurs, and the same bond contributes more than one peak to a Raman spectrum, it is known as an overtone. These levels are normally presented in the form of a Morse curve. This is shown in Figure 3(f) and displays the quantised energy as a function of the internuclear separation. With each individual bond and individual vibration type contributing a set of overtones Raman spectra could become very complicated. However, perhaps fortunately, overtones are extremely weak and rarely present in Raman spectra for reasons described by the quantum theory of Raman spectroscopy which is discussed in Appendix B. The inelastic scattering tends only to involve the first level of quantised nuclear movement as other levels are of extremely high energy and somewhat less likely to occur.

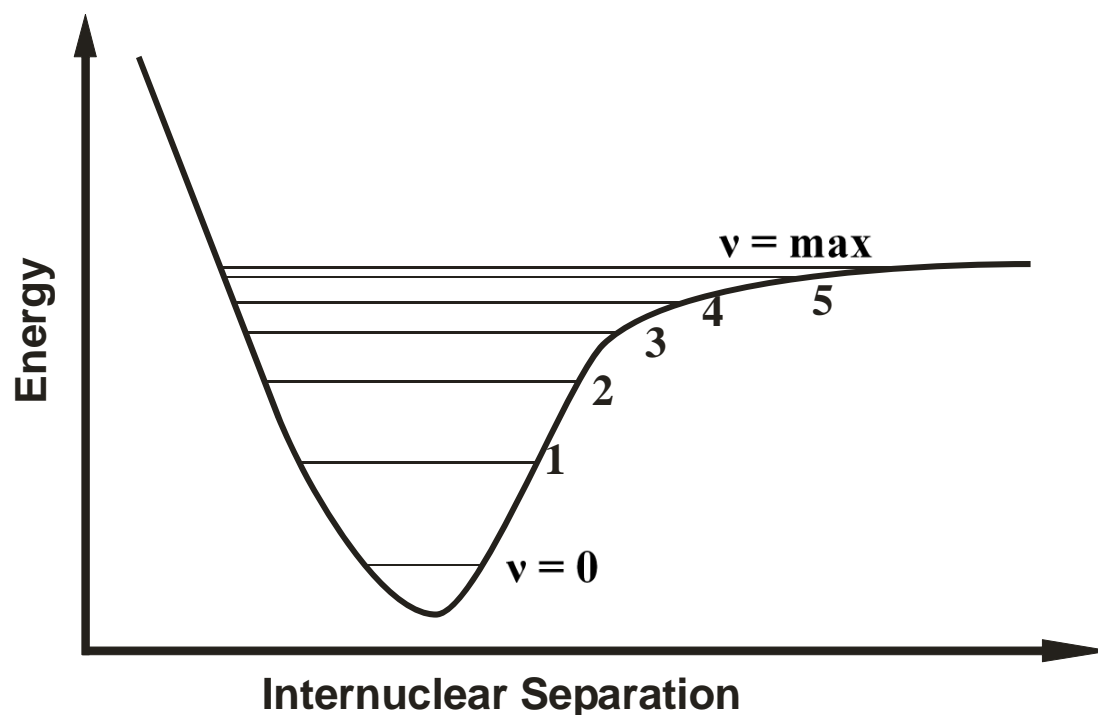


Figure 3(f). A Morse curve showing the quantised extent of a vibration between two intra molecular atoms.

Raman spectra can be complex and this may be seen as daunting initially but it only serves to yield more information about the sample under study.

One of the final key aspects in the understanding of Raman spectra is the scale in which they are normally presented. Raman spectra are often recorded initially as a function of wavelength but are more commonly plotted in a scale called relative wavenumbers that is measured in  $\text{cm}^{-1}$ . Raman spectra essentially display the energy shift, of the measured photon, away from the exciting line which relates directly to the energy of the vibration induced by the photon upon scattering. Remembering that the scattering process is independent of wavelength we consider some small energy packet  $\Delta E$ , which corresponds to a vibrational energy gap, and think about inducing inelastic scattering with two different wavelengths, one in the blue and one in red portion of the visible electromagnetic spectrum. Looking at equation 3.2 we can see

that the blue photon, by virtue of a shorter wavelength, will have a much higher energy than a red photon.

$$E = h \frac{c}{\lambda} \quad (3.2)$$

Where: E = the photon energy  
h = Planck's constant  
c = speed of light  
 $\lambda$  = photon wavelength

When these photons undergo inelastic scattering they will lose a portion,  $\Delta E$ , of their energy. As a percentage of the total energy this will be much more for the red photon in comparison to the blue one. Physically this manifests itself as two different shifts in the wavelength despite the same loss in energy. The relative wavenumbers scale is introduced to combat this effect and to display the same shift for a scattering event no matter what wavelength was used in the excitation. The energy, or Raman, shift in relative wavenumbers can be calculated using equation 3.3. A Raman spectrum of aspirin, acquired with our Raman tweezers system, is shown in figure 3(g) presented with the wavenumber scale.

$$\nu = \frac{1}{\lambda_i} - \frac{1}{\lambda_s} \quad (3.3)$$

Where:  $\nu$  = Raman shift measured in  $\text{cm}^{-1}$   
 $\lambda_i$  = Wavelength of the incident Radiation  
 $\lambda_s$  = Wavelength of the scattered Radiation

Figure 3(g) shows a recorded Raman spectrum of aspirin plotted as a function of wavenumbers. In most cases a sample will produce Raman peaks in the region of approximately 50-4000  $\text{cm}^{-1}$ . In figure 3(g) only the region from 500 to 2000  $\text{cm}^{-1}$  was recorded, this region is known as the 'finger print region' and contains the majority of the most detailed and pertinent information on the chemical composition. Figure 3(h) shows a diagram detailing the bond types present in the region 50-4000  $\text{cm}^{-1}$ , this

gives a good indication of the energy required to power vibrational motions but is only a guide and there are exceptions. This generally occurs when a single bond between the atoms is very strong or the atoms are 'heavy' requiring a large energy to vibrate thus perhaps presenting in a region of the Raman spectra normally associate with higher energy bond motions. Reference 5 provides a more in depth examination of the various bond vibrations and their relation to energy. As much of the detailed and pertinent chemical information is contained within the finger print region this thesis will only deal with this section in its interpretation of biochemical data retrieved with Raman spectroscopy from cells.

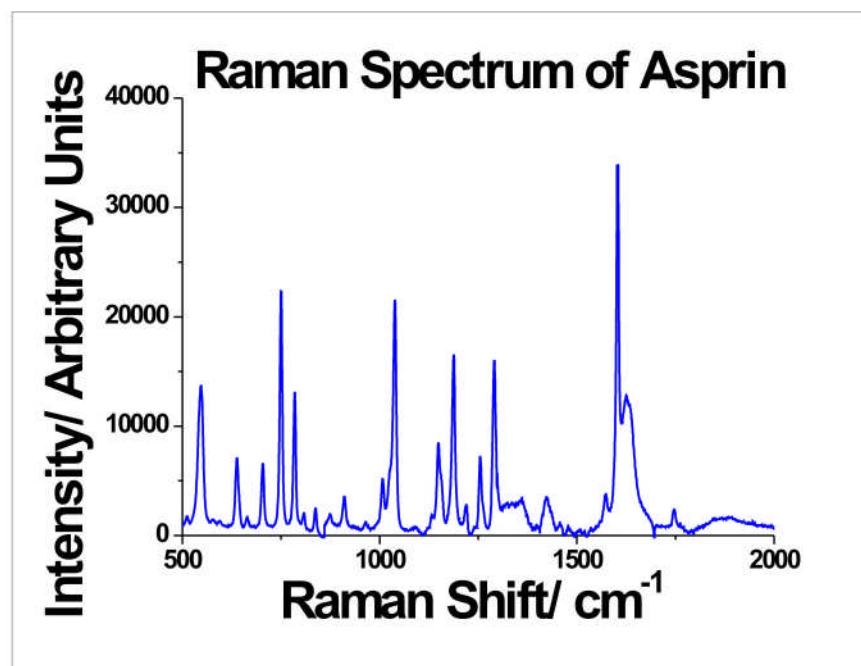


Figure 3(g). Raman Spectrum of Aspirin plotted as a function of wavenumber.

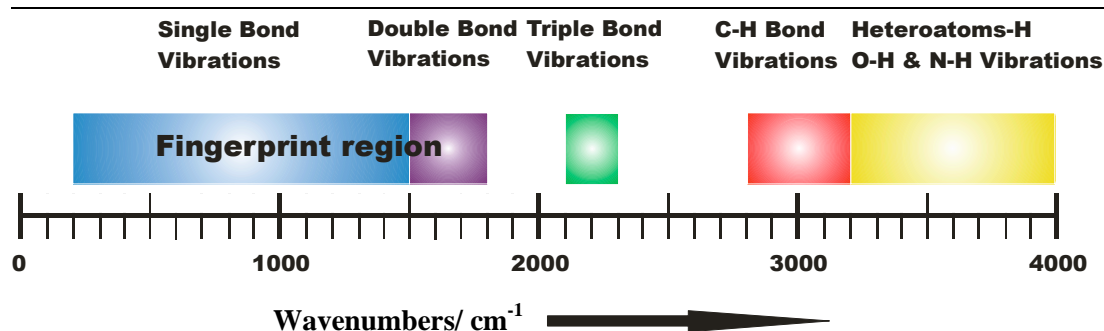


Figure 3(h). A schematic guide to the types and positions of the peaks, arising from the relevant chemical bonds, in a typical Raman Spectrum.

Raman spectroscopy is a powerful technique probing the chemical composition of samples but is a complimentary technique often used with IR spectroscopy to probe samples as they both probe the vibrational energy levels of molecules. IR spectroscopy, see section 2.3.6, is a technique that probes vibrational energy levels through absorption of Infrared radiation. These techniques are described as complimentary as strong Raman bands are weak or non existent in IR spectra and vice versa. The origin of this exclusion rule lies in the physical processes underpinning absorption and inelastic scattering. Inelastic scattering events cause a large polarisation in the electron cloud in comparison to the absorption process which requires a change in the molecular dipole moment. If we consider an example of a very simple triatomic CO<sub>2</sub> molecule we can observe the possible vibrations as shown in Figure 3(i). If we consider the symmetric stretch, shown in Figure 3(i), we can see that it causes a change in polarisability but no change in the electric dipole thus is a Raman active transition. The following two situations in Figure 3(i) show situations where there is a large change in the dipole thus these are Infrared absorption transitions and do not present on the Raman spectra. For simple triatomic molecules, where there is a centre of symmetry, this mutual exclusion rule holds true, however for diatomic molecules, larger complex molecules and for group vibrations the situation is not quite so clear cut and many vibrations induce both a change in

---

polarisability and in the dipole thus appear in both spectra and have varying degrees of scattering 'strength' [5].

This effect has interesting consequences for the polarisation of the scattered light. Raman scatter is partially polarised; more generally the input polarisation can be linked to the polarisation of the Raman scattered light. When the interaction is with a molecule displaying a totally symmetric stretch, even in randomly orientated media, the Raman scattered light is almost all in the same polarisation plane as the input light. This effect is often made use of in Raman spectrometers to probe further the molecular properties. However this becomes more complicated when the interaction is with highly ordered samples or molecules, such as DNA which, where the polarisation tends to align to the scattering structure.

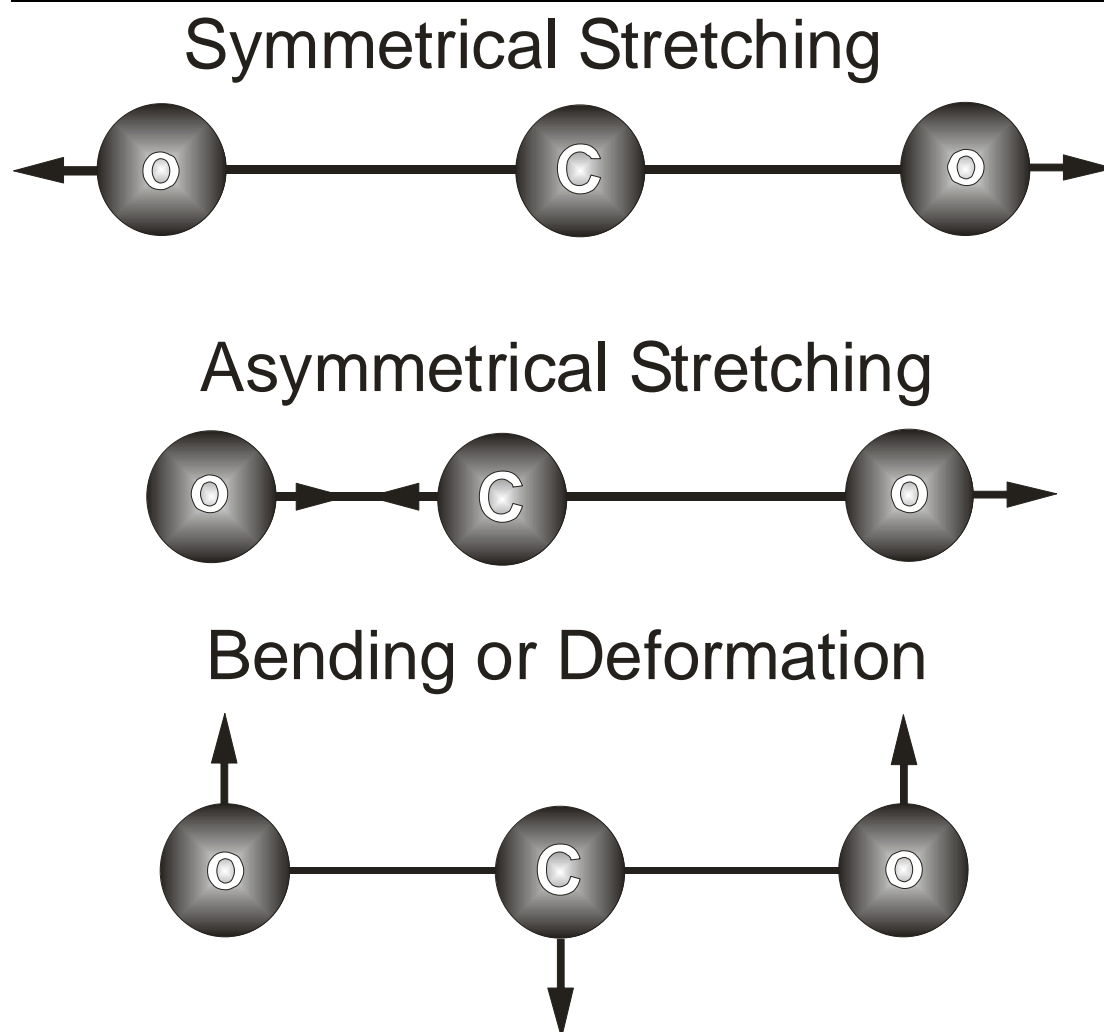


Figure 3(i). Depiction of the vibrational modes of a triatomic CO<sub>2</sub> molecule

These are the main principles of Raman spectroscopy describing conceptually the origin of the technique and how the results are presented. A more detailed mathematical discussion of the principles of Raman spectroscopy follows designed to give a further insight and understanding of this technique.

### 3.3 The Classical Theory of Raman Spectroscopy

The classical theory of Raman spectroscopy [6] gives a good conceptual understanding, as we will see, of the origins and physical processes that underpin Raman spectroscopy. In our discussion we will be considering a molecule that experiences an input electric field and thus scatters the light. The classical theory of

---

light scatter from molecules describes the scattered electric field,  $\mathbf{E}_{sc}$ , as the result of an oscillating dipole induced on a molecule by the presence of some input electric field  $\mathbf{E}_{in}$ . The induced dipole moment in the molecule, created by  $\mathbf{E}_{in}$ , is described in the most general manner by:

$$\underline{\mu}(t) = \underline{\alpha}(t) \underline{E}_{in}(t) \quad (3.4)$$

Where:  $\underline{\mu}(t)$  = the time dependant induced dipole moment  
 $\underline{\alpha}(t)$  = the time dependant polarisability tensor  
 $\underline{E}_{in}(t)$  = the time dependant input electric field

At the most basic level we can see that, as the polarisability tensor and input electric light field can be represented by harmonic functions, there will be a ‘beating’ effect between the two time dependant quantities of the electric field and polarisability tensor thus a number of additional frequency components will be generated.

At this point it is useful to understand conceptually the nature of polarisability and how it is represented. The polarisability is a quantity that essentially represents how ‘easy’ it is to distort the electron cloud, normally the larger the molecule the easier it is to polarise the electron cloud. More formally the polarisability tensor is a response function that represents the volume and shape of the electron cloud at a particular time. The polarisability is represented in tensor form as it links the response of the electron cloud in the three Cartesian directions to the polarisation of the input electric field. This is an important point as this describes the relationship between the polarisation of the incident beam and that of the scattered beam that is experimentally observed. The polarisability, of the molecule in question, is not a fixed quantity; rather it is sensitive to ongoing processes in the molecule and its environment. It is for this reason that the polarisability is represented as a time dependent function. Examples of factors that can affect the polarisability tensor include the constant motion and rotation that most molecules will undergo near room temperature,

---

reconfigurations in the electron cloud through absorption processes or thermal promotion of electrons and nuclear motion in the molecule itself. The polarisability plays an important role in scattering from molecules and a full mathematical derivation of the tensor and its implications can be seen in reference 7. With a working knowledge of the nature of the polarisability tensor we are in a position to proceed on with this discussion.

The time dependant incident electric field can be described as follows:

$$E_{in} = E_{in,0} \cos(\omega_0 t) \quad (3.5)$$

Where:  $E_{in}$  = Intensity of the input electric field at time  $t$   
 $E_{in,0}$  = Maximum intensity of the input electric field  
 $\omega_0$  = angular frequency of the input electric field

Considering this we can now construct an expression for the induced dipole moment:

$$\underline{\mu}(t) = \underline{\alpha}(t) \underline{E}_{in} = \underline{\alpha}(t) E_{in,0} \cos(\omega_0 t) \quad (3.6)$$

Where:  $\underline{\mu}(t)$  = the induced dipole moment  
 $\underline{\alpha}(t)$  = the polarisability tensor

If the molecule, interacting with the incident light field, vibrates we may represent the time dependant nuclear displacement, from the equilibrium position, with the harmonic term:

$$s = s_0 \cos(\omega_n t) \quad (3.7)$$

Where:  $s$  = the nuclear displacement at some time  $t$   
 $s_0$  = the maximum nuclear displacement  
 $\omega_n$  = the angular frequency of nuclear vibration

As mentioned before, the polarisability, of the molecule, is dependant upon the environmental state of the molecule and the nuclear vibrational motion will causes a time dependant variation in the polarisability tensor. This relationship, between the polarisability and nuclear vibration, can be written as a Taylor expansion as follows:

$$\underline{\alpha}(t) = \alpha_0 + \left( \frac{\partial \alpha}{\partial s} \right)_0 s + \frac{1}{2} \left( \frac{\partial^2 \alpha}{\partial s^2} \right)_0 s^2 + \dots \quad (3.8)$$

Where:  $\alpha_0$  = the polarisability tensor at the equilibrium nuclear position

$\left( \frac{\partial \alpha}{\partial s} \right)_0$  = the time varying polarisability tensor, as a function of  $s$ , evaluated at the equilibrium position

The third term in equation 3.8 represents the second order nonlinear dependence of the polarisability upon vibration. However for small vibrations, thus small  $s$ , the relationship between polarisability and nuclear movement is a linear one thus we need only consider the first two terms in equation 3.8.

If we now employ the new expression for vibration dependant polarisability in our consideration of the induced dipole moment we can write:

$$\underline{\mu}(t) = \underline{\alpha}(t) E_{in,0} \cos(\omega_0 t) \quad (3.9)$$

$$= \alpha_0 E_{in,0} \cos(\omega_0 t) + \left( \frac{\partial \alpha}{\partial s} \right)_0 s E_{in,0} \cos(\omega_0 t) \quad (3.10)$$

$$= \alpha_0 E_{in,0} \cos(\omega_0 t) + \left( \frac{\partial \alpha}{\partial s} \right)_0 s_0 E_{in,0} \cos(\omega_0 t) \cos(\omega_n t) \quad (3.11)$$

In order to simplify this expression we can employ the trigonometric identity given by equation 3.12.

$$\cos A \cos B = \frac{1}{2} (\cos[A + B]) + (\cos[A - B]) \quad (3.12)$$

This gives us the resulting expression for the induced dipole moment and hence expression for the scattered electric field as:

$$\begin{aligned} \underline{\mu}(t) = & \underbrace{\alpha_0 E_{in,0} \cos(\omega_0 t)}_{\text{term a}} + \underbrace{\frac{1}{2} \left( \frac{\partial \alpha}{\partial s} \right)_0 s_0 E_{in,0} [\cos\{(\omega_0 + \omega_n)t\}]}_{\text{term b}} \\ & + \underbrace{\frac{1}{2} \left( \frac{\partial \alpha}{\partial s} \right)_0 s_0 E_{in,0} [\cos\{(\omega_0 - \omega_n)t\}]}_{\text{term c}} \end{aligned} \quad (3.13)$$

---

This equation describes the scattered electric field from an induced dipole and contains some interesting aspects describing the scattered electromagnetic field. The first marked term, *term a*, describes the Rayleigh scattering component where there is no change in frequency and the polarisability tensor remains unchanged and describes the relationship between the polarisations of the input and scattered electric fields. *Term b* describes an additional higher frequency component in the scattered field that corresponds to the anti-stokes scattering, in a similar fashion *term c* describes an additional component in the field with reduced frequency that corresponds to the stokes scattering. In both these cases the change in frequency is proportional to the frequency of bond vibration in the molecule; we should also note that equation 3.13 describes only the frequency changes associated with one bond, when considering a Raman spectrum of a complete molecule we need to sum over all the vibrating bonds. Equation 3.13 also contains some other important information; the first is that the varying polarisability tensor, as a result of bond vibration, will mean the polarisation of the Raman scattered field will have an altered relationship with the input polarisation allowing further opportunity to gain information about a specific bond through examination of the polarisation of the Raman scattered field. The second interesting aspect pertaining to the variation of polarisability with nuclear vibration is that if the derivative term goes to zero term b and term c will also collapse to zero. The first obvious possibility for this is no nuclear movement in the molecule thus only Rayleigh scattering will be observed, the second is that the nuclear movement causes no change in polarisability therefore no Raman scatter and it is this second possibility that underpins the broad selection rule for Raman scattering events that the incoming light field must induce a change in polarisability of the molecule for Raman scattering to occur.

---

---

The classical theory of Raman spectroscopy gives a good conceptual understanding of the fundamental processes that contribute to the inelastic scattering of light, however it struggles to explain some observed phenomena in Raman spectra such as the quantised nature of the observed vibrations and the links between molecular properties and those of the Raman scattered light. To fully understand all the properties of the inelastically scattered light and their relationship with the molecular properties of the scatterer a quantum mechanical approach is necessary. Although not presented in this chapter, as an understanding of the quantum theory of Raman spectroscopy is not strictly necessary to interpret the results presented in this thesis, interested readers can find a presentation of the quantum theory of Raman scattering in appendix B.

### 3.4 References

- [1] Smekal A. **Zur Quantentheorie der Dispersion**. Naturwissenschaften 1923; **43**: 873-875
- [2] Raman CV and Krishnan KS. **A new type of secondary radiation**. Nature 1928; **121**: 501-502
- [3] Smith E and Dent G. **Modern Raman Spectroscopy: A practical approach**. 2005; John Wiley & Sons: pp. 72
- [4] Wilson J and Hawkes J. **Optoelectronics and introduction 3<sup>rd</sup> edition**. 1998; Prentice Hall Europe: pp. 501
- [5] Smith E and Dent G. **Modern Raman Spectroscopy: A practical approach**. 2005; John Wiley & Sons: pp. 11-20
- [6] Ferraro JR, Nakamoto K and Brown CW. **Introductory Raman Spectroscopy**. 1994; Academic Press: pp. 13-22

---

[7] Laserna JJ. **Modern Techniques in Raman Spectroscopy**. 1996: John Wiley &

Sons: pp. 3-12

---

# 4. Optical Trapping: An Introduction and Theory

---

*The invention of the single beam optical trap spawned an entirely new research field and has become common place in many others, supplementing techniques and opening up areas of investigation that were previously inaccessible. The following discussion addresses the theory that underpins the optical trap and examines briefly its impact in the biomedical sciences. Finally the dual beam trap, which is enjoying a recent resurgence in interest, is also considered and its potential applications are discussed.*

---

## 4.1 Introduction to Optical Trapping

In 1986 a seminal paper was published in Optics Letters that spawned an entirely new field of research that in particular would lead to great leaps in understanding in single molecule biophysics and cell biology, enhance existing spectroscopy techniques and even the furthering of our understanding in fundamental light matter interactions. That paper, by Ashkin *et al*, was ‘Observation of a single-beam gradient force trap for dielectric particles’ [1] which describes what is more frequently described as the ‘Optical Tweezers’ and was the culmination of works that centered on the phenomenon of radiation pressure, the result of the transfer of momentum from photons to an object.

Optical tweezers is a term used to describe a technique that uses strongly focussed laser light to hold and manipulate microscopic particles, from tens of

---

---

nanometres up to tens of microns, in three dimensions with little or no damage. A single laser beam focussed to a diffraction limited spot attracts small dielectric particles into the region of highest intensity due to the intensity gradient of the light. The particles that can be manipulated range from small silica and polymer spheres through to single biological cells all using only a few tens of milliwatts of laser power.

The concept of light being able to exert a force was considered as far back as 1873 when Maxwell was considering the implications of his theory of electromagnetism [2] and in 1901 Lebedev showed the first demonstration of radiation pressure deflecting atoms away from a detector with the use of an arc lamp [3]. It was however with the invention of the laser that investigations into this effect enjoyed a resurgence when in 1970 Ashkin, then at Bell Laboratories, published a manuscript detailing the optical trapping, due to the transverse optical gradient force, and acceleration along a propagating  $TEM_{00}$  mode laser beam due to the scattering force, of micron sized particles. Ashkin went on to demonstrate, in this publication, how two counter propagating  $TEM_{00}$  light beams could hold a high index micron sized particle at an equilibrium position where the scattering forces and gradient forces from the laser beams are balanced, this geometry is often referred to as a dual beam trap. The following year Ashkin demonstrated the use of a focussed  $TEM_{00}$  laser beam to levitate silica particles, balancing the scattering forces against the force due to gravity, to deliver particles to a dual beam trap [4]. It was then in 1986 that Ashkin published his research on single beam gradient traps demonstrating a method of optically confining small particles which can be readily incorporated into commercially available microscopes. Ashkin went on to demonstrate the potential of

---

---

this technique, especially in the biological arena, by trapping and manipulating single bacterial cells and viruses [5&6].

This work showed the potential of this technique and the optical tweezers tool has taken many forms and found many applications throughout all the natural sciences. As this discussion on optical trapping progresses we will examine the origins of trapping and the forces involved that allow particles to be confined in the optical gradient potential. A discussion of the operation of dual beam traps will also be considered as their use is finding renewed interest in applications in the biomedical sciences. Furthermore we will see how a basic optical tweezers setup is constructed and discuss the impact this technique has had on the biomedical sciences.

## 4.2 The Origins and Forces involved in Optical Trapping

As previously mentioned the origin of radiation pressure is the interaction of a photon with matter that results in some change of photon momentum. If we consider the example, figure 4(a), of a photon, with a momentum described by equation 4.1, incident on a mirror and is subsequently reflected, a change in momentum will occur. If momentum of the system is to be conserved, as it must, the mirror must experience a change in momentum thus a force from the photons.

$$P = \frac{h}{\lambda} \quad (4.1)$$

Where:  $P$  = the photon momentum  
 $h$  = Planck's constant  
 $\lambda$  = the photon wavelength

The force imparted by the photons is on the order of femtonewtons. This is extremely small and has little impact on the mirror however for small micron sized particles this force is significant.

The understanding of the mechanisms that allow the optical trapping can be understood in two regimes: The Mie regime and the Rayleigh regime, figure 4(b).

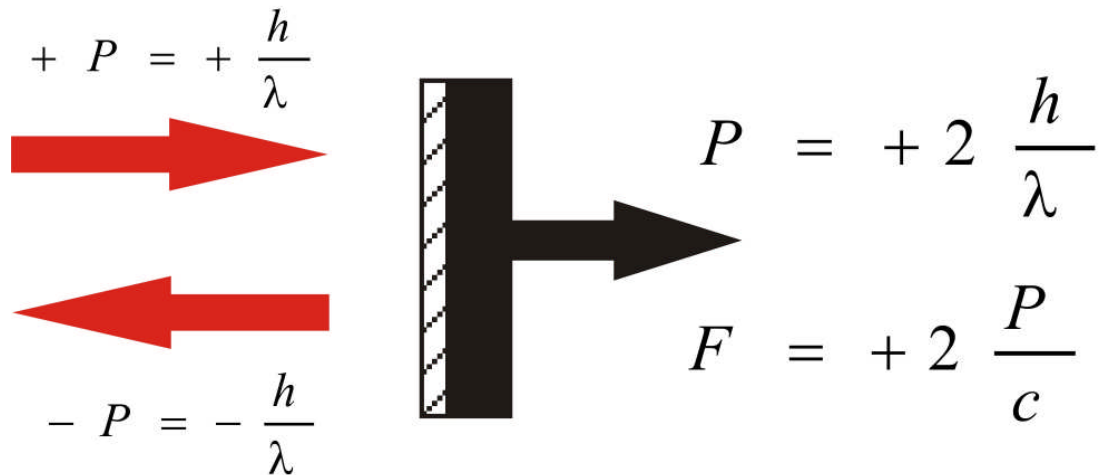
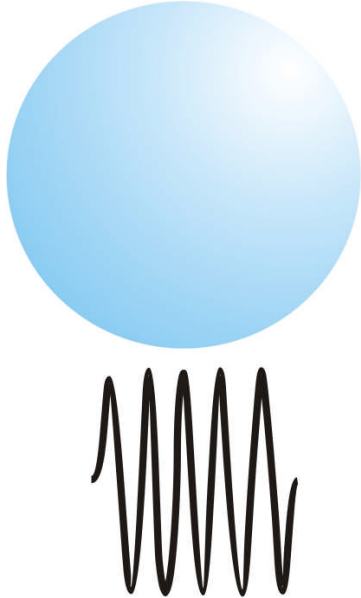


Figure 4(a). If a photon, with momentum  $P = +h/\lambda$ , is incident upon a mirror and undergoes a reflection it will leave with a momentum  $P = -h/\lambda$ . In order to conserve momentum the photon must impart a momentum of  $P = +2 h/\lambda$  to the mirror. This change in momentum for the mirror will mean the photon has imparted a small force on the mirror of  $F = 2P/c$ .

The Mie regime addresses situations where the particle being trapped is much larger than the wavelength of the light being used for trapping; in this situation a consideration using ray optics approach is appropriate. The Rayleigh regime considers the situation where the particle is smaller than the wavelength of the trapping radiation; in this situation a ray optics approach is not sufficient rather it is more appropriate to consider the electric field in the trapping region. With the Mie regime accounting for particles with diameters much larger than the trapping wavelength and the Rayleigh regime accounting for particles with diameters much smaller than the trapping wavelength, there remains a region in the middle where the particle being trapped has a diameter similar to that of the wavelength of the trapping light. This regime is not as well understood as the others but is the regime in which much optical trapping occurs thus we shall discuss the progress in this area later in this section.

## Mie Regime



## Rayleigh Regime



Figure 4(b). In the Mie regime the Particle diameter is much larger than the wavelength of the incident radiation, in contrast to the Rayleigh regime where the diameter of the particle is smaller than the incident radiation.

### 4.2.1 Optical Trapping in the Mie Regime

The Mie regime, as already stated, deals with situations where the diameter of the particle is much larger than the wavelength of the trapping radiation and thus we may, in this situation, neglect the effects of diffraction and use a ray optics approach in the analysis of the forces involved.

Initially we will begin by considering a small dielectric particle that has a higher refractive than the surrounding medium, such as a silica particle in water or a biological cell in a growth medium. In this situation the particle will behave in a similar manner to a small lens refracting any rays incident upon it. If we think again about the inherent momentum  $P$  carried by photons, as described by equation 4.1, then a particle causing refraction of a stream of photons will cause a change in their

---

momentum, thus by conservation of momentum and Newton's third law, the photons will impart an equal and opposite change in momentum to the particle hence applying a small force to it.

Considering first the transverse attraction, or transverse gradient force, we think of a situation, depicted in figure 4(c), where a small high index particle is offset in relation to a Gaussian laser beam. A Gaussian laser beam is chosen here as it is the most commonly used beam, to trap high index particles, in optical trapping and the natural output of most lasers. A Gaussian beam has a high intensity central region spatially decaying at right angles to the propagation direction; a schematic of a Gaussian beam profile can be seen at the top of figure 4(c). Examining the particle, in figure 4(c), its right edge is close to the intense central region and will refract the photons to the left, thus by Newton's third law the particle will experience a force,  $F_a$ , to the right proportional to the number of photons undergoing the refraction process. Now looking at the left side of the particle, it too is refracting photons but this time to the right. Again by Newton's third law the particle will then undergo a force,  $F_b$ , to the left proportional to the number of photons undergoing the refraction process. Due to the Gaussian beam shape the right edge of the particle, experiencing a high intensity, will refract many more photons than the left edge, in an area of low intensity. This will result in  $F_a$  being much larger  $F_b$  giving a net force to the right into the most intense part of the beam. Eventually the particle will come to rest, in the transverse plane, when the particle sits in the centre of the beam and  $F_a$  and  $F_b$  are balanced. In the transverse plane particles are drawn to the highest intensity region of the beam due to its inherent intensity gradient. The same argument can be made for the axial trapping but is a little less intuitive.

---

---

The situation and the forces involved in the axial trapping process are shown in Figure 4(d); this shows the two outermost rays in the beam being strongly focussed by a high numerical aperture lens. Below the focus the rays are incident upon the high index particle; at the particle interface there is a small reflection giving scattered light that will result in a force, labelled with  $F_s$  in Figure 4(d). The remaining photons, in the rays, are refracted and also generate a force labelled by  $F_r$ . These forces contain vector components in both the horizontal and vertical directions; if the particle is in the centre of the beam, as shown, the horizontal components will cancel leaving only the vertical vector to be evaluated. The force propelling the particle away from the focus arises from the scattering of light from the particle at the medium/particle interface. The force drawing the particle towards the beam focus arises from the vertical component of the force imparted to the particle by the refracted photons. When a high NA lens is used, the upwards force from the refracted photons, more commonly referred to as the axial gradient force, is much larger than the force from the scattering, thus the particle is drawn into the focus.

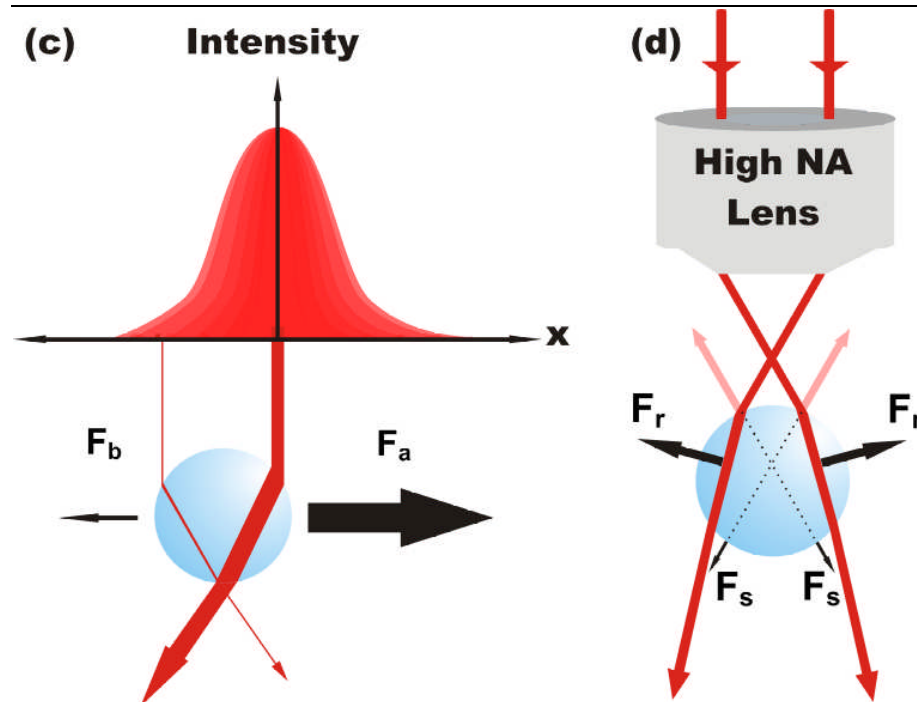


Figure 4(c&d). Figure 4(c) shows a schematic of the forces involved in the transverse gradient force that draws particles the laser beam. Figure 4(d) shows a schematic of the forces involved in the axial gradient force that draws the particle into the focus of the beam.

From this argument we can appreciate that the greater the vertical component of the refraction force the greater the gradient force and thus axial trapping will be. This requirement for a strong vertical component underpins the need for a high NA lens that can aggressively focus light, figure 4(e) shows three rays with different angles of incidence on a particle and demonstrates the greater the angle of incidence the greater the vertical force component. Thus for effective optical trapping in three dimensions with a single beam, a high NA lens must be employed.

The axial trapping, in the Mie regime, can be described in a more quantitative manner [7] and calculated from the Fresnel reflection and transmission coefficients. The scattering force is given by equation 4.2 and the gradient force is described by 4.3. These equations can be combined to give the total  $F$  described by equation 4.4. These are involved equations but the interesting thing to note is the dependence on incidence and refraction angles and the independence of the forces on the radius of the

trapped particle. Despite the lack of dependence on particle radius it does not imply that particles with infinitely large radii can be readily trapped. In our discussion we neglected the force due to gravity, as mass of particle scales as radius cubed large particles are difficult to manipulate.

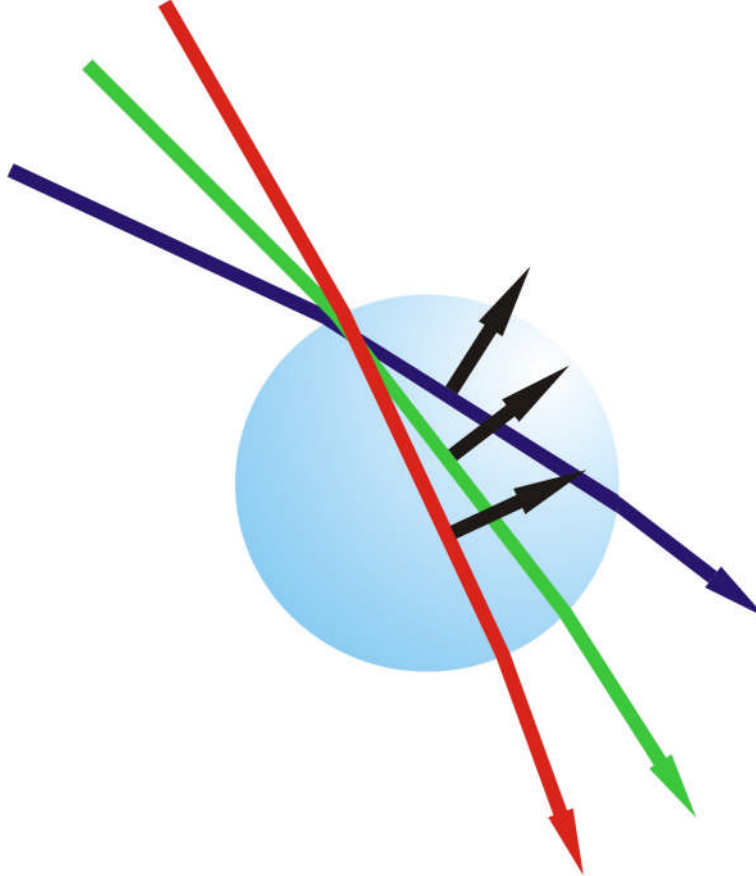


Figure 4(e). A diagram showing the resultant vector forces, black arrows, from the refraction of rays at different incident angles. The greater the angle of incidence the greater the vertical component of the resultant force resulting in an increase in the gradient force and stronger optical trapping.

$$F_s = \frac{n_m P}{c} \left( 1 + R \cos 2\theta + \frac{T^2 [\cos(2\theta - 2\phi) + R \cos 2\theta]}{1 + R^2 + 2R \cos 2\phi} \right) \quad (4.2)$$

$$F_g = \frac{n_m P}{c} \left( R \sin 2\theta + \frac{T^2 [\sin(2\theta - 2\phi) + R \sin 2\theta]}{1 + R^2 + 2R \sin 2\phi} \right) \quad (4.3)$$

Where:  $F_s$  = Scattering Force

$F_g$  = Gradient Force

$n_m$  = Refractive index of surrounding medium

$\theta$  &  $\phi$  = Angles of incidence and refraction respectively

$R$  = Fresnel reflection coefficient

$T$  = Fresnel transmission coefficient

$P$  = Photon momentum

---

The total force can be described as:

$$F = \frac{Qn_m P}{c} \quad (4.4)$$

Where:  $F$  = the total force

$Q$  = the Dimensionless trapping efficiency

The Mie regime gives a good conceptual explanation of the underpinning forces that the optical tweezer relies upon to draw small dielectric particles into the intense region of a focussed laser beam. It should also be noted that particles with a refractive index lower than the surrounding medium can also be trapped but require a different beam shape. The low index particles will refract the light away from them thus will be repelled from the intensity region and a Laguerre-Gaussian beam is required to trap the particles in its dark central core. The ray-optics analysis gives a good approximation for Mie particles; however a different approach is required for Rayleigh particles.

#### 4.2.2 Optical Trapping in the Rayleigh Regime

The Rayleigh regime deals with the situation in which the particle is much smaller than the wavelength of the trapping light. The ray optics approach is no longer satisfactory, as only a portion of light wave interacts with the particle, and it is more appropriate to consider the interaction of the particle and the electric field imposed by the light.

If we consider a small polarisable particle in the presence of a light wave, it will experience an approximately uniform electric field. This electric field will create a polarisation in the individual atoms, making up the particle, and hence induce an electrical dipole in the particle. As the overall system, of light field and particle, will

---

strive to attain the lowest possible energy state, the particle is drawn to the region of highest field intensity to enable a minimisation of the energy. Figure 4(f) shows a schematic of a polarised particle in a uniform electric field. The applied field induces a dipole in the particle, however in this uniform field there is no net force on the particle. In order to induce a net force in the particle a gradient must be introduced into the electric field, in the case of optical trapping this is achieved by focussing the light. As there is a much higher field intensity acting at on one sign of the dipole than the other a net force is induced on the particle and thus it is drawn towards the focus of the electric field, this is shown in figure 4(g). The focussing of the light field creates a local minimum in potential energy in the field that creates a gradient force which draws in the particle so that overall the system may reduce its energy.

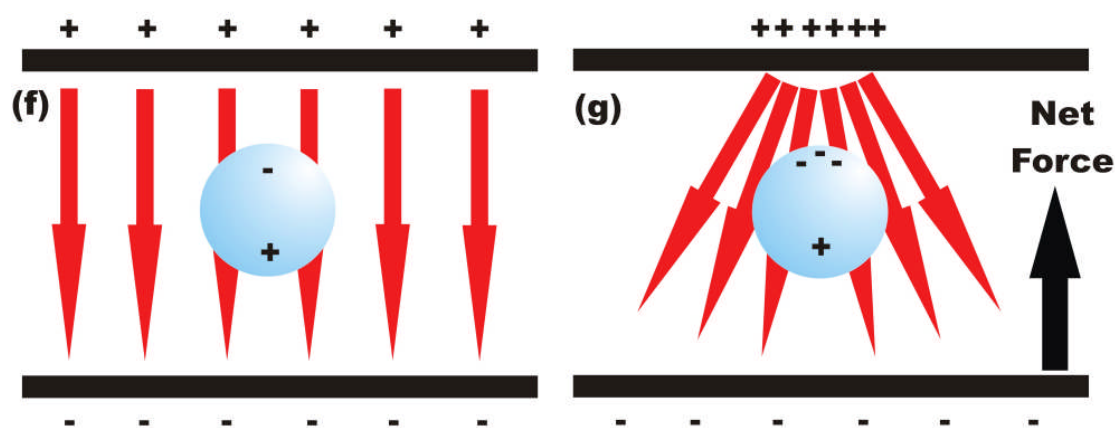


Figure 4(f & g). Figure 4(f), the induced dipole in a small dielectric particle placed in an external uniform field, the uniform field induces a dipole but there is no net force. Figure 4(g), a small dielectric particle placed in an external nonuniform-electric field, the field induces a dipole in the particle but the gradient in field intensity means a net force is induced on the particle that results in it being drawn to the region of highest intensity.

In the Rayleigh regime, as in the Mie regime, the gradient force drawing the particle into the focus of the beam is countered by the scattering forces that tend to push the particle away from the focus. These two forces are readily separated in the Rayleigh regime and the origin of the scattering force can be attributed to the absorption and reemission, of the incident light, by the dipole induced in the particle.

The absorption and re-emission results in a net force in the direction of the propagating light field thus driving the particle away from the focus. The forces involved in the Rayleigh regime can be described more quantitatively as follows [1].

For a Rayleigh particle in a medium of index  $n_m$  the scattering force, in the direction of the incident power is:

$$F_{scat} = \frac{n_m P_{scat}}{c} \quad (4.5)$$

In terms of the field intensity this can be shown to be:

$$F_{scat} = \frac{I_o}{c} \frac{128\pi^5 r^6}{3\lambda^4} \left( \frac{m^2 - 1}{m^2 + 2} \right)^2 n_m \quad (4.6)$$

Where:  $I_o$  = Incident field intensity  
 $\lambda$  = Wavelength of incident radiation  
 $r$  = Particle radius  
 $m$  = Effective refractive index

The gradient force, experienced by the particle, is proportional to the polarisability of the Rayleigh particle:

$$\begin{aligned} F_{grad} &= -\frac{n_m}{2} \alpha \nabla E^2 \\ &= -\frac{n_m^3 r^3}{2} \left( \frac{m^2 - 1}{m^2 + 2} \right) \nabla E^2 \end{aligned} \quad (4.7)$$

Where:  $\alpha$  = Polarisability of the particle  
 $E$  = Electric field vector

As in the Mie regime the ratio of the gradient force to scattering force must be greater than 1 for axial trapping, the ratio is given by

$$\frac{F_{grad}}{F_{scat}} = \frac{3\sqrt{3}}{64\pi^2} \frac{n_m^2}{\left( \frac{m^2 - 1}{m^2 + 2} \right)} \frac{\lambda^5}{r^3 \omega_o} \quad (4.8)$$

Where:  $\omega_o$  = size of the Gaussian beam waist

In reality we require this ratio to be much higher than 1 for stable axial trapping but there are some interesting points arising from equation 4.8. The first point to note is that the ratio is independent of beam intensity although in reality with other factors

---

such as Brownian motion acting on sample the laser intensity is a consideration. The second point of note is the direct proportionality of the ratio to wavelength indicating longer wavelength sources would provide more effective trapping, though this is balanced by the need to focus the light to as small a spot as possible to create a strong gradient. There is a possible exception to this that arises in the trapping of small metallic particles, which behave as dielectrics when they have radii on the order of tens of nanometres. There is evidence to suggest that at certain wavelengths in the visible region, where the metallic particles absorb the light to create surface plasmons, the trapping is enhanced [8]. The final points are that the ratio is inversely proportional to beam waist implying the need for high NA focussing lenses to give the maximum gradient and the ratio is also inversely proportional to particle size. It should be noted however that infinitely small particles can not be trapped as after  $\sim 18\text{nm}$  the number of polarisable atoms becomes insufficient to sustain a strong gradient force [9]. The Rayleigh concepts for understanding optical trapping are very effective for small nanometre sized particles and allow a further understanding of the role of strong optical gradients in optical trapping.

#### **4.2.3 Optical trapping when particle diameter $\sim$ to the trapping wavelength**

When considering the trapping of particle with radii  $\sim 1\mu\text{m}$  in between the Mie and Rayleigh regimes the theory becomes involved and more difficult although recent progress has been made [10]. Any theory describing this regime must take into account the diffraction of the light by the trapped particles and the optical field surrounding the trapped particle. This regime can be described by the Lorenz-Mie theory [11] that describes the behaviour of the electric field around the particle and takes into account wavelength, particle size and refractive index. However this theory

---

---

is limited as it describes the interaction of particles with plane waves and cannot describe Gaussian TEM<sub>00</sub> beams that are normally used in optical trapping. In order to address this issue an updated version of this theory was presented by Goubet *et al* [12] that has become known as the generalised Lorenz Mie theory (GLMT) and can describe the interaction of particles with any arbitrary beam shape. GLMT has established itself as the leading theory in this area and is proving very successful in describing light particle interactions. In reality particles with  $r \sim \lambda$  trap very effectively and are widely employed in optical trapping, often as molecular handles.

In this thesis the particles trapped fall mostly into the Mie regime such as large silica or polymer microspheres as well as biological cells ranging from 5 $\mu\text{m}$  up to 50  $\mu\text{m}$ .

### 4.3 The Basic Optical Tweezers Set-Up.

Optical traps have taken many functional forms but there are a few major concerns that must be addressed when designing a system:

- Trapping wavelength
- Laser beam profile
- Microscope objective used for trapping
- Trap geometry

The choice of laser wavelength will depend largely on the intended application; in this thesis optical traps are often used to interrogate biological cells thus a wavelength must be chosen such that the possibility of photo-damage is kept to a minimum. The mechanism that leads to photo-damage is the absorption of light causing heating and tearing of bonds, thus a trapping wavelength must be chosen where the cells have absorption minima. This will almost certainly mean a choice of

---

---

laser in the Infrared region of approximately 750nm-1.2 $\mu$ m, as this region has a much lower absorption than visible wavelengths. Studies on photo-damage have thrown up evidence for several possible mechanisms powering the observed damage. The first study, we will consider [13], examined damage caused by infrared laser radiation on *E. coli* and Chinese Hamster Ovary (CHO) cells and cited a single photon mechanism for damage. This report found minimum damage at 785nm, 830nm and 970nm although damage also remains reasonably low at 1064nm, a widely used wavelength in trapping. A chart, taken from reference 13, displaying the correlation between wavelength and photodamage can be seen in figure 4(h). The photo-damage did not correlate directly to the absorption spectra of water or oxygen but is more likely the result of absorption by specific photopigments. The fact that the absorption profile of *E. coli* and CHO cells was similar indicates the damage mechanism may be similar in both prokaryotic and eukaryotic systems. The second study [14], also examining damage in the infrared, cites a multiphoton absorption process for the damage causing the release of reactive and destructive chemicals. Localised heating has also been cited as a possible mechanism for photo-damage through absorption of the light, mainly by water [15]. All these studies drive home the importance of choosing a laser wavelength with low absorption in cells for maximising their study in optical traps.

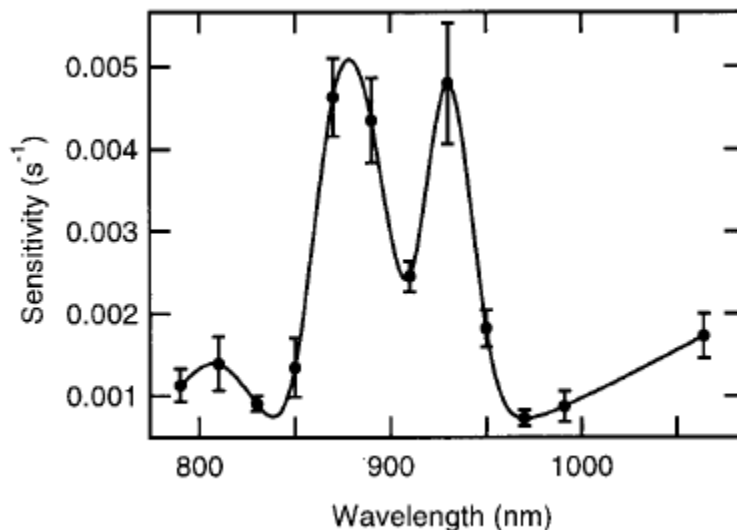


Figure 4(h). Chart, taken from reference 13, showing the correlation between photodamage and wavelength in *E. coli*.

As well as the wavelength, the laser beam shape is also an important factor to be considered in optical trapping. A TEM<sub>00</sub> Gaussian beam profile is normally used to create the trapping gradient, but another important factor is the  $M^2$  parameter. This parameter essentially describes how close to a perfect Gaussian the beam is, with an  $M^2$  value of 1 describing a perfectly Gaussian output, whilst increasing  $M^2$  values describe increasingly irregular beam shape. For the trapping of small Rayleigh particles where the gradients are critical very low  $M^2$  values are required, however for larger Mie particles the importance of the beam quality diminishes slightly as the particles are often larger than the beam thus allowing the use of more cost effective sources such as shaped diode lasers.

As we have established from our look at the theory of optical trapping a high NA lens is required to form aggressive gradients. Again this is especially true for Rayleigh particles but the NA can be decreased slightly for Mie particles. This requirement almost certainly means the use of microscope objective lens' which can have numerical apertures (NA) of up to 1.4. These microscope objectives are often oil immersion or water immersion, the use of oil or water between the front objective

lens and the sample, normally contained in a glass cover slip ‘sandwich’ allows the light to be focussed much more tightly giving increased gradients. The demand for high gradients and viewing constraints will almost certainly mean that  $\times 100$  NA 1.25-1.4 oil immersion objectives will be required for trapping Rayleigh particles, however for Mie particles the conditions can be relaxed and objectives with NA of 0.7-0.9 and magnifications of 50x upwards can be used.

The final consideration is the geometry of the trap, although optical traps have taken many forms they tend to fall into two broad categories: conventional optical tweezers and the inverted optical tweezers. The conventional optical tweezers utilises a beam travelling downwards such that the gradient force, drawing the particle into the beam focus, works against both the scattering force and gravity. In the inverted tweezer geometry an upward travelling beam is employed such as the gradient force works with gravity against the scattering force to trap the particle. A schematic of a basic inverted tweezer is shown in Figure 4(i); this is the geometry of trap that is used throughout this thesis.

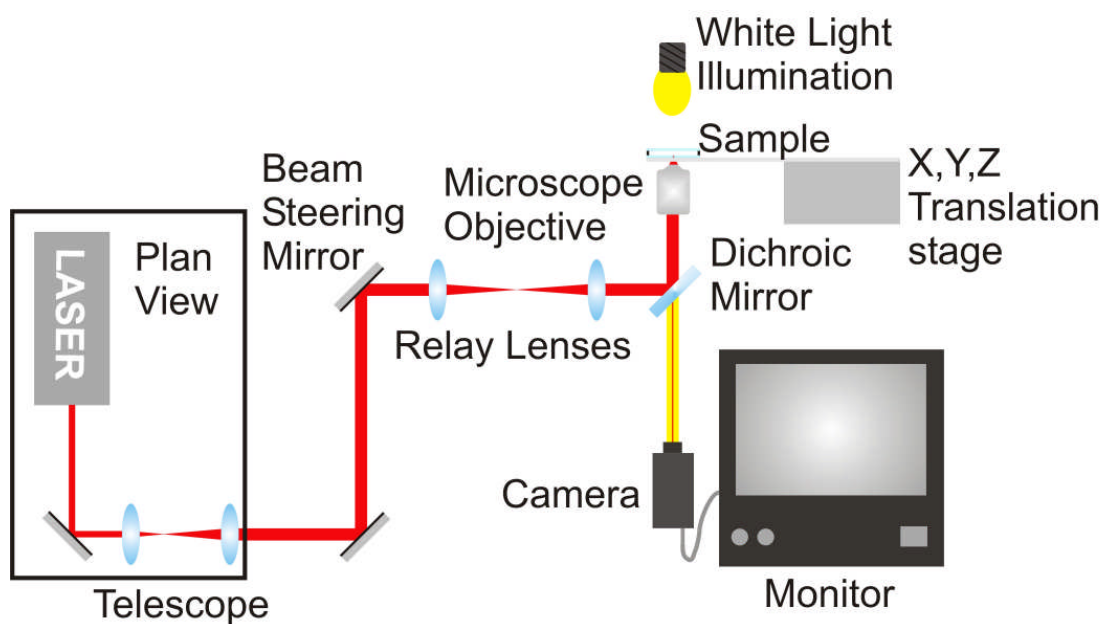


Figure 4(i). Schematic of a basic inverted optical tweezer

In most optical tweezers the beam is initially expanded up to the diameter of the back aperture of the microscope objective in order to ensure the largest gradient possible. The beam is then lifted vertically to the beam steering mirror that, in conjunction with the relay lenses, can be used to move the trap and hence manipulate particles. The relay lenses are used to match the laser beam to the microscope optics, this geometry assumes the use of an infinity corrected microscope objective. In infinity corrected microscopes the objective produces trains of parallel rays from each point on the object being imaged, a subsequent collection lens is then required to focus the rays down and form the image. The first lens forms a focussed spot in the microscope image plane, thus the second relay lens behaves as the collection lens and transmits a parallel train of rays to the microscope objective via the 45° dichroic mirror. The microscope objective then focuses the laser light down to a diffraction limited spot for trapping. The samples are normally contained between two glass cover slips separated by a vinyl spacer. These vinyl spacers are normally square with a 1 cm diameter hole in the centre that is 80µm deep to contain the sample. The sample is then placed above the microscope objective and aligned, to the objective, with the use of a three dimensional translation stage. The sample is illuminated with a white light source and the same objective, used for the trapping, collects the white light image from the trapped particles, which is passed through the dichroic mirror, and is then focussed down to an image on the camera connected to a monitor for viewing. As previously mentioned the optical tweezer has taken many forms but this is the basic arrangement that underpins their operation.

---

---

## 4.4 Applications of Optical Traps in Biology

Optical trapping has found widespread application in the biomedical sciences as they offer non-invasive and precise micromanipulation of particles in closed chambers that form sterile environments.

The first applications of optical traps in biology were in the optical manipulation of bacteria and viruses by Ashkin [6] where they were able to trap and observe the reproduction cycle of *E. coli* bacteria; they also demonstrated how the shape of the cell is important in the trapping dynamics. Much of the initial work done with optical tweezers revolved around cells. However as the field progressed, work was performed on smaller subcellular structures manipulating organelles inside cells; some important early work was performed on chromosomes inside living cells to investigate the cell division process [16]. As the technique has advanced, much focus has been directed towards the small scale molecular motors operating in cells, and some of the most fascinating research has concentrated on measuring the forces exerted by and the behaviour of single molecule motor proteins in cells [17]. As well as the very small, the single beam optical tweezer is involved in some exciting work with cells such as optically guided neuron growth [18]. Furthermore advanced trapping geometries have led to new techniques such as optical fractionation where a pattern of optical traps can be used to sort different sized particles and types of cells [19]. Optical tweezers can also be used to enhance existing techniques such as Raman spectroscopy to create the new technique of Raman tweezers microscopy [20]. It is difficult to cover all the applications that optical tweezers has become involved in as they are so numerous and this section is only designed as a very brief guide; however a dedicated review of the subject can be found in reference 21.

---

## 4.5 Dual Beam Optical Traps

Dual beam traps [4], as the title suggests, utilise two counter propagating beams to trap and manipulate particles. Although often regarded as a step in the progress towards the single beam trap, dual beam traps have enjoyed a recent resurgence of interest, especially in the area of cell manipulation. The single beam optical tweezer is an extremely useful tool but can struggle to manipulate large cells at low powers, increasing the power to try and create a more stable trap can lead to photo-damage; the alternative is the use of the dual beam trap. In this section we will consider the operation of the dual beam trap, in particular the fibre optical light force trap, and why it is particularly useful in the field of cell manipulation.

### 4.5.1 The Fibre Optical Light Force Trap

The free space dual beam trap described by Ashkin [4] is useful and has been used in recent studies on optical binding [22]; however the focus of the resurgence in interest has surrounded the fibre optical light force trap. The fibre optical trap was demonstrated in 1993 by Constable *et al* [23], in this technique two optical fibres are used to deliver light to the sample forming a three dimensional optical trap for small dielectric particles by placing the two fibres opposite each other creating two counter propagating light fields. A schematic of the trapping arrangement can be seen in figure 4(j). The attractiveness of this technique lies in its simplicity to implement; very little optics are required, only those to couple light into the fibres are necessary and the use of fibre pigtailed laser diodes can negate the use of optics completely. A commercial microscope is suitable for viewing the fibres and samples; the fact the trapping is decoupled from the microscope means that greater viewing and manipulation is possible. As the fibres can be widely separated,  $\sim 100\text{-}200\mu\text{m}$ , and

still maintain stable trapping other probes can be easily introduced, such as a Raman or fluorescence probes. Furthermore the fact that the fibres can be so widely separated means the trapping volume can be up to  $\sim 5$  orders of magnitude greater than that of the single beam trap. The use of fibres to deliver the light also means that there are no constraints on laser beam quality as the fibres will spatially clean the mode and output a Gaussian profile of laser light.

The fibre optical light force trap provides a simple implementation of a dual beam trap that opens up the possibility of stably trapping ‘large’ objects with relatively low power densities.

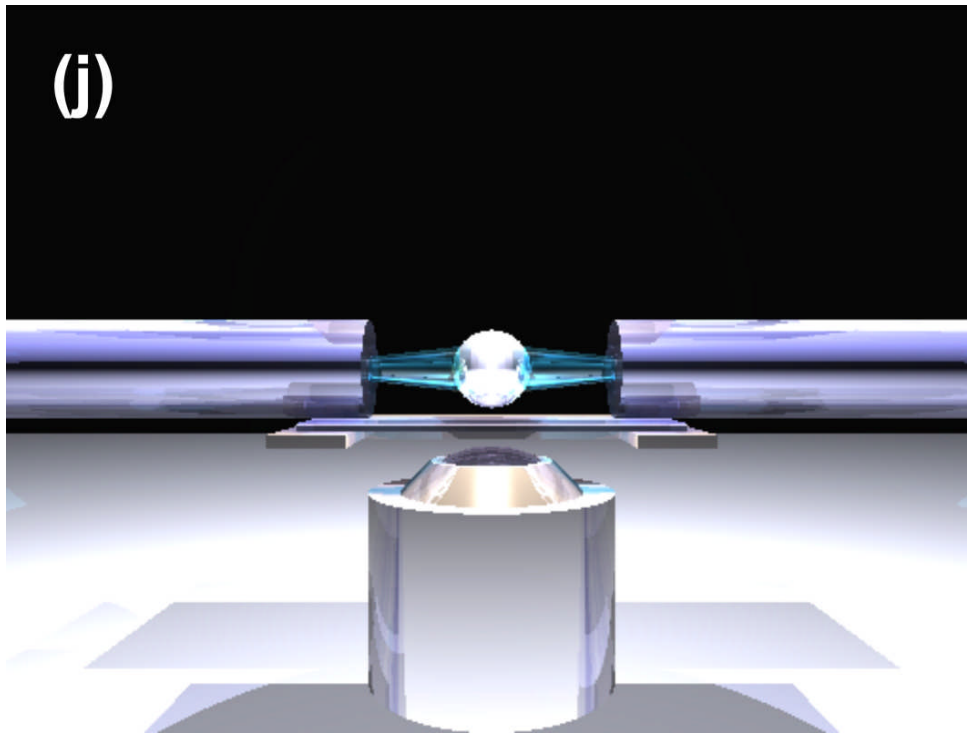


Figure 4(j). Schematic of the operation of a dual beam fibre trap.

#### 4.5.2 Operation and Theory of the Fibre Trap.

In considering the operation of the fibre optical light force trap we must first consider the output of the light from the fibre; in this discussion we will assume that singlemode fibre is used to form the trap. The output of singlemode fibre has a

---

Gaussian profile, due to the nature of the guided mode, thus no beam shaping or beam alteration is required, however unlike the single beam trap the fibre outputs a weakly diverging beam. A schematic of the Gaussian beam divergence can be seen in Figure 4(k). Although this beam will induce a weak gradient force, in a direction towards the fibre, the divergent nature of the beam means the scattering forces dominate and push the particles away from the fibre. Despite the weakly diverging beam, the Gaussian profile still means there is a transverse gradient drawing particles in towards the beam. Although as the beam propagates the Gaussian profile will spread and the gradient will become less aggressive and will result in less effective transverse trapping, as shown in Figure 4(k). If we were to observe a single fibre placed in a suspension of particles we would observe the particles being transversely drawn into the propagating light beam and being accelerated along the axial beam propagation path. If two fibres are set opposing each other, the particles will feel opposing scattering forces from each fibre, thus if the optical power from each fibre is identical, the particles will come to rest at a point exactly between the two fibres. Therefore the scattering force from each fibre accounts for the axial stability with the transverse gradient force accounting for the transverse stability of the particle in the trap; a schematic of the forces acting on the particle in a dual beam fibre trap can be seen in Figure 4(l). It should be noted that the particles can be translated between the two fibres easily by adjusting the relative powers in each fibre and thus creating many stable trapping points between the fibres. A final interesting point about the operation of the fibre trap lies in the small axial gradient force induced by the weakly diverging beam. The fibre trap is mostly employed in trapping large Mie particles thus if we think about the ray optics approach, the Mie particle will focus slightly the diverging beam, thus by considering figure 4(l) we can observe there will be a small backwards

---

force induced. In a dual beam trap this will result in a small axial stretching force. For rigid particles, such as silica spheres, this will have no effect but for soft dielectric objects such as cells this will result in a visible stretching. In fact work was published using this effect to test the elasticity of cells detecting the greater elasticity in cells often associated with the onset of neoplasia and using it as a diagnostic technique to screen for cancer [24].

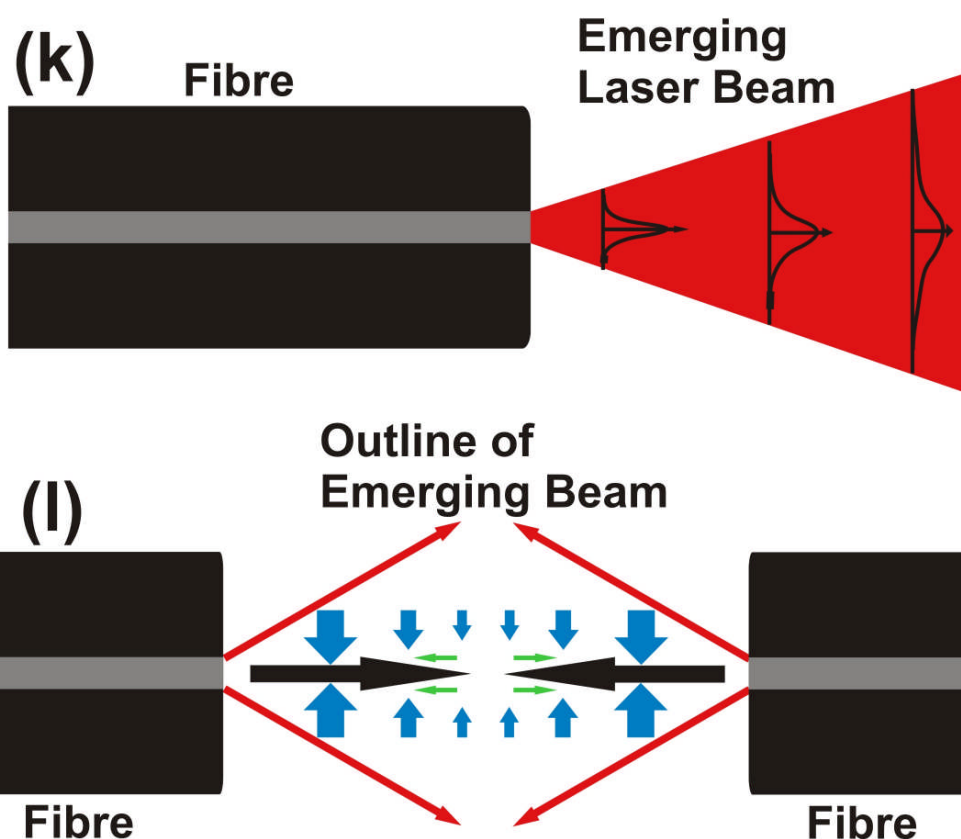


Figure 4(k&l). Figure 4(k) shows a schematic of the effect of the weak beam divergence on the Gaussian beam profile resulting in weaker transverse trapping the further the particle is from the fibre face. Figure 4(l) indicates the forces, and their relative magnitudes, operating in the fibre trap. The red arrows show an emphasised outline of the beam divergence, the black arrows refer to the direction and magnitude of the scattering force, the blue arrows refer to the direction and magnitude of the transverse gradient force and the green arrows refer to the direction and magnitude of the axial gradient force.

As with the single beam trap the fibre optical trap can be described in a more quantitative manner. The transverse gradient force operates on the same principles as that of the single beam trap already discussed thus we will concentrate our attention

on the axial scattering forces. We consider a situation where we have a fibre trap, as shown in figure 4(1), in which care has been taken to avoid interference effects thus the forces involved are merely the sum of the two light fields calculated individually. If each fibre carries some power, and we represent the output beam with a Gaussian profile, then the intensity of the light at the fibre face is given by:

$$I_0 = \frac{2P}{(\pi\omega_0^2)} \quad (4.9)$$

Where:  $I_0$  = Intensity at the fibre face  
 $P$  = Power carried in the fibre  
 $\omega_0$  = Gaussian beam waist

If we then think about the light scattering from a particle, the scattering force imparted to a particle of radius  $r$ , by the light field, is given by:

$$F_{scat} = \frac{(\pi r^2)IQ_{PR}}{c} \quad (4.10)$$

Where:  $F_{scat}$  = Scattering force on the particle  
 $r$  = radius of particle  
 $c$  = speed of light  
 $Q_{PR}$  = Radiation pressure coefficient

The radiation pressure coefficient  $Q_{PR}$  is defined as the ratio of the momentum acquired by the target to the electromagnetic momentum contained in the lightfield before the scattering event [25]. Considering now two counter propagating beams, one travelling in direction  $+z$  and the other in the direction  $-z$ , we define a position  $z = 0$  which is the centre point between the two fibres. We must also introduce now an approximation into this analysis such that we consider the intensity and phase of the trapping beams to be constant over the area of the sphere. We can then express the total scattering force as:

$$F_{total} = \frac{\alpha P_{+z} Q_{PR,+z} / \omega_{0,+z}^2}{1 + d_{+z}^{-2} (S/2 + z)^2} - \frac{\alpha P_{-z} Q_{PR,-z} / \omega_{0,-z}^2}{1 + d_{-z}^{-2} (S/2 - z)^2} \quad (4.11)$$

$$\text{Where: } \alpha = \frac{2r^2}{c}$$

$$d^I = \frac{\lambda}{(\pi\omega_0^2)}$$

$S$  = the separation of the two fibre faces

$\lambda$  = the wavelength of the trapping laser

An interesting aspect of this equation is that when the light fields are balanced the particle will be at rest somewhere between the fibres and is thus stably axially trapped. Any perturbation of the particles position will then result in a net restoring force that can be described by Hooke's spring law  $F = -k\epsilon$  where  $\epsilon$  is the displacement  $z - z_{eq}$ , where  $z_{eq}$  is the equilibrium position, and  $k$  is derived from equation 4.11 and is given by

$$k = 16\pi^2 a S \left[ \frac{P_{-z} Q_{PR,-z} \omega_{0,-z}^2}{\lambda_{-z}^2 (S^2 + 4d_{-z}^2)^2} + \frac{P_{+z} Q_{PR,+z} \omega_{0,+z}^2}{\lambda_{+z}^2 (S^2 + 4d_{+z}^2)^2} \right] \quad (4.12)$$

There is, as we have seen, also a backwards axial force caused by the weak gradient of the emitted light, this is described by the axial gradient force discussed in the single beam tweezer. A detailed analysis of the force in fibre optical traps can be found in reference 18.

### 4.5.3 Applications of the Fibre Optical Trap

The fibre optical trap has only recently emerged as a tool for manipulating biological matter; however it is finding applications in situations where the single beam trap would normally struggle. One of the most interesting applications has involved the use of the stretching phenomena in the trap as a cancer diagnostic, based on a morphology change in the cell that means it becomes more flexible with the onset of neoplasia [24], the fibre trap has also been used to study cell properties and

---

their dynamics in the trap [26 & 27]. As science turns its attention to the study of large cells in isolation the fibre trap is likely to play an evermore important role in the field of biomedical sciences. The fibre optical trap could potentially be used to hold and trap stably large cells such that we could introduce a Raman probe to study the trapped cells allowing us to study large trapped cells with Raman spectroscopy whilst retaining all the original advantages that single beam tweezers bring to the study of smaller particles.

## 4.6 Conclusions

Optical traps have found widespread use in the biomedical sciences and even opened up new fields of study due to their compatibility with microscopy, ease of implementation and ability to manipulate cells with little chance of photodamage. The applications have become numerous and widespread and the technique is constantly being developed and employed in new areas thus the future for optical trapping is bright and exciting. Furthermore the fibre optical light force trap could become important in the study of large cells that the single beam tweezers struggles to manipulate.

## 4.7 References

- [1] Ashkin A, Dziedzic JM, Bjorkholm JE and Chu S. **Observation of a single-beam gradient force optical trap for dielectric particles.** Optics Letters 1986; **11**: 288-290
- [2] Maxwell JC. **Treatise on electricity and Magnetism.** 1873; Oxford UK: Clarendon Press
- [3] Lebedev PN. **Experimental Examination of Light Pressure.** Ann Der

---

Physik 1901: **6**: 433

- [4] Ashkin A. **Acceleration and trapping of particles by Radiation Pressure.**  
Physical Review Letters 1970; **24**: 156-159
- [5] Ashkin A and Dziedzic JM. **Optical trapping and manipulation of viruses and bacteria.** Science 1987; **235**: 1517-1520
- [6] Ashkin A, Dziedzic JM and Yamane T. **Optical Trapping and manipulation of single cells using infrared laser beams.** Nature 1987; **330**: 768-771
- [7] Ashkin A. **Forces of a single-beam gradient laser trap on a dielectric sphere in the ray optics regime.** Biophysical Journal 1992; **61**: 569-582
- [8] Pelton M, Liu M, Kim HY, Smith G, Guyot-Sionnest P and Scherer NF. **Optical Trapping and alignment of single gold nanorods using plasmon resonances.**  
Optics Letters 2006; **31**: 2075-2077
- [9] Hansen PM, Bhatia VK, Harrit N and Oddershede L. **Expanding the Optical Trapping Range of Gold Nanoparticles.** Nano Letters 2005; **5**: 1937-1942
- [10] Neuman KC and Block SM. **Optical Trapping.** Review of Scientific Instruments 2004; **75**: 2787-2809
- [11] Mie G. **Beitrage zur Optik truber Meiden, Speziell Kolloideler Metalosurgen.** Ann der Physik 1908; **25**: 377-452
- [12] Gouesbet G, Maheu B and Gehan G. **Light scattering from a sphere arbitrarily located in a Gaussian beam, using a Bromwich formulation.**  
Journal of the Optical Society of America A 1988; **5**: 1427-1443
- [13] Neuman KC, Chadd EH, Liou GF, Bergman K and Block SM. **Characterisation of Photodamage to Escherichia Coli in Optical Taps.** Biophysical Journal 1999; **77**: 2856-2863
- [14] Koenig K, Liang H, Berns MW and Tromberg BJ. **Cell damage in near**
-

---

**infrared multimode optical traps as a result of multiphoton absorption.**

Optics Letters 1996; **21**: 1090-1092

- [15] Liu Y, Sonek GJ, Berns MW and Tromberg BJ. **Physiological monitoring of optically trapped cells: assessing the effects of confinement by 1064nm laser tweezers during microfluourometry.** Biophysical Journal 1996; **71**: 2158-2167
- [16] Berns MW, Wright WH, Tromberg BJ, Profeta GA and Andrews JJ. **Use of a laser-induced optical force trap to study chromosome movement on the mitotic spindle.** Proceedings National Academy of Sciences 1989; **86**: 4539-4543
- [17] Asbury CL, Fehr AN and Block AM. **Kinesin moves by an Asymmetric Hand –Over-Hand Mechanism.** Science 2002; **302**: 2130-2134
- [18] Stevenson DJ, Lake TK, Agate B, Garces-Chavez V, Dholakia K and Gunn-Moore F. **Optically Guided Neuronal growth at near infrared wavelengths.** Optics Express 2006; **14**: 9786-9793
- [19] MacDonald MP, Spalding GC and Dholakia K. **Microfluidic Sorting in an Optical Lattice.** Nature 2003; **426**: 421
- [20] Xie CA, Dinno MA and Li TQ. **Near-infrared Raman Spectroscopy of single optically trapped biological cells.** Optics Letters 2002; **27**: 249-251
- [21] Kuyper CL and Chiu DT. **Optical Trapping: A versatile technique for Biomanipulation.** Applied Spectroscopy 2002; **56**: 300A-312A
- [22] McGloin D, Carruthers AE, Dholakia K and Wright EM. **Optically bound microscopic particles in one dimension.** Physical Review E 2004; **69**: 021403
- [23] Constable A, Kim J, Mervis J, Zarinetchi F and Prentiss M. **Demonstartion of a fibre-optical light-force trap.** Optics Letters 1993; **18**: 1867-1869
- [24] Guck J, Ananthakrishnan R, Moon TJ, Cunningham CC and Kas J. **Optical**
-

---

**deformability of soft biological dielectrics.** Physical Review Letters 2000; **84**:  
5451-5454

[25] Van De Hulst HC. **Light Scattering by small particles.** 1981; Dover

Publications: pp. 14

[26] Wei MT, Yang KT, Karmenyan A and Chiou A. **Three-Dimensional optical force field on a Chinese Hamster Ovary cell in a fibre-optical dual-beam trap.** Optics Express 2006; **14**: 3056-3064

[27] Metzger NK, Jess PRT, Paterson L, Wright EM and Dholakia K. **Optical Binding of Chinese Hamster Ovary cells.** Proceedings of SPIE 2005; **5930**: 0M-1

## 4.8 Bibliography

Paterson L. **Novel Techniques in Optical Micromanipulation.** Ph.D thesis 2003;  
University of St. Andrews: 6-38

Brown BA and Brown PR. **Optical Tweezers: Theory and current applications.**  
American Laboratory 2001; **Nov**: 13-20

Dholakia K and Spalding GC. **Introduction to Optical Tweezers and Optical Micromanipulation.** 2005 Spie Educational Services; **SC655**

McGloin D. **Optical Tweezers: 20 years on.** Philosophical Transactions of the Royal Society A 2006; **364**: 3521-3527

---

# 5. Raman Tweezers Microspectroscopy: An Introduction and Research Perspective.

---

*Raman Tweezers Microspectroscopy has, in recent times, attracted much attention as a non invasive tool for the interrogation of biomedical samples in particular single cells. This discussion introduces the technique, which is a combination of optical trapping and traditional Raman spectroscopy, and goes on to give a review of the key publications in the development of the field and in its application to the biomedical sciences.*

---

## 5.1 Introduction

With ever increasing interest in the study of single biological cells and their behaviour, it is important to find a tool that can isolate and probe the biochemical behaviour of individual cells. Fluorescence spectroscopy and infra-red absorption spectroscopy are potential techniques that could probe the biochemical nature of single cells. Fluorescence spectroscopy however often depends upon chemical markers therefore not allowing many biochemicals to be studied simultaneously. Natural cellular fluorescence can be studied but the signal is the amalgamation of many biochemicals and it is difficult to attribute subtle changes in fluorescence background to individual molecules or processes. Infrared spectroscopy, unlike

---

---

fluorescence spectroscopy, is molecule specific and could potentially monitor the behaviour of several single biomolecules simultaneously. However infrared spectroscopy requires advanced sample preparation and is difficult to use in water due to high absorption, thus it is difficult to study cellular samples in solution. Furthermore the experimental arrangement for infrared microspectroscopy can potentially be very involved and difficult to optically align. Emerging from these potential techniques, for cellular study, is Raman spectroscopy. This technique is molecule specific and easily combined with microscopy thus allowing the relatively easy study of many biomolecules and processes within cells in solution. However, Raman scattering is a weak process and thus takes a long time to collect a signal which can be easily masked by fluorescence. In order to improve this situation enhancement techniques have been employed based on metallic surfaces, Surface enhanced Raman spectroscopy (SERS), and by matching the exciting laser source to an electronic transition in the molecule of interest to 'drive' the Raman scattering from that bond, this enhancement method is known as Resonance Raman spectroscopy. While extremely successful, SERS requires a metallic surface to be in close proximity to the substance of interest which in the case of cellular studies requires the inserting of gold particles into the cell which then aggregate and form the required metal surface. This method does give a strong enhancement but only close to the metallic cluster thus the whole cell cannot be probed simultaneously. Resonance Raman spectroscopy also provides a large signal enhancement but only for a few molecular bonds that have electronic transitions matching the input laser frequency. Thus we need some technique that can improve the signal to noise ratio of traditional Raman spectroscopy to allow us to study the behaviour of entire cells simultaneously. By combining Raman spectroscopy with optical trapping we have a method that can

---

---

trap a cell of interest in the Raman probe beam whilst isolating it from any surrounding sources of fluorescence interference. This combination of Raman spectroscopy and optical trapping provides an improvement in signal to noise ratios and makes more feasible the effective study and monitoring of single biological cells.

## 5.2 Raman Tweezers Microspectroscopy

Raman tweezers microspectroscopy is the combination of traditional Raman spectroscopy, optical tweezers and optical microscopy to enable practical, precise and highly informative interrogation of micron sized samples. The techniques are very compatible as the microscope objective, and viewing optics, employed for optical trapping are highly suitable for the delivery of a laser probe to induce Raman scattering in the sample. In fact a separate beam is typically not required; rather a carefully chosen trapping beam may be used to excite the Raman scattering process as well as trapping the object under study. The Raman scatter can then be collected by the same objective, used for trapping and excitation, and passed to a spectrograph, for analysis, in what would be traditionally known as the  $180^\circ$  geometry. Furthermore this combination of techniques requires little alteration to a standard optical tweezers setup and requires only one specialist optical element, the holographic notch filter. This is a special filter that operates on a holographic grating recorded in an optically clear gelatine medium. The grating however provides very strong optical blocking of a narrow wavelength band of only a few hundred wavenumbers. This allows the blocking of the strong Rayleigh scatter from the laser whilst permitting the Raman scatter to pass through unabated.

With interest increasing in the study of single cells and sub-cellular components Raman spectroscopy provides a very attractive prospect, especially as

---

---

one single spectrum can potentially reveal their chemical composition. However the relatively weak nature of the Raman scattering process means that lengthy acquisition times are required that can be on the order of tens of seconds even up to minutes. When studying epithelial cells, whose natural instinct is to grow on surfaces in the lab, the substrate on which they are growing, normally glass, can often be a source of laser induced auto fluorescence that drowns out the weak Raman signal. The natural state of some cell types is in solution, and not in tissue layers, such as red and white blood cells and types of stem cell. Problems can occur when studying these samples as the cell under study can often drift out of the probe beam before an acceptable Raman signal can be acquired. This leads to further problems if the same cell is to be probed repeatedly as Brownian motion can cause the cell to migrate away and it may be impossible to relocate. Often studies on single cells are extremely difficult and studies on cells attached to surfaces often require specialised and expensive surfaces, such as quartz, to avoid the fluorescence. Short excitation wavelengths are another option to avoid fluorescence but this option can be extremely damaging to cells. The incorporation of optical tweezers into Raman spectroscopy systems has circumvented a great many of these problems. For cells in suspension optical tweezers can be used to hold the cell in the focal point during the spectral acquisition and can furthermore be used to store the cell for long periods of time for further interrogation. Problems with interfering surfaces can be reduced by using the optical tweezers, normally in conjunction with a confocal arrangement [1], to isolate the cell under study away from the surface and record spectra with minimum fluorescence interference. In practice however, using glass and infrared wavelengths, a considerable fluorescence background is still recorded but the Raman signal is distinguishable; it is then still useful to use quartz coverslips to keep the employment of background subtractions

---

---

and extra data filtering to a minimum. Furthermore Raman tweezers is also extremely useful in the study of cells, not normally found in suspension, under certain conditions; firstly these cells can be put into suspension with the use of trypsin-ethylenediaminetetraacetic acid (trypsin-EDTA), an enzyme that breaks the tethers binding the cells to the surface and each other, for study. Secondly and perhaps one of the most important examples is in the study of medical samples where the material comes in single cell format or in small clumps of cells. The prime example of this is cervical smears, although there are other examples such as lung tissue extracted via a bronchoscope. These materials are normally fixed, thus by default, will remain in the single cell format that Raman tweezers can be used to interrogate.

The addition of optical tweezers to traditional Raman spectroscopy has opened up a new range of samples that can be readily studied as the optical tweezers allows the holding and storing of samples in the Raman probe beam whilst simultaneously isolating the sample from interfering surfaces. The techniques are ideal for combination as the highly focussed beam spot needed for optical trapping also provides the required power to obtain a precise Raman signal from the sample under study.

### **5.3 Raman Tweezers Microspectroscopy: A Research Review**

The field of Raman tweezers is a relatively new one and has built upon a large body of work in traditional Raman spectroscopy; however it has expanded rapidly as researchers recognise its potential benefits and articles have appeared in a broad variety of journals representing the technique's employment in many fields. This research review will concentrate on the origin of Raman tweezers and its subsequent employment in the interrogation of single cells.

---

The origins of Raman Tweezers lie in the desire to study the chemical dynamics of small micron sized particles isolated from their environment. R. Thurn and co-workers combined the optical levitation trap with Raman spectroscopy to study small dielectric micron sized particles [2], furthermore they also noticed enhancements in the spectra as a result of whispering gallery modes in the particle enhancing certain wavelengths [3], this enabled accurate sizing of the particles and formed the basis of what is now more commonly known as Cavity Enhanced Raman Spectroscopy (CERS) [4]. The publication of Ashkin's seminal paper on the single beam gradient trap, or optical tweezers, paved the way for the incorporation of the optical trap into Raman spectroscopy, in 1994 Lankers *et al* published work that demonstrated the optical trapping, and simultaneous recording of Raman spectra, from micro droplets in emulsion [5]. This group used the new Raman Tweezers setup in many chemical applications including the study of gas bubble composition and interfaces [6]. Most of this work was carried out with the use of Argon ion lasers emitting light in the short wavelength region of the visible spectrum. This causes a large fluorescence emission from the sample and in 1998 Ajito [7] demonstrated a Raman tweezers system based around a near infrared laser source, for the study of single toluene micro droplets in water, that virtually eliminated interference from fluorescence. This paper is also notable for probably the first demonstration of a system based around holographic notch filters, which allows the simplification of the optical arrangement. This system allowed the effective study of advanced chemical events [8] and was used in the first study of organic micro and nano particles [9 & 10]. The same research group made the first use of Raman tweezers to study biological samples in 2002 by trapping and obtaining Raman spectra from synaptosomes obtained from rats and dispersed in a phosphate buffer [11]. The

---

---

potential of this technique in the examination and understanding of biological systems was quickly recognised and in 2002 Xie *et al* demonstrated the use of Raman tweezers in the examination of human red blood cells and yeast cells [12]. These early papers demonstrated the potential of Raman tweezers to gain information from biological systems and the subsequent flurry of publications dealt with employment of Raman Tweezers to study biological systems and improvements in the technique to gain better and more sensitive information.

In 2003 Cherney *et al* published work on the analysis of lipid vesicles detecting their structure, including changes within the structure with temperature, and their individual contents [13]. Also in 2003 Xie *et al* presented a study of the denaturising process in E coli and Enterobacter aerogenes bacteria [14] and a work detailing improvements in the Raman tweezers analysis by using a shifted excitation technique that can reduce artefacts, in the spectra, introduced by fluorescence [15].

In 2004 the technique of Raman tweezers was applied further in the biomedical sciences, Chan *et al* demonstrated the use of the technique to identify single bacterial spores suggesting the possibility of including Raman tweezers in a flow cytometry type scheme [16], the ability of the technique to discriminate between, and identify the ratio of individual chemicals present, in single microbial cells was also demonstrated by Huang *et al* [17]. Ajito *et al* demonstrated the use of Raman tweezers, in perhaps one of the first examples of the technique being employed to understand a biochemical system, to study the behaviour of neurons and the release of neurochemicals when stimulated [18]. The use of Raman tweezers in the investigation of lipid vesicles was reported by Sanderson & Ward and Cherney *et al* where the technique was able to probe the chemical composition and contents of the vesicles as well as measure the structural changes in the lipids, imposed by optical forces from

---

---

the tweezer, respectively [19 & 20]. Xie *et al* demonstrated the first use of the technique to trap and probe organelles inside living cells, making use of the tweezers predisposition to draw in high index particles in whatever medium, the response of cells to temperature was also described in this report [21]. Improvements to the technique, published in 2004, included the investigation of various wavelengths, in the probing of red blood cells, to take advantage of Resonance Raman effects [22 & 23]. This paper also introduced the use of separate lasers for trapping and for the resonance Raman probe to allow the cell to be trapped with a infrared wavelength to minimise photodamage whilst the visible lasers were used to excite the resonance Raman effect. The use of separate lasers, for trapping and Raman excitation, was also investigated by Creely *et al* and Gressner *et al*; in the first instance the second wavelength was used for maximising the trapping position for Raman and storing a yeast cell for up to two hours without damage [24], the second article also uses the second beam to maximise trapping position of the particle for Raman study and for the trapping of small metal coated particles for use as a surface enhanced [25] Raman spectroscopic probe [26].

2005 also produced an exciting range of publications describing system improvements and biomedical applications for Raman tweezers. Xie *et al* used Raman tweezers to identify bacteria types in solution using advanced statistical processing to aid the Raman interpretation [27]. Singh *et al* used Raman tweezers to measure the biochemical response of yeast cells put under environmental stress demonstrating how Raman tweezers can be used to monitor the behaviour of entire biochemical systems [28]. Deng *et al*, in a similar fashion described the response of red blood cells when exposed to alcohol [29]. Also studying red blood cells were Ramser *et al* who published a report detailing a microfluidic flow system where red blood cells could be

---

held in a Raman tweezers probe beam and various solutions could be flowed passed and the cells biochemical response measured [30]. Mannie *et al* published a work detailing the Raman spectroscopic analysis of the activation of human T cells, a hot topic in current biology, where they measured the biochemical changes occurring in the different phases of T-cell activation [31]. Raman tweezers was employed, for probably the first time, in a rudimentary optical sorting experiment where a mixed population of live and dead yeast were tested and moved to a relevant chamber dependant upon the Raman ‘diagnosis’ [32]. Probably the most significant improvement to the Raman tweezers technique in 2005 came from Creely *et al* and through the combination of Raman with an advanced form of holographic tweezing to hold large cells for mapping [33]. The single beam gradient trap can often struggle to manipulate large cells thus the holographic optical tweezers creates several trap sites around the cell to hold it more effectively, furthermore the traps are dynamic and can be moved around allowing them to scan the cell over a Raman probe beam. The only disadvantage to this technique is the complex optics required and the weak nature of the optical trapping with the multiple trap sites. This paper demonstrated a real need to expand the Raman tweezers capability to allow the study of large cellular samples and as we shall see later in this thesis the original dual beam trap may provide a solution to this problem. Finally in 2005 Hamden *et al* published a work describing the identification of derived cells infected with Kaposi’s sarcoma associated herpes-virus that is known to cause cancer, the ability to diagnose cancer in single cells has long been thought as one of the key applications in this field [34].

In 2006, following the publication of Hamden *et al*, two more papers emerged demonstrating the ability of Raman tweezers to diagnose cancer in single cells; the first publication, by Chan *et al*, discriminated between cells from normal and

---

---

neoplastic Haematopoietic cell lines [35], secondly Chen *et al* discriminated between healthy and cancerous cells obtained from patient biopsy's who were diagnosed with colorectal cancer [36]. These two papers, along with that of Hamden *et al*, are important demonstrations of the capability of Raman tweezers in a diagnostic role. Other notable publications in 2006 were involved in the monitoring of the yeast cell cycle [37] by Singh *et al* and cell growth dynamics in an optical trap measured with Raman Tweezers by Volpe *et al* [38]. The paper on cell growth dynamics was an important publication as it demonstrated how the movement of cells in single beam traps can cause variations in the acquired Raman spectrum, this only goes to demonstrate further the importance of stably trapping cells for Raman examination. Finally in 2006 a paper was published by Ojeda *et al* [39] demonstrating the possibility of analysing and identifying chromosomes.

This brief review deals only with biomedical samples studied with Raman tweezers, there is also a large body of work carried out, and continues to be carried out with more traditional systems. It would be an oversight not to consider this work as many valuable publications have arisen from the field; substantive reviews on traditional Raman microspectroscopy can be found in references 40 & 41, which covers single cell, biopsy and fibre optical probe investigations. In subsequent experimental chapters this work shall be considered along side that done in Raman tweezers where appropriate.

Raman tweezers microspectroscopy is attracting increasing attention as a technique for investigating biological samples as well as in a diagnostic capacity with medical samples. More and more researchers are making use of this technique, reflected in the increasing number of publications across a wide variety of journals.

---

## 5.4 Conclusions

Since the initial demonstration of Raman tweezers microspectroscopy applied to cells by Xie *et al* in 2002 a flurry of publications has followed reflecting the continued and increasing interest in this technique. The experiments presented in this thesis aim to both extend the abilities of the Raman tweezers technique and exploit its powerful analysis abilities to study biological systems. The initial experiment studies the behaviour of the Raman system and aims to demonstrate how a simple technique in optical trapping can be used to obtain rapid representative spectra of populations of cells. The following experiment aims to build upon the cancer studies of Chan *et al* [35] and Chen *et al* [36] only in this experiment Raman tweezers spectroscopy is applied to study the progression of cervical neoplasia. In the penultimate study an advanced Raman tweezers experimental geometry is presented to further the work of Creely *et al* [33] improving the trapping and flexible analysis of large cells with the use of a fibre optical light force trap rather than a holographic trapping system. In the publications presented many of the authors demonstrate the potential of Raman tweezers spectroscopy to monitor biological systems and perform clinical diagnostics however the main drawback preventing the widespread use of Raman spectroscopy remains the long signal integration times and the final study in this thesis aims to tackle this important problem.

Raman tweezers microspectroscopy is becoming a popular and powerful technique and this thesis aims to build upon published works to address some of the important issues facing Raman tweezers and demonstrate further its ability to study complex biological systems.

---

## 5.5 References

- [1] Pawley JB. **Handbook of Biological Confocal Microscopy**. 1995; Springer  
Science and media: pp. 19-36
- [2] Thurn R and Kiefer W. **Raman-Microsampling Technique Applying Optical Levitation by Radiation Pressure**. Applied Spectroscopy 1984; **38**: 78-83
- [3] Thurn R and Kiefer W. **Observations of structural resonances in the Raman spectra of optically levitated dielectric microspheres**. Journal of Raman Spectroscopy 1984; **15**: 411-413
- [4] Symes R, Sayer RM and Reid JP. **Cavity enhanced droplet spectroscopy: Principles, perspectives and prospects**. Physical Chemistry Chemical Physics 2004; **6**: 474-487
- [5] Lankers M, Popp J and Kiefer W. **Raman and Fluorescence Spectra of Single Optically Trapped Microdroplets in Emulsions**. Applied Spectroscopy 1994; **48**: 1166-1168
- [6] Lankers M, Popp J, Rossling G and Kiefer W. **Raman Investigations on laser-trapped gas bubbles**. Chemical Physics Letters 1997; **277**: 331-334
- [7] Ajito K. **Combined Near-Infrared Raman Microprobe and Laser Trapping System: Application to the Analysis of a Single Organic Microdroplet in Water**. Applied Spectroscopy 1998; **52**: 339-342
- [8] Ajito K, Morita M and Torimitsu K. **Investigation of the Molecular Extraction Process in Single Subpicolitre Droplets Using a Near-Infrared Laser Raman Trapping System**. Analytical Chemistry 2000; **72**: 4721-4725
- [9] Ajito K and Torimitsu K. **Near-infrared Raman spectroscopy of single particles**. Trends in Analytical Chemistry 2001; **20**: 255-262
- [10] Ajito K and Torimitsu K. **Single nanoparticle trapping using a Raman**
-

- 
- tweezers microscope.** Applied Spectroscopy 2001; **56**: 541-544
- [11] Ajito K and Torimitsu K. **Laser trapping and Raman spectroscopy of single cellular organelles in the nanometre range.** Lab on a Chip 2002; **2**: 11-14
- [12] Xie C, Dinno M and Li YQ. **Near-infrared Raman spectroscopy of single optically trapped biological cells.** Optics Letters 2002; **27**: 249-251
- [13] Cherney DP, Conboy JC and Harris JM. **Optical Trapping Raman Microscopy Detection of Single Unilamellar Lipid Vesicles.** Analytical Chemistry 2003; **75**: 6621-6628
- [14] Xie C, Li YQ, Tang W and Newton RJ. **Study of dynamical processes of heat denaturation in optically trapped single microorganisms by near-infrared Raman spectroscopy.** Journal of Applied Physics 2003; **94**: 6138-6142
- [15] Xie C and Li YQ. **Confocal micro-Raman spectroscopy of single biological cells using optical trapping and shifted excitation difference techniques.** Journal of Applied Physics 2003; **93**: 2982-2986
- [16] Chan JW, Esposito AP, Talley CE, Hollars CW, Lane SM and Huser T. **Reagentless Identification of Single Bacterial Spores in Aqueous Solution by Confocal Laser Tweezers Raman Spectroscopy.** Analytical Chemistry 2004; **76**: 599-603
- [17] Huang WE and Griffiths RI. **Raman Microscopic Analysis of Single Microbial Cells.** Analytical Chemistry 2004; **76**: 4452-4458
- [18] Ajito K, Han C and Torimitsu K. **Detection of Glutamate in Optically Trapped Single Nerve Terminals by Raman Spectroscopy.** Analytical Chemistry 2004; **76**: 2506-2510
- [19] Sanderson JM and Ward D. **Analysis of liposomal membrane composition using Raman Tweezers.** Chemical Communications 2004; **10**: 1120-1121
-

- 
- [20] Cherney DP, Bridges TE and Harris JM. **Optical Trapping of Unilamellar Phospholipid Vesicles: Investigation of the Effect of Optical Forces on the Lipid Membrane shape by Confocal-Raman Microscopy.** Analytical Chemistry 2004; **76**: 4920-4928
- [21] Xie C, Goodman C, Dinno M and Li YQ. **Real-time Raman spectroscopy of optically trapped living cells and organelles.** Optics Express 2004; **12**:6208-6214
- [22] Smith E and Dent G. **Modern Raman Spectroscopy.** 2005; Wiley Publishing: pp. 93-112
- [23] Ramser K, Logg K, Goksor M, Enger J, Kall M and Hanstorp D. **Resonance Raman spectroscopy of optically trapped functional erythrocytes.** Journal of Biomedical Optics 2004; **9**: 593-600
- [24] Creely CM, Singh GP and Petrov D. **Dual wavelength optical tweezers for confocal Raman spectroscopy.** Optics Communications 2004; **245**: 465-470
- [25] Smith E and Dent G. **Modern Raman Spectroscopy.** 2005; Wiley Publishing: pp. 113-127
- [26] Gessner R, Winter C, Rosch P, Schmitt M, Petry R, Kiefer W, Lankers M and Popp J. **Identification of Biotic and Abiotic Particles by Using a Combination of Optical Tweezers and In Situ Raman Spectroscopy.** ChemPhysChem 2004; **5**: 1159-1170
- [27] Xie C, Mace J, Dinno MA, Li YQ, Tang W, Newton RJ and Gemperline PJ. **Identification of Single Bacterial Cells in Aqueous Solution Using Confocal Laser Tweezers Raman Spectroscopy.** Analytical Chemistry 2005; **77**: 4390-4397
- [28] Singh GP, Creely CM, Volpe G, Grotzsch H and Petrov D. **Real-Time Detection**
-

- 
- of Hyperosmotic Stress Response in Optically Trapped Single Yeast Cells Using Raman Microspectroscopy.** *Analytical Chemistry* 2005; **77**: 2564-2568
- [29] Deng JL, Wei Q, Zhang MH, Wang YZ and Li YQ. **Study of the effect of alcohol on single human red blood cells using near-infrared laser tweezers Raman spectroscopy.** *Journal of Raman Spectroscopy* 2005; **36**: 257-261
- [30] Ramser K, Enger J, Goksor M, Hanstorp D, Logg K and Kall M. **A microfluidic system enabling Raman measurements of the oxygenation cycle in optically trapped red blood cells.** *Lab on a Chip* 2005; **5**: 431-436
- [31] Mannie MD, McConnell TJ, Xie C and Li YQ. **Activation-dependant phases of T cells distinguished by use of optical tweezers and near infrared Raman spectroscopy.** *Journal of Immunological Methods* 2005; **297**: 53-60
- [32] Xie C, Chen D and Li YQ. **Raman sorting and identification of single living micro-organisms with optical tweezers.** *Optics Letters* 2005; **30**: 1800-1802
- [33] Creely CM, Volpe G, Singh GP and Petrov D. **Raman imaging of floating cells.** *Optics Express* 2005; **13**: 6105-6110
- [34] Hamden KE, Bryan BA, Ford PW, Xie C, Li YQ and Akula SM. **Spectroscopic analysis of Kaposi's sarcoma-associated herpesvirus infected cells by Raman tweezers.** *Journal of Virological Methods* 2005; **129**: 145-151
- [35] Chan JW, Taylor DS, Zwerdling T, Lane SM, Ihara K and Huser T. **Micro-Raman Spectroscopy Detects Individual Neoplastic and Normal Haematopoietic Cells.** *Biophysical Journal* 2006; **90**: 648-656
- [36] Chen K, Qin Y, Zheng F, Sun M and Shi D. **Diagnosis of colorectal cancer using Raman spectroscopy of laser-trapped single living epithelial cells.** *Optics Letters* 2006; **31**: 2015-2017
- [37] Singh GP, Volpe G, Creely CM, Grotsch H, Geli IM and Petrov D. **The lag**
-

---

**phase and G1 phase of a single yeast cell monitored by Raman**

**microspectroscopy.** Journal of Raman Spectroscopy 2006; **37**: 858-864

[38] Volpe G, Singh GP and Petrov D. **Dynamics of a growing cell in an optical trap.** Applied Physics Letters 2006; **88**: 231106-231108

[39] Ojeda JF, Xie C, Li YQ, Bertrand FE, Wiley J and McConnell TJ.

**Chromosomal analysis and identification based on optical tweezers and Raman spectroscopy.** Optics Express 2006; **14**: 5385-5393

[40] Notingher I and Hench LL. **Raman microspectroscopy: a non-invasive tool for studies of individual living cells *in vitro*.** Future Drugs 2006; **3**: 215-234

[41] Crow P, Stone N, Kendall CA, Persad RA and Wright MPJ. **Optical diagnostics in urology: current applications and future prospects.** British Journal of Urology International 2003; **92**: 400-407

## **5.6 Bibliography**

Singh GP. **Raman Microspectroscopy of Optically Trapped Cells.** 2006 PhD Thesis; Institut de Ciències Fotoniques: 14-18

---

# 6. The Construction and Evolution of the Raman Tweezers System

---

*The construction of a Raman Tweezers Spectroscopy system requires care and consideration in the choices of experimental apparatus and parameters to maximise the Raman signal collected and the tweezing capability of the system all whilst considering the implications of the final application of studying biological cells. In this discussion we consider the key parameters in designing the system and the methods and materials used to construct our initial setup. The alignment, calibration, testing and data processing will be covered and the discussion will finish with a look at how the system evolved throughout the research covered in this thesis.*

---

The combination of Raman spectroscopy and optical tweezers is in theory relatively straight forward requiring little alteration to the standard single beam optical tweezers. There is however some important questions we must ask ourselves such as what laser wavelength we require and how much optical power will be required?, What are the requirements of our optical system? And will we require any specialist optical elements? In this chapter we will address these questions and discuss the practical aspects of Raman tweezers spectroscopy.

## 6.1 Considerations in the Construction of a Raman Tweezers Experimental Setup

Raman micro-spectroscopy and optical trapping, as we have discussed, are ideal techniques for combination as the highly focussed spot used in optical trapping

---

---

is highly suitable for providing the excitation of the Raman scatter thus a single laser beam may be used for both. Although these techniques are suitable for combination there are some factors that we must consider carefully to maximise the instrument design:

- Trapping and excitation wavelength
- Microscope objectives used
- Possible confocal arrangements
- Introduction of the laser into the optical system and efficient collection optics

When thinking about the choices for these parameters we must keep in mind the application of the system, which is the probing and study of biological cells, as this will have a direct bearing on the informed choices we must make.

### **6.1.1 The choice of trapping and excitation wavelength**

We will begin by thinking about the choice of wavelength for the optical tweezers aspect of the experimental system. The cells investigated in this thesis can be thought of as Mie particles thus the optical trapping is described by the Ray optics approach and we are largely independent of wavelength in this respect. Our choice of wavelength is thus dominated by the response of cells at the available laser wavelengths. As we do not wish to damage the cells we are probing, in order to avoid changing the system we are studying, we must choose a wavelength where cells exhibit minimum photodamage. The wavelengths at which minimum cell damage occurs, as discussed in section 4.3, are 785nm, 830nm and 970nm in order of decreasing damage. Laser sources are available at all wavelengths thus the choice will be determined by the requirements of the Raman aspect of this system. Due to the weak nature of Raman spectroscopy (the chance of a photon inelastically scattering is

---

---

around one in thirty million approximately) we naturally want to maximise the signal. The intensity of the Raman scattered light is proportional to  $1/\lambda^4$ , thus shorter wavelengths will give a much larger signal, however at short wavelengths cells can be killed or severely damaged even at low optical intensities due to large absorption so longer wavelengths must be used. Traditionally Raman spectroscopy was performed with a dispersive instrument at near UV wavelengths or at 1064nm using a Fourier transform instrument, the longer wavelength allowed higher powers to be used, without damaging samples, thus compensating for the falling efficiency in the Raman scattering. However when dealing with cells, 1064nm causes more damage than the previously mentioned wavelengths [1] so their use is more preferable due to reduced photodamage and increased scattering efficiency. Fourier instruments were traditionally used in the near infrared as spectrographs were not very efficient at these wavelengths. However, advances in grating technology have made dispersive spectrographs in the near infrared the instrument of choice giving efficient and high resolution dispersion of the collected signal, thus our choice between 785, 830 and 970nm will be dominated by the detector performance. One of the greatest advances in Raman spectroscopy, and many other spectroscopy's, has been the development of the deep cooled CCD camera allowing low intensities to be easily collected without being adversely affected by noise. At room temperature a large number of electrons, in the pixels, can be thermally released rather than optically released. When we then have a low optical signal, as is the case in Raman spectroscopy, it can be difficult to discern due to the high noise. The deep cooling of the CCD cameras reduces this noise to a minimum allowing detection of low light signals. These detectors are mostly made from silicon which has a wavelength dependant efficiency that can be seen in figure 6(a).

---

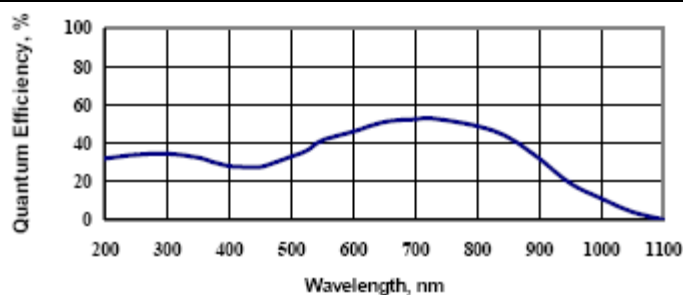


Figure 6(a). Quantum Efficiency of the silicon based CCD camera used in our Raman Tweezers system, this efficiency curve is typical of front illuminated silicon CCD cameras.

As we can see, from figure 6(a), the quantum efficiency reaches a maximum around 700nm and tails off rapidly after approximately 950nm. Raman scattering manifests itself as intensity peaks ‘red’ shifted from the incident laser line. The important fingerprint region we are interested in recording reaches to approximately 1800 wavenumbers. If we consider our three prospective wavelengths, and convert the  $1800\text{ cm}^{-1}$  wavenumber point into nanometres for the three wavelengths, then we find that an incident beam of 785nm will produce a spectra extending to 914nm. In a similar fashion an incident beam at 830nm will produce a spectra extending to 975nm and an incident laser beam of 970nm will produce a spectra extending to 1175nm. We can thus see that an incident beam of 785nm will produce Raman spectra that will fall in a region of relatively good quantum efficiency. The excitation with 970nm will produce Raman spectra in an area of very poor quantum efficiency, with excitation at 830nm the spectra will fall in a region of reasonable quantum efficiency.

Considering all these factors an excitation at 785nm is the best option, the increased scattering efficiency, which comes with using a shorter wavelength, and the produced spectra falling in a region of good quantum efficiency means that lower powers and shorter spectral acquisition times can be used in recording Raman spectra that may cancel out the very small increase in potential photodamage at this wavelength compared to 830nm or 970nm. Thus in our system a 785 nm diode laser is

---

used. Use of this wavelength also brings the advantage of good quality and cost effective laser diode sources.

### **6.1.2 Microscope objectives**

The requirement for optical trapping, to isolate our sample away from interfering surfaces, means that that a high numerical aperture (NA) objective is required. This will almost certainly mean the use of a x100 magnification oil immersion objective as these have the greatest NA available. Oil immersion objectives allow a greater NA as the drop of oil, placed between the nose of the objective and glass coverslip on the sample chamber, matches the refractive index between the lenses in the microscope objective and glass coverslip of the sample chamber. The use of high NA objectives also has the advantage of collecting a larger volume of the Raman scattered light, which is scattered into a spherical volume. The main possible drawback is the very small volume sampled; a x100 NA 1.25 objective will produce a laser focal spot approximately 500nm in diameter. If we want to sample a larger area a smaller magnification must be used, however this often means a compromise in NA thus less effective trapping. A trial and error approach to this problem, throughout this thesis, led to the conclusion that it is possible to use a x50 NA 0.9 oil immersion objective. Despite the lower trapping power it is still sufficient for the study of most Mie particles whilst allowing the examination of an increased area. The choice of microscope objective will depend largely on the specifics of the application and must be chosen with it in mind.

### 6.1.3 Confocal apertures

Confocal microscopy is an established and important technique throughout the biomedical sciences [2]. The technique allows optical sectioning of samples by placing an aperture in the image plane of the microscope, this allows the rejection of spurious signals from regions surrounding the object under study and the size of the aperture placed in the image plane determines the depth of the sample studied and the area in the plane of examination. A schematic showing how the technique operates is displayed in figure 6(b).

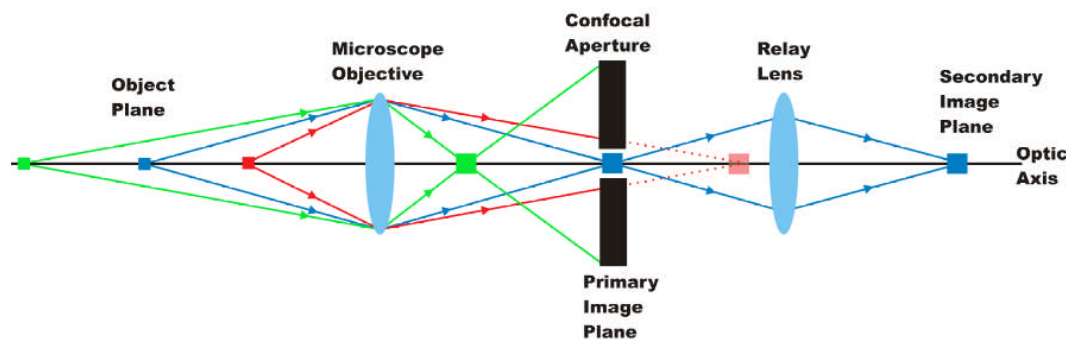


Figure 6(b). Schematic demonstrating the operation of a confocal aperture. The blue object is the object of interest whilst the red and green objects provide potential sources of interference.

As can be seen in figure 6(b) the confocal aperture either blocks the rays, from the interfering objects, forming an image of the object in the primary image plane (red rays) or stops the rays from an image, already formed in the primary image plane (green rays), reaching the relay lens to form an image in the secondary image plane where the signal is detected. Thus the confocal aperture only allows the formation of an image, of the object of interest, in the secondary image plane. Interestingly, as we can see from the figure, that if we wish to measure the objects individually, scanning the confocal aperture would allow us to form images of each object separately in the secondary image plane, this is the basis of scanning confocal microscopy. Although this technique is very powerful it is not perfect and as we can infer from figure 6(b),

any rays from the interfering objects travelling close to the optic axis will still pass through the confocal aperture creating a source of noise or interference.

The confocal aperture will define a cylinder in the object plane, which is proportional to the physical size of the confocal aperture, and can be calculated as follows [3]:

The radius of the cylinder in the object plane, imposed by the confocal aperture, is related to the actual size of the aperture through the microscope magnification as described in equation 6.1.

$$r_0 = \frac{r}{M} \quad (6.1)$$

Where:  $r_0$  = radius of confocal cylinder in object plane  
 $r$  = physical radius of confocal aperture  
 $M$  = magnification of microscope

The depth of the confocal cylinder, which is related to the numerical aperture, is given by equation 6.2

$$d = r_0 \cot(\alpha) \quad (6.2)$$

Where:  $d$  = depth of confocal cylinder  
 $r_0$  = radius of confocal cylinder

and where

$$\alpha = \sin^{-1}(NA/n) \quad (6.3)$$

Where:  $NA$  = numerical aperture  
 $n$  = is the refractive index of the medium between the microscope objective and the sample

Confocal arrangements can be created in two ways in Raman spectroscopy, or indeed any in any system that uses a spectrograph and CCD to collect and measure the light. The first method is the traditional lens based system shown in figure 6(b). The second method utilises the imaging properties of spectrographs and CCD cameras. When coupling the light for examination into the spectrograph an image is usually formed at the entrance slit, this means that the slit can be closed down and clip the image in the x plane. After the light is separated out by the grating and imaged onto the camera the y plane still retains it's original image height, thus by only

---

selecting a few rows of pixels on the CCD camera the image can be clipped in the  $y$  plane. The use of only a few pixels and the entrance slit, we form an aperture that will then define the confocal depth [4]. The second method reduces the complexity of the optics and alignment but reduces the flexibility of the spectrograph settings.

Confocal imaging is a powerful tool often incorporated into Raman Tweezers systems. Although the tweezers reduces the interference from the surroundings, by isolating our particle of interest, interference can still affect the quality of the recorded signal and thus confocal optics are very useful.

#### **6.1.4 Introduction of the laser into the optical system and efficient collection optics**

Traditionally in Raman spectroscopy the Raman scatter is collected at right angles to the incident laser beam in order to try and reduce the collected Rayleigh scatter that can swamp the Raman signal. A complicated set of band pass filters and triple grating spectrographs are normally required to be able to record an acceptable signal: all of this can make the optical alignment of the system very difficult. However the invention of the holographic notch filter, an important step in the development of modern Raman systems, can reduce the alignment difficulty and greatly simplify the experimental apparatus. The holographic notch filter is an optical component that is essentially a holographic type Bragg grating written into gelatine that reflects only a very narrow band of wavelengths, a few nanometres, and allowing everything else to pass. These filters are used in Raman spectroscopy to suppress the Rayleigh scattered light and typically have an optical suppression of OD4. OD stands for optical density and is a measure of the filter's absorbance per unit length that can be calculated according to equation 6.4. The use of holographic notch filters means a

---

---

single grating spectrograph can be used and no further band pass filters are required.

This filter also allows the same objective to be used to excite the Raman scatter, trap the object of interest and collect the Raman scatter as the laser can be introduced via the notch filter into the objective and the collected Raman scatter will pass through the filter and can be sent to the spectrograph, this essentially means a simplification in the optics and thus a much more efficient collection of the Raman signal.

$$OD_{\lambda} = -\frac{1}{l} \log_{10} \left( \frac{I_0}{I} \right) \quad (6.4)$$

Where:  $OD_{\lambda}$  = Optical density at wavelength  $\lambda$   
 $l$  = distance light travels through the sample measured in cm  
 $I_0$  = Intensity of the incident light beam  
 $I$  = Intensity of transmitted light beam

## 6.2 The Raman Tweezers spectroscopy system

Now we have examined the most important parameters in the design of a Raman tweezers spectroscopy system (RTS) we can now tackle the construction and materials used in the RTS system throughout this thesis. A schematic depicting the RTS apparatus can be seen in figure 6(c).

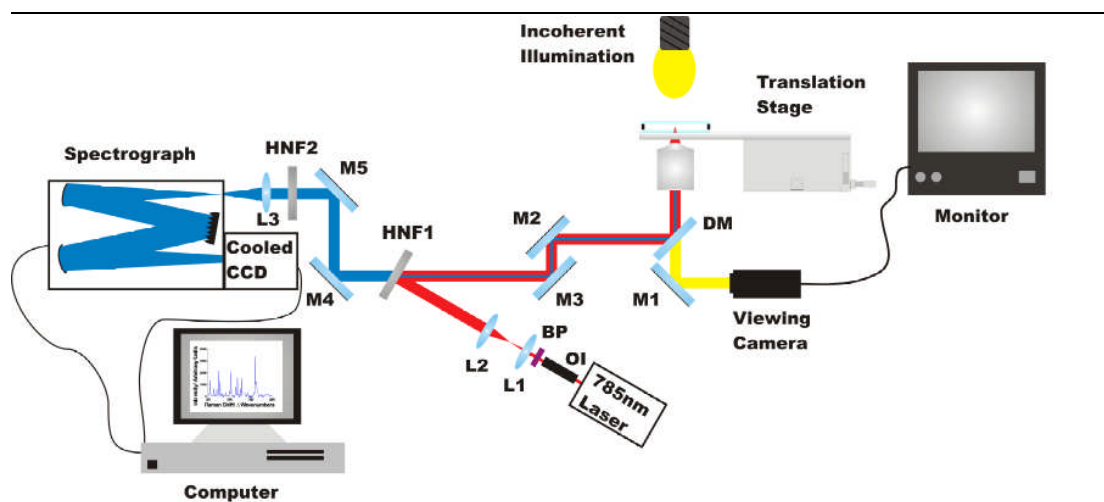


Figure 6(c). A Schematic of the basic RTS system used in this thesis. Abbreviations are as follows: DM - Dichroic Mirror, M – Mirror, L – Lens, OI – Optical Isolator, BP – Bandpass Filter and HNF – Holographic Notch filter.

Our initial setup was guided by published designs that had been used to successfully probe biological cells [5]. The initial system was constructed with the Thorlabs cage system and the details of the setup are as follows.

A 785 nm diode laser was used as the trapping and Raman excitation source. Two diode lasers were tested in this role, a Hitachi 50mW circularised laser diode (HL7851G) and Sanyo 80mW circularised laser diode (DL-7140-201S). Both laser diodes were circularised by Blue Sky research with the use of a micro lens placed directly onto the face of the diode chip to give an  $M^2$  value suitable for trapping. The main difference between the two sources is their relative linewidth, the Hitachi diode has a measured linewidth of 3.4 MHz [6], and the Sanyo diode has a measured linewidth of 20 MHz [7]. It was found that both lasers were suitable, despite the larger linewidth of the Sanyo, as the resolution of the spectrograph and CCD camera is on the order of tens of GHz. The Sanyo laser was preferred as the higher power proved to be useful as the laser has to travel through many optics and despite antireflection coatings, a sizeable portion of the laser power is lost. The laser diode was placed in a

---

collimating tube (Thorlabs) and set into a homemade temperature controlled mount in order to minimise wavelength drift. The temperature is maintained with the use of a peltier element, transferring heat between the laser mount and heat sink, and managed by a temperature controller from Wavelength Electronics (model-MPT-2500).

Diode lasers are very good sources for Raman spectroscopy but are susceptible to feedback thus our laser beam is passed through an optical isolator. Early experiments showed that the laser was susceptible to large mode hops that would produce two uncontrollable separate Raman spectra. The use of an optical isolator, coupled with the temperature stabilisation, resulted in a wavelength stable source with a drift less than the resolution of the spectrograph/CCD system suitable for long term Raman measurements.

The laser beam is then passed through a bandpass filter to remove the spontaneous fluorescence from the laser gain bandwidth. The cooled CCD is a very sensitive instrument and can pick up this emission, from the laser chip, that will interfere with the Raman signal. At 785nm the fluorescence extends to approximately  $950\text{ cm}^{-1}$ , this will mask weaker Raman peaks containing important information thus the fluorescence must be removed. The filter used was an interference filter from Comar (785 IH 25), this is very effective but only transmits seventy percent of the laser intensity thus the extra power provided by the Sanyo laser is extremely useful.

The laser beam is then expanded with the use of lenses L1 and L2. The expansion of the beam is important in order to fill the back aperture of the microscope objective to maximise the optical trapping aspect of the system.

To allow the use of one objective for Raman excitation and collection a holographic notch filter is used (Tydex Notch-4 @  $30^\circ$ ) to reflect the beam onto the optical trapping beam path. As we have discussed, the notch filter provides very high

---

suppression of the laser line thus reflects it and essentially behaves as a mirror for the laser line. The notch filter used has a suppression bandwidth  $500\text{cm}^{-1}$ , this will mean we cannot see the Raman lines within  $250\text{cm}^{-1}$  of the laser line; however this is not a problem for the experiments presented in this thesis.

Mirrors M3 and M2 and the dichroic mirror are used to align the beam precisely into the microscope objective. The alignment of the beam can be checked by watching the reflection pattern, of the laser beam from a microscope slide placed on the sample stage, in the viewing camera. When aligned the laser beam will appear to travel in and out radially from a single spot on the monitor screen, when the slide is brought in and out of focus. If the beam is not correctly aligned it will appear to 'walk' across the screen. The dichroic mirror is a hot mirror (Edmund optics NT43-955) that reflects the infrared laser light and passes the visible light to allow viewing of the sample, although it still passes a little laser light that is very useful in the aligning of the system.

The microscope objective used in the initial system was an Olympus x100 NA 1.25 oil immersion microscope objective and was found to perform well. The immersion oil used was sourced from Cargille (Type DF) and is an ultra low fluorescence oil suitable for spectroscopic applications.

The imaging system, used to view the samples, was constructed from a standard halogen bulb that illuminated the system, the microscope objective that forms the magnified image on the CCD imaging camera (Pulnix) and the monitor that is used to display the image on the camera. This was a simple but effective system, the only drawback was the illumination had to be switched off during Raman acquisition as the light contains an infrared portion that swamps the Raman signal.

---

The sample stage is constructed with a home made metal plate, with a hole drilled in it to allow access to the sample by the microscope objective, mounted on an x,y,z translation stage (Newport 562F). This allows us to move a trapped particle around inside the sample chamber and away from interfering surfaces. In RTS systems, in comparison to many optical tweezers systems, the laser beam remains fixed and the environment, around the trapped particle, is moved rather than the beam moving the particle around the sample chamber. The reasons for this will become clearer as we discuss alignment procedures but the Raman collection path is fixed thus moving the beam, and thus the source of the Raman excitation will mean a reduced collection efficiency or total loss of signal.

The Raman signal that will be collected by the microscope objective from the trapped sample will be reflected by the dichroic mirror and will travel along the same beam path as the laser to the holographic notch filter. As the holographic notch filter has a very narrow suppression band it will reflect the collected Rayleigh scatter and transmit the Raman scatter.

Mirrors M4 and M5 are used to steer the Raman beam onto the spectrographs optical axis.

A second holographic notch filter (Tydex Notch-4 @ 90°) is used to block any remaining Rayleigh scatter that can swamp the Raman signal.

Lens 3 is chosen to match the spectrograph f- number and couple the Raman scatter efficiently onto the spectrographs optical axis.

The spectrograph (Jobin Yvon Triax 550) is an imaging spectrograph with a focal length of 550mm. The spectrograph is equipped with a 300 lines/mm grating and a 1200 lines/mm grating to allow different resolutions. The imaging spectrograph works by imaging the signal at the entrance slit of the spectrograph onto the grating,

---

---

the diffracted light is then imaged again onto a detector. The spectrograph is a one to one imaging system; this means that a single frequency beam incident upon an entrance slit with a width of  $x \mu\text{m}$  will produce a spot of  $x \mu\text{m}$  in size at the spectrograph detector plane. This has important consequences for the resolution of the system, even though the spot was single frequency it still produced a spot size akin to the size of the entrance slit, if two frequencies are incident upon the same entrance slit and the grating does not separate them spatially by more than  $x \mu\text{m}$ , in the detector plane, we will not be able to resolve them, thus the width of the entrance slit has direct bearing on the resolution of the system, the narrower the entrance slit the greater the resolution. The second factor affecting the resolution is the detector used; the detector used throughout this thesis is a thermoelectrically cooled CCD camera (Jobin Yvon Symphony OE STE). The detector is cooled to  $-70^{\circ}\text{C}$  to reduce thermal noise in the camera and allow sensitive detection of the weak Raman signal. The CCD chip itself is a pixel array  $1024 \times 512$  with individual pixel size  $26 \mu\text{m}$ . This will define our system resolution as we cannot resolve spatially beneath  $26 \mu\text{m}$  thus the minimum useful entrance slit of the spectrograph will also be  $26 \mu\text{m}$ . The resolution possible with this system using the  $300 \text{ lines/mm}$  grating is  $0.15\text{nm}$  and using the  $1200 \text{ lines/mm}$  grating is  $0.035\text{nm}$ .

The CCD camera and spectrograph are computer controlled using the Synergy software (Jobin Yvon) that allows the calibration of the instrument and the defining all the appropriate parameters.

In the initial system no physical confocal system was employed, where confocal imaging of the Raman signal was required the method employing the spectrograph entrance slit and CCD camera was used as discussed in section 6.1.3 and presented in reference 4.

---

---

## **6.3 Construction, Alignment, Calibration and Testing of the RTS system**

### **6.3.1 Construction, Alignment and Calibration**

The alignment of the RTS system is done as a stage in the construction of the system. The RTS system is constructed around holographic notch filter 1, as shown in figure 6(c). Holographic notch filters are extremely sensitive to angle of incidence, deviating from the designed angle of incidence results in a change of the wavelength band reflected, thus this element must remain fixed in position. The holographic notch filter is fixed at its designed operation angle, in our case this was  $30^\circ$ . The laser was then directed to be incident upon the notch filter at the correct angle so it behaves as a strong mirror for the laser wavelength. Once the laser beam path was set correctly the band pass filter and the optical isolator were placed in the beam path to clean up the laser emission and stabilise the diode. The optical tweezers portion of the system was then constructed, from Thorlabs cage system, and the laser beam aligned vertically into the objective. With the tweezers correctly aligned, the alignment of the Raman path could then be started. A helium neon (He-Ne) laser (Melles Griot 25 LHR 213) was then introduced into the system, as can be seen in Figure 6(d), through the dichroic mirror, used to reflect the laser beam vertically into the objective, and aligned along the same path as the incoming 785nm laser beam. The He-Ne laser simulates the collected Raman signal, which is too weak to be seen by infrared cards or viewers, which would be collected by the objective and passed back to HNF1 along the same beam path as the incident 785nm laser beam.

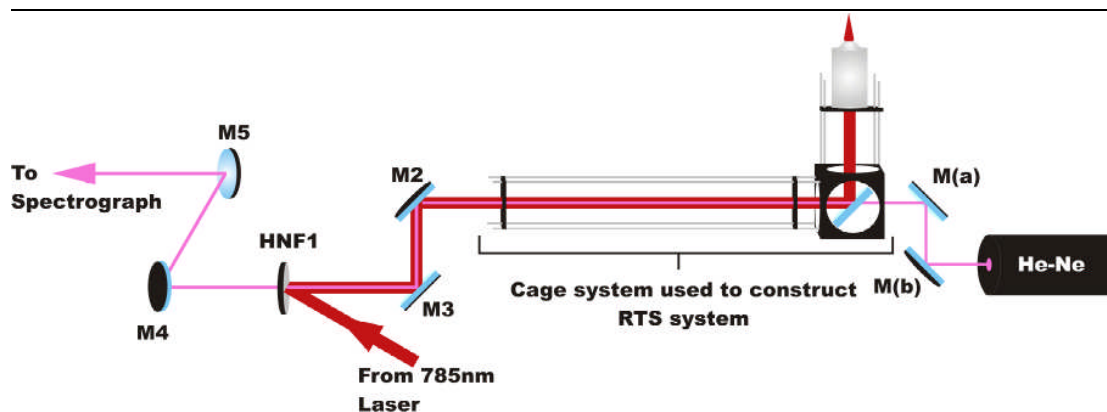


Figure 6(d). A diagram depicting the alignment procedure of the RTS system. The He-Ne laser, whose alignment is controlled by mirrors M(a) & M(b), simulates the beam path of the collected Raman scatter, which is too weak to be visualised, so it can be correctly aligned into the spectrograph.

When the He-Ne beam reaches the holographic notch filter it passes through, as the Raman scatter would, and is then aligned into the spectrograph by mirrors M4 and M5. The spectrograph is pre-aligned internally by the manufacturer thus we must only ensure that the He-Ne beam passes through the centre of the entrance slit and subsequently strikes the centre of the spectrograph's internal collection mirror. A lens is then used, L3 in figure 6(c), to focus the Raman scatter onto the spectrograph's entrance slit and to match the f-number of the spectrograph in order to maximise the signal to noise ratio.

Once this initial alignment has been completed the system is then tested and the fine alignment undertaken. The first task in this step is to ensure that the spectrograph and CCD system are correctly calibrated, this is done with the use of a mercury discharge lamp and the calibration software contained in the Synergy package that controls the spectrograph and CCD. Again using the Synergy software the wavelength of the laser can be recorded and used to calibrate the spectrograph and CCD system into wavenumbers in preparation for taking the Raman spectra, this will allow us to compare our experimental data with well characterised compounds to ensure the system is working well. Once these steps have been completed a disperse

sample of 5 $\mu$ m polystyrene spheres is placed in a sample chamber constructed from a type 1 large cover slip (22 x 50 mm) as the base, a vinyl spacer with a central hole to form the chamber and a type 1 coverslip (22 x 22 mm) to form the lid. A schematic of the sample chamber can be seen in figure 6(e). In fact this is the layout for the sample chambers used throughout the course of this thesis.

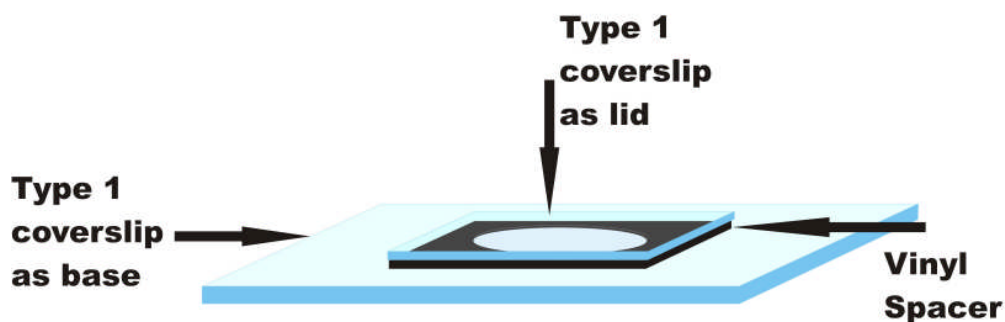


Figure 6(e). A depiction of the construction of the sample chamber used in the calibration process and in experiments throughout this thesis.

A drop of immersion oil is placed on the objective and the sample chamber placed on the translation stage. The 785nm laser is then set to an optical power of 20mW and used to optically trap one of the polystyrene spheres. As well as trapping the sphere, the laser will simultaneously excite the Raman scattering process thus the Raman scatter should be collected and guided, by the optics, to the spectrograph. The spectrograph was initially set with a wide entrance slit and the full CCD pixel area was used, the computer was then set to continuously acquire spectra to try and observe the Raman spectrum of polystyrene from the trapped particle. If the initial alignment was performed correctly, the Raman spectra of the polymer sphere should be visible which can be seen in figure 6(f). The spectrum of this material is very well known and well characterised [8] so is useful for testing the system to ensure it is working correctly. Once the polymer spectrum has been observed the signal intensity can be maximised by adjusting the mirrors M4 and M5, in Figure 6(c), which control the beam path into the spectrograph. Another important factor in maximising the

---

signal intensity is ensuring the laser beam traps the particle in the microscope objectives focal plane. The signal collection efficiency of microscope objectives falls off rapidly as the point of signal origin moves away from the focal plane, this can be maximised by adjusting lens L2, in figure 6(c), along the beam path thus adjusting the laser focus position hence the position of the trapped object. The final task in the fine alignment of the system is the adjustment of the entrance slit and the selection of the pixel rows used for taking data. As we have previously mentioned the entrance slit is an important factor in determining the resolution of the spectrograph so we want it as narrow as possible without adversely affecting the signal intensity thus it is imperative that the focus of the coupling lens, into the spectrograph, coincides with the entrance slit. This can be maximised by continuously narrowing the entrance slit whilst moving lens L3, as shown in figure 6(c), along the Raman scatter beam path to obtain the maximum signal. The final task is then to choose the number of rows of pixels used on the camera for detection; this may seem counterintuitive to start with but is important.

## Raman Spectrum of Polystyrene

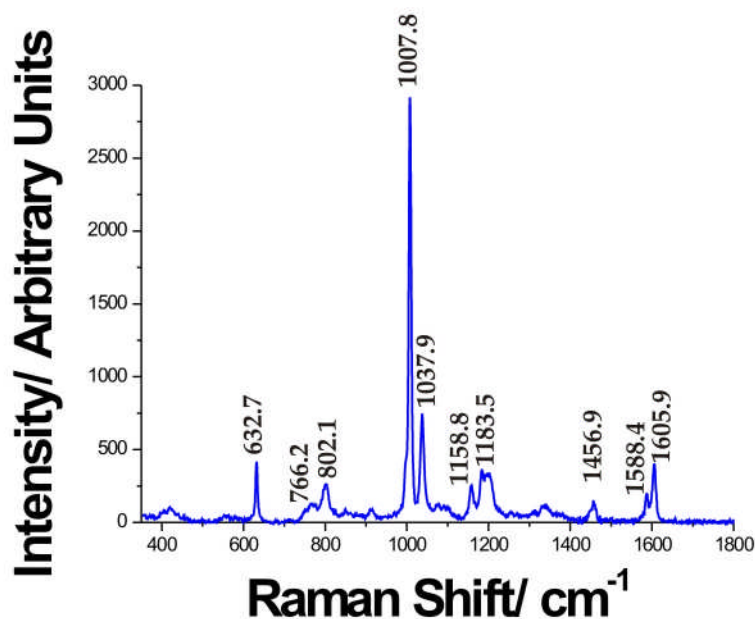
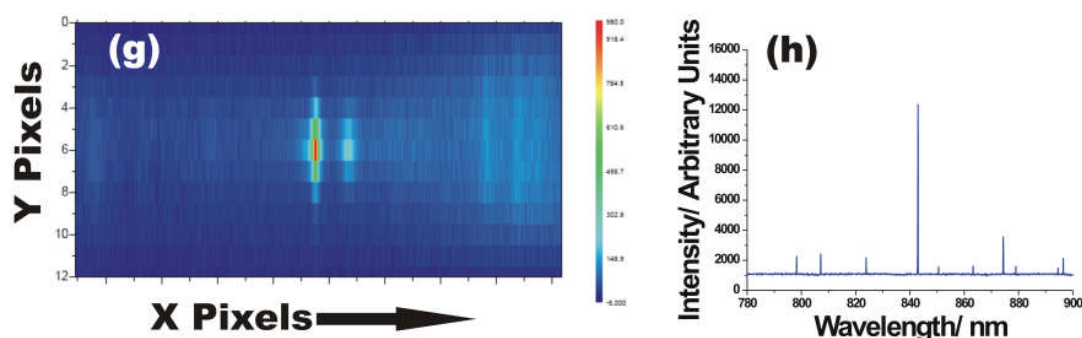


Figure 6(f). Raman spectra of Polystyrene; the laser power, for this acquisition, was 20mW before the objective and the acquisition time was 2 seconds and the spectrograph grating used was the 1200 lines/mm.

As we have discussed previously the spectrograph is an imaging system; although in the horizontal plane the grating separates the light into a wavelength dependant stripe, the vertical plane will remain unchanged thus the height of the image at the entrance slit will be the height of the image in the detector. The detector is made up of a pixel array of 1024 x 256 pixels each 26  $\mu\text{m}$  square with a physical size of 26.6 x 6.7 mm, the image at the slit typically has a height of 75-100  $\mu\text{m}$  meaning we use only a small fraction of the chip area, in fact only three or four rows of pixels actually integrate signal. The remaining pixels only integrate noise from the camera electronics and thermal noise. Figure 6(g) shows an intensity image of a few pixel rows of the CCD camera capturing the strong central Raman peaks of polystyrene at 1007.8 and 1037.9  $\text{cm}^{-1}$ . The image only occupies five of the twelve rows thus the remaining rows appear blue and are integrating only noise. Another phenomenon these cameras are susceptible to are cosmic rays that appear as strong spikes on the spectra, reducing the

area reduces the probability of a cosmic ray affecting a spectra. Figure 6(h) shows a spectra acquired for four minutes in a dark room without any sources turned on, thus the spurious spikes are a result of cosmic rays striking the CCD chip.



Figures 6(g&h). Figure 6(g) shows an image of a few rows of pixels on the CCD camera, the Raman signal only covers a fraction of the available rows thus the remaining rows integrate noise and is best to discard their information. Figure 6(h) shows a spectrum taken with the CCD without any sources turned on; the spikes are the result of cosmic rays striking the CCD chip, reducing the number of pixels used reduces the probability of cosmic rays interfering with a Raman acquisition.

### 6.3.2 Testing the Raman Tweezers system and Data Treatment

Once the alignment and calibration was complete the system was tested for performance by taking spectra and comparing them with known published spectra. The spectra in figure 6(f), of polystyrene, compares favourably with those previously published [5, 9 & 10]. There is some disagreement as to the exact peak positions, for example the large central peak near  $1000\text{cm}^{-1}$  is reported at positions from  $1000\text{cm}^{-1}$  [9] up to  $1007\text{cm}^{-1}$  [10], our positions are thus at the top end of this band. The variations in the reported positions are most likely the result of small variations in the calibration of individual systems. The RTS system was recalibrated several times throughout this thesis and the central peak continues to fall very close to this reported value. As well as testing polystyrene other substances were tested such as glucose, the spectrum of which can be seen in figure 6(i). To ensure the correct operation of the

RTS system the results were compared against previously published spectra and again compared favourably [11].

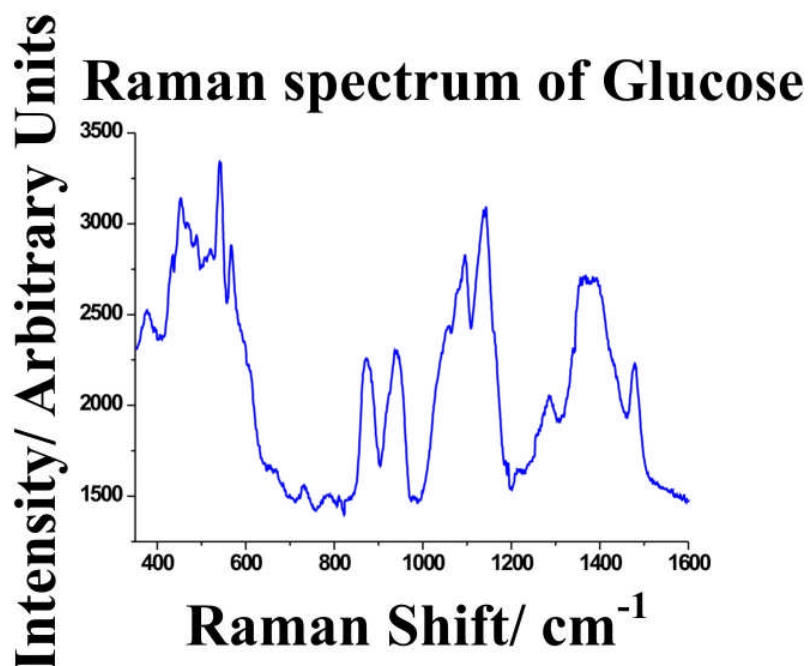
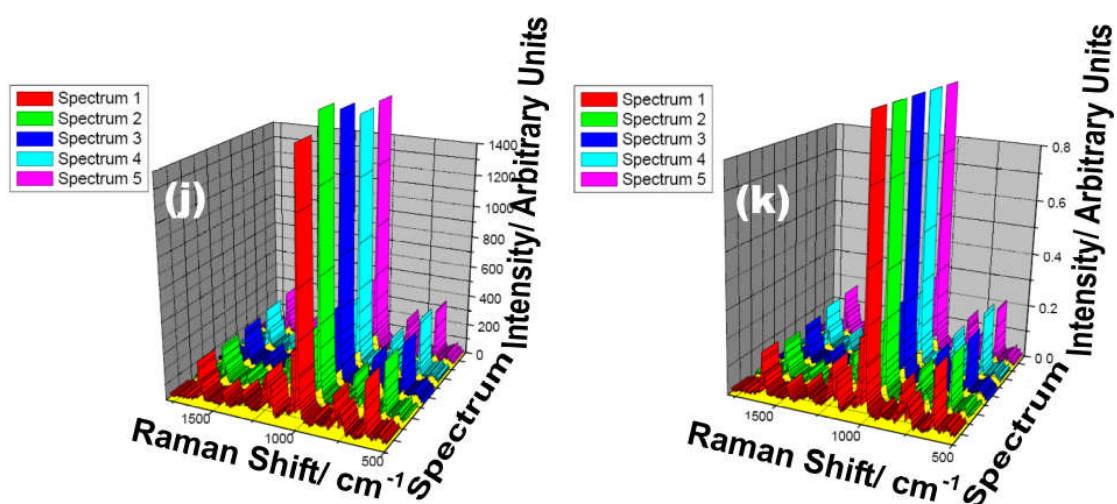


Figure 6(i). Raman spectrum of Glucose; the laser power, for this acquisition, was 20mW before the objective, the acquisition time was 20 seconds and the spectrograph grating used was the 1200 lines/mm.

Satisfied the RTS system was working correctly we examined the temporal behaviour of the Raman spectra. A diagram showing five successive Raman spectra of polystyrene can be seen in figure 6(j).



Figures 6(j&k). Figure 6(j) shows the temporal evolution of the Raman spectrum of a 5 $\mu$ m trapped polystyrene sphere; the laser power, for the acquisition, was 20mW, the acquisition time for each spectra was 2 seconds and the 300 lines/mm grating was used. Figure 6(k) shows the same data set after undergoing normalisation.

Figure 6(j) shows how the intensity of the Raman spectra varies with each acquisition; this is not a fault with the system but rather is down to small fluctuations in laser power and the result of the statistical Raman process. What does remain constant however is the ratios between the peaks, a change in peak ratios would indicate a chemical change in the area being probed, thus we can normalise the data to make the spectra more readily comparable and help make any change in peak ratios more easily visible without being obscured by intensity fluctuations. There are three ways to normalise data; the first way is the simplest and involves dividing each point in the spectra by the height of the largest peak, this method is simple but not extremely accurate for complex spectra but works well however for spectra similar to polymer where there is only a few sharp spikes and very low area under the curve, this was in fact the method used to normalise the data in figure 6(k). The second method is known as an intensity normalisation or normalisation to one and involves the division of each point on the spectra by the area under the curve according to equation 6.5.

$$I(p)_n = \frac{I(p)}{\sum_1^{1024} I(p)} \quad (6.5)$$

Where:  $I(p)_n$  = normalised intensity at pixel p  
 $I(p)$  = Intensity at pixel p

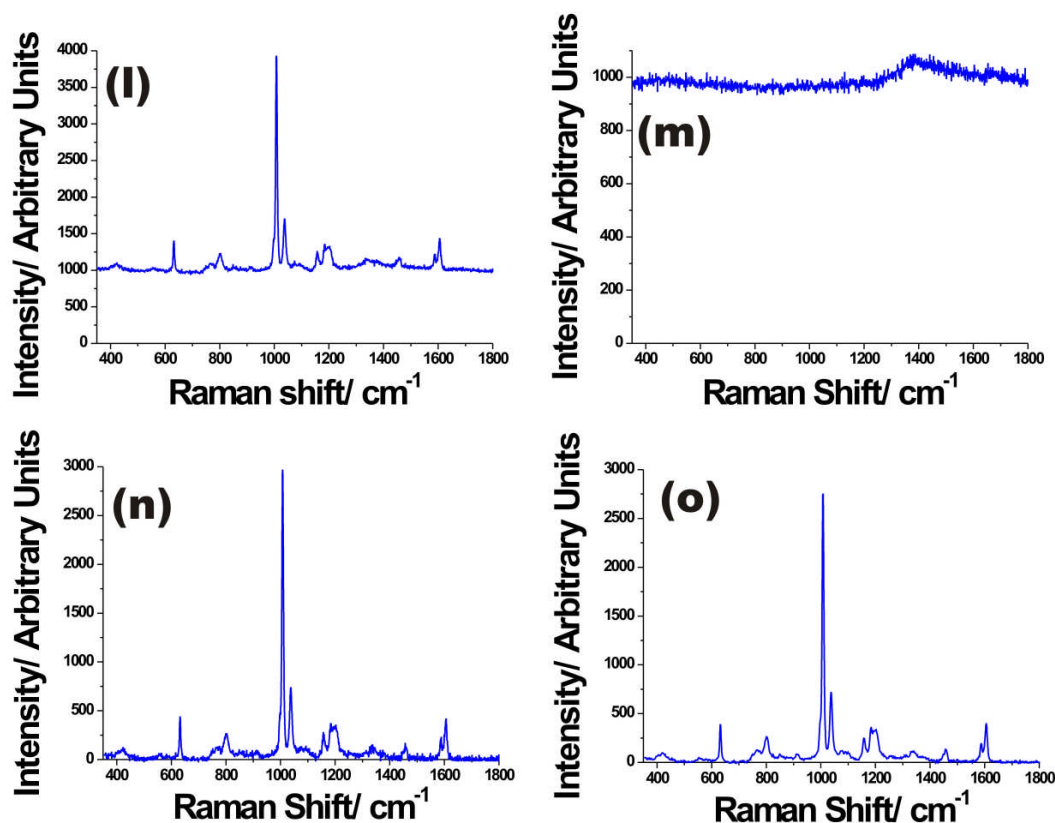
The Raman spectrum is an intensity spectrum but there are occasions when it may contain negative numbers, as the result of subtractions that we will discuss subsequently, thus the intensity normalisation is less suitable and an amplitude normalisation is required according to equation 6.6.

$$I(p)_n = \frac{I(p)}{\sqrt{\sum_1^{1024} (I(p))^2}} \quad (6.6)$$

---

The amplitude normalisation is very effective but it is preferable to use the intensity normalisation for spectra as the squaring process, in the amplitude normalisation, will bias the result towards the large peaks and any relevant information contained in weaker peaks may be masked or have its influence reduced.

As well as the normalisation process the raw data is often subjected to two more statistical processes to help improve our understanding of the data. The first is background subtraction; despite confocal arrangements and the use of optical trapping, to isolate the particle of interest away from interfering surfaces, there is normally a background component in the spectra upon which the Raman spectrum sits. This can be a problem with long acquisitions, as silica has strong laser induced auto fluorescence at our excitation wavelength. This can be reduced by using quartz coverslips and using a background subtraction. Again if we consider the polystyrene spectrum seen in figure 6(f), this particular spectrum has undergone background subtraction. A spectrum was taken from the trapped particle and immediately afterwards the particle was 'kicked' out of the trap and a background spectrum was then taken, it is important take the background before readjusting the setup as the z focussing position is extremely important in the amount of auto fluorescence collected. Figure 6(l) and figure 6(m) show the raw signal and its corresponding background respectively.



Figures 6(l,m,n&o). Figure 6(l) shows the raw polystyrene Raman spectra and its corresponding background spectrum in figure 6(m). Figure 6(n) shows the background subtracted polystyrene spectrum. Figure 6(o) shows the smoothed background subtracted polystyrene Raman spectrum.

We can see, in figure 6(l), that the Raman spectrum sits on a background that is shown in figure 6(m). The background consists of two parts, the smooth trend that is a result of the laser induced auto fluorescence and the ‘fuzzy’ pattern that is the result of thermal noise in the camera head. The background is subtracted from the signal to leave only the Raman signal as shown in Figure 6(n). The second statistical process, used in the treatment of spectra, is smoothing. Despite having removed the auto fluorescent background the ‘fuzzy’ component still remains on the spectra in figure 6(n), this is because it is the result of thermal noise which is a very close approximation to true white noise thus cannot be accounted for as it is truly random. This noise can mask fine detail in peaks and obscure weak peaks, but it can be

---

removed by the smoothing process which picks out the trend of the spectra from the noise. Two types of smoothing were used in this thesis; adjacent averaging and Fast Fourier Transform (FFT) smoothing. Adjacent averaging averages a data point with a set number of points either side of it, this method is useful but obviously the averaging process may destroy weak peaks. FFT smoothing removes high frequency Fourier components, this method is much more successful and is the one used to smooth the spectrum in figure 6(n) to produce the spectrum in figure 6(o), this makes it much easier to discern the smaller peaks and fine detail in peaks. Smoothing is an extremely useful operation but does alter the data, thus where absolute measurements are performed no smoothing is applied to the data and it is restricted to supporting arguments based on the visual inspection of Raman spectra.

This Raman tweezers setup was found to be very successful and was the culmination of several experiments on different suitable geometries and optical components. Initially we investigated a system based on cheap commercially available glass filters to attempt the construction of a low cost Raman tweezers system. However it was discovered to be very difficult as the suppression of the Rayleigh scattered light was not strong enough and it stopped us from seeing the weak Raman signal in the spectrograph. Also constructed was a Raman tweezers system based on two opposing microscope objectives, one used to trap the object under study and excite the Raman scatter and a second objective to collect the Raman scatter. A schematic of this setup can be seen in figure 6(p). This setup allows us to use a simple inverted tweezer to trap the object and simultaneously excite the Raman scatter. The second objective is then used to collect the scatter and send it to the spectrograph. In theory this geometry should simplify the alignment procedure as no He-Ne will be required because the trapping beam can be collected and aligned into the

---

---

spectrograph. Furthermore the number of optics the Raman scatter passes through is reduced thus less signal is lost. However in practice this system is quite tricky to get right as it is difficult to align well the two microscope objectives and also requires a greater complexity in the experimental arrangement. A standard Raman tweezers system was also constructed and worked well but the inverted system was preferred because of the advantages of using inverted optical tweezers for low power trapping where gravity aids the gradient force in drawing the particle into the beam focus. These systems were all evaluated on the way to developing our working system, described in this section, on which confident measurements could be undertaken.

The construction and alignment of the initial system has been described here along with the methods used to treat the data. Even though the system continually evolved throughout duration of the work this thesis describes, the alignment principles and apparatus remained for the most part constant. In the next section we will see how the system evolved to become more suitable for our applications.

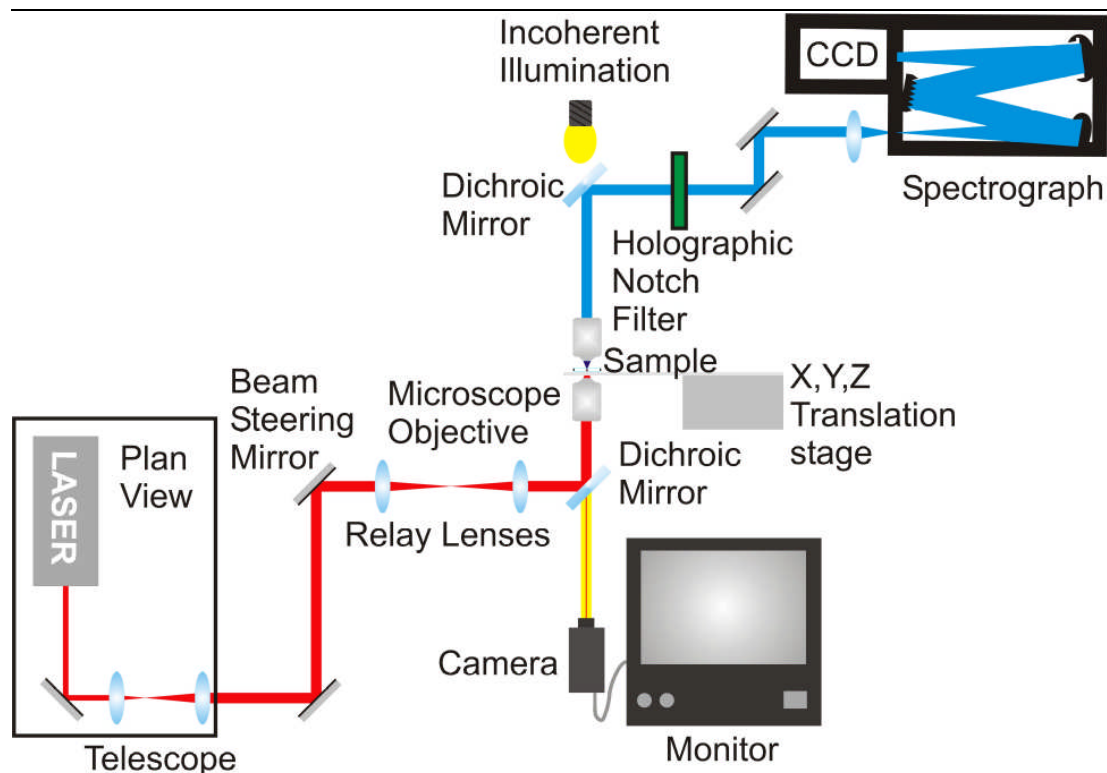


Figure 6(p). Schematic of the dual objective Raman tweezers system evaluated during the construction of our initial Raman tweezers system. This system allows us to use a standard optical tweezers to trap an object and excite the Raman scatter whilst a second objective can be used to collect the Raman scatter and send it to the spectrograph

## 6.4 Evolution of the Raman Tweezers Spectroscopy System

The initial RTS system performed well but as experience with the system mounted and specific applications presented themselves the system evolved to suit the specific needs of the applications and as a result of the experience gained. Specific evolutions of the system, designed for a particular application, will be discussed in the relevant chapter but there were a couple of major changes to the RTS system that deserve to be noted here.

The first major evolution applicable throughout all the experiments undertaken in this thesis was the introduction of a temperature controlled sample stage, a schematic of the stage can be seen in figure 6(q). As the experiments, described in this thesis, concern the monitoring of biological cells a heated sample stage was deemed

necessary to keep the cells alive and in surroundings as close to their natural conditions, 37°, as possible during the measurements. Although the time required to take a single spectrum of a cell is relatively short the entire time a sample may be on the stage is substantial and the cells will almost certainly begin to die and divert from their normal behaviour, this may alter the experimental results or mask the signal we are looking for, thus the heated stage is important.

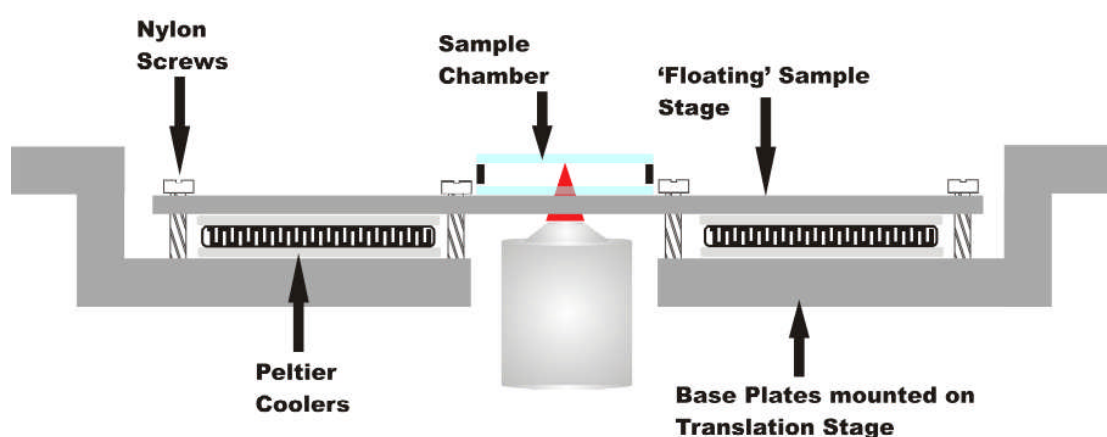


Figure 6(q). Diagram detailing the construction and components used in the thermally controlled temperature stage.

The stage is constructed from aluminium; the base plates are attached to the translation stage that acts as a heat sink for the heated sample stage. On the base there are two Peltier elements (Melcor CP1.0-127-08) around the hole in the base, which allows the microscope objective to reach the sample, that facilitate the transfer of heat between the base and sample stage. The sample stage essentially 'floats' on the Peltier elements but is anchored in place by nylon screws that prevent uncontrolled thermal transfer between the base plates and the sample stage. The temperature is controlled by a thermal control unit (Wavelength Electronics MPT-2500) that monitors the stage temperature, via a thermister bonded to the sample stage with thermal bonding glue, and appropriately adjusts the current in the Peltier elements to maintain the stage at a constant 37°. The stage worked well and was able to keep cells comfortable for several hours but it does have some drawbacks. The hole in the centre of the stage, to

---

allow the objective to be brought up to the sample, means that the portion of stage under the sample chamber, and a portion of the sample chamber itself, is not directly heated, this leads to thermal gradients over the sample that are not ideal for the cells, experimentally temperature gradients of up to 3° centigrade were observed meaning not all cells will be at the correct temperature. The objective, being made of metal, will also conduct thermal energy away from the sample. The only real solution for these problems is to place the entire setup inside an incubator, as is the case for many commercial microscopes, and apply an objective heater to the objective. This is a very costly exercise however and our stage performs adequately for the type of experiments carried out in this thesis thus was used as is shown in figure 6(q). In keeping cells alive we must also consider the CO<sub>2</sub> supply reaching the cells which require an atmosphere of 5% CO<sub>2</sub> to control the surrounding ph for optimum growth. Obviously in the sample chamber the cells are not getting the required amount of carbon dioxide; however in the time periods we were examining the cells this did not appear to have a detrimental effect on the cells. If we wish to carry out a lengthy examination of cells it is possible to add a chemical called hepes that is capable of controlling the sample ph.

The second and most major evolution in the system was the introduction of a commercial microscope (Nikon TE2000U) as the base for the RTS system as opposed to the initial setup constructed from Thorlabs cage system. The main advantages of the commercial microscope is that it is extremely robust, has a high quality prealigned optical beam path, the high quality in built viewing system and use of an objective wheel means it is very easy to swap objectives during an experiment. The Nikon TE 2000 system is an infinity corrected microscope system. This essentially means the microscope objective produces a parallel train of rays from each point on the image.

---

This means the beam emerging from the microscope objective will be a diverging one, as can be seen in figure 6(r); thus in order to form the image another lens must then be used. The advantage of this system is that other optical elements can be placed in the beam path between the objective and the imaging lens without overly affecting the imaging beam path and allowing other techniques to more easily integrated with microscopy.

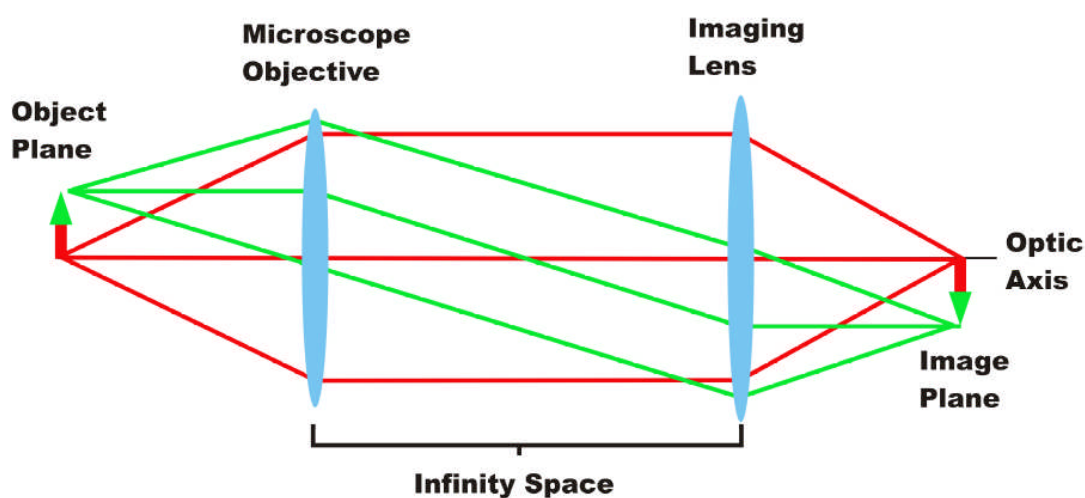


Figure 6(r). Schematic of the optical path of an infinity corrected microscope, the microscope objective produces a parallel train of rays from each point on the object that manifests itself as a diverging beam leaving the microscope objective and an imaging lens is then used to form the image. The space between the objective and imaging lens is referred to as the infinity space and allows other optical elements to be placed in this space without overly affecting the imaging path. The distance between the objective and imaging lens is not important but as can be seen from the diagram the larger the distance the smaller the field of view of the microscope.

A schematic of the new microscope system can be seen in figure 6(s). The microscope based system uses most of the same parts as the initial system with two new additions, a 45° notch filter (Tydex notch-4) was acquired and an external confocal system was applied to the Raman scatter beam. The external confocal system was used, rather than the previous spectrograph and camera based one, to restore the flexibility in the spectrograph parameters to maximise experimental conditions. The laser beam is prepared in the same manner as the in the initial system but is directed through the microscopes epi-port, using mirrors M1 and M2, onto the 45° notch filter in the

infinity space between the microscope objective and imaging lens. The laser beam is directed vertically into the microscope objective to form the trap and excite the Raman scatter. The Raman scatter is then collected and passed through notch filter onto the imaging lens that forms the image, via the flip mirror, outside the microscope body. The flip mirror allows the Raman scatter to exit the left port of the microscope to the spectrograph or can be used to direct the bright field image of the trapped object to the camera attached to the right hand microscope port. A confocal aperture is then placed in the image plane and the remaining light is re-collimated by lens L1. Mirrors M3 and M4 are then used to align the Raman scatter into the spectrograph and lens L2 reforms the Raman image at the entrance slit of the spectrograph. A photograph of the Raman collection portion of the microscope setup can be seen in figure 6(t). The alignment of the new system is undertaken in much the same way as the initial system; the tweezer is initially aligned, the objective is removed and the He-Ne passed through the microscope body, out the left hand port of the microscope and can then be aligned into the spectrograph.

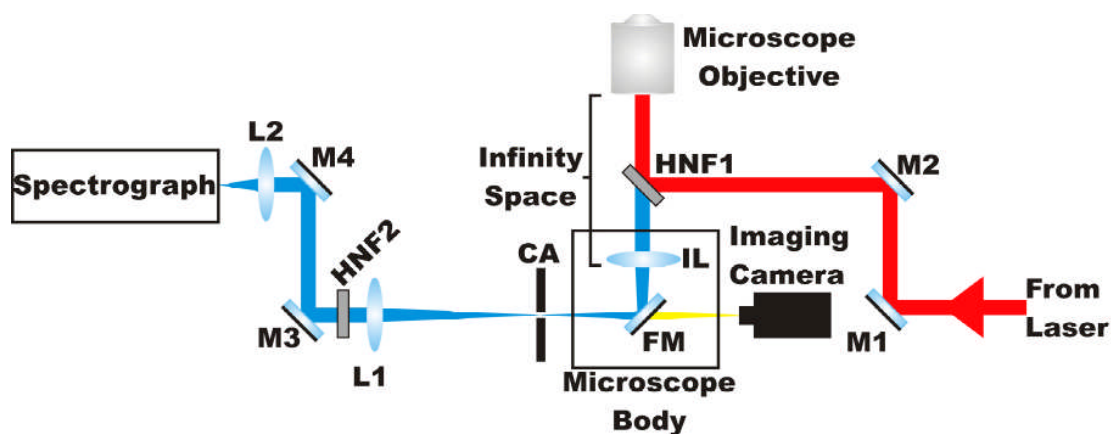


Figure 6(s). Schematic of the experimental arrangement of the microscope based RTS system. Abbreviations are as follows: M - mirror, L - lens, FM - flip mirror, IL - imaging lens, HNF - holographic notch filter and CA - confocal aperture.

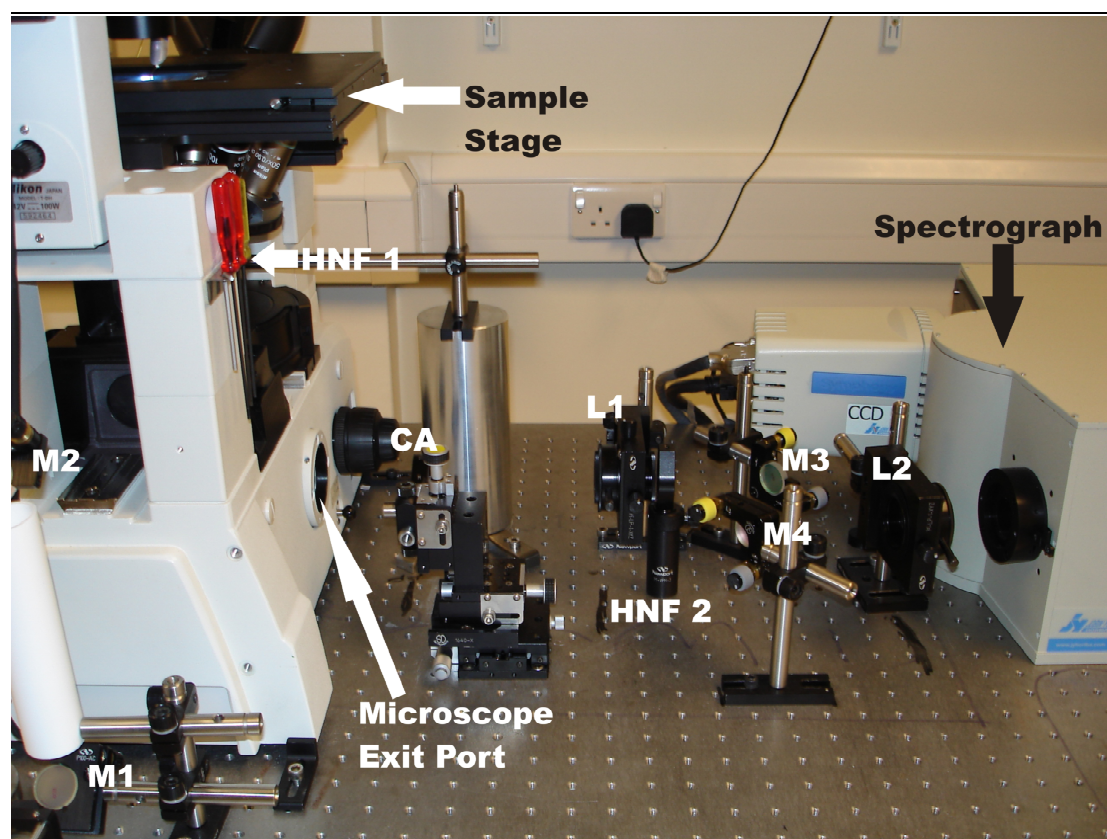


Figure 6(t). Photograph of the microscope based RTS system; abbreviations are the same as those in figure 6(q).

The main advantage of the microscope based RTS system, as can be seen in figure 6(s), is that the input laser beam path and the Raman scatter collection path are virtually independent. This means that the alignment of each path can be tweaked individually to maximise the collection of the Raman signal. Previously on the initial system, if the alignment drifted out it often meant a complete rebuild but on the microscope system this is avoided and is thus much more robust. The main drawback of this new arrangement is that the object trapped cannot be simultaneously viewed and interrogated with the Raman system; it was not felt that this was a serious problem as the illumination lamp had to be turned off anyway during Raman acquisition as it interferes with the signal. The new microscope based RTS system was found to be very useful and robust and therefore employed in the experiments detailed in chapters 8, 9 and 10.

---

We have described the major evolutions that the system underwent throughout the course of the research presented in this thesis. There were of course specific alterations to the setup to accommodate particular applications but as mentioned these will be described in the relevant chapters.

## 6.5 References

- [1] Neuman KC, Chadd EH, Liou GF, Bergman K and Block SM. **Characterisation of Photodamage to Escherichia coli in Optical Traps.** Biophysical Journal 1999; **77**: 2856-2863
- [2] Pawley JB. **Handbook of biological confocal microscopy.** 1995; Springer science and business media: pp. 1-14
- [3] Koppel DE, Axelrod J, Schlessinger J, Elson EL and Webb WW. **Dynamics of Fluorescence Marker Concentration as a Probe of Mobility.** Biophysical Journal 1976; **16**: 1315-1329
- [4] Williams KPJ, Pitt GD, Batchelder DN and Kip BJ. **Confocal Raman Microspectroscopy using a Stigmatic Spectrograph and CCD Detector.** Applied Spectroscopy; **48**: 232-235
- [5] Xie C, Dinno MA and Li YQ. **Near-infrared Raman spectroscopy of single optically trapped biological cells.** Optics Letters 2002; **27**: 249-251
- [6] Lancaster GPT. **Experimental Studies of Diode Lasers and Cold Atom Guiding.** 2001 PhD Thesis University of St. Andrews: 73-80
- [7] Gabbanini C, Fioretti A, Lucchesini A, Gozzini S and Mazzoni M. **Cold Rubidium molecules formed in a magneto-optical trap.** Physical Review Letters 2000; **84**: 2814-2817
- [8] Singh GP. **Raman Microspectroscopy of Optically Trapped Cells.** 2006 PhD

---

Thesis; Institut de Ciencies Fotoniques: 72

- [9] Bridges TE, Houlne MP and Harris JM. **Spatially Resolved Analysis of Small Particles by Confocal Raman Microspectroscopy: Depth Profiling and Optical Trapping.** Analytical Chemistry 2004; **76**: 576-584
- [10] Gessner R, Winter C, Rosch P, Schmitt M, Petry R, Kiefer W, Lankers M and Popp J. **Identification of Biotic and Abiotic Particles by Using a Combination of Optical Tweezers and In Situ Raman Spectroscopy.** ChemPhysChem 2004; **5**: 1159-1170
- [11] Berger AJ, Itzkan I and Feld MS. **Feasibility of measuring blood glucose concentration by near infrared Raman spectroscopy.** Spectrochim Acta A Molecular Biomolecular Spectroscopy 1997; **53(A)**: 287-292

---

# 7. Simultaneous Raman Micro- Spectroscopy of Optically Trapped and Stacked cells

---

*Optical stacking is a phenomenon observed in optical traps where multiple particles align in a vertical stack along the beam propagation axis close to the beam focus. The implementation of this effect requires no extra equipment or involved procedures thus is ideal for use with Raman Tweezers. In this study we will examine how increasing depth of stacked particles affects the collected Raman signal and see how this technique may be used to obtain rapid, clear and representative spectra from cell populations*

---

## 7.1 Introduction and Experimental Aims

We have seen in the preceding chapters how the compatible techniques of Raman spectroscopy and optical tweezers can be combined, with relative ease, to form the powerful new technique of Raman tweezers. We have also seen the advantages this new technique brings to cellular studies in comparison with traditional Raman spectroscopy. Most of the current published work has concentrated on studying single particles or cells, but a unique property of optical tweezers offers the possibility of studying many particles simultaneously. This property is optical stacking [1] and is a phenomenon observed in optical traps where multiple particles

---

---

are simultaneously trapped and align vertically along the beam axis, a schematic of this can be seen in figure 7(a). This effect was predicted theoretically by Gauthier and Ashman [2] and many groups have subsequently observed the phenomenon [1, 3]. In optical stacking a particle may be drawn into the trapping laser beam by the transverse gradient force and then drawn into the focus by the axial gradient force where a particle is already trapped, the new particle then stacks up underneath the particle already in the trap held underneath by the axial and transverse gradient forces. Optical stacks of microparticles can be constructed in two ways; the first is with the use of the axial gradient force holding the particles close to the focus of the laser beam and the second method utilises radiation pressure to hold a stack of particles against the upper coverslip of the sample chamber. In the second method, the one shown in figure 7(a), the beam is focussed on the upper coverslip and the transverse gradient force draws particles into the beam and the radiation pressure pushes them along the beam axis towards the focus where they are held in a stack. This method allows the creation of much more stable stacks with lower optical powers and thus is the method used throughout this chapter to create the stacks. We should note that the technique of stacking requires no extra equipment or variations in the experimental apparatus as it will occur naturally in the optical tweezers. This effect is typically avoided in colloidal studies as most experiments undertaken often want to study just one trapped particle; however in Raman tweezers microspectroscopy it can be put to use in the evaluation of more than one cell simultaneously.

This technique would be useful in the examination of populations of cells where a particular aspect of a cell culture is of interest rather the behaviour of an individual cell, this is possible as the stacking technique probes several cells simultaneously and provides a pseudo average of the biochemical status of the cell

---

ensemble. The technique does not provide a true average due to the variation in microscope collection efficiency with distance from the focal plane thus the cells will each have a different weighting factor in the ‘averaged’ signal. This pseudo averaging then will help smooth out variations in individual cell spectra, such as variations due to cells being in different points of the cell cycle, and make clearer the behaviour of the cell population. Furthermore the stacking and thus simultaneous examination of multiple cells will reduce the number of acquisitions required to study a cell population reducing the overall experimental time.

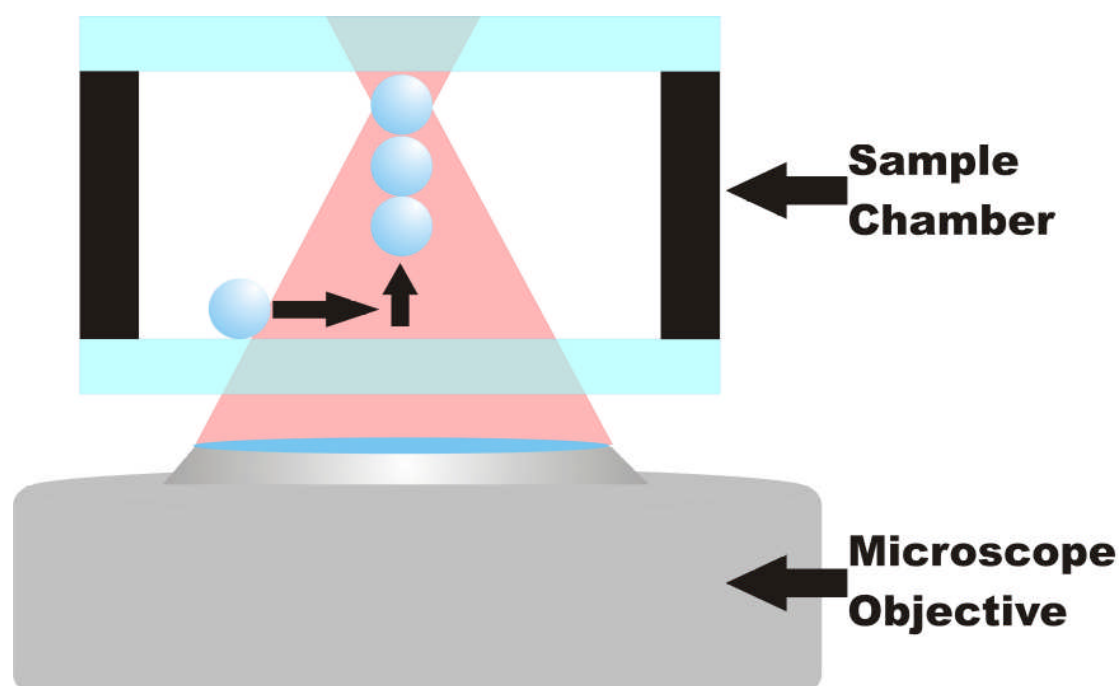


Figure 7(a). Schematic of stacking in an optical tweezers; if a particle is trapped in the focus of the trap another particle can be drawn into the focussed beam by the transverse gradient force and then drawn towards the focus by the gradient and radiation pressure forces, by this process several particles can be stably stacked.

Specific applications where the pseudo averaging property of stacking may be useful include the Raman spectroscopic study of small cell populations pre-selected by methodologies such as optical sorting [4], micro fluorescence activated cell sorting [5] or dielectrophoresis [6]. One can then evaluate their true biochemical nature that is not probed the sorting technique; the stacking may come in specifically useful in the

---

study of sorted cancerous cell populations. Recent research has shown the ability of Raman tweezers spectroscopy to discriminate between cancerous and healthy populations by the use of statistical models that essentially detect increased S-phase activity [7]. In unsynchronised, as is normal, healthy populations any cell undergoing replication will likely flag up as cancerous creating a false positive. The stacking technique with its pseudo averaging ability has the promise to alleviate these concerns and allow the collection of a signal representative of the whole population allowing conformation of samples sorted by these other techniques.

In 2004 Bridges *et al* [8] published work detailing the effect on the Raman signal of increasing the size of polymer spheres adhered to a glass surface, inside an imposed confocal volume, by monitoring the intensity of the Raman bands. They also developed a theoretical model that was in good agreement, for the most part, with the observed results that showed a near linear initial increase in signal intensity followed by Lorentzian type decay as the confocal volume became filled. After filling the confocal volume the intensity showed only a minor increase despite continuous increases in the size of the particles. Although we might expect the signal to increase linearly until the confocal volume was filled and then display no further increase, the decrease in collection efficiency of the microscope objective, as we move from the focal plane, plays an important role and accounts for the Lorentzian profile of the collected signal intensity as the particle fills the confocal volume. The small increase in intensity of the collected Raman signal, for increasing depths, once the confocal volume has been filled is a result of the imperfect nature of the confocal system that in reality cannot completely exclude signals from outside the confocal volume. This paper demonstrates how Raman microspectroscopy may be used in depth profiling and for spatial analysis of small particles but does not investigate how the intensity of

---

---

the collected signal behaves in much larger confocal volumes, for multiple trapped particles, for non-uniform objects such as cells and does not investigate any implications, of increasing sample volume, on the signal to noise ratios. The use of optical trapping and stacking, compared to the particles fixed on the slide, will allow an investigation of the importance of sample depth vs. sample volume by creating similar sample depths with different sized particles to gain further understanding of the behaviour of the collected signal and any advantages it may bring in our Raman Tweezers studies.

In this chapter we aim to investigate the effect of increasing the axial mass in the Raman probe volume by stacking polymer microparticles of different sizes in the Raman tweezers beam and measuring the Raman signal. We also aim to investigate the effect of this technique when applied to cells, in particular we wish to evaluate any changes in the spectra due to stacking and any effect the stacking has on the signal to noise ratio of the Raman spectra acquired from the cells.

## 7.2 Experimental Methods and Procedures

To allow us to study the effect of increasing the mass of material in the Raman probe volume we stacked and obtained spectra from up to five polystyrene microspheres from monodisperse solutions of polymer microspheres, Duke scientific, of sizes 5 $\mu\text{m}$ , 10  $\mu\text{m}$  and obtained spectra from single polystyrene microspheres of sizes 20 $\mu\text{m}$  and 25 $\mu\text{m}$ . Polystyrene microspheres were chosen as the Raman spectrum of polystyrene is well known and has well defined spectral features, a Raman spectrum of polystyrene can be seen in figure 7(b) accompanied by the chemical bond assignments for the Raman peaks [8, 9]. To evaluate quantitatively the effect of the stacking process the intensity of the 1008 $\text{cm}^{-1}$  peak was monitored as the particles

---

were stacked. Finally, in order to evaluate the effect of the stacking process on cells, we stacked up to three red blood cells (RBC) and up to three yeast cells. The details of the experimental setup, sample preparation and experimental procedures are described below.

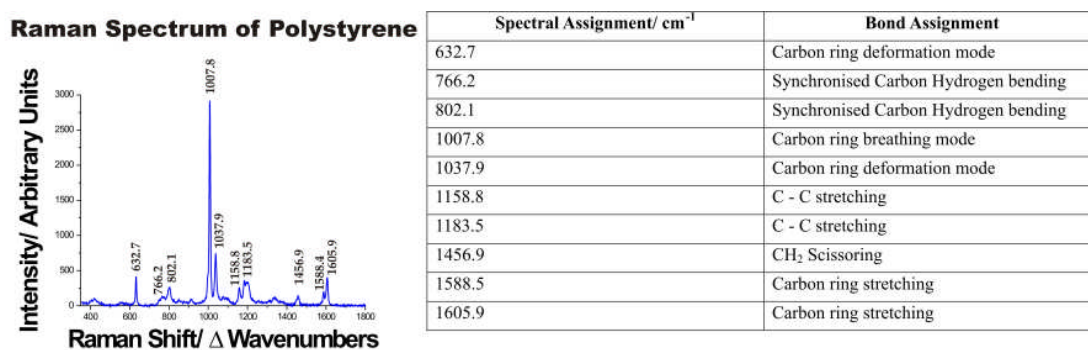


Figure 7(b). Raman spectrum of Polystyrene accompanied by a table displaying the chemical bond assignments for the observed Raman peaks.

### 7.2.1 Experimental Setup

The Raman Tweezers system used to perform the stacking experiments is the same as that described in detail in section 6.2 and shown in figure 6(c) with one small addition. An additional 1070nm Ytterbium fibre laser, IPG photonics YLM-5-1070-LP, is sent into the system, in a similar manner to the system described by Singh et al in 2004 [10]. This laser is required to support the stacking process as the building and holding of large numbers of stacked particles requires more optical power than is available from the diode laser exciting the Raman transitions and normally used in the tweezing and Raman excitation process. This laser is introduced into the system with the use of a short pass filter that will reflect the 1070nm laser light into the optical tweezers but allow any collected Raman signal to be passed through the filter to the spectrograph; a schematic of the altered system can be seen in figure 7(c). The beam is expanded with lenses L4 and L5, to maximise trapping efficiency, and introduced

into the optical tweezers via the short pass filter, which in combination with M6 can be used to align the beam correctly.

We want to examine how the Raman signal evolves with increasing mass in the Raman probe volume thus we want to avoid setting a confocal volume that will affect the data. To this end no external confocal arrangement is included in the setup and the entrance slit of the spectrograph is opened relatively wide,  $500\mu\text{m}$ , and a large CCD area is also used to avoid filtering the signal. This obviously has implications for the resolution of the system; this is affected by two parameters, the size of the image at the entrance slit and the grating used. The spectrograph is equipped with two gratings, a 300 lines/mm and 1200 lines/mm grating; the 1200 lines/mm grating was used for the studies on the polymer microspheres and RBC's, the 300 lines/mm grating was used for the studies on yeast. In combination with a measured image size of  $100\mu\text{m}$  the system has a resolution of  $8\text{cm}^{-1}$  using the 300 lines/mm grating and a resolution of  $2\text{cm}^{-1}$  when using the 1200 lines/mm grating.

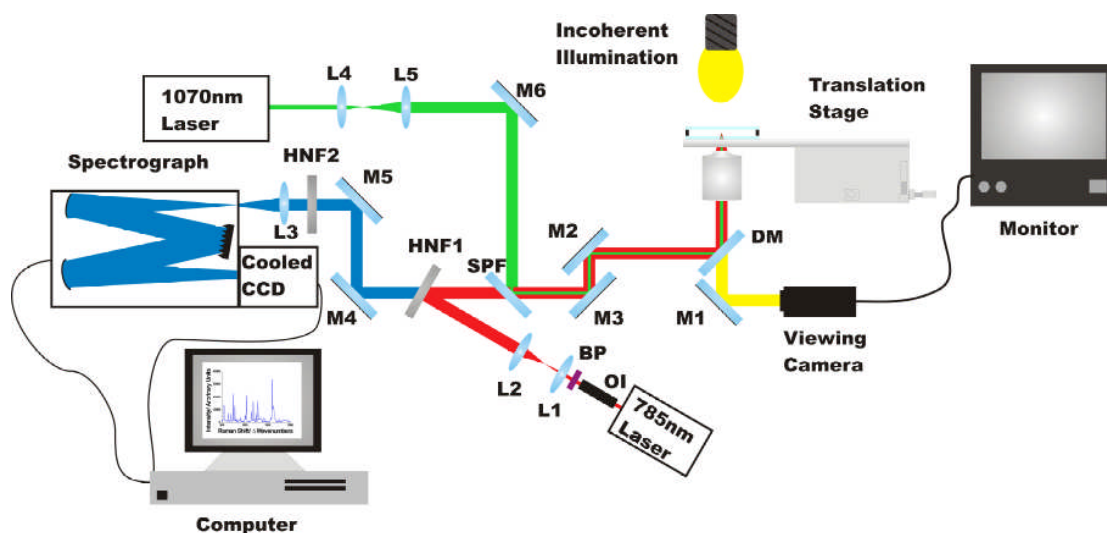


Figure 7(c). A schematic of the Raman system used in this study, it is the same Raman system as described in detail in section 6.2 with the addition of a 1070nm fibre laser to aid the trapping and stacking process. Abbreviations are as follows: M - mirror, L - lens, OI - optical isolator, BP - bandpass filter, DM - dichroic mirror, HNF - holographic notch filter and SPF - short pass filter.

---

### 7.2.2 Samples and Preparation

The polystyrene microspheres were suspended in deionised water to form dilute solutions, it is important that the solutions are dilute to avoid interference when taking data from the optically stacked particles. If the solution is too dense, particles not involved in the stacking process may jump into the trap and alter the experimental conditions. Twenty micro-litres of the sample is then pipetted into the sample chamber, as described in section 6.3.1, and placed on the sample stage for analysis.

The red blood cells were acquired from a volunteer with the use of a heparin coated capillary, to avoid the whole blood clotting, and were then suspended in RPMI 1640 supplemented with 10% fetal calf serum (FCS). The cells were then incubated at 37° until required for the experiment. The cells were again pipetted into a sample chamber for Raman analysis.

The *Saccharomyces cerevisiae* yeast cells were cultured in a Petri dish and kept at room temperature. Although this is not the ideal growth temperature for yeast, which is 30°, the cell type is hardy and able to function in the slightly lower temperature and made the growing and spread of the culture manageable. When the cells were required for Raman analysis a swab of the culture was taken and suspended in saline tween 80 medium; the sample was then pipetted into a chamber and placed on the sample stage for analysis.

### 7.2.3 Experimental procedures

Once the polystyrene sphere samples had been prepared the 785nm laser was set to give 30mW optical power at the back aperture of the microscope objective. Although the 1070nm laser was available to aid the stacking process it was found experimentally only to be required for the stacking of the yeast cells. Initially one

---

sphere of 5  $\mu\text{m}$  size was trapped and ten spectra each of duration 2s were acquired from the sample, a second sphere is then stacked under the first and again ten spectra of 2s duration were acquired. This process is repeated for stacks of up to five particles and in the same manner for the 10 $\mu\text{m}$  spheres. Only single 20 $\mu\text{m}$  and 25 $\mu\text{m}$  spheres are probed as they are too large to be stacked, the experimental conditions are however kept the same and ten 2s acquisitions are taken to compare with the stacked particles. All other experimental parameters were kept constant throughout the experiments on the polymer microspheres to allow an accurate comparison of the data.

In studying the RBC's up to three cells were stacked; the only change in the experimental parameters, from those used to study the polystyrene microspheres, was the acquisition time. The scattered Raman signal from cells is much weaker than that of polymer and a 60s integration time was required to obtain a good quality Raman spectrum.

For the studies of the yeast cells the 300 lines/mm grating was used to examine the acquired Raman spectra. Again spectra were acquired from up to three stacked yeast cells using an integration time of 30s. In stacking the yeast cells 20mW of laser power from the 1070nm was required to aid the building and maintaining of the stack of cells.

#### **7.2.4 The experimental method for stacking microparticles**

The stacking of optical microparticles is a relatively straight forward process and can be achieved as follows. In our experiments we stacked microparticles by focussing the beam at the top of the sample chamber and trapping a series of particles. The first important procedure is to be certain the focal plane of the microscope

---

objective and the laser focus are coincident. This can be achieved by taking an ordinary coverslip and making a small mark on it with an ink pen. By imaging the mark on the surface of the coverslip and then adjusting lens 2, in figure 7(c), until the smallest laser beam spot, reflecting off the top surface of the coverslip, is observed on the monitor we can ensure the imaging and laser foci are coincident. Once we have ensured the laser focus and microscope image plane are coincident we can begin the stacking process. We begin by moving the stage around until we find a particle and place the laser beam over it so it becomes trapped in the beam focus; we then move the particle to the top of the sample chamber. We can tell when it hits the top of the chamber as the particle, that remains in focus as it is trapped, suddenly defocuses; the stage is moved such that the particle is at the top of the chamber but remains in focus. We can then stack a particle beneath the first one by moving the stage in the x, y plane until we find another particle. Most particles will be close to the bottom and appear as dark ‘fuzzy’ spheres on the monitor as they are out of focus; we then move the stage so the laser is over the microparticle at the bottom of the sample chamber. The transverse gradient force will draw the sphere into the laser beam and the axial gradient force, assisted by the scattering force, will draw the particle towards the focus where it will be stored under the already trapped particle. On the monitor the out of focus sphere will appear to be drawn into the beam and then suddenly move into focus as it becomes trapped in a stack beneath the originally trapped particle. Using this method we can stack several microspheres in a vertical stack.

When using the auxiliary 1070nm laser to aid the stacking we must ensure that the two beams overlap exactly to maintain a high Raman collection efficiency. We can overlap the two beams, once they have been aligned into the microscope objective, by looking at the laser beam reflections, from a glass coverslip, on the

---

---

viewing monitor and moving them so that they overlap with the alignment mirrors. It is important to move only the 1070nm beam as movement of the aligned 785nm beam will decrease the Raman collection efficiency. To check the alignment we stack three 5 $\mu$ m polystyrene spheres with the 785nm Raman probe beam whilst the 1070nm beam is blocked. If we view the stack in the monitor and simultaneously block the 785nm beam and unblock the 1070nm beam, so that the stack is now being held by the 1070nm beam, we should observe no movement of the stack of particles if the beams are correctly overlapped. If we do observe movement, the beams are not correctly overlapped and can be adjusted using mirror M6 and the SPF as shown in figure 7(c). Once the alignment has been done and the stacks formed we are ready to carry out quantitative measurements.

All the data was acquired using the above procedures and on the described experimental setup seen in figure 7(c).

### 7.3 Experimental Results and Discussion

Data sets were acquired according to the above procedures and the acquired data showed high repeatability across all the data sets showing a standard deviation in the data of less than 2%.

To gain an initial understanding of the behaviour of the Raman signal, as an increasing mass is placed in the examination volume, we looked at the acquired signal from single optically trapped spheres of sizes 5, 10, 20 & 25  $\mu$ m. It should be noted that the 20 and 25  $\mu$ m spheres were only transversely trapped and not axially trapped as they are much too large to be axially trapped with such small power as provided by the laser exciting the Raman transitions. The results can be seen in figure 7(d).

---

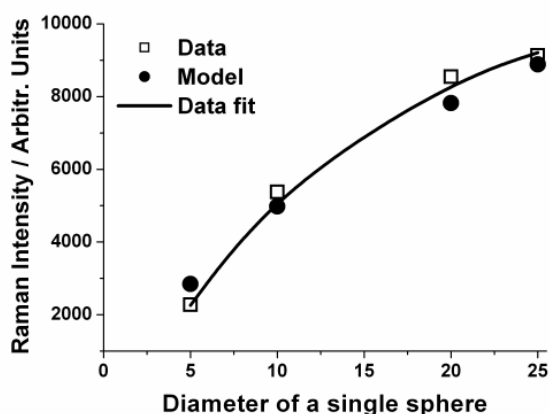


Figure 7(d). Evolution of the intensity of  $1008\text{cm}^{-1}$  peak, of polystyrene, with an increase in the diameter of a single trapped polymer microsphere.

The first point that is evident from the chart is that a linear increase in the diameter of the microparticle does not result in a linear increase in signal intensity. Rather, as demonstrated by Bridges *et al* [8], there appears to be an initial linear section followed by a non linear asymptotic approach to a maximum value. The origin of this shape is dominated by the collection efficiency profile of the microscope objective; the objective is extremely efficient close to the focal plane but as the object moves away from the focal plane the collection efficiency drops off rapidly in a Lorentzian fashion. A collection efficiency profile for the microscope objective used in this experiment can be seen in figure 7(e).

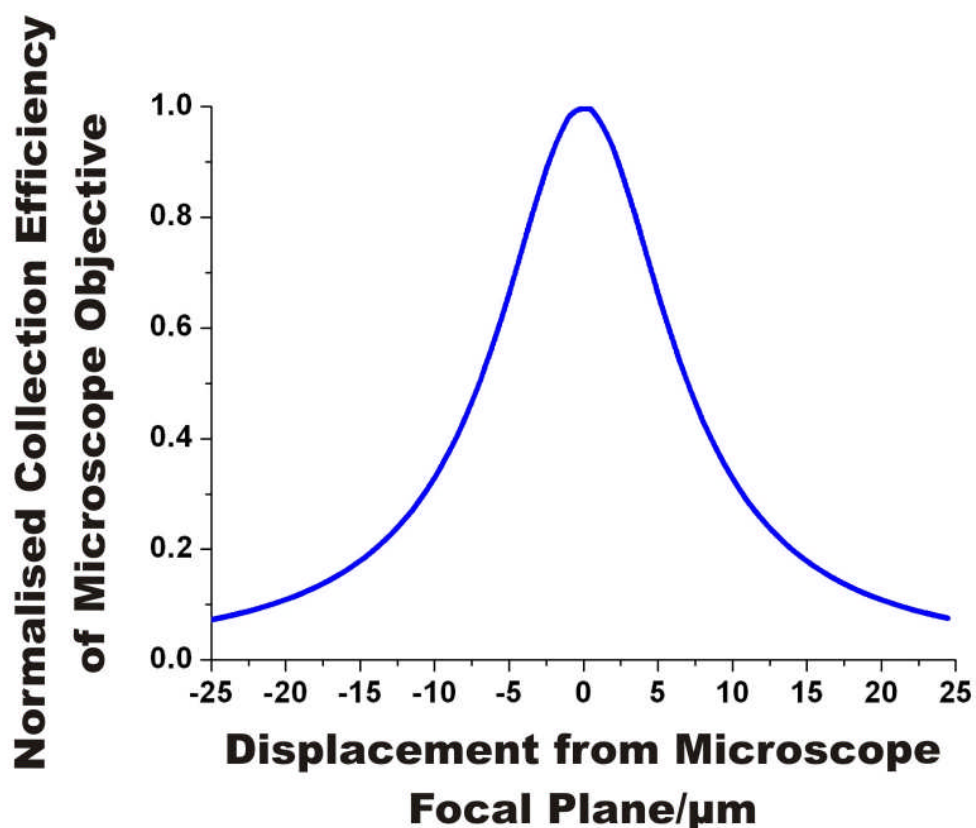


Figure 7(e). Graphical representation of the normalised collection efficiency, calculated using the model in reference 8, of the microscope objective, used in this experiment, as we move from the focal plane.

What is interesting is that the additional volume increase, obtained by examining a larger diameter particle, is not all exposed to the laser hence much of the particle is not contributing Raman scatter or if exposed to the laser is far off axis where the collection efficiency is quite poor and hence contributes little to the total signal collected. This will also influence the shape of the curve to an extent and opens up an interesting question of whether the total volume of the sphere is important or the total depth of the sample is important or indeed a combination of these two factors. The second interesting point of note is that the experimental data is in good agreement with the theoretical model, developed by Veneranda Garcés-Chávez a colleague on the project, based on the collection efficiency of the microscope objective and other experimental parameters.

---

In order to explore further the question of the importance of depth vs. total particle volume in Raman tweezers we stacked up to five 5 and 10  $\mu\text{m}$  microspheres and acquired the data displayed in figures 7(f) and 7(g). As we observed in figure 7(d) the data in both figures 7(f) and 7(g) show the characteristic shape dominated by the microscope collection efficiency and the experimental data agrees well with the theoretical model for the 5  $\mu\text{m}$  spheres and is in reasonable agreement for the 10  $\mu\text{m}$  spheres. The most interesting aspect of this data becomes evident when we combine the data sets on one chart with those of single 20 and 25  $\mu\text{m}$  spheres and can be seen in figure 7(f).

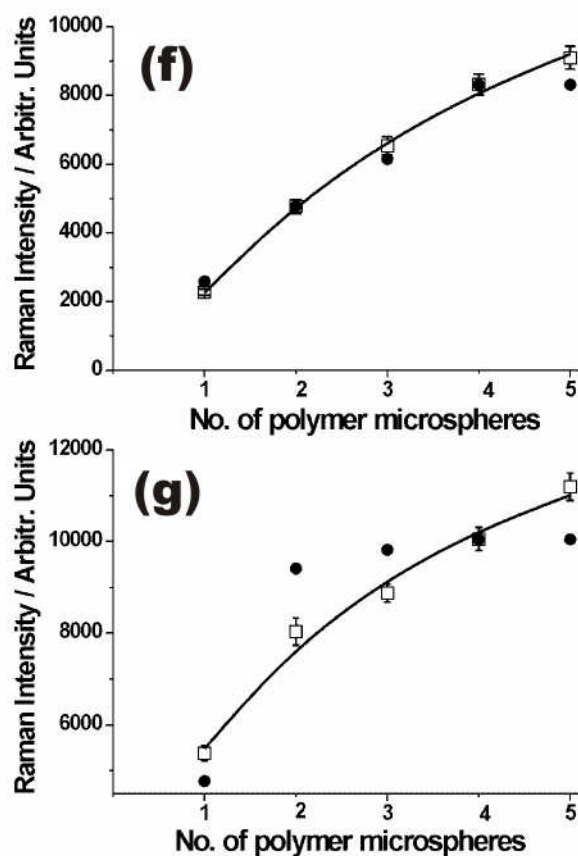


Figure 7(f & g). Figure 7(f) shows intensity of the  $1008\text{ cm}^{-1}$  Raman peak, of polystyrene, with increasing number of stacked  $5\mu\text{m}$  microspheres. Figure 7(g) shows intensity of the  $1008\text{ cm}^{-1}$  Raman peak, of polystyrene, with increasing number of stacked  $10\mu\text{m}$  microspheres.

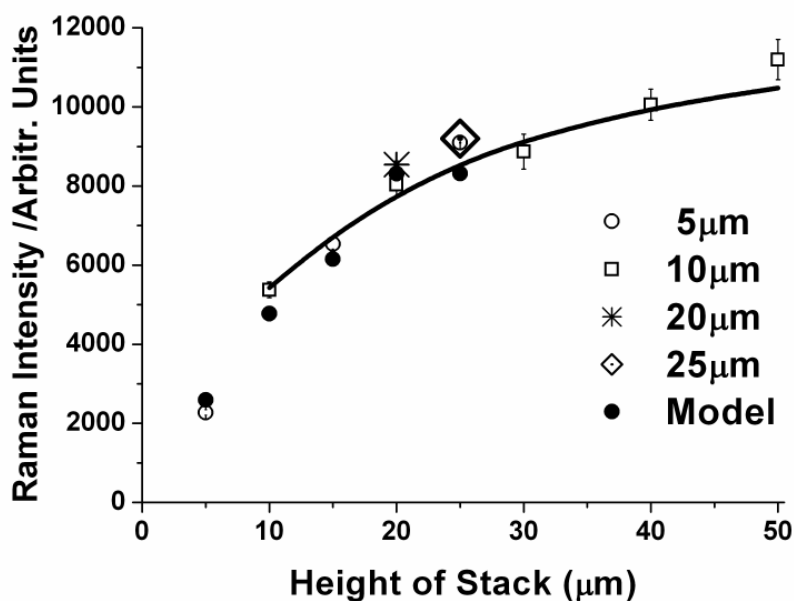


Figure 7(h). A chart displaying the intensity of  $1008\text{ cm}^{-1}$  Raman peak, of polystyrene, for both data sets of stacked  $5$  and  $10\mu\text{m}$  microspheres. Also included are data from single  $20$  and  $25\mu\text{m}$  microspheres and the results of the theoretical model.

Observing figure 7(h) we can see the familiar shape of the curve we discussed when considering figures 7(f) and 7(g) but the most interesting aspect of this chart is the close coincidence of data points representing a single 10  $\mu\text{m}$  sphere and two 5  $\mu\text{m}$  spheres. This result is not what we may have expected as the total mass in the beam is different for the two situations, as volume scales as  $r^3$ , rather only the total depth remains the same, this effect is illustrated in figure 7(i). We can also see the same coincidence in the data points at depths of 20 and 25  $\mu\text{m}$ . The underlying origins of this effect can be more readily understood if we add a further data set to figure 7(h) of five stacked 2  $\mu\text{m}$  spheres, the data from the 2  $\mu\text{m}$  spheres was acquired in the same manner as previously described for the 10 and 5  $\mu\text{m}$  spheres. The results can be seen in figure 7(j).

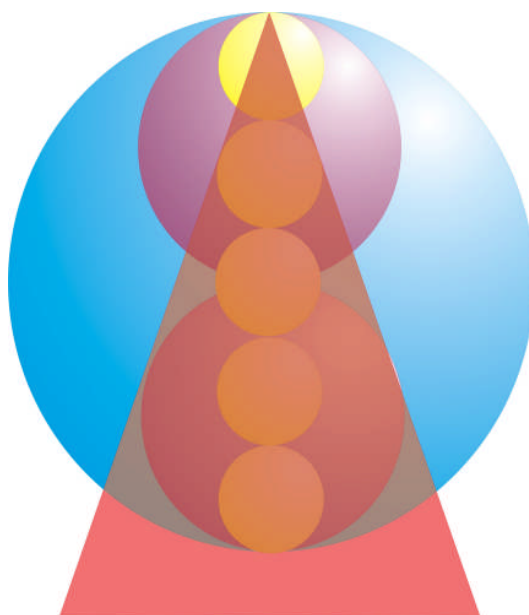


Figure 7(i). Diagram depicting the volume occupied by a single 10  $\mu\text{m}$  sphere, shown in blue, in comparison to two 5  $\mu\text{m}$  spheres, shown in purple, and five 2  $\mu\text{m}$  spheres, depicted in yellow. Although the total depth of the stacks of particles remains constant the physical volume, occupied by the particles, is very different. Also shown in the diagram is a depiction of the focussed laser beam shown in red.

What is immediately obvious from figure 7(j) is that the data collected from the 2  $\mu\text{m}$  spheres does not fit into our pattern of total stack depth being more important than the overall volume occupied by the stacked spheres, only the data from one sphere

---

---

appears to fit with the other data. The reason for this becomes clear if take a second look at figure 7(i), where the 2  $\mu\text{m}$  spheres and a depiction of the laser beam have been superimposed onto the 10 and 5  $\mu\text{m}$  spheres. It becomes clear that the shape of the focussed beam, used for the trapping, plays an important role in the collected signal intensity. There are a couple of important considerations, when considering the effect of the beam shape on the collected signal intensity, which may appear obvious but should be kept in mind. The first is that we can only collect signal from areas where the laser beam interacts with the spheres and secondly, as the beam focuses the power density increases that means the intensity of the Raman scatter will increase as they are directly proportional. If we consider first the 5 and 10  $\mu\text{m}$  spheres we can see that the beam is interacting with virtually the same amount of polystyrene thus the signal intensities collected are very similar. However if we look at the stack of five 2  $\mu\text{m}$  spheres they only fill a small portion of the available laser beam thus the collected Raman signal is much weaker, this accounts for the data collected at sample depths of ten microns but does not account for the coincidence in the data at twenty microns sample depth where the four 5 $\mu\text{m}$  spheres will be much narrower than the laser beam width in comparison to the two 10 $\mu\text{m}$  spheres. This effect is accounted for through a combination of the poor microscope collection efficiency so far from the focal plane and the much reduced power density in the beam so far from the focus. This means that there is little Raman scatter collected from the extra volume of polystyrene in the two 10  $\mu\text{m}$  spheres hence produces the similar values, of collected Raman intensity, for the four 5  $\mu\text{m}$  spheres and the two 10  $\mu\text{m}$  spheres.

---

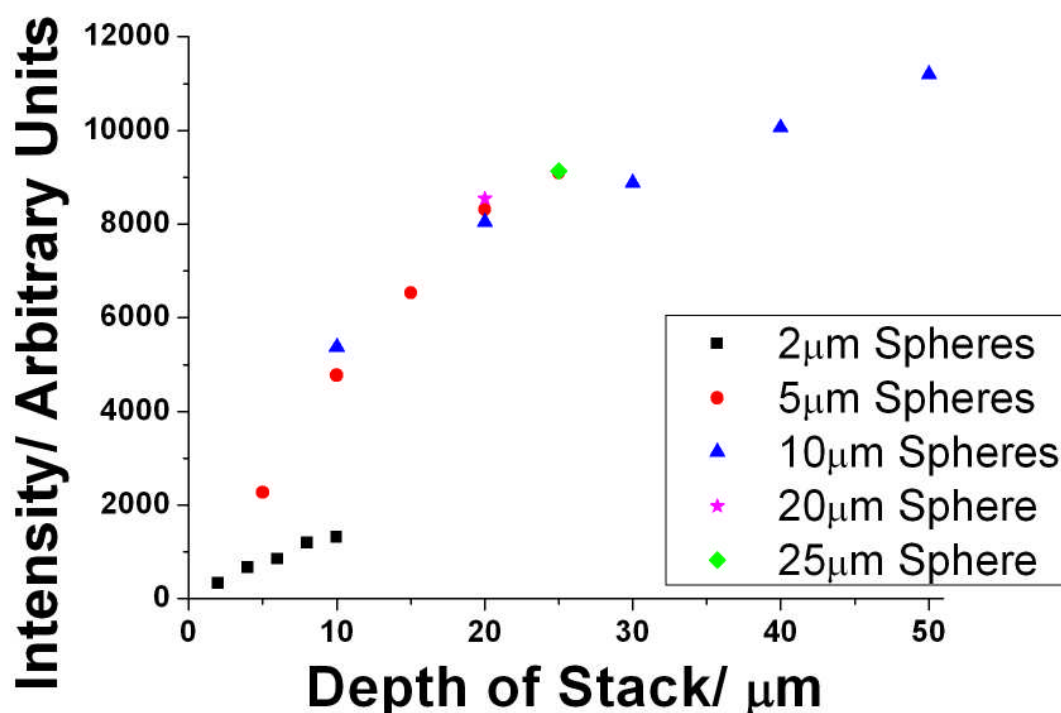


Figure 7(j). A chart displaying the intensity of  $1008\text{cm}^{-1}$  Raman peak, of polystyrene, for data sets of stacked 2, 5 and 10  $\mu\text{m}$  microspheres, also included are data from single 20 and 25  $\mu\text{m}$  microspheres.

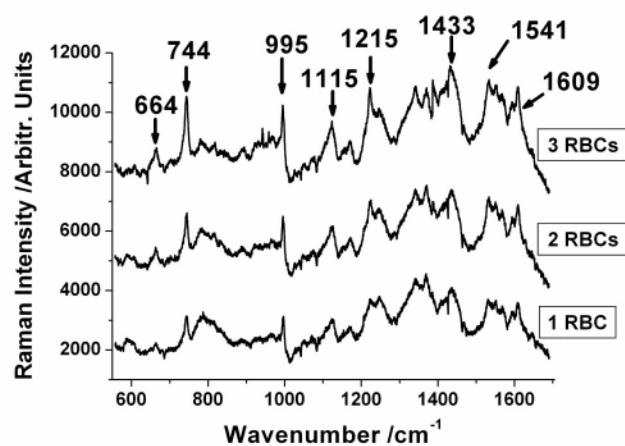
The conclusions we can take from this study, on the stacking of polystyrene microspheres, are that the majority of the collected Raman signal comes from a depth of - 10  $\mu\text{m}$  from the focal plane of the microscope and increasing the mass beyond this does add to the collected signal intensity but with ever decreasing importance as we move further from the focal plane. What is a very obvious but potentially useful conclusion is that increasing the number of spheres increases the signal intensity; this could be particularly valuable in the study of weak Raman scatters. By increasing the mass, or number of particles, higher signal intensities can be obtained, hence a reduced time could be used to obtain quality Raman spectra from what are traditionally known as weak Raman scatters.

One area of study where the additional signal obtained by the stacking technique could prove extremely useful is in the study of biological cells, an area that

---

has enjoyed a large growth of interest in recent times. Cellular samples tend to be weak Raman scatters and acquisition times to obtain a quality signal are often on the order of several minutes so the stacking technique could provide a reduction in acquisition time by increasing the overall signal. Furthermore the engagement of many cells simultaneously in the stacking technique will provide a signal that is a pseudo average of the cells, removing to some extent the effects of inter cell variations, such as position in the cell cycle, thus giving a truer representation of the behaviour of the cellular population under study. The use of the stacking technique, in the study of cell populations, offers up the opportunity to gain rapid and representative spectra without the need to make long acquisitions from single cells and averaging their resultant spectra.

In order to evaluate the potential of this technique we stacked up to three red blood cells according as described in section 7.2.3. The resulting spectra, which agree well with previously published spectra for RBC [11], can be seen in figure 7(k) accompanied by a chemical assignment for the major Raman bands [11, 12].



Raman Peak Position/ $\text{cm}^{-1}$	Bond Assignment
664	Haemoglobin vibration $\nu_7$
744	Haemoglobin vibration $\nu_{14}$
995	$[\delta(\text{C}_\beta\text{C}_i)]$
1115	Pyrrole half ring stretching $\nu_{22}$
1215	$[\delta(\text{C}_m\text{H})]$
1433	Pyrrole half ring stretching $\nu_4$
1541	$\nu_{11}(\text{C}_\beta\text{C}_\beta)$
1609	Oxygenated Haemoglobin $\nu(\text{C}_\alpha=\text{C}_\beta)$

Figure 7(k). Raman spectra of up to three stacked Red Blood Cells, the spectra have been offset to ease viewing. Accompanying the spectra are chemical bond assignments for the major Raman peaks.

Looking at figure 7(k) we can immediately see that by increasing the number of cells in the stack we increase the intensity and clarity of the Raman peaks, perhaps most importantly peaks that are small and indiscernible with one RBC become clear and evident with three stacked RBCs. In order to demonstrate this point more effectively figure 7(l) shows a bar chart detailing the signal to noise ratios for a few of the major Raman peaks as up to three cells are stacked. A quick visual inspection demonstrates that the stacking technique results in sizeable increases in the signal to noise ratio that should lead to rapid and detailed spectra. A detailed examination of the spectra in figure 7(k) reveals one of the most interesting aspects of this study, we observe two sets of peaks that present different relative intensities:  $1215 \text{ cm}^{-1}$  and  $1250 \text{ cm}^{-1}$ ;  $744 \text{ cm}^{-1}$  and  $780 \text{ cm}^{-1}$  as we increase the number of cells stacked. This may under some circumstances be construed as a chemical change but in this situation is more likely due to be the result of intra-population variation in the cells that we have talked about

in this discussion. The cells will all be in different phases of growth, as the culture has not been synchronised. Thus they have a different balance of biochemicals that may alter slightly the peak ratios. As more cells are stacked these variations in the acquired spectra are reduced and a truer picture of the population emerges.

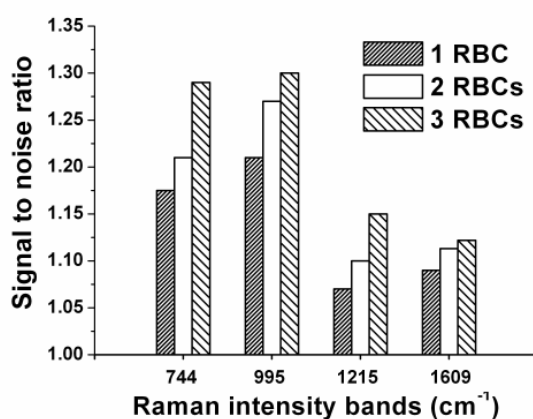
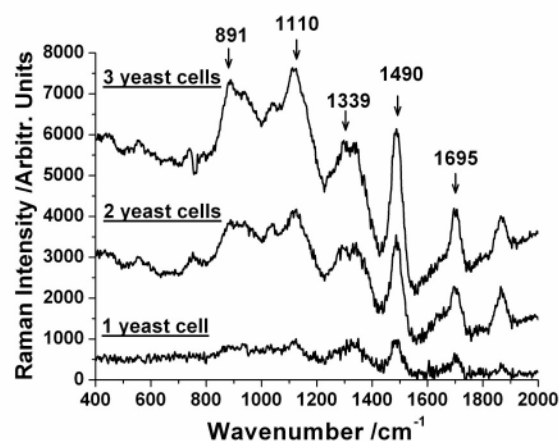


Figure 7(l). Chart displaying the Signal to noise ratios for a few of the major Raman peaks of Red Blood Cells as up to three cells are stacked.

As well as studying red blood cells, *Saccharomyces cerevisiae* yeast cells were also studied to evaluate the performance of the stacking technique when applied to non-uniform cellular samples. As before, spectra were acquired from up to three stacked cells according to the procedures described in section 7.2.3. The results, which agreed well with previously published spectra [13], can be seen in figure 7(m) accompanied by a chemical assignment for the major Raman peaks [13].



Raman Peak Position/ $\text{cm}^{-1}$	Bond Assignment
891	DNA backbone
1110	C-N
1339	Amide III deformation
1490	Lipids
1695	Amide I deformation

Figure 7(m). Raman spectra of up to three stacked yeast cells, the spectra have been offset to ease viewing. Accompanying the spectra are chemical bond assignments for the major Raman peaks.

Inspecting figure 7(m) we can readily observe how the stacking process dramatically increases the intensity of the Raman peaks especially at 891 and 1339  $\text{cm}^{-1}$  where the peaks were barely discernable with only one cell in the trap. This demonstrates effectively how the stacking process allows us to extract detailed spectra in short times from biological cells. We should note that the peak at 1890  $\text{cm}^{-1}$  is unexpected and it is believed to be a remnant from the pump source, at 980nm, of the 1070nm fibre laser used in this experiment to support the stack, the reason it increases with the number of stacked cells is most likely down to the cells acting as a small ‘mirror’ hence more cells, more of the pump source is reflected.

## 7.4 Conclusions

The technique of optical stacking requires no alteration to existing Raman tweezers setups and can be readily employed. It is often avoided as researchers often wish to study single particles or single cells but we have seen how optical stacking

---

can be used in Raman tweezers to provide rapid representative spectra of small cell populations without the need to resort to averaging over spectra from several individually studied cells.

We began by studying trapped and stacked polystyrene microspheres to evaluate how the intensity of the Raman signal evolved as we stacked ever increasing numbers of particles and particles of different sizes. We found that the collected intensity, of the Raman signal, was governed by three main factors: the collection efficiency profile of the microscope objective, the shape of the focussed laser beam and the area of the beam occupied by the trapped spheres. We found close to the beam waist it is important to have particles stacked that are larger than the beam as it is close to the waist that the microscope collection efficiency is high and the laser power density is also high meaning a strong Raman signal is collected. We can continue to stack particles to increase the mass of polystyrene in the beam but as we move further away from the beam waist the microscope collection efficiency and laser power drops off so the effect is less pronounced. By stacking particles in the Raman tweezers laser beam we can increase our signal allowing us to acquire quality spectra faster.

The area where this technique could be extremely useful is in the study of small cell populations. The stacking technique allows us to obtain good quality Raman spectra in relatively short timescales from samples that are traditionally thought of as weak Raman scatterers. By stacking red blood cells and yeast cells we seen how we may increase the signal and improve the signal to noise ratios. Furthermore as we are probing several cells simultaneously we obtain a pseudo average of the population reducing the effects, on the Raman spectra, of intra population variation. The stacking technique allows us to gain rapid and representative Raman spectra of small cell populations.

---

---

We should stress that this technique requires little or no alteration to existing Raman tweezers setups allowing rapid and representative signals to be acquired without complicated instrumentation or statistical processing.

## 7.5 References

- [1] Paterson L. **Novel Micromanipulation Techniques in Optical Tweezers**. 2003  
PhD Thesis; University of St. Andrews: 39-51
- [2] Gauthier RC and Ashman M. **Simulated dynamic behaviour of single and multiple spheres in the trap region of focussed laser beams**. *Applied Optics* 1998; **37**: 6421-6431
- [3] Zemanek P, Jonas A, Sramek L, Liska M: **Optical trapping of nanoparticles and microparticles by a Gaussian standing wave**. *Optics Letters* 1999; **24**:1448-1450
- [4] MacDonald MP, Spalding GC and Dholakia K. **Microfluidic sorting in an optical lattice**. *Nature* 2003; **426**: 421-424
- [5] Fu AY, Spence C, Scherer A, Arnold FH and Quake SR. **A microfabricated fluorescence-activated cell sorter**. *Nature Biotechnology* 1999; **17**: 1109-1111
- [6] Chiou PY, Ohta AT and Wu MC. **Massively parallel manipulation of single cells and microparticles using optical images**. *Nature* 2005; **436**: 370-372
- [7] Chan JW, Taylor DS, Zwerdling T, Lane SM, Ihara K and Huser T. **Micro-Raman spectroscopy detects individual neoplastic and normal haematopoietic cells**. *Biophysical Journal* 2006; **90**: 648-656
- [8] Bridges TE, Houlne MP and Harris JM. **Spatially Resolved Analysis of Small Particles by Confocal Raman Microspectroscopy: Depth Profiling and Optical Trapping**. *Analytical Chemistry* 2004; **76**: 576-584

- 
- [9] Gessner R, Winter C, Rosch P, Schmitt M, Petry R, Kiefer W, Lankers M and Popp J. **Identification of Biotic and Abiotic Particles by Using a Combination of Optical Tweezers and In Situ Raman Spectroscopy.** ChemPhysChem 2004; **5**: 1159-1170
- [10] Creely CM, Singh GP and Petrov D. **Dual wavelength optical tweezers for confocal Raman spectroscopy.** Optics Communications 2005; **245**: 465-470
- [11] Xie C, Dinno MA and Li YQ. **Near-infrared Raman spectroscopy of single optically trapped biological cells.** Optics Letters 2002; **27**: 249-251
- [12] Ramser K, Logg K, Goksor M, Enger J, Kall M and Hanstorp D. **Resonance Raman spectroscopy of optically trapped functional erythrocytes.** Journal of Biomedical Optics 2004; **9**: 593-600
- [13] Xie C and Li YQ. **Confocal micro-Raman spectroscopy of single biological cells using optical trapping and shifted excitation difference techniques.** Journal of Applied Physics 2003; **93**: 2982-2986

---

# 8. Early Detection of Cervical Neoplasia by Raman Microspectroscopy

---

*One of the most promising applications for Raman spectroscopy is in the field of cancer diagnostics as the technique can readily probe the biochemical nature of samples without the need for markers or advanced preparation offering the opportunity of making an early and objective diagnosis. In this chapter we examine the potential of our Raman tweezers system to detect the presence of Human Papillomavirus induced cervical neoplasia and demonstrate the compatibility of this technique with current medical screening methods and clinical practice.*

---

## 8.1 Motivations

Cervical cancer is the second most common cancer in women worldwide and infection with oncogenic, or ‘high-risk’, human papillomavirus (HPV) types is the most significant risk factor in its aetiology [1]. HPV is present in 99.7% of invasive cervical cancers [1, 2] and, therefore, early detection of the effects of HPV infection, particularly when accompanied by neoplastic changes, could improve the diagnosis of HPV-associated neoplasia. Raman spectroscopy is emerging as a powerful diagnostic technique in the field of cancer medicine and in this chapter we will see how Raman tweezers spectroscopy can be used to detect the presence of the

---

---

Human Papillomavirus in primary human cell cultures thus allowing us detect the earliest neoplastic changes associated with the onset of cervical cancer. The ability to study single cells easily with use of Raman tweezers spectroscopy makes it extremely compatible with the samples gathered from pap smears demonstrating how this technique sits easily with current screening practices for cervical cancer.

## **8.2 Prospects for Raman spectroscopy in Cancer diagnostics**

One of the most promising areas of application for Raman spectroscopy is in that of cancer diagnostics. Current methods of detecting and diagnosing cancers range from patient self examination through to dedicated screening programmes such as mammography and pap smears. If these methods flag up something abnormal a biopsy normally follows whereupon a pathologist will subsequently examine the acquired cells or tissue specimens and determine a diagnosis based upon any morphological abnormalities. This subjective analysis method is effective but often results in a significant number of false positives/negatives [3] that can lead to cancers going undetected and some patients having unnecessary invasive medical procedures. For these reasons an objective screening technique that can confidently detect neoplastic changes at the very earliest stages would be extremely advantageous to improve patient survival and provide effective treatments.

Optical diagnostic techniques, such as drug-assisted tumour fluorescence [4], natural tissue fluorescence [5] or Fourier transform infrared spectroscopy [6] have attracted much interest recently as they offer the possibility of non-intrusive objective diagnostics both *in vitro* and *in vivo*. Emerging as a forerunner from these diagnostic technologies is Raman spectroscopy as it probes the biochemical nature of the samples, without the need for chemical markers or patient ingested fluorescent drugs,

---

opening up the possibility of not only detecting the cancer but potentially grading the extent of neoplastic development. Furthermore Raman spectroscopy requires little sample preparation and is compatible with endoscopic techniques [7].

With the potential benefits of using Raman spectroscopy in cancer diagnostics many groups have investigated its use to discriminate between normal and potentially cancerous samples. Much of this work has centred on traditional Raman spectroscopy and has been used to study biopsy samples of a large number of cancers from Breast cancer [8] to prostate cancer [9] and even brain tumours [10]. Although the inclusion of an exhaustive list is not appropriate here a good review detailing these studies can be found in reference 11. The analysis of biopsy tissues has been very successful and has been followed by an interest in the analysis of neoplastic development at the single cell level as biopsy tissue will contain many components from the extracellular matrix that may cause interference in the acquired Raman spectra. Although we should note that there are components, such as collagen, in the extra cellular matrix that are important in tumour formation and development. However the very earliest stages in neoplastic development will occur in the cells and thus Raman studies at this level have attracted a lot of interest. Raman microspectroscopy has been used to study gastric adenocarcinoma cells derived from biopsy samples [12], derived healthy and cancerous human liver cell lines [13] and biopsy derived prostatic adenocarcinoma cell lines [14] to name a few. Notably this last paper was able to grade the neoplastic development represented by the different derived cell lines.

As we have discussed throughout this thesis Raman tweezers microspectroscopy is an excellent tool, for many reasons, for the study of single cells; thus it was not long before the potential of Raman tweezers spectroscopy, to discriminate between healthy and abnormal cells, was recognised and to date three

---

---

papers have been published detailing its use in this field. In 2005 Hamden et al detailed work examining transformed cells infected with Kaposi's sarcoma-associated herpesvirus, a known tumour causing virus, and were able to discriminate between infected and uninfected cells [15]. This was followed up by work published by Chan *et al* showing how Raman tweezers spectroscopy could be used to discriminate between neoplastic lymphocytes and their normal counterpart cell line [16]. Finally, also in 2006, Chen et al published research discriminating between cells obtained from normal tissue and tissues with colorectal cancer [17]. Raman Tweezers spectroscopy is inspiring interest for use as a cancer diagnostic due to the biochemically sensitive nature of Raman spectroscopy and the advantages that are brought to the technique through the optical trapping aspect of the system.

### **8.3 Cervical cancer and the Human Papillomavirus**

In order to understand the full implications of our results it is useful to understand how the virus influences the host cell and disrupts its normal function resulting in neoplastic development. Upon infection the HPV virus attaches to host cells via cell surface heparan sulphate [18], once inside the cell the virus migrates to the host cells nucleus. As HPVs only code for 8-10 proteins they must harness the host cells own transcription and replication machinery in order to proliferate. A schematic of the HPV circular DNA genome can be seen in figure 8(a) [19] and shows a number of gene sequences that are each involved in the host infection and viral replication process.

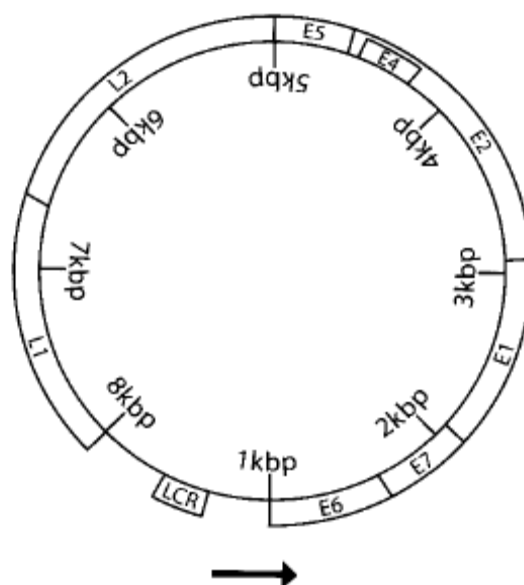


Figure 8(a). A schematic of the circular HPV genome [19] showing the important reading frames that play a role in the potential development of cervical neoplasia.

The process begins when the host cells transcription factors, proteins that mediate DNA reading and the subsequent building of the DNA encoded proteins and other products, interact with the long control region (LCR) of the viral genome and subsequently begin the transcription of the E6 and E7 genes. The main function of the HPV E6 and E7 proteins is to subvert cell growth pathways and modify the cellular environment in order to facilitate viral replication. The first gene to be transcribed is the E6 gene whose product binds to and inactivates the tumour suppressor protein, p53, negating the ability of the cell to repair its DNA and most importantly undergo apoptosis. In dangerous known cancer causing strains of HPV, such as HPV-16, HPV-18 and HPV-33, the binding of the E6 gene product to p53 is strong. The next gene to be transcribed is the E7 gene whose product binds to and inactivates pRb, blocking the formation of Cyclin Dependent Kinases, that could block the cell cycle, and allowing the release of the transcription factor E2F-1 that drives the cell into S phase [20]. Again in known cancer causing strains of HPV, the binding of the E7 gene products to pRb is strong. The E7 gene is known to be able to extend the lifespan of primary keratinocytes and is capable of immortalising these cells [21]. The E1 gene is

---

transcribed next, the E1 gene product is essential for DNA replication and binds to the long control region of the viral genome and is believed to facilitate DNA replication through physical interaction with numerous components of the cellular DNA machinery [22, 23]. The process begins to wind down with the transcription of the E2 gene; the E2 gene product binds to the promoters from which the transcription of the E6 and E7 genes are initiated thus suppressing the expression of the E6 and E7 gene products [24]. This essentially acts to allow the release of host cells p53 and pRb proteins and with it a return to the normal differentiation process of the host cell. Next in the sequence the E5 gene is transcribed releasing a protein that increases protein kinase activity, an enzyme that alters proteins, resulting in continued growth and proliferation of the host cell [25]. The final genes, E4 L1 and L2, govern the formation and release of viral particles from the host cell to allow the infection process to continue in surrounding cells [19]. The aggressive viral strains continue to infect the host cell by incorporating themselves into the host cells DNA.

The more aggressive strains of HPV, such as types 16, 18 and 33, can lead to cancer due to the fact that when they incorporate themselves into the human genome the E2 gene is often damaged thus the virus is no longer regulating the expression of its E6 and E7 genes [26]. As the E6 and E7 genes interfere with the cell growth pathways, not allowing the cell to effectively exit the cell cycle to repair DNA or allow the initiation of the apoptosis process, this allows the proliferation of mutations in the DNA to go unchecked which can eventually lead to neoplasia.

Although infection with HPV will not necessarily lead to cancer it is believed that dangerous strains of the virus, HPV-16, HPV-18 and HPV-33, are a necessary factor in the development of cervical cancer [1], thus the Raman spectroscopic study of and subsequent detection of samples expressing HPV would allow us to detect the

---

---

possibility of cancer at the earliest possible stage potentially improving patient outcome and care.

## **8.4 Experimental Aims**

In this chapter we aim use our Raman tweezers spectroscopy system to discriminate initially between primary human keratinocytes, a normal healthy cell culture, and CasKi cells, an HPV type-16containing cervical carcinoma derived cell line. This represents a discrimination between healthy and an advanced form of cervical cancer. To examine further the discriminatory ability of Raman tweezers we then aim to discriminate between primary human keratinocytes and the same cells expressing the HPV 16 E7 protein, which has been shown to lead to keratinocyte immortalisation, representing the detection of possible cervical cancer development at the earliest possible stage.

Finally, we aim to investigate the effects of fixation, which is carried out routinely on clinical samples, on the ability of Raman spectroscopy to discriminate between these cell types. Fixation is a chemical process by which cells, and indeed tissues, are preserved from decay terminating any ongoing biochemical reactions. This preserves the sample for microscopic study in a stable intact, but obviously dead, manner.

These studies should allow us evaluate the effectiveness of Raman tweezers in the detection of cervical neoplasia and evaluate the compatibility of this technique with current clinical practice.

---

## 8.5 Previous Studies on Cervical Neoplasia

Much of the optical based detection of cervical neoplasia has centred on fluorescence and Infrared spectroscopy [5, 6]. There have been however a few studies examining the use of Raman spectroscopy to detect cervical abnormalities. In 1998 Mahadevan-Jansen *et al* examined biopsies, with Raman spectroscopy, that were pathologically graded as normal, metaplastic and displaying cervical intraepithelial neoplasia (CIN) [27]. The researchers were able to discriminate between them with the aid of a diagnostic algorithm based on Raman peak ratios. In 2001 the same group published work [28] detailing an *in vivo* Raman probe that the authors successfully used to discriminate between healthy tissues and squamous dysplasia, a precursor to cervical cancer. Most recently, in 2006, Krishna *et al* published work where they showed how Raman spectroscopy could be used to discriminate between normal and malignant biopsy samples with aid of the statistical technique principle component analysis [29]. The use of statistical models is an important part of the diagnostic process as it removes the subjective analysis of the spectra by the researcher's eye and allows for a more objective analysis.

The use of Raman spectroscopy at a single cell level, similar to material available from Pap smears, to detect the presence and effect of HPV has yet to be evaluated and offers up a unique opportunity to exploit the benefits and advantages of Raman tweezers spectroscopy. In fact, as we have seen, Raman tweezers spectroscopy has been used in the examination of Kaposi's sarcoma-associated herpesvirus in haematopoietic cells [15] so it should be ideal for the study of the Human Papillomavirus.

---

## 8.6 Materials and Experimental Methods

### 8.6.1 Raman Tweezers experimental setup

For this experiment we used the evolved Raman tweezers microspectroscopy system, based around the commercial microscope, developed throughout this thesis and detailed in section 6.4. Although this is a very effective system the large nature of the cells, used in this study, makes them very difficult to axially trap so we must examine them on the surface of the sample chamber. Due to the large fluorescence of silica coverslips we used quartz coverslips to form our sample chamber as they have significantly lower fluorescence and allow the acquisition of good quality Raman spectra. We should note that the construction of the sample chamber remains the same as that described in section 6.3.1. Despite losing the ability to z-trap the cells we still retain the advantage of transverse trapping avoiding any possibility of the cell drifting out of the laser beam during Raman acquisition.

To probe the cells, a Nikon 50x NA 0.9 oil immersion microscope objective was used to focus the laser onto the sample and was used in combination with 200 $\mu\text{m}$  pinhole placed at the image plane of the microscope to form a confocal volume of diameter 4  $\mu\text{m}$  and depth of 3  $\mu\text{m}$ . This confocal volume allows us to suppress any remaining fluorescence from the quartz coverslips whilst allowing us to probe a large area of the cells nucleus, where most of the important information concerning the effects of the virus is likely to be. Although we should note the large confocal volume is also likely to partially examine the membrane and cytoplasm above and below the nucleus. The laser power was set to give 16mW of optical power at the focus which in combination with a spectral acquisition time of 120s allowed us to collect good quality Raman spectra that had a resolution, using the 300 lines/mm grating, of approximately  $6\text{cm}^{-1}$ .

---

This experimental arrangement and set of experimental parameters was used to examine all samples studied in this chapter.

### **8.6.2 Cell types, cell culture and sample preparation**

Three cell types were used in these studies: PHKs, PHKs expressing the HPV-16 E7 protein and CasKi cells. These cells were largely cultured and prepared by Dan Smith and colleagues in the molecular and structural virology group at the Bute medical school in St. Andrews.

Primary (normal) human keratinocytes (PHKs) from neonatal foreskin (Cambrex) were used as normal cells and cultured, by Dan Smith, in keratinocyte growth medium-2 (KGM-2) containing the supplied supplements (PromoCell) as described in reference 30.

To create Primary Human Keratinocytes expressing the HPV-16 E7 protein healthy PHKs were infected according to the following procedure by Rachel Lyman and subsequently cultured by Dan Smith. A retroviral packaging line (PA317) containing wild-type HPV 16 E7 cloned into the pLXSN vector and under the control of the Moloney murine leukemia virus (MoMuLV) promoter-enhancer sequences [31] was obtained from the ATCC, and cultured in Dulbecco's modified Eagle's medium containing 10% fetal calf serum. To generate keratinocytes expressing HPV 16 E7, the packaging line was left overnight in KBM-2 to allow viral particles to accumulate. The virus-containing supernatant was filtered (0.45  $\mu\text{m}$  cellulose acetate filter), then combined with an equal volume of KBM-2 containing hexadimethrine bromide (polybrene) at 12  $\mu\text{g}/\text{ml}$ . Five ml of this solution was added to monolayer PHKs at approximately 10 % confluency in 25  $\text{cm}^2$  flasks, and left in direct contact with the cells for 7 h to allow infection to occur. Fresh medium was then applied and the

---

---

supernatant discarded. Cells were allowed to recover for 24 h, followed by selection with 150  $\mu\text{g/ml}$  G418 for 4 days. After this time, all non-infected control cells exposed to the same concentration of G418 were dead.

CaSki cells, cultured partially by Dan Smith, were obtained from the ATCC and cultured at 37°C in Dulbecco's Modified Eagle Medium (DMEM) supplemented with Fetal Calf Serum (10% by volume), penicillin (100mg/ml), streptomycin (100U/ml) and glutamine (2mmol/L).

To compare live and fixed cells, cells were fixed, by Dan Smith, in ethanol as follows: growing cells were harvested using trypsin-EDTA, pelleted by centrifugation at 600g for 5 min, resuspended in PBS, pelleted and resuspended in 70% (v/v) ethanol. The samples were stored under ethanol in a freezer until required for examination.

### **8.6.3 Experimental procedures**

Initially, before commencing Raman acquisitions, we need to prepare the samples. If we are studying live cells the cultures had to be removed from the incubator and put into suspension. These cells are epithelial cells and as such their natural state is to grow in layers so when they are growing in the incubator they form a layer attached to the bottom of the culture flask. The cells are 'bathed' in 2 ml of trypsin EDTA, an enzyme that cleaves the collagen fibres that attach the cells to the flask, to release them from the flask. The cells then have 8 ml of their respective growth medium added that deactivates the trypsin, to stop it causing any damage to the cells, and resulting in a suspension of cells. The cells won't begin to reattach to their container for approximately two hours giving a window for Raman examination. When we are ready to undertake the spectroscopy 20  $\mu\text{l}$  of cell suspension is pipietted

---

---

into a quartz sample chamber and transferred to the heated microscope stage. The cells are suspended in growth medium containing nutrients; however they are dilute enough such that no detectable Raman signal is acquired from them in time required to examine the cells. If we are to study fixed cells we remove a vial of the cells, suspended in ethanol, from the freezer and spin the cells into a pellet, at the bottom of the vial, using the centrifuge set to 400g. The ethanol has a very strong Raman signal and must be removed as it would potentially mask the Raman signal from the cells. Once the cells have been centrifuged, a pipette is used to remove the ethanol leaving only the pellet of cells at the bottom of the vial. The cells are then suspended in phosphate buffered saline (PBS) which like the growth medium displays no Raman signal in the time required to analyse the cells. Again 20 $\mu$ l is pipetted into a quartz sample chamber and transferred to the Raman tweezers system.

Once we have our sample on the microscope stage the flip mirror is set to the camera position and a cell can be visualised on the monitor. The z focus of the microscope is adjusted until the cells nucleus becomes clearly visible, under bright field illumination, and is then moved over the laser beam. The flip mirror is set to the Raman position and a spectrum is then acquired. Once the spectrum is acquired the cell is again visualised on the monitor and moved sideways out of the laser beam so we may acquire a background spectrum. Even though we have imposed a confocal volume there is still measurable fluorescence interference thus we want to measure it so it can be later subtracted. This process is repeated on different cells to build up a library of Raman spectra for each cell type. It is important to take a background for each cell as they vary in size thus have different proximities to the quartz coverslip which is the largest factor influencing the shape of the background fluorescence.

---

Spectra were taken from several different cultures of each cell type to ensure the repeatability of the results and in total, single spectra and backgrounds were acquired from 33 live PHKs, 33 live PHKs expressing HPV 16 E7, 32 live CasKi, 50 fixed PHKs and 50 fixed PHKs expressing HPV 16 E7 and 48 fixed CasKi. With our data sets acquired we can then think about the spectral processing and analysis. Spectra were acquired, using the previously mentioned parameters, in the range of 782 to 937 nm in order to record the position of the laser and the Raman spectra simultaneously which could then be subsequently used to calibrate the spectra into wavenumbers.

#### **8.6.4 Spectral Analysis**

Spectral analysis is an extremely important part of the diagnostic process. One of the main potential advantages of using Raman spectroscopy is that it could provide an objective diagnosis. However visually inspecting spectra, whilst providing us with an understanding of the underlying biochemical processes, reintroduces an element of subjectivity. To combat this, statistical techniques have been developed based on spectral attributes such as peak height ratios [27]; however establishing itself as the leading technique in this area is principle component analysis (PCA) [32]. PCA is a type of multivariate analysis that allows reduction of the large amount of spectral data to only a few important components by finding combinations of the original dimensions that represent the largest variations between the data sets. These combinations are known as principal components. Principle components are essentially a set of spectra that show where the variations between the input data sets occur and to what extent. This is useful as it allows us to link the components to biochemical changes occurring between the different cell types studied. The first

---

principle component contains information on the largest and most important variations; the second principle component contains the second most prominent variations and so on. Principle component analysis is a 'blind' technique, as it does not remember the origin of any input spectra, thus does not have a biased output increasing the objectivity of this analysis method. After the principle components have been created the original spectra are then compared to them and assigned a score for each component. This score is then plotted on a chart, with one principle component representing one axis, where spectra, and hence cells, with similar spectral make ups tend to cluster together. Conversely this also means that different cells should tend to separate on the charts, allowing us to make a diagnosis. A fuller explanation of how this technique works is contained in appendix A.

The spectral analysis begins by subtracting each cells individual background from its spectra, this was done at the beginning of the process as it was presumed that the experimental parameters would not change or drift over the 5 minutes required to obtain the signal and background. These subtracted spectra are then input into a mathematical programme, kindly written by Michael Mazilu a colleague on the project, which measures the laser line position, on each spectrum, and subsequently aligns them all. This is important as the data was acquired over a period of four months and during that time the laser was changed resulting in the acquired spectra showing very marginal laser wavelength shifts. The shifts in laser wavelength, due to the nature of the Raman effect, cause a shift in the position of the Raman peaks which would effect the PCA routine resulting in a diagnosis not based entirely upon the biochemical state of the probed cells. Once this has been done the spectra are normalised, according to area under the curve, to remove any influence of laser power fluctuations over the long experimental period. The spectra can be normalised as,

---

---

although the total intensity may vary, the Raman peak ratios should remain constant. Finally the spectra are converted into  $\text{cm}^{-1}$  and clipped down to the region between 600 and  $1800 \text{ cm}^{-1}$ , known as the fingerprint region. The fingerprint region contains the most pertinent Raman information thus the spectral regions outside this are cut to avoid inputting extra 'noise' into the statistical analysis. The spectra are now ready to be input into the PCA routine, kindly developed by Michael Mazilu, which will output charts displaying the scores of each spectrum with respect to the principle components.

Finally, using the outputted PCA charts we applied an algorithm, kindly developed by Michael Mazilu, to discriminate between the data sets and give numerical values for the sensitivity and specificity of the technique. Sensitivity and specificity is a common measure used in the discrimination between medical samples that gives an indication of how well a diagnostic system is performing. In our case sensitivity refers to the number neoplastic cells identified correctly and the specificity refers to the number of healthy cells correctly classified as healthy. Maximising both parameters is obviously extremely desirable however it is best to maximise sensitivity initially to pick up as many neoplastic cells as possible thus the algorithm works by maximising sensitivity although without excessive cost to the specificity. This allowed us to evaluate the effectiveness of Raman spectroscopy to discriminate between healthy and neoplastic samples.

## **8.7 Results**

### **8.7.1 Spectral Interpretation and Discussion**

Good quality Raman spectra were acquired from all samples, whether live cells or cells fixed in 70% (v/v) ethanol. The resultant average spectra of both the live

---

cells and fixed cells can be seen in figures 8(b) and 8(c) respectively. A tentative biochemical assignment for the peaks displayed in figures 8(b & c) can be seen in figure 8(d) [16, 33 & 34].

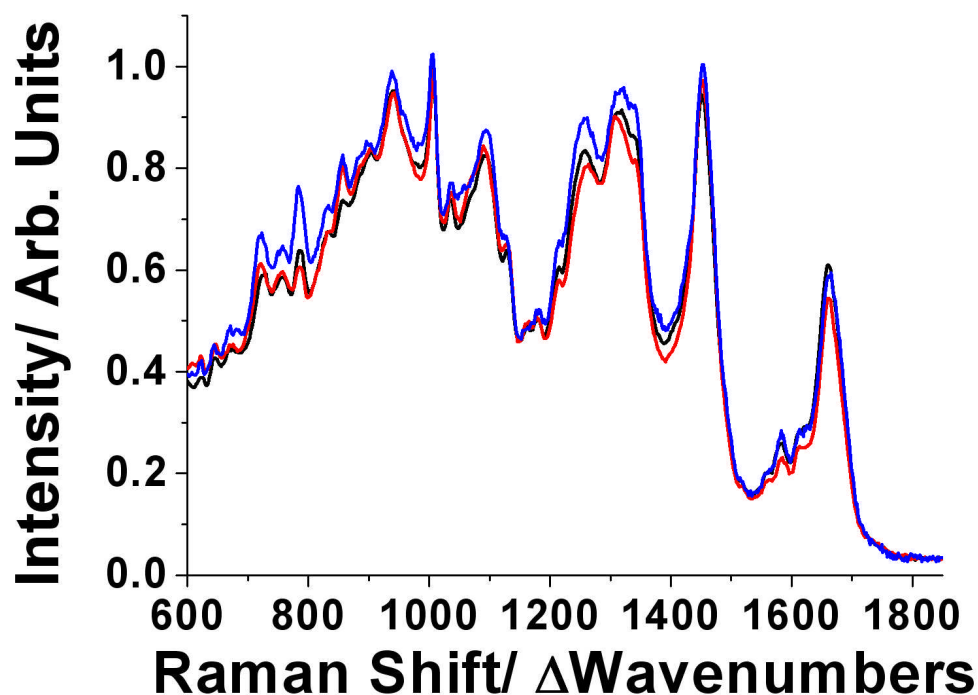


Figure 8(b). Comparison of the average Raman spectra of live PHK (Black), live PHK E7 (Red) and live CasKi (Blue) cells.

Comparison of the spectra obtained from live CaSki and live PHK E7 cells shows large increases in virtually all peaks in CaSki cells. These correspond to large increases in proteins, lipids and in DNA content, consistent with changes associated with neoplastic development. In particular, there is a previously indiscernible peak associated with lipid skeletal stretching at  $1057\text{ cm}^{-1}$ . There is a small decrease in the  $1661\text{ cm}^{-1}$  peak but the significance of this is unclear. CasKi cells represent an advanced form of cervical cancer thus are largely proliferating uncontrolled resulting the large increases in DNA, proteins and lipids. We must exercise some slight caution in this analysis as there is a possibility that variations in peak intensity, although largely down to the effects of neoplastic changes in the CasKi cells, may be

---

influenced by the fact we are also observing the fact that these are indeed two different cell types. A truer measure of the capabilities of Raman spectroscopy, to discriminate between healthy cells and those displaying the effects of HPV infection, is to examine the spectra pertaining to PHK and PHK E7.

Comparison of PHK and PHK E7 cells shows that these cell types are very similar. This is consistent with the fact that these cells differ only in the expression of a single viral protein, but there are some subtle and interesting variations. Peaks at 621, 645, 854  $\text{cm}^{-1}$  corresponding to phenylalanine, tyrosine and proline/tyrosine respectively all show an increase in the PHK E7 spectra. Furthermore there are increases in the peaks pertaining to lipids at 720, 1129 and 1452  $\text{cm}^{-1}$ . Conversely, significant decreases are observed at 788, 1340 and 1582  $\text{cm}^{-1}$  that correspond collectively to decreases in the density of the DNA bases. The remaining significant decreases occur at 1220, 1258 and 1661  $\text{cm}^{-1}$ , which are related to a reduction in the density of amide III ( $\beta$  sheet) and amide I ( $\alpha$  helix) respectively. If we think briefly again about the influence of the E7 viral protein, which blocks the formation of CDKs that could block continuation of the cell cycle, and facilitates the release of E2F-1 driving the cell into the S phase of the cell cycle, we can reconcile the observed spectral variations between PHK and PHK E7. Keeping in mind that we are examining the nucleus of the cells the increases in lipids and amino acids, the building blocks of proteins, reflect the fact that PHK E7 have a higher increased metabolic activity and turnover. The reduction in the signal from DNA, in the PHK E7 spectra, points to a reduced density in the probe volume suggesting that the normally densely packed supercoiled DNA is transcriptionally active. This would also tie in with the reduction in signal from amide I and amide III, which are moieties associated with the protein backbone that influence protein structure and function. As measurements were made from the

---

---

nucleus, it is likely that histones, which are responsible for maintaining the DNA in a tightly wound state within the nucleus, are the source of these amide peaks. The reduction in signal from amides, pointing to a reduction in their density within the probe volume, supports the conclusion that the normally densely packed supercoiled DNA is open and transcriptionally active. The conclusions drawn from the examination of the Raman peaks agrees well with what is known in the biomedical community about the influence HPV and also agrees with previous studies that examined other cell types with Raman micro spectroscopy [16]. However, there are some changes in the spectra that cannot be reconciled, such as the E7 spectra displaying an increase in the DNA base guanine at  $675\text{ cm}^{-1}$  and a small increase in DNA backbone signal at  $1093\text{ cm}^{-1}$ . Also, in the CaSki spectra there is a small decrease, by comparison with the PHK spectra, in amide I at  $1661\text{ cm}^{-1}$ : this might have been expected to be enhanced in CaSki cells, which are metabolically active and may be a result of the CasKi being a different cell type. However overall the spectral changes observed in this study are explicable in terms of the known biological differences between the cell types analysed.

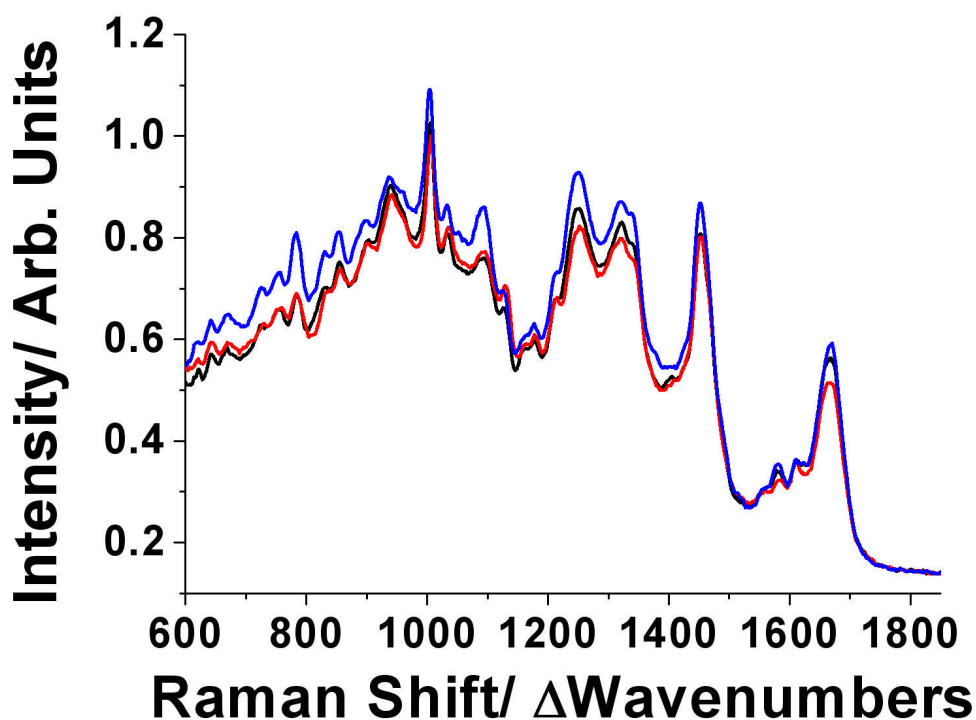


Figure 8(c). Comparison of the average Raman spectra of fixed PHK (Black), live PHK E7 (Red) and live CasKi (Blue) cells.

An important aspect of this study is the evaluation of how cell fixation affects the spectra obtained by Raman spectroscopy and whether this approach can still identify the differences between neoplastic and normal cells. The average spectra of the fixed cell types can be seen in figure 8(c). There is a visible change in the overall background shape in comparison with live cells (figure 8(b) versus figure 8(c)). This appears to be mostly the result of large reductions in the peaks at  $936$  and  $1090\text{ cm}^{-1}$  corresponding to DNA backbone stretches in both cases: this may be explained by the fact that ethanol is a precipitating fixative. However, despite this, the major differences between the cell cultures, discussed with respect to the live spectra, remain intact and visible in the fixed spectra with the exception of the peak at  $788\text{ cm}^{-1}$ , which corresponds to the DNA bases thymine and cytosine. These may be affected by fixation, although those peaks showing differences between cell types and those corresponding to the DNA bases adenine and guanine remain unaffected. We

will be able to probe the effects of fixation further in the next section when we look at the diagnostic ability of Raman spectroscopy, using PCA, where we shall see if it is still possible to discriminate between the cell types even after fixation.

Peak Position/ $\text{cm}^{-1}$	Assignment
621	C-C twist in phenylalanine
645	C-C twist in tyrosine
671	C-S stretching in cystine
720	C-N stretching in lipid/ adenine
755	Symmetric ring breathing in tryptophan
788	DNA: O-P-O backbone stretching/ thymine/ cytosine
833	DNA: O-P-O backbone stretching/ out of plane ring breathing in tyrosine
854	Ring breathing in tyrosine/ C-C stretching in proline
900	C-C skeletal stretching in protein
939	C-C skeletal stretching in protein
1006	Symmetric ring breathing mode of phenylalanine
1036	C-H in plane bending mode of phenylalanine
1071	Skeletal C-C stretch in lipids
1095	DNA: O-P-O backbone stretching
1129	Skeletal C-C stretching in lipids
1160	C-C stretching in protein
1180	Cytosine/ guanine/ adenine
1215	Amide III: $\beta$ -sheet
1258	Amide III: $\beta$ -sheet/ adenine/ cytosine
1308	$\text{CH}_2$ deformation in lipids/ adenine/ cytosine
1340	Polynucleotide chain (DNA bases)
1452	$\text{CH}_2$ deformation in lipids
1580	Adenine/ guanine
1610	C=C bending in phenylalanine and tyrosine
1661	Amide I: $\alpha$ -helix

Figure 8(d). A table displaying a tentative chemical bond assignment for the Raman peaks in figures 8(b & c)

### 8.7.2 Can Raman spectroscopy discriminate between healthy cells and those affected by HPV?

As we have previously mentioned, the ability of Raman spectroscopy to discriminate between the cell types analysed was assessed by PCA. The ability of Raman spectroscopy to discriminate between PHK and PHKE7, PHK and CasKi and

---

PHKE7 and CasKi was evaluated. As well as comparing the cell types individually all three cell types were simultaneously subjected to the PCA process to see if they can be discriminated in just one statistical step. Live and fixed cells were evaluated separately as the fixation process, as we have seen, causes spectral changes that would show up in the PCA analysis; however the key question in this evaluation was if the technique could discriminate between the fixed sets of cells. If this were possible it would demonstrate the compatibility of Raman spectroscopy with current clinical practice.

The table in figure 8(e) gives the sensitivity and specificity of this approach for the discrimination between each pair of cells. In this case sensitivity and specificity are defined according to standard medical definitions where: sensitivity is defined as the ratio of the number of true positives to the sum of true positives and false negatives and the specificity is defined as the ratio of the number of true negatives to the sum of true negatives and false positives. It is interesting to note that the sensitivity ranged from 73 % to 80 % percent for the live samples but was higher, from 91 % to 96%, for the fixed samples. Importantly, Raman spectroscopy was able to distinguish not only between normal (PHK) and transformed (CaSki) cells but also between normal (PHK) cells and these cells expressing the HPV 16 E7 protein. Promisingly, the technique could also distinguish between PHK E7 and CaSki cells indicating that Raman spectroscopy can distinguish between various stages in the development of cervical neoplasia. We can also see relatively high specificity's for our comparisons; they are not quite as high as the sensitivities, partly due to the way the diagnostic model behaves, but also because of the physical attributes the PCA is detecting through analysing the spectra. The PCA is essentially picking up increased s

phase activity in the cell culture thus any normal cell at the peak of its s phase may appear as neoplastic under PCA analysis.

---

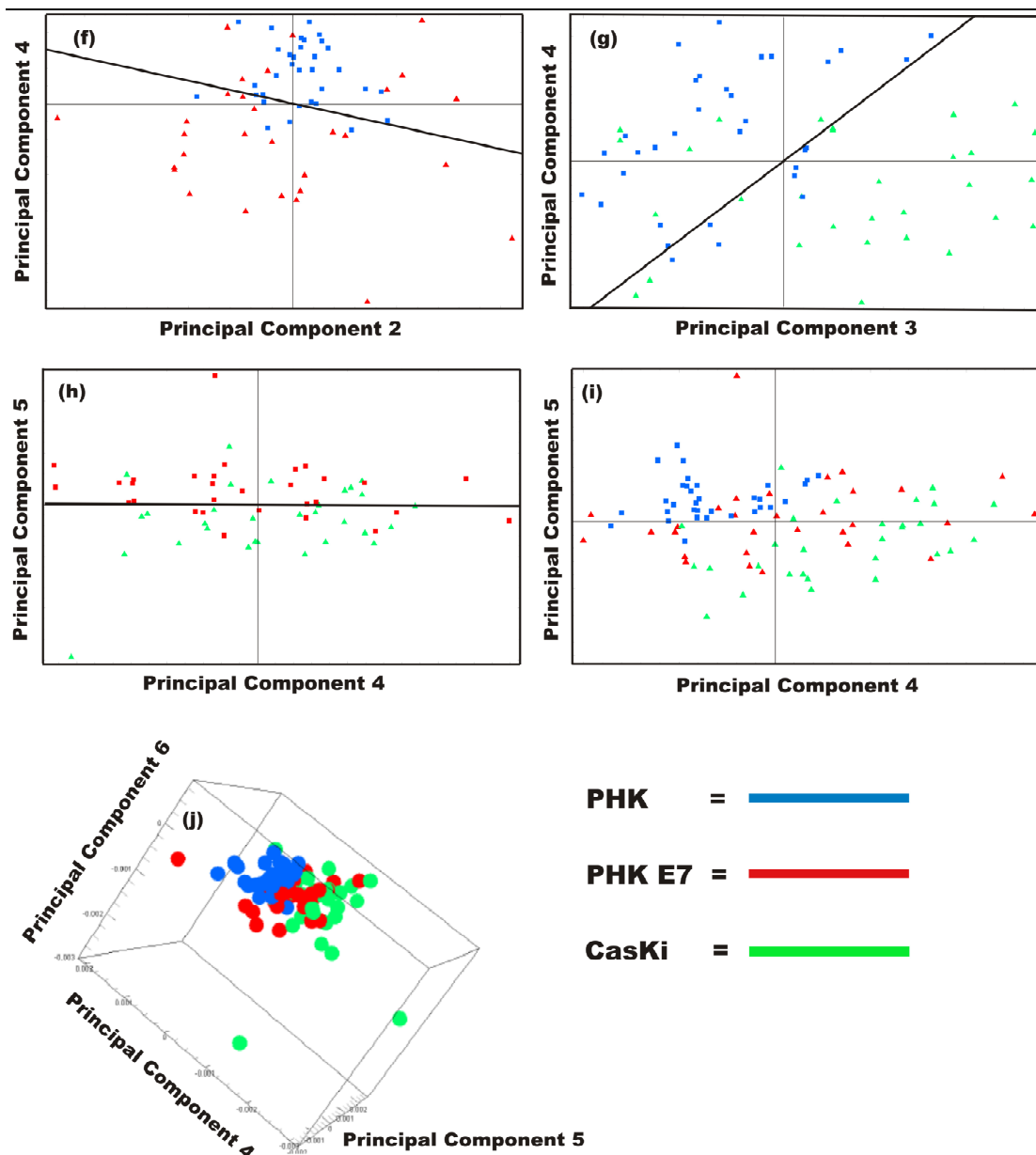


---

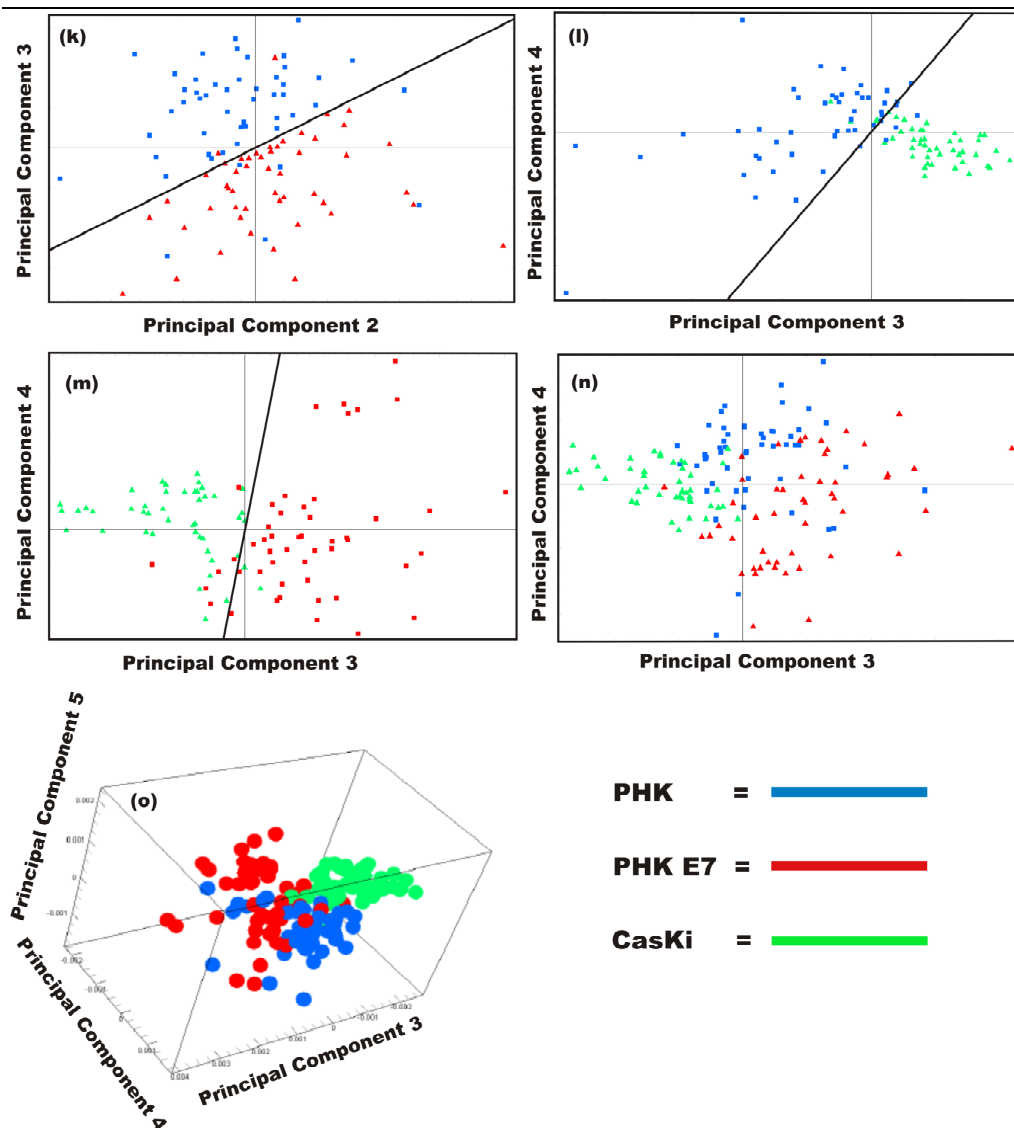
<b>Comparison</b>	<b>Sensitivity</b>	<b>Specificity</b>
PHK vs. PHK E7 (Live)	73 %	88 %
PHK vs. CaSki (Live)	80 %	76 %
PHK E7 vs. CaSki (Live)	73 %	73 %
PHK vs. PHK E7 (Fixed)	96 %	88 %
PHK vs. CaSki (Fixed)	91 %	90 %
PHK E7 vs. CaSki (Fixed)	95 %	88 %

Figure 8(e). Table showing the sensitivity and specificity of the principal component analysis for the discrimination between the cell types indicated.

The actual PCA charts for comparisons between the live cell sets can be seen in figures 8(f, g, h, i & j). Also, the PCA charts for comparisons between the fixed cell sets can be seen in figures 8(k, l, m, n & o). As mentioned previously PCA works in such a manner that similar spectra, and hence cells, cluster together on the chart; each cell is represented by one data point on the chart. Conversely this also means that different cells should tend to separate on the charts.



Figures 8(f, g, h, i & j). Figure 8(f) shows the PCA chart for the comparison between PHK and PHK E7. Figure 8(g) shows the PCA chart for the comparison between PHK and CasKi. Figure 8(h) shows the PCA chart for the comparison between PHK E7 and CasKi. Figure 8(i) shows all the diagnostic separation achieved when all three cell types are examined simultaneously. Finally figure 8(j) shows how the addition of a third principle component may help increase the separation between the data sets.



Figures 8(k, l, m, n & o). Figure 8(k) shows the PCA chart for the comparison between PHK and PHK E7. Figure 8(l) shows the PCA chart for the comparison between PHK and CasKi. Figure 8(m) shows the PCA chart for the comparison between PHK E7 and CasKi. Figure 8(n) shows all the diagnostic separation achieved when all three cell types are examined simultaneously. Finally figure 8(o) shows how the addition of a third principle component may help increase the separation between the data sets.

The sensitivities provided by Raman spectroscopy, in our study of HPV infected cells, were extremely good; however we can not fail to notice that the technique discriminates better between fixed cell sets in comparison to the live cells. Although this may be due to the smaller sample set used in the analysis of live cells, the more likely explanation is hinted to by the fact that different principal components were

---

used to discriminate between the cell types, as shown in figures 8(f-o). As we mentioned Principal component analysis compresses the large amount of spectral information into a few important factors that describe the major variations between the spectral data sets. The first principal component describes the greatest variation and the second principal component describes the next most significant variation and so on. Now if we consider again figures 8(b) and 8(c) there is background intensity, upon which the Raman spectra sit, that is most likely the result of cell autofluorescence. This is important as in all situations; the first principal component appears predominantly to describe the inter-sample variation in autofluorescence, which cannot be directly attributed to the cellular changes that separate the samples. Supporting this argument is that any attempted discrimination based on principal components that contain contributions from the fluorescence background yield poor sensitivities. Compounding this variation in autofluorescent background, most likely due to intra-sample variation, also contributes to the second principal component: this means that successful discrimination based on this component must be treated with some caution. However this also presents a problem as the second principal component, in this analysis, also carries the most pertinent Raman information so, if the second principal component is discarded, this information is lost and discrimination based upon the third and fourth principal components, which contain less Raman information, will be less robust.

To demonstrate this point, a plot of the principle components used to separate the live PHK and CasKi samples is shown in figure 8(p). As a principle component describes variations between the Raman spectra we would expect that it would approximate a flat line around zero with spikes coming off where we have variation in the discrete Raman peaks. However if we look at principle component 1 in figure 8(p)

---

---

we can see it looks just like a spectra on a slope through zero. This is a result of this component describing variation in autofluorescent background alone which cannot be attributed to the HPV induced neoplasia. Looking now at the second principle component it is again on a slope but no longer looks like a spectra and does contain some spikes. These spikes represent the most important Raman variations between CasKi and PHK but we must discard them as a result of the autofluorescence affecting the principle component. Now in principle component 3 we can see exactly what we would expect, a flat line with spikes coming off it displaying no components as a result of autofluorescence. The same effect can be seen in principle component 4 but this does not contain as much information as component 3. The discrimination between live PHK and CasKi was based on the 3<sup>rd</sup> and 4<sup>th</sup> principle components we see here in figure 8(p), however it may have been much stronger had we been able to use the important Raman information in principle component 2.

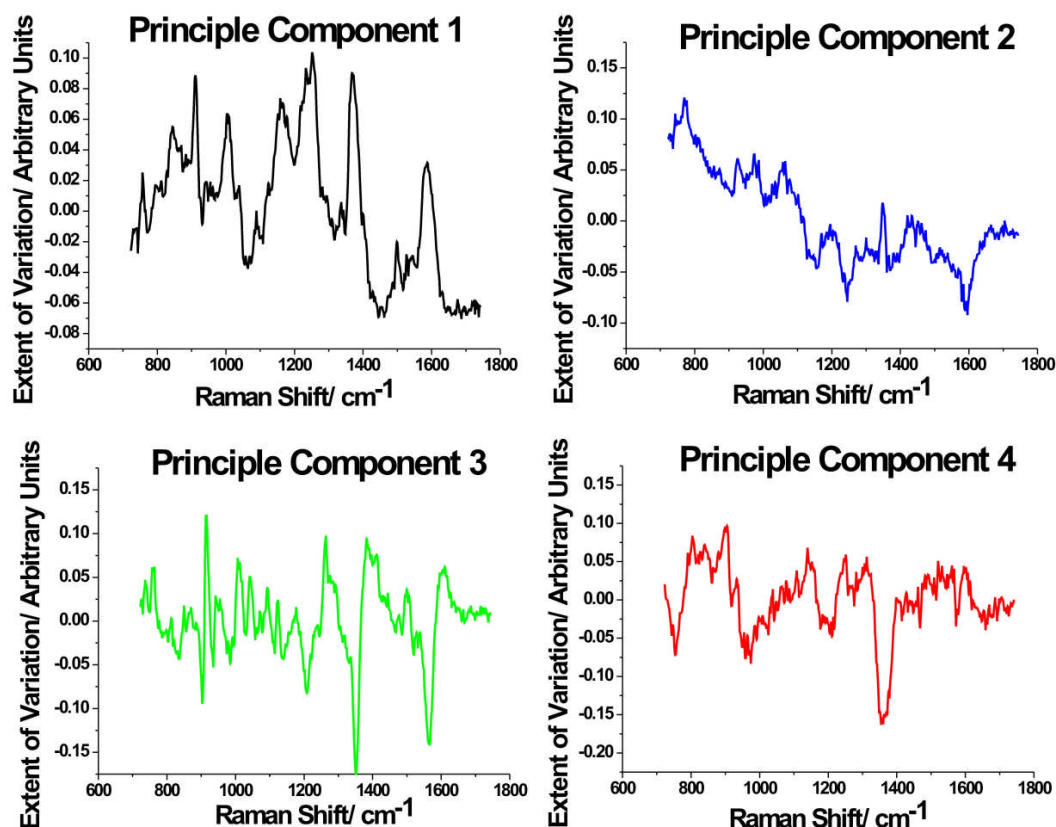


Figure 8(p). Principle components generated by the analysis of live PHK and CasKi.

If we now look at the principle components used to discriminate between fixed sample sets. The second and third principal components were used to discriminate between fixed PHK and PHK E7, figure 8(k). As the PHK E7 sample was derived from PHKs by retroviral transduction, there is very little inter-sample variation in cellular autofluorescence. Therefore, the second and third components, which contain the most pertinent Raman information, can be used to discriminate between these cell types resulting in excellent sensitivity and specificity. By contrast, discrimination between CaSki cells and PHKs, and CaSki cells and PHK E7 cells (figures 8(l) and figure 8(m) respectively) requires use of the third and fourth principal components, as the first two components contain autofluorescent background information. This is consistent with the fact that CaSki cells were derived from a cervical carcinoma unrelated to the origin of the PHKs. However, efficient discrimination between these

---

cell types is still achieved with sensitivities of over 90% as shown in figure 8(e). Now looking at the live sample comparisons we see that they two show a similar trend. The first principal component accounts for variations in autofluorescence between for the PHK vs. PHK E7 comparison, the second principal component then describes variation in Raman signatures. However, the third component appears to describe another subtle variation in fluorescence background that means that any pertinent Raman information contained within this component is discarded. Use of the fourth component, which contains less discriminatory information, results in weaker discrimination between the sample sets. Comparing the live PHK and live CaSki cells, the first two components carry information mostly related to variations in autofluorescence so the third and fourth principal components carry the majority of the Raman information, resulting in the most successful discrimination in this set. The comparison of live PHK E7 and CaSki suffers heavily, with the fourth and fifth components the first two that are not influenced by fluorescence, resulting in the weakest discrimination in the set. This effect is also prevalent in the 3D plot, figure 8(j), which shows that addition of the sixth principal component to help discrimination has little effect. The use of lower principle components generally results in much weaker diagnostics for the live sample sets. What however is the origin of this extra autofluorescence?

A clue, to the origin of the extra autofluorescence, lies in the consideration of the comparisons of discriminations between live and fixed PHK vs. PHK E7. As we mentioned we were able to use the 2<sup>nd</sup> and 3<sup>rd</sup> principle component for the fixed comparison but in the live comparison the 3<sup>rd</sup> principle component contained some weak fluorescence information thus we had to rely on the 2<sup>nd</sup> and 4<sup>th</sup> principle components. If we look again to the actual average spectra of the fixed and live PHK

---

---

spectra, figures 8(b) and 8(c), the only difference between them was a reduction in the DNA backbone signal. We may thus infer that the source of the extra autofluorescence was from the DNA itself that was denatured, to an extent, during fixation.

The use of Raman spectroscopy in combination with Principle component analysis allows us to discriminate reliably between normal keratinocytes and the transformed cervical carcinoma-derived cell line CaSki. More specifically, Raman spectroscopy can identify cells expressing the HPV 16 E7 gene accurately and objectively, suggesting that this approach may be of value for the identification and discrimination of the different stages of HPV-associated neoplasia. The ability to detect the effects of the virus in fixed samples also demonstrates the compatibility of Raman spectroscopy with current cervical screening methods. Furthermore the fact that many of these samples were stored under the fixing agent for some time before examination, up to three months in some cases, further demonstrates the compatibility of Raman spectroscopy with application to stored clinical samples.

## **8.8 Conclusions**

The use of Raman spectroscopy in cancer diagnostics has been attracting much interest, and rightly so, as it offers the possibility of objective and accurate diagnosis at an extremely early stage in cancer development. Raman tweezers spectroscopy has been recently used in the area of cancer diagnostics to examine colorectal cancer and neoplastic lymphocytes bringing not only the diagnostic power of Raman spectroscopy to this field but also the advantages supplied by optical tweezers. Using our Raman tweezers system we studied HPV induced cervical neoplasia. This is an excellent opportunity for the application of Raman tweezers as it

---

---

is extremely suited to the study of single cells, similar to material available from Pap smears, the current medical screening technique for cervical cancer.

In order to evaluate the potential of Raman tweezers in the early detection of cervical neoplasia we acquired and analysed spectra from normal healthy PHKs and compared them to CasKi cells, a cervical carcinoma derived cell line, representing an advanced stage of cervical cancer. We also compared our PHK spectra with those acquired from PHKs infected with HPV expressing the E7 viral protein. Being able to detect the HPV and its effects on the cell would represent the detection of a high risk population group that may go on to develop cervical neoplasia at the earliest possible stage as the link between HPV and cervical cancer is well known. Furthermore we also compared spectra from live and fixed cells; although we expected the fixation process to alter the spectra, the ability to detect differences between the healthy and abnormal cells even when fixed would further demonstrate the compatibility of this technique with current medical practice.

The Raman tweezers system performed well acquiring good quality spectra from the samples, however the large cells could not be z trapped so we had to rely on quartz coverslips to reduce interfering fluorescence from the surface the cells were sitting on. We shall see however in the subsequent chapter how advanced Raman tweezers geometries can be used to overcome these problems.

Examining and comparing the acquired average spectra for PHK, PHK E7 and CasKi we found that CasKi cells, in comparison to the normal PHK cells, showed large increases at all peaks, representing increases in DNA, protein and lipid content, except at the  $1661\text{cm}^{-1}$ , a peak pertaining to amide I, which showed a small decrease. The increases in DNA, protein and lipid content are consistent with the onset of advanced neoplasia, however the significance of the decrease in the  $1661\text{cm}^{-1}$  peak is

---

---

unclear. It is possible that these results could be biased by the fact we are examining two different cell types so a more insightful examination is between that of PHK and PHK E7, the same cells infected with HPV-16 expressing the E7 protein. We found that the spectra are very similar, as we might expect, but found the key differences of decreased amide and DNA density and increased lipid and protein content. This is again consistent with the known effects of the E7 viral protein causing increased metabolic activity. Furthermore we found the same effects to be visible in the average spectra from the fixed samples, although the overall spectral shape was altered due to decreases in peaks pertaining to DNA backbone. This is likely a result of the fixation process denaturing the DNA backbone to some extent. These results, explained by the known effects of HPV infection, demonstrate the ability of Raman spectroscopy to monitor the biochemical changes associated with the early stages of the development of cervical neoplasia.

One of the most promising aspects of the use of Raman spectroscopy in cancer diagnostics is that it offers the possibility of objective diagnosis. We used the statistical technique of PCA to analyse and diagnose our spectra, hence cells, resulting in sensitivities of up to 96% for the comparison of fixed PHK vs. PHK E7. However we surprisingly found the PCA analysis performed better for the fixed samples. This was suggested to be a result of the fixation process leading to a reduction in cellular laser induced autofluorescence, which is not likely to be related to the cells neoplastic state, removing its influence on the statistical analysis. The fact that we observed the fixation process reduced DNA backbone signal in the average spectra points to it being the source of the interfering autofluorescence that reduced the sensitivities of the analysis on the live cell spectra. The results of the analysis were very favourable,

---

especially for the fixed samples, and could possibly be further improved by the use of more advanced statistical analysis techniques such as linear discriminant analysis [9].

These results point to the ability of Raman spectroscopy to analyse and diagnose HPV associated cervical neoplasia in an accurate and objective manner. Furthermore the ability to perform the analysis on fixed samples points to the compatibility of this technique with current medical practice. The next step in this research would of course be to move on and analyse the material retrieved from pap smears to assess the performance of the technique in a clinical environment.

## 8.9 References

- [1] Walboomers JM, Jacobs MV, Manos MM, Bosch FX, Kummer JA, Shah KV, Snijders PJF, Peto J, Meijer CJLM and Munoz N **Human papillomavirus is a necessary cause of invasive cervical cancer worldwide.** *Journal of Pathology* 1999 Sep; **189**: 12-19
- [2] Bosch FX, Manos MM, Munoz N, Sherman M, Jansen AM, Peto J, Schiffman MH, Moreno V, Kurman R and Shah KV. **Prevalence of human papillomavirus in cervical cancer: a worldwide perspective.** *Journal of the National Cancer Institute* 1995; **87**: 796-802
- [3] Ronco G, Giorgi-Rossi P, Carozzi F, Dalla Palma P, Del Mistro A, De Marco L, De Millo M, Naldani C, Pierotti P, Rizzolo R, Sergnan N, Schincaglia P, Zarzi M, Confortini M and Cuzick J. **Human papillomavirus testing and liquid-based cytology in primary screening of women younger than 35 years: results at recruitment for a randomised controlled trial.** *Lancet Oncology* 2006;**7**: 547-55
- [4] Nadeau V, Hamdan K, Hewett J, Sibbett W, Tait I, Cuschieri A and Padgett M.
-

- 
- Endoscopic fluorescence imaging and point spectroscopy system for the detection of gastro-intestinal cancers.** Journal of Modern Optics 2002; **49**: 731-41
- [5] Mitchell MF, Cantor SB, Ramanujam N, Tortolero-Luna G and Richards-Kortum R. **Fluorescence spectroscopy for diagnosis of squamous intraepithelial lesions of the cervix.** Obstetrics Gynaecology 1999; **93**: 462-70
- [6] Cohenford MA and Rigas B. **Cytologically normal cells from neoplastic cervical samples display extensive structural abnormalities on IR spectroscopy: Implications for tumour biology.** Proceedings of the National Academy of Sciences 1998; **95**: 15327-15332
- [7] Crow P, Molckovsky A, Stone N, Uff J, Wilson B and WongKeeSong LM. **Assessment of fiberoptic near-infrared raman spectroscopy for diagnosis of bladder and prostate cancer.** Urology 2005; **65**:1126-1130
- [8] Haka AS, Shafer-Peltier KE, Fitzmaurice M, Crowe J, Dasari RR, Feld MS. **Diagnosing breast cancer by using Raman spectroscopy.** Proceedings of the National Academy of Sciences 2005; **102**: 12371-12376
- [9] Stone N, Kendall C, Smith J, Crow P and Barr H. **Raman spectroscopy for identification of epithelial cancers.** Faraday Discussions 2004; **126**: 141-157
- [10] Krafft C, Sobottka SB, Schackert G and Salzer R. **Near infrared Raman spectroscopic mapping of native brain tissue and intracranial tumors.** The Analyst 2005; **130**: 1070-1077
- [11] Notingher I and Hench LL. **Raman microspectroscopy: a non-invasive tool for studies of individual living cells in vitro.** Expert Review of Medical Devices 2006; **3**: 215-234
- [12] Shen AG, Ye Y, Zhang JW, Wang XH, Hu JM, Xie W and Shen J. **Screening of**
-

- 
- gastric carcinoma cells in the human malignant gastric mucosa by confocal Raman microspectroscopy.** *Vibrational Spectroscopy* 2005; **37**: 225-231
- [13] Hawi SR, Campbell WB, Kajdacsy-Bulla A, Murphey R, Adar F and Nithipatikom K. **Characterisation of normal and malignant human hepatocytes by Raman microspectroscopy.** *Cancer Letters* 1996; **110**: 35-40
- [14] Crow P, Barass B, Kendall C, Hart-Prieto M, Wright M, Persad R and Stone N. **The use of Raman spectroscopy to differentiate between different prostatic adenocarcinoma cell lines.** *British Journal of Cancer* 2005; **92**: 2166-2170
- [15] Hamden KE, Bryan BA, Ford PW, Xie C, Li YQ and Akula SM. **Spectroscopic analysis of Kaposi's sarcoma-associated herpesvirus infected cells by Raman tweezers.** *Journal of Virological Methods* 2005; **129**: 145-151
- [16] Chan JW, Taylor DS, Zwerdling T, Lane SM, Ihara K and Huser T. **Micro-Raman Spectroscopy Detects Individual Neoplastic and Normal Haematopoietic Cells.** *Biophysical Journal* 2006; **90**: 648-656
- [17] Chen K, Qin Y, Zheng F, Sun M and Shi D. **Diagnosis of colorectal cancer using Raman spectroscopy of laser-trapped single living epithelial cells.** *Optics Letters* 2006; **31**: 2015-2017
- [18] Giroglu T, Florin L, Schafer F, Streek RE and Sapp M. **Human Papillomavirus infection requires cell surface heparin sulphate.** *Journal of Virology* 2001; **75**: 1565-1570
- [19] Burd EM. **Human Papillomavirus and Cervical Cancer.** *Clinical Microbiology Reviews* 2003; **16**: 1-17
- [20] Southern SA and Herrington CS. **Disruption of cell cycle control by human papillomaviruses with special reference to cervical carcinoma.** *International Journal of Gynaecological Cancer* 2000; **10**: 263-274
-

- 
- [21] Halbert CL, Demers GW and Galloway DA. **The E7 gene of human papillomavirus type 16 is sufficient for immortalization of human epithelial cells.** Journal of Virology 1991; **65**: 473-478
- [22] Kuo SR, Liu JS, Broker TR and Chow LT. **Cell free replication of the human Papillomavirus DNA with homologous viral E1 and E2 proteins and human cell extracts.** Journal of Biological Chemistry 1994; **269**: 24058-24065
- [23] Conger KL, Liu JS, Kuo SR, Chow LT and Wong TSF. **Human Papillomavirus DNA Replication. Interactions between the viral E1 protein and two subunits of human DNA polymerase & primase.** Journal of Biological Chemistry 1999; **274**: 2696-2705
- [24] Bernard BA, Bailly C, Lenoir MC, Darmon M, Thierry F and Yaniv M. **The human Papillomavirus type 18 (HPV 18) E2 gene product is a repressor of the HPV 18 regulatory region in human keratinocytes.** Journal of Virology 1989; **63**: 4317-4324
- [25] Martin P, Vass WC, Schiller JT, Lowry DR and Velu TJ. **The Bovine Papillomavirus E5 transforming protein can stimulate the transforming activity of EGF and CSF-1 receptors.** Cell 1989; **59**: 21-32
- [26] Schwarz E, Freese UK, Grissman L, Mayer W, Roggenbuck B, Stremlau A and Hausen HZ. **Structure and transcription of human Papillomavirus sequences in cervical carcinoma cells.** Nature 1985; **314**: 111-114
- [27] Mahadevan-Jansen A, Mitchell MF, Ramanujam N, Malpica A, Thomsen S, Utzinger U and Richards-Kortum R. **Near infrared Raman spectroscopy for in vitro detection of cervical precancers.** Photochemistry and photobiology 1998; **68**: 123-132
- [28] Utzinger U, Heintzelman DL, Mahadevan-Jansen A, Malpica A, Follen M and
-

- 
- Richards-Kortum R. **Near infrared Raman spectroscopy for in vivo detection of cervical precancers.** Applied Spectroscopy 2001; **55**: 955-959
- [29] Krishna CM, Prathima NB, Malini R, Vadhiraja BM, Bhatt RA, Fernandes DJ, Kushtagi P, Vidyasagar BM and Kartha VB. **Raman spectroscopy studies for diagnosis of cancers in human uterine cervix.** Vibrational Spectroscopy 2006; **41**: 136-141
- [30] Southern SA, Lewis MH and Herrington CS. **Induction of tetrasomy by human papillomavirus type 16 E7 protein is independent of pRb binding and disruption of differentiation.** British Journal of Cancer 2004; **90**: 1949-1954
- [31] Halbert CL, Demers GW and Galloway DA. **The E6 and E7 genes of human papillomavirus type 6 have weak immortalizing activity in human epithelial cells.** Journal of Virology 1992; **66**: 2125-34
- [32] Brenton RG. **Chemometrics: data analysis for the laboratory and chemical plant.** 2003; John Wiley & Sons: 184-219
- [33] Jess PRT, Garces-Chaves V, Smith D, Mazilu M, Paterson L, Riches A, Herrington CS, Sibbett W and Dholakia K. **A dual beam fibre trap for Raman micro-spectroscopy of single cells.** Optics Express 2006; **14**: 5779-5791
- [34] Crow P, Stone N, Kendall CA, Uff JS, Farmer JA, Barr H and Wright MPJ. **The use of Raman spectroscopy to identify and grade prostatic adenocarcinoma in vitro.** British Journal of Cancer 2003; **89**: 106-108.
-

---

# 9. A Dual Beam Fibre Trap for Raman Microspectroscopy of Single Cells

---

*Raman tweezers spectroscopy has become a useful tool in the examination of single biological cells. However the technique has some shortfalls as it cannot easily trap and spatially examine large cells. In this discussion we will see the advantages that can be gained from decoupling the Raman and tweezing functions and how the use of a dual beam fibre trap, as the primary trapping mechanism, can allow us to study large biological cells in detail whilst retaining the original advantages that make Raman tweezers spectroscopy such an attractive prospect.*

---

## 9.1 Introduction and Motivations

### 9.1.1 Introduction and issues in tweezing large cells for study with Raman tweezers microspectroscopy

We have seen how Raman microspectroscopy builds up a chemical fingerprint of the substance we are studying and how the incorporation of optical tweezers allows us to isolate our object of interest, from interfering surfaces, and hold it stably in three dimensions whilst we acquire our Raman spectra. Previously the study of single cells was very difficult. Cells often would have to be grown or fixed onto expensive ultra low fluorescence substrates to avoid the drift of cells out of the laser beam. Raman tweezers microspectroscopy has thus made the study of single cells much more accessible and the technique has been employed in studies ranging from the

---

---

monitoring of the yeast growth cycle [1] to the behaviour of T-cells [2] and even in the diagnosis of cancer [3].

Whilst combined Raman tweezers spectroscopy has provided many important advantages for the study of biological cells there remains some shortfalls in the ability of the technique. Raman tweezers spectroscopy is ideal for the study of smaller cells such as red and white blood cells, small yeast or bacterial cells and subcellular organelles, which have sizes ranging from approximately five to ten microns. Optical tweezers however, whilst although employed extremely successfully throughout biology, struggles to manipulate larger biological cells that have sizes over approximately fifteen microns. Thus it is more difficult to study them with Raman tweezers spectroscopy. It is possible to increase the laser power to attempt to trap large objects stably; however when studying biological cells the use of such large powers in the focussed beam spot, required for trapping, will carry an extremely high risk of causing photodamage. This essentially means that, in the study of large biological cells, we have lost the ability to 3D tweeze the cells away from the coverslips, which are large sources of fluorescence interference, and with it one of the major advantages of Raman tweezers forcing us to fall back on the use of expensive coverslips made from quartz or calcium fluoride. We should note however that the cell does remain trapped by the transverse gradient force, acting parallel to the coverslips, thus it cannot drift out of the beam easily during Raman interrogation thus this advantage is retained in the study of large cells. The important aggressive focussing used in optical tweezers also leads to an inherent shortfall in Raman tweezers microspectroscopy. The aggressive focussing creates the required small focal spot, on the order of half a micron using a 100x NA 1.25 objective, which generates the gradient force. However as we noted in chapter 7 the intensity of the

---

---

Raman scatter is proportional to the power density of the laser, thus most of the collected Raman scatter is from a very small area in the cell and is therefore not representative of behaviour of the whole cell. This can be easily remedied by using a lower magnification microscope objective to give a larger focal spot, however this invariably means a reduction in the numerical aperture and a loss of three dimensional trapping. Again we must examine the cells resting on specialised coverslips if we want to engage the whole cell area. Although the use of high NA high magnification objectives makes studying the entire cell simultaneously difficult, it opens up the possibility of studying and mapping the intracellular organelles and biochemical behaviour in fine detail. In fact there is great interest in this; Krafft *et al* [4] mapped cells fixed to a quartz slide with traditional Raman microspectroscopy and Feofanov *et al* mapped cells to monitor the interaction of intracellular organelles with therapeutic drugs, also with traditional Raman microspectroscopy [5]. In 2004 Xie *et al* applied Raman tweezers to trap and acquire spectra from the nucleus in pine cells [6], although the nucleus was trapped the cells were grown onto a coverslip thus these papers did not utilise the full potential of Raman tweezers to manipulate the cells away from interfering surfaces. The small focal spot in Raman tweezers should be ideal for subcellular analysis; however cells in single beam gradient optical tweezers often move, rotate and pivot around the beam axis. The single beam gradient trap, as we have seen, draws to the beam focus the area of highest refractive index, the eukaryotic cell however is far from uniform having many high index organelles. The largest of these organelles, the nucleus, is normally drawn too the beam focus and becomes the primary trapping site of the cell. However the forces experienced by the other organelles, imposed by the light, results in the cell often moving substantially in the trap as the organelles attempt to move closer to the beam focus. This makes it

---

---

extremely difficult to acquire a spectrum from one small volume. This movement of cells in optical traps also affects the Raman spectra of smaller cells [7] thus a method of stably trapping cells is an important issue.

Considering these factors it would be extremely useful to develop a system that could stably trap large or small cells for Raman examination whilst retaining the advantages of current Raman tweezers systems.

### **9.1.2 Proposed systems to extend the functionality of Raman tweezers**

Examining large cells and performing subcellular analysis can be very difficult in Raman tweezers and the research field has thus seen a recent move towards separating the Raman and trapping aspects to create more versatile and capable systems that can examine a wider variety of biological samples.

The move towards separate trapping beam and Raman probe beam provides the advantage of selecting the wavelength and power for the individual trapping and Raman probe functions to optimise the functionality and flexibility of the system. Furthermore this would allow us to use the tweezing beam to position the object for examination precisely in the Raman probe beam and also use a very low power trapping beam for storing cells until they are required for examination. The first move towards this type of system was demonstrated by Xie *et al* in 2002 [8] where, although the authors did not use two separate beams, they introduced a system where only 2mW of optical power was required for trapping but could be ramped up to 20mW to acquire quality Raman spectra. The authors identified the need for a more flexible system to study biological cells and this power ramping system reduced the cells exposure to the laser reducing the chances of photodamage. The first demonstration of the use of two separate beams was carried out by Ramser *et al* [9] in

---

---

2004; in this publication the authors study red blood cells with resonance Raman spectroscopy. To obtain the resonance enhancement wavelengths in the visible are required thus continuously trapping the cell with these wavelength will cause massive photodamage to the cells. In order to circumvent this, the authors use a separate infrared trapping beam, at 830 nm, delivered to the sample via a second opposing microscope objective in the manner depicted in figure 9(a). This arrangement allows the long term trapping of the cell at a wavelength and power that will cause little photodamage and to obtain enhanced rapid Raman signals. Also in 2004 Gessner *et al* [10] evaluated three decoupled experimental geometries applied in the study of biological cells. The first geometry was identical to that used by Ramser et al but the second used only one microscope objective to deliver the trapping and excitation wavelengths, which were 632.8 nm and 514.5nm respectively, to the sample as depicted in figure 9(b). This geometry is much simpler to create and align but does require careful choice of optics although this is not normally a serious problem. The final geometry used a converted fibre probe as the excitation source introduced at  $90^\circ$  to a traditional Raman tweezer, as shown in figure 9(c), however the focussed laser beam, of the Raman tweezer, was only used for trapping and collecting the scattered Raman signal. This system also has the advantage of reduced complexity in the experimental arrangement but as with the first and second arrangement fails to address the issue of trapping large cells or obtaining site specific Raman spectra on stably trapped cells.

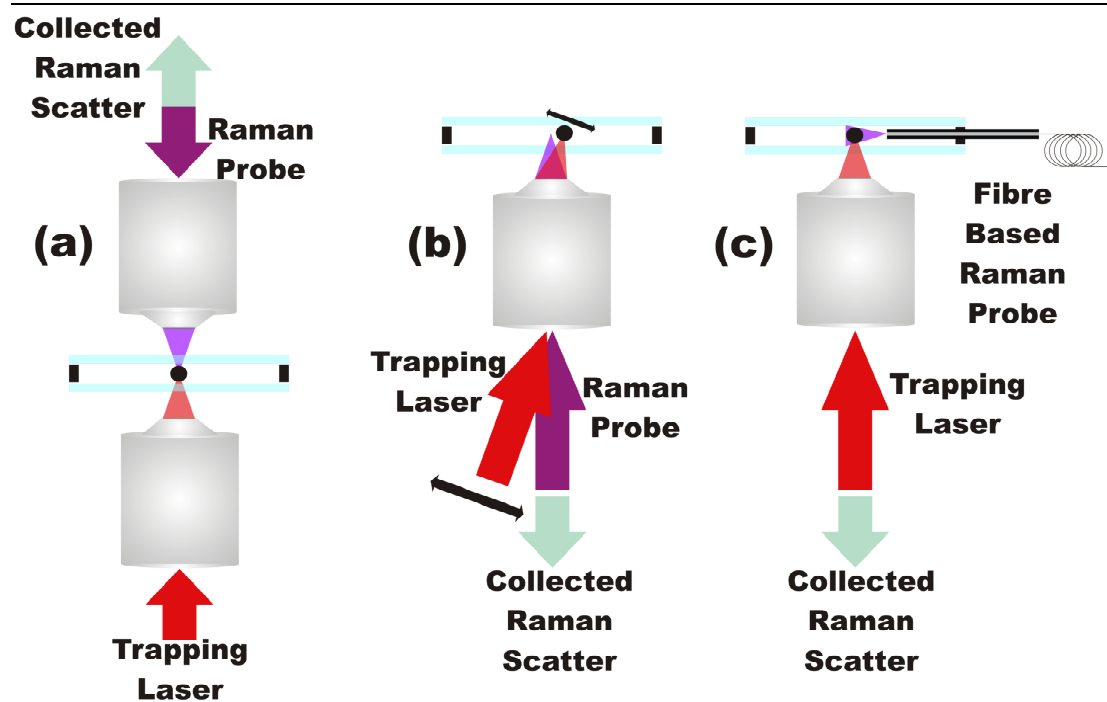


Figure 9(a, b & c). Figure 9(a) depicts a decoupled Raman Tweezers system where the trapping and Raman probe beams are introduced to the sample via two separate microscope objectives. Figure 9(b) depicts a decoupled Raman system where the Raman probe and trapping beam are introduced to the sample via the same microscope objective, this system offers reduced complexity in experimental apparatus. Figure 9(c) depicts a decoupled Raman Tweezers system where the trapping beam is introduced through a microscope objective and the Raman probe beam is introduced to the sample via a fibre optic probe.

Finally in 2004 Creely *et al* [11] also produced a decoupled system based on figure 9(b), in this paper they used the full potential of the decoupled tweezer to move the cell, under study, in and out of the Raman probe, this allowed accurate background readings to be more easily conducted and most importantly allowed extremely good alignment of the cell in the Raman probe to maximise signal collection. Although successful this paper does not address the issues of trapping and acquiring signals from large cells. In order to address the problems of trapping cells stably and allowing the production of Raman maps from trapped cells Creely *et al* [12] demonstrated the implementation of an advanced decoupled system, still based on the geometry in figure 9(b), using holographic optical tweezers as the trapping mechanism.

---

Holographic optical tweezers utilises a hologram, in this case generated by a spatial light modulator (SLM), to create an array of trap sites. SLMs are pixelated devices that can be used to create a phase only hologram such that when a light beam is incident upon the device, it creates a phase pattern on the laser wavefronts. When this phase pattern is Fourier transformed, i.e. when the laser is focussed by the microscope objective, it creates an array of laser trap sites in the microscope objective focal plane. An SLM is a dynamic instrument that means the number and position of the laser trapping spots can be adjusted. Creely *et al* used this instrument to create an array of traps around the edge of a cell to support it and trap it in a stable manner. The dynamic nature of the spatial light modulator allows the movement of the cell over a separate Raman probe beam so a Raman image of the cell can be produced. The drawbacks of this experimental arrangement are the complex nature of the equipment and most importantly the Raman probe pulled the cell under study out of the holographic tweezers unless very low optical power was used,  $\sim 1\text{mW}$ , in the Raman probe meaning long acquisition times. Furthermore the multiple single gradient trap sites, of the holographic optical tweezers, may affect the cell function over long periods of time as they are likely to attract the internal organelles. This paper was successful in stably trapping and creating a Raman map of a cell however the cell studied was a transformed white blood cell, approximately  $15\ \mu\text{m}$  in size, thus did not demonstrate the ability of the technique to study very large cells.

---

### 9.1.3 The use of fibre optical traps to trap cells for Raman analysis

In order to address the issues of stably trapping cells, especially large cells, in a manner that allows us to engage the whole cell or obtain subcellular Raman images whilst minimising potential for photodamage or affecting the cell function, we propose the use of a decoupled Raman tweezers system based on a fibre optical light force trap. This system would allow us to readily examine cellular objects whilst retaining all the original advantages that have made Raman tweezers an exciting and attractive prospect.

As we have seen in chapter 4, prior to the realisation of the single beam optical trap (optical tweezers) [13], the first actual trap demonstrated by Ashkin in 1970 employed two divergent counter-propagating beams [14]. This trap was revisited in 1993 by Constable and co-workers [15] who generated a version using two co-axial optical fibres. This dual beam trap has many advantages over the single beam optical tweezers that are important for the purposes we have discussed here. Firstly the trap does not require high numerical aperture optics and may be realised with weakly divergent beams. In turn this indicates the prospect of a reduction in photodamage or any two-photon induced damage [16] due to a reduced optical density. The dual beam fibre trap also encompasses another key attribute: it can hold large objects readily due to the large encatchment area and beam divergence. Finally due to its geometry it may be readily incorporated into a microfluidic flow system for cell analysis, a current hot topic in Raman tweezers spectroscopy as groups drive towards a flow cytometry style system based on Raman spectroscopy. Indeed recent studies have shown the use of a cell stretcher where a dual beam system was used to elongate cells in a manner dictated by their internal elasticity: in turn this allows one to distinguish between normal and tumour cells [17]. This system should allow us to use the fibre optical trap

---

as the primary trapping mechanism whilst the Raman tweezers beam can accurately probe the sample.

In this chapter we will see how a fibre optical light force trap may be incorporated readily into a Raman tweezers system and discuss some of its advantages and disadvantages, we shall also see how this trap can be used to interrogate biological cells and be incorporated into rudimentary microfluidic systems.

## **9.2 Experimental apparatus and Procedures**

The construction and implementation of fibre optical traps is in essence a relatively straight forward process but there some factors that we must be aware of in our experimental choices and procedures. We will address these issues in this section.

### **9.2.1 Experimental apparatus and construction**

The fibre optical light force trap is readily incorporated into a conventional Raman tweezers system as the two optical fibres, forming the trap, are placed on the sample stage above the Raman tweezers system. The fibre optic launching system can then be placed conveniently on the optical table. A schematic of the fibre optical Raman tweezers setup can be seen in figure 10(d).

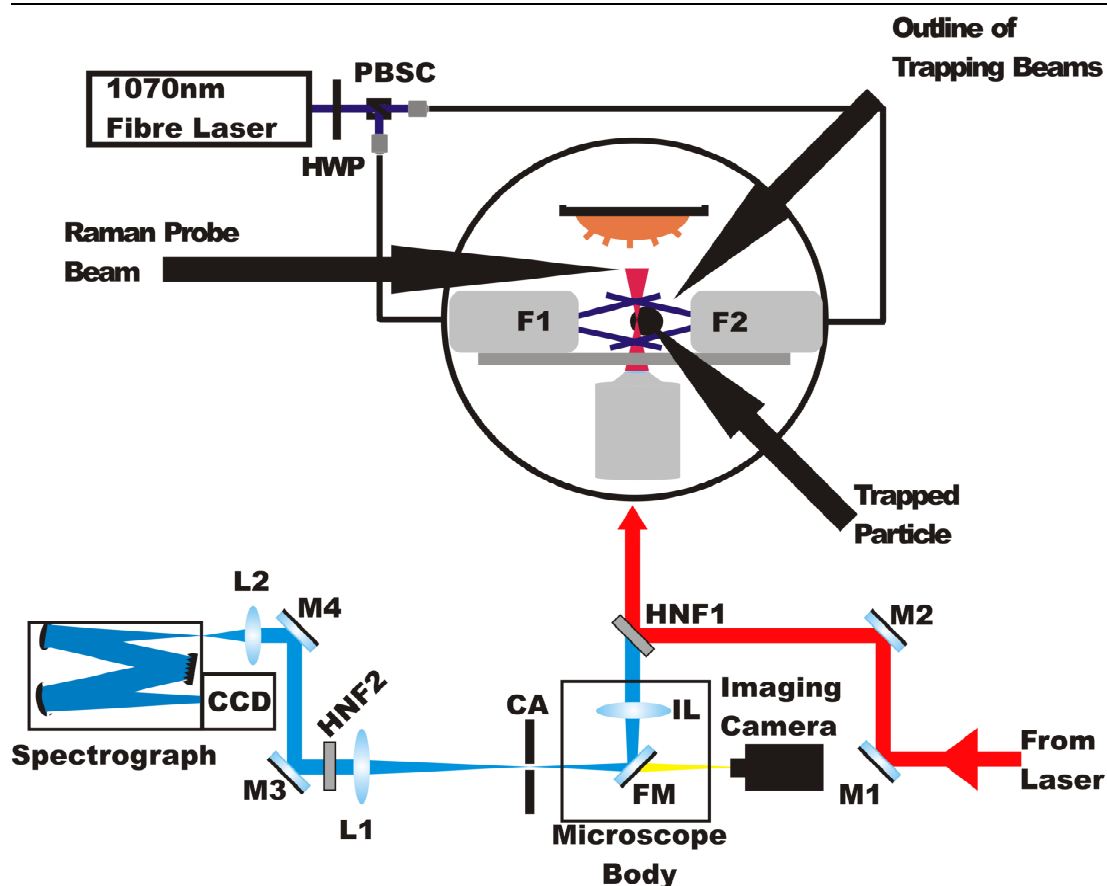


Figure 9(d). A schematic of the Fibre optical Raman tweezers setup, in this system the fibre trap sits on the microscope stage above the conventional Raman tweezers. Abbreviations are as follows: M – mirror, L – lens, HNF – holographic notch filter, CA – confocal aperture, FM – flip mirror, IL – imaging lens, F – fibre, HWP – half wave plate and PBSC – polarising beam splitter cube.

Looking at figure 9(d), the conventional Raman tweezers portion of the experimental setup should be recognisable as the evolved system, based around a commercial microscope, developed in this thesis and discussed in section 6.4, thus we will concentrate on the fibre optical portion of this setup as this is merely placed on the microscope stage to form the completed fibre optical Raman tweezers system.

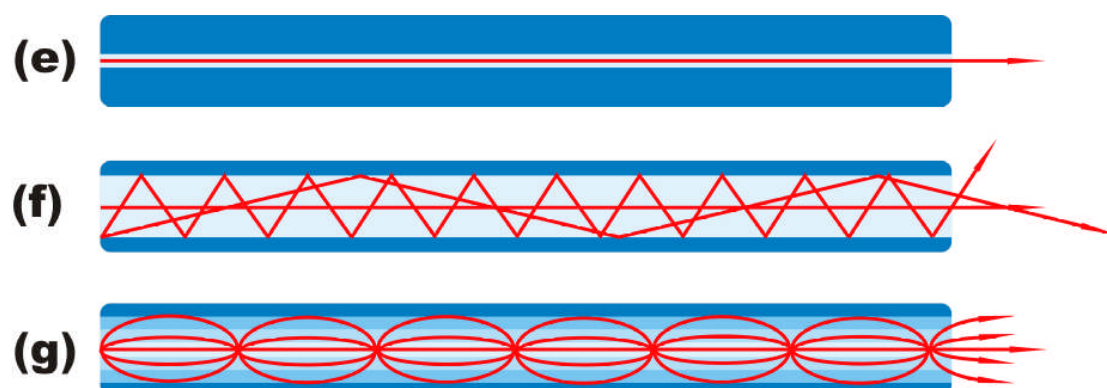
In constructing the fibre trap there are three main issues we must consider, the first issue is the type of fibre optical cable we use, the second is the launching of the laser light into the optical fibres and finally the formation of the trap on the microscope stage.

---

**9.2.1.1 Choice of Fibre optical cable**

The choice of fibre optic cable type used in the experiment, to form the fibre trap, will be dominated ultimately by the application and can be selected from three broad categories of fibre types: single mode fibre, step index multimode fibre and graded index multimode fibre. Single mode fibre has a very narrow core, around  $6\mu\text{m}$ , that allows only one light mode to propagate; this can be seen in figure 9(e). This has the advantage that the output beam has a very pure diverging near Gaussian profile that is excellent for trapping, the main disadvantage of using this fibre is that it is difficult to get large optical powers into the core as it is so narrow. Step index multimode fibre has a large core all of one index; this offers the light many possibilities of travelling along the fibre, as can be seen in figure 9(f). This has the advantage of allowing large amounts of optical power to be coupled into the fibre, however the different path lengths of the light beams travelling in the fibre ultimately leads to an interference pattern formed at the output creating a 'speckled' output beam thus it is not so good for trapping. Finally, graded index multimode fibre has a variable index core such that the light is not totally internally reflected, at the core cladding boundary, rather it is guided along the fibre by the refractive index variation, as can be seen in figure 9(g). The advantage of this fibre is that any rays travelling along the centre of the core experience a high refractive index thus travel more slowly than those taking a longer path length travelling along the outer edges of the core where the refractive index is lower, this keeps the wave fronts of the laser beam closer together and reduces the speckling on the output beam. Graded index multimode fibre allows large amounts of power to be carried in the fibre whilst maintaining a reasonable output beam, the beam has a Lorentzian type profile but still displays some speckling so is fine for trapping but not quite as good as single mode fibre.

---



Figures 9(e, f & g). Figure 9(e) depicts light travelling in a single mode fibre. Figure 9(f) depicts light travelling in a step index multimode fibre. Figure 9(g) depicts light travelling in a graded index multimode fibre.

With these factors in mind we choose graded index multimode fibre for use in the trapping of large objects, greater than  $50\ \mu\text{m}$  in diameter; although the output laser beam is not perfect the large particles have a greater diameter than that of the beam and will thus ‘not notice’ the speckled intensity pattern of the output beam. The actual fibre used was  $62.5/125\ \mu\text{m}$  (core size/ cladding size) graded index fibre sourced from Newport. For the trapping of the smaller and medium sized particles and cells, from  $7$  to  $50\ \mu\text{m}$ , we choose single mode fibre due to its superior output beam characteristics that are extremely suitable for trapping. The singlemode fibre used was  $6.6/125\ \mu\text{m}$  singlemode fibre sourced from Thorlabs. Although it is more difficult to couple large powers into singlemode fibre we were able to couple in more than enough for our trapping experiments.

### 9.2.1.2 Fibre optic launch system

The requirements for our fibre launch system is that we couple light into two fibres and have the ability to adjust the relative power in the fibres so that when our trap is formed we may move the trapped object between the two fibre faces via the scattering force. The laser we choose for this experiment was a linearly polarised

1070nm fibre laser, IPG photonics VLM-5-1070-LP; this wavelength is far from that of the Raman probe, at 785nm, so should not cause interference in the acquired Raman spectra whilst also maintaining a low chance of causing any photodamage [19]. This is then passed through a half wave plate and onto a polarizing beam splitter cube; this allows us to split the beam in two and with the use of the half wave plate adjust the relative power in each beam. The laser light is then coupled into the optical fibres through x10 microscope objectives with the use of commercial fibre launch stages (Elliot Scientific MDE510). Although a x10 objective will not create a beam spot the same size as single mode fibre core it matches the numerical aperture of the fibre more effectively thus is a more efficient choice. A picture of the setup can be seen in figure 9(h).

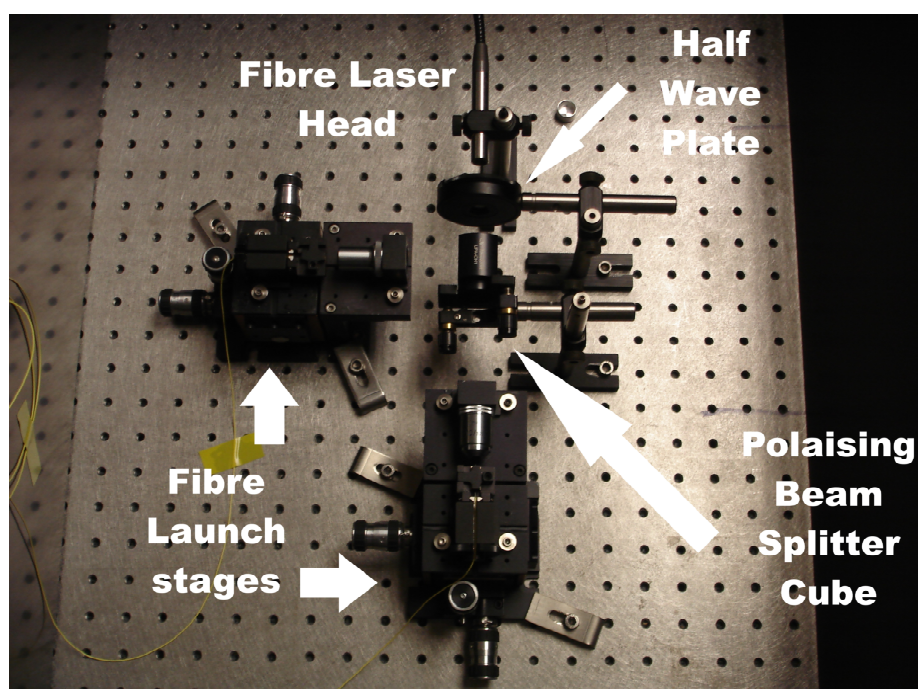


Figure 9(h). A picture of the launch system used in the fibre optical Raman tweezers experimental setup.

The alignment procedure for the setup, in figure 9(h), begins by setting the laser head at the same height as the centre of the back aperture of the microscope objectives. The laser is then passed through the half wave plate and into the beam splitter to crate the two beams. Using a power meter the half wave plate is adjusted to balance the power

---

in each split beam. The fibre launch stages holding the microscope objectives can be aligned by moving them across the beam, a reflection from the back lens of the microscope objective can be clearly seen on the back of the half wave plate holder after passing back through the beam splitter cube, when this reflection appears as a perfect circle the stage is aligned. Absolute critical alignment is not required as the fibre holder is placed on a moveable stage to compensate. Once this has been done the fibres must be placed into the holders, seen opposite the microscope objectives on the fibre launch stages in figure 9(h). The fibres however must be cleaved to create a smooth face for maximum coupling efficiency. First any outer sheaths and coatings must be removed; this is done by placing the fibre in acetone for a few minutes. The acetone weakens and swells the plastic coverings that can then be pulled off, the fibre is then wiped using lens tissue dipped in isopropanol and cleaved using a commercial cleaver (Fujikara CT-07). The fibres are then placed in the holders. The free ends of the fibre optic cables are then cleaved in an identical manner to produce a quality output beam. The free ends are then shone into an optical power meter and the translation stage on the fibre launch stage is adjusted until a maximum output power is achieved. The construction of the launch system is now complete and we can begin building the trap. One final consideration in the preparation of the fibres is to ensure that they have a length difference greater than the coherence length of the laser. This ensures no standing waves are created in the trap between the two laser faces. Using this system we can obtain launch efficiencies up to forty percent for single mode fibre and up to eighty percent for the multimode fibre. In combination with the 5W power available from the fibre laser means we have ample power available for our trapping experiments and coupled with the half wave plate polarising beam splitter cube combination we have dynamic control over our trapped particles. The final task

---

---

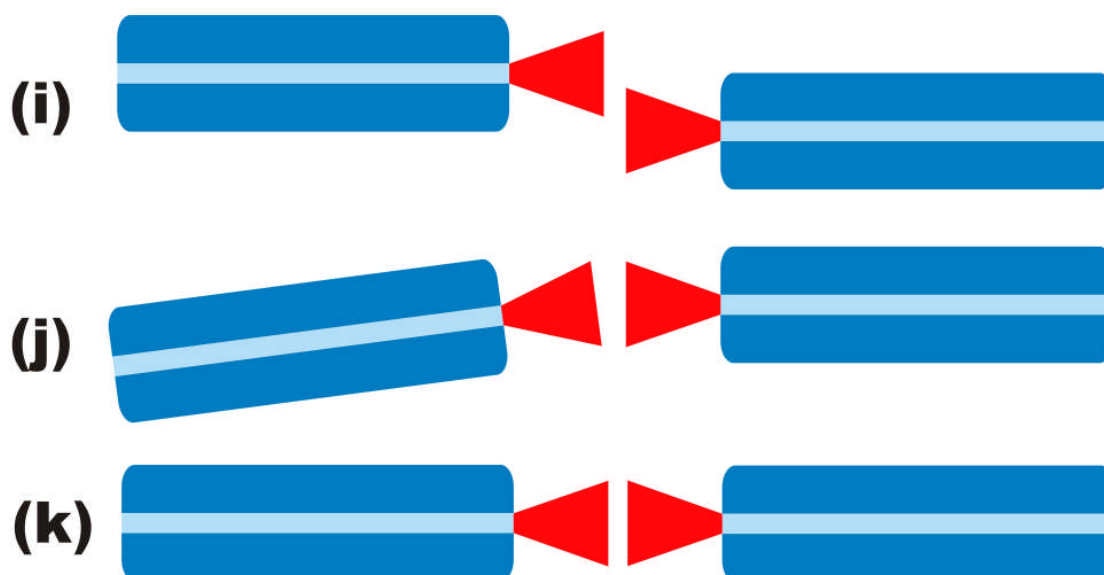
before constructing the trap itself was to characterise the output of the fibres with respect to the input laser power so we may know the power emanating from the fibres during experimentation.

### **9.2.1.3 Constructing the fibre optical trap**

With the launch system constructed we must actually construct the trap itself, in theory this is straight forward as it is just two fibres placed opposite each other. The reality is slightly more complicated however and we must consider how we are going to view the trap, fix the fibres in place and how we may align the fibres. The fibres themselves are relatively large, in comparison to the objects we will study, so a 10x or 20x objective is required to be able to view the fibres for alignment, this conflicts with the requirement for high spatial resolution spectroscopy. The use of a commercial microscope, containing an objective turret, means that we can switch objectives at will through the experiment without disturbing the trap. The choice of objective raises another key issue; the 100x objective preferred to obtain high spatial resolution has a very short working distance of only 230  $\mu\text{m}$ . In the fibre trap the trapped particles will sit on an axis, between the two fibre cores, 62.5  $\mu\text{m}$  above the coverslip on which the samples are placed, this leaves us with a working distance of a little under 170  $\mu\text{m}$ . As the microscope is inverted and we must pass the laser through the coverslip, on which the fibres and samples are placed. This means we must choose a very thin cover slip, less than 170  $\mu\text{m}$  thickness, so that we may move the objective close enough to focus on samples. In fact a type 0 coverslip, a standard commercially available thickness, was used to place the samples on as it has an average thickness of only 100  $\mu\text{m}$  allowing further flexibility in the focussing and allowing for the possibility of three dimensional sample mapping. With imaging issues addressed we must think about

---

alignment and construction of the trap. The two optical fibres need to be counter propagating and aligned both in terms of transverse alignment and in terms of angular alignment, figures 9(i) and 9(j) show these possible misalignments respectively. We do not need to worry about vertical alignment as two fibres sit on the same surface. Figure 9(k) shows a schematic of the correct alignment. In order to achieve a good alignment we fixed one of the fibres to the coverslip and mounted the second on a translation stage so that it could be aligned correctly against the first fibre. Physically this meant securing the coverslip to the microscope stage with tape and again securing one of the fibres to the coverslip with tape. The second, movable fibre was placed in a holder constructed from a 25 gauge medical needle glued to an optical post and attached to a commercial translation stage (Newport M-562), which was screwed onto the microscope stage. A photograph of the equipment can be seen in figure 9(l). The translation stage could be used to align the fibre in the transverse direction and control the fibre separation; the angular alignment was done by observing the fixed fibre on the monitor and merely rotating the post, on which the fibre is mounted, until a matching angle is achieved. The moveable fibre is placed on the slide at a slight downward angle to ensure the natural elasticity in the fibre forces it flat against the coverslip.



Figures 9(i, j & k). Figure 9(i) depicts the fibre trap transversely misaligned, in this situation the light from the lower fibre will push the particle away until it feels the transverse gradient force of the upper fibre and get drawn into the upper beam and again pushed away until it will feel the transverse gradient force from the lower fibre setting up a circular motion for the particle. Figure 9(j) depicts and angular misalignment in the fibre trap, in this instance there is a net force pushing particles sideways out of the trap. Figure 9(k) depicts a well aligned fibre trap the particles will be stably trapped between the two fibres.

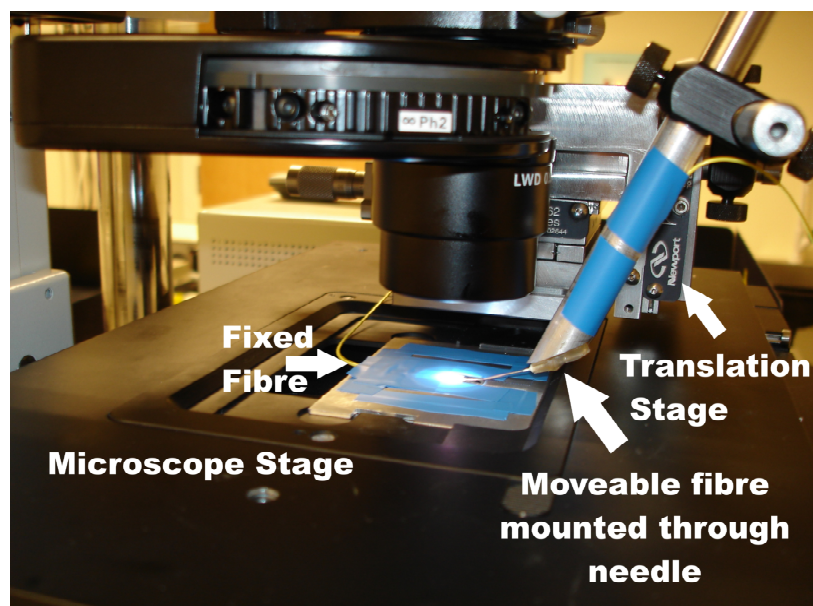


Figure 9(1). A picture of the fibre trap placed on the microscope stage.

The alignment of the system can be performed crudely by eye initially and then with the use of the microscope camera to make the fine corrections and ensure it is aligned

---

correctly. Finally the alignment can be checked by passing the laser through one of the fibres and blocking the beam entering the second fibre. If the fibres are aligned correctly the laser light will couple from one fibre through into the 'dark' fibre and a laser spot will appear on the other side of the beam block used to stop light entering the objective of the dark fibre launch stage.

This is a rudimentary but extremely effective method of creating a fibre trap above a conventional Raman tweezers system that can be used to trap and hold large objects whilst we perform Raman measurements on them.

### **9.2.2 Sample preparation**

In this series of experiments on the fibre optical trap, biological cells, polystyrene microspheres and ethylene dimethacrylate (EDMA) microspheres are investigated and were prepared in the following manner.

Separate mono disperse dilute solutions of 50 and 100  $\mu\text{m}$  polystyrene spheres, sourced from Duke Scientific, were prepared by diluting the spheres in deionised water. Dilute samples are preferred to avoid interference from large numbers of surrounding particles.

For an experiment evaluating the ability of the system to probe different particles simultaneously held in the fibre trap a 50/50 mixed solution of 5 $\mu\text{m}$  polystyrene spheres and 7 $\mu\text{m}$  EDMA spheres was prepared. This mixture was also diluted with deionised water to avoid interference.

For the cellular based studies we used primary human keratinocytes (PHK), kindly provided and cultured by Dan Smith, human promyelocytic leukemia (HL60) cells and human cervical squamous carcinoma (SiHa) cells. The cells were prepared as follows: Primary (normal) human keratinocytes (PHKs) from neonatal foreskin

---

(Cambrex) were cultured in keratinocyte growth medium-2 (KGM-2) containing the supplied supplements (PromoCell) as described in reference 20. The HL60 human promyelocytic leukemia cell line was grown in RPMI 1640 medium containing 10% fetal calf serum (FCS) as described in reference 21. The SiHa cells are a cell line derived from carcinoma of uterus I, and grown in Dulbecco's Modified Eagle's Medium containing 10% fetal calf serum (FCS) and 1% penicillin, streptomycin and glutamine (PSG) as described in reference 22.

### 9.2.3 Fibre optical trap operation and evaluation

In this section we will see how the fibre trap operates and we will come across the main disadvantages of the fibre optical trap.

With the fibre trap set on the microscope stage, as described in the previous section, we are ready to put the sample on the coverslip. Five hundred microlitres is pipeted onto coverslip over the top of the two fibres; this is the first main disadvantage of the fibre trap, the sample is not contained in a chamber and is open to the air. Thus the sample cannot be kept sterile and will evaporate away causing currents within the liquid droplet, containing the sample. In order to combat this, a further one to two millilitres is placed around the fibres so the evaporation does not affect the sample close to the fibres, furthermore the temperature in the lab is set to a minimum to slow the evaporation process. In our studies the sterility of the cellular samples is not a problem as we do not wish keep the cells and culture them further.

Once we have the sample on the stage we turn on fibre trap laser and wait for a sample to be captured between the two fibres. This is the second disadvantage of the fibre trap; with a single beam gradient tweezers we can move the stage to find a particle that will be drawn into the laser beam, however as the fibres are fixed on the

---

stage we must wait for a particle to pass between the fibres and become trapped. Due to the very large capture area of the fibre trap we normally do not have to wait for very long to capture and trap a particle. The situation is different when we are dealing with small cells and particles, up to approximately ten microns, the Raman probe beam can be used to trap the small particles and lift them into the fibre trap where the large trapping force pulls the particle out of the single beam tweezer onto the axis between the two fibre faces. When dealing with biological cells, as they are slightly more buoyant compared to solid polystyrene spheres, it is possible to use a 20x objective, through which the Raman probe beam is passed, to slowly levitate cells through radiation pressure into the fibre trap.

Once our particle is in the trap it is unlikely to be exactly in the centre and will certainly drift off to one fibre faces due to an imbalance of optical powers emanating from the fibres. The position of the particle can be then altered by adjusting the half wave plate, in the launch system, resulting in a change in power coming from each fibre. Using this method it is possible to obtain a stably trapped particle; furthermore it is possible to trap the particle at several stable positions between the two fibres by adjusting the half wave plate suitably. Although no formal investigations were carried out we found it was possible, using only forty milliwatts of power from each fibre, to separate the fibre faces to such an extent as they were out of the field of view of the microscope, using a 10x objective, and still keep a 50  $\mu\text{m}$  polystyrene particle trapped. Furthermore experimentally we observed that reasonably large misalignments in the trap did not adversely affect the trapping due to the strong nature of the transverse gradient force, although again no formal investigations were carried out. The strong and robust trapping of the fibre trap, coupled with the large possible fibre face separations makes it very easy to incorporate other probes and allow them

---

---

to study the trapped sample. Using our Raman Tweezers system we can now probe the chemistry of the particle we have trapped.

When we have our particle trapped we can turn the objective turret to select an objective for Raman studies. In the experiments in this chapter we used two objectives for exciting and collecting the Raman signal, the first was a Nikon x100 NA 1.25 oil immersion objective and the second was a Nikon x50 NA 0.9 oil immersion objective. As we must keep the Raman probe fixed, to maximise Raman collection efficiency, the particle must be moved over the Raman probe beam. This can be done in two ways; firstly by using the optical forces to move the particle between the two fibres until it is over the probe and secondly by moving the microscope stage on which the fibre trap is placed. The first method only allows one dimension of movement thus we moved the microscope stage to select the portion of trapped particle we wanted to study and position it over the Raman probe; the robustness of the fibre trap means that it was unaffected by the sample stage movement. When we turned on the Raman probe, which had an optical power of 30mW, we did notice some interference on the position of the particles held in the fibre trap. As the Raman probe is still essentially a single beam gradient trap it exerts a force on the particle held in the fibre trap, this was not found to be a problem as an equilibrium position was reached between the forces, exerted by the two traps, and we were able to study the particle at will. This perturbation of the particle in the trap was not observed for trapped cells, most likely due to their non uniform structure and varying density. It is pertinent to mention at this point that when trapping cells in the fibre trap they are extremely stable and strongly trapped. This is most likely due to the large trapping area of the fibre trap, due to the diverging nature of the beams, that results in more of the cell being involved in the trapping process thus the refractive index variations are not as

---

---

important as in single beam tweezers where the trapping area is only a few microns at the largest. When we have selected the area on the trapped particle we wanted to study the flip mirror, in the microscope, was changed from the viewing position to the Raman collection position and we were able to acquire a quality signal. If multiple measurements were to be made on the particle we reselected the viewing position, of the microscope, moved the next area to be interrogated over the Raman probe and selected the Raman position on the microscope to collect a signal.

Our particles could be trapped in the fibre trap and, by selecting a higher magnification microscope objective, could be examined with the Raman probe beam. Using the above methods we were able to carry out the experiments described in the results section.

### 9.3 Experimental Results

To demonstrate the usefulness and full potential of the fibre optical trap we undertook a series of experiments using the fibre trap as the primary trapping mechanism to hold particles whilst we interrogated them with a Raman probe beam introduced from below.

As we have previously mentioned the use of a fibre optical light force trap opens up the possibility of stably trapping large objects with reduced power densities and without the need for holographic beam shaping or multiple trap sites. As an example, figure 9(n) shows a fibre optical light force trap, with graded index multimode fibres, being employed to trap and move a 100 micron object using 800 mW of light travelling in each fibre, resulting in an output irradiance of  $5.2 \times 10^8$  W/m<sup>2</sup>. We believe this is the largest optically trapped object reported to date.

There are some extra experimental considerations we must keep in mind when trapping these very large spheres. The first consideration is the weight of the particle; as we increase the radius  $r$  we increase the mass by a factor of  $r^3$ . For a particle with a diameter of  $100\mu\text{m}$  the mass will obviously be very substantial. This means that the particle is not likely to sit on the trapping axis directly between the centres of the two fibre cores but will sit beneath this axis where the upward transverse gradient force balances the force on the particle due to gravity. The particle can also be translated and stably held at several positions between the fibres by varying the powers emanating from each fibre. As the particle sits below the trapping axis it is difficult to be certain that we are trapping the particle completely in three dimensions. In order to ensure we are trapping the particle in three dimensions a slight alteration had to be made to the sample slide. Instead of using one glass slide and placing the fibres on it a more advanced sample slide was created, as shown in figure 9(m), which formed a deep well beneath the trap allowing us to ensure the particle was completely three dimensionally trapped.

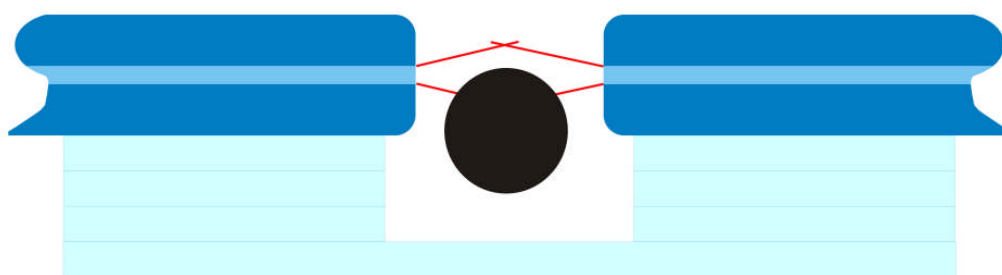


Figure 9(m). Schematic of the sample chamber used to trap the  $100\mu\text{m}$  spheres, the formation of the chamber beneath the fibres ensures that we are trapping the particle in three dimensions.

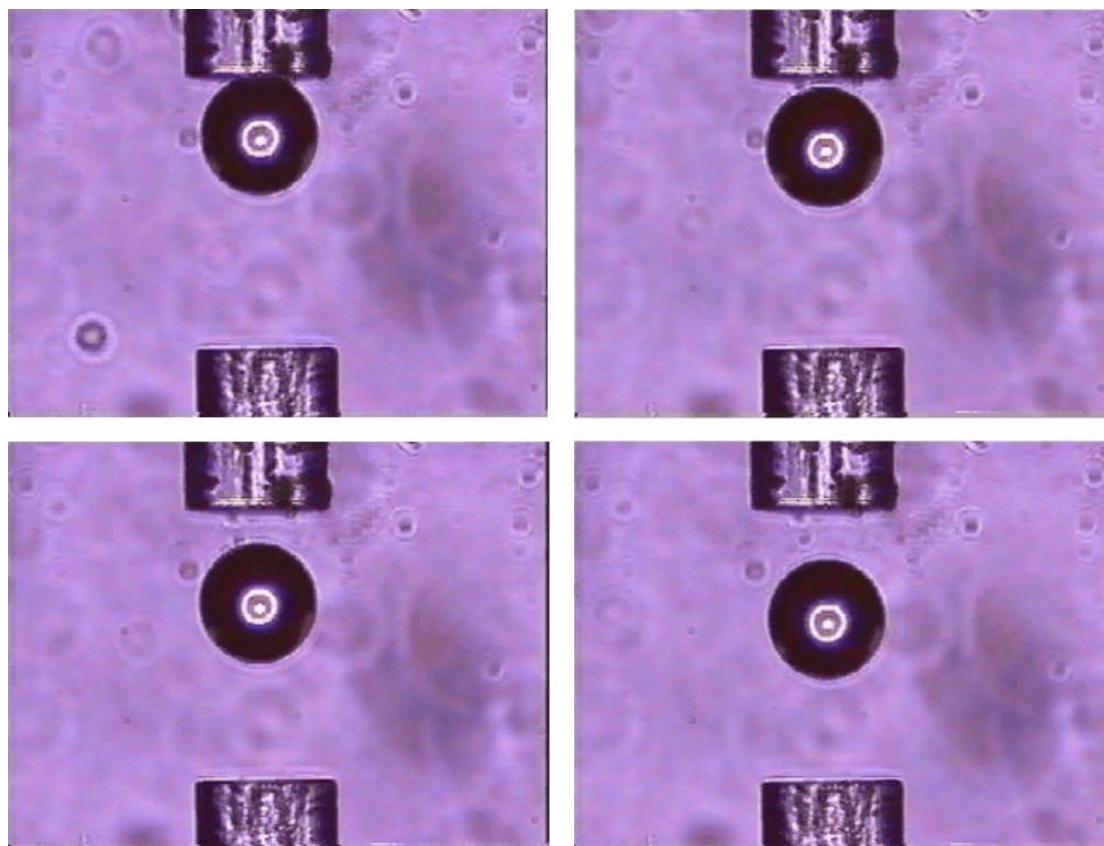


Figure 9(n). A 100 micron polymer sphere trapped in a fibre optical light force trap, viewed from below. The fibre trap uses 62.5/125 $\mu\text{m}$  (core size/ cladding size) multimode fibre, a trapping power of 800mW in each fibre arm and a fibre separation of 240 $\mu\text{m}$ . The series of images shows how the particle can be translated from one fibre to the centre of the trap just by adjusting the half waveplate, in the fibre launch setup.

Although the optical power seems quite high a look at the irradiance,  $5.2 \times 10^8 \text{ W/m}^2$ , tells us that the power density is in fact lower than that of the 30mW focussed Raman probe beam which has an irradiance of  $4 \times 10^{10} \text{ W/m}^2$ . It is this fact that is key in the reduced probability of photodamage when trapping cells in a fibre trap compared with a traditional single beam tweezer. We should stress that the trapping of a particle this size is far beyond the capabilities of single beam tweezers and using the fibre trap we can not only trap but also retain the advantages that single beam tweezers provides for smaller particles such as moving particles away from interfering surfaces.

---

As we discussed, this novel geometry allows us to separate the trapping and Raman probe functions giving us local control over where in the trapped particle we examine. To demonstrate this a 50 micron polystyrene sphere was trapped in the fibre optical light force trap, using a power setting of 40 mW emanating from each singlemode fibre (irradiance  $4.6 \times 10^9 \text{ W/m}^2$ ) and a fibre separation of  $175 \mu\text{m}$ . Using the mechanical motion of the sample stage, upon which the fibres are placed, the particle was then scanned across the Raman probe beam. The intensity of the Raman probe beam was set to 30 mW (irradiance of  $4 \times 10^{10} \text{ W/m}^2$ ) and focused onto the sample with a Nikon x50 NA 0.9 oil immersion objective, the Raman signal at each scan step was then integrated for two seconds. The particle was scanned perpendicularly to the fibre trap trapping axis in 5 micron intervals measured with the use of a calibration grid. A calibration grid was imaged with the microscope enabling us to calibrate a five micron movement into a fixed distance on the monitor. A conversion grid was then drawn up on acetate and placed on the monitor to allow us to measure five micron intervals when looking at our trapped particles on the monitor. The intensity of the  $1000 \text{ cm}^{-1}$  benzene ring breathing mode in polymer was monitored as the particle was scanned to demonstrate the system's ability to measure the depth of the particle at each point, we should note that no confocal arrangement was used in order to collect as much information as possible. The results can be seen in figure 9(o).

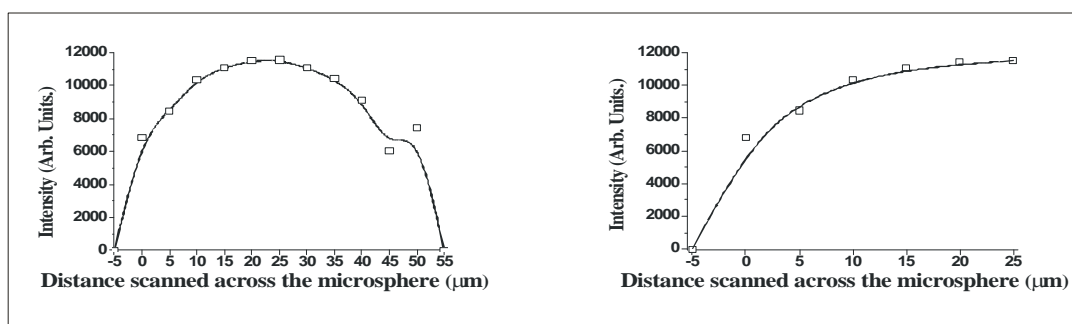


Figure 9(o). Left Chart shows the variation in Raman intensity, of the  $1000\text{cm}^{-1}$  benzene ring breathing mode of polystyrene, as the microsphere is scanned across the Raman excitation laser. The Right hand chart shows a fit of the data obeying a Lorentzian relationship that we became familiar with in chapter 8.

From figure 9(o) we see that as the depth of the particle decreases, due to its spherical nature, the Raman intensity falls off proportionately with the depth as we move from the centre of the sphere. The right hand chart shows the Raman intensity of half the scanned particle displaying the familiar Lorentzian shape that we became familiar with in chapter 8. We also observe a small unexpected dip in intensity at  $45\mu\text{m}$  into the scan, on the left hand chart; we believe this is due to a defect in this microsphere and serves to further show the sensitivity of this technique. We believe that this was a defect, as we scanned over the area several times and the same intensity dip was observed. These results show that this method allows us to gain sensitive localized information from large objects.

To show the ability of the system to trap and hold multiple particles of different species and chemically identify them, we used the Raman probe laser to trap and load the fibre trap with particles of different materials. Polymer particles ( $5\mu\text{m}$ ) and ethylene dimethacrylate (EDMA) particles ( $7\mu\text{m}$ ) were loaded into the fibre trap creating a colloidal conglomerate of these objects. Once in the fibre trap, the objects may be moved by varying the intensity of the optical field from each fiber permitting us to record the local Raman signal from this sphere amalgamation giving chemical

information from the trapped particles. The trapping and Raman excitation powers, as well as the fibre type used are the same as those described for the experiment with the 50 micron sphere and the fibre face separation was 65 $\mu\text{m}$ . The results can be seen in figure 9(p).

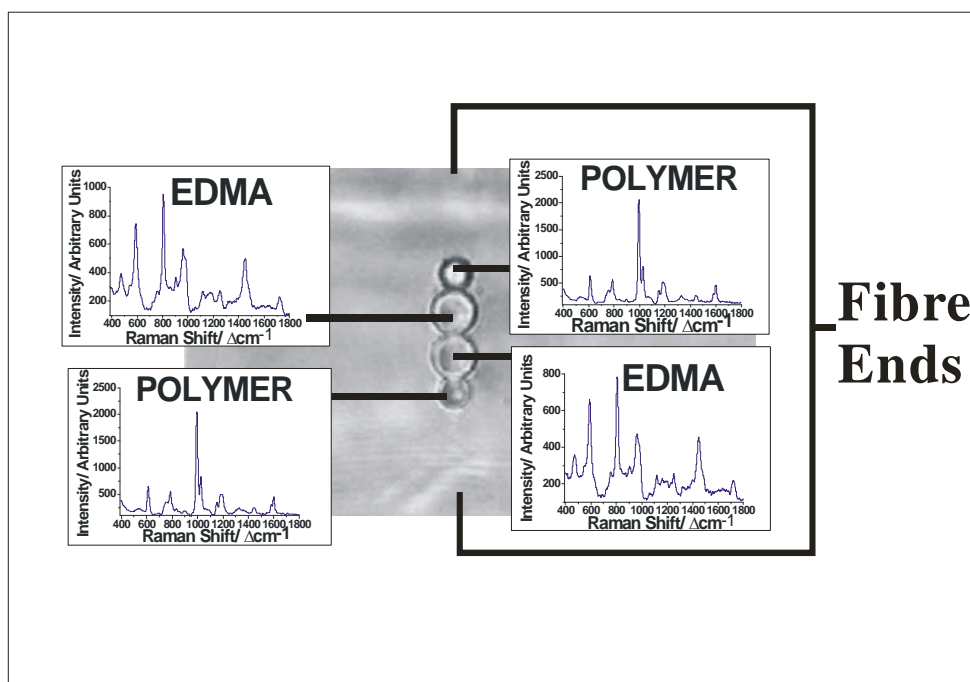


Figure 9(p). A conglomerate of spheres in the fibre trap created from two 7 $\mu\text{m}$  EDMA spheres and two 5 $\mu\text{m}$  polymer spheres. They are shown with their measured Raman spectra demonstrating the ability of this technique to gain localized sensitive chemical information.

Figure 9(p) shows that the fibre trap allows us to not only store multiple particles, but also to perform localized Raman spectroscopy and distinguish easily different types of particle purely by adjusting the laser power, to move different particles over the Raman probe beam, or by moving the fibre positions, relative to the Raman excitation laser beam, via mechanical movement of the sample stage.

The examination of the polystyrene and EDMA spheres demonstrate both the ability of the fibre trap to capture multiple particles and the combined fibre trap Raman tweezers system to chemically analyse samples. However the area of application that this arrangement is likely to have the largest impact is in that of the study of single cells.

---

In order to examine the potential of this technique, in the area of single cell examination, we trapped and acquired localized Raman signals from a primary human keratinocyte (PHK) cell. PHKs are normal cells that form the lining of the skin. They are approximately 30 $\mu$ m in diameter and have relatively small nuclei, with abundant cytoplasm, giving them a low nucleo-cytoplasmic ratio. This presents a significant challenge to trapping technologies and demonstrates clearly the utility of the approach described here. In order to confirm this we attempted to tweeze HL60 cells and SiHa cells with a single beam trap formed with a Nikon x100 NA 1.25 oil immersion objective and a power of 80mW (irradiance of  $1 \times 10^{11}$  W/m<sup>2</sup>) at 1070nm, a comparable power to that utilized by the fibre trap. The SiHa cells were chosen as they are very similar to PHK having a low nucleo-cytoplasmic ratio. We found that with this large power of 80mW it was possible to tweeze the smaller HL60 cells, approximately 8 microns in diameter. These cells are reasonably easy to tweeze as they have a high nucleo-cytoplasmic ratio meaning there are few other high index organelles able to compete for position in the trapping beam. However there was little control over the trapping position and such high power increases the risk of two photon damage cellular damage [16]. We found that the orientation of the cells in the single beam trap was not stable. Two trapping sites were observed on the cell, the nucleus and the membrane; this is most likely due to the non uniform cell density. Over periods of a few seconds the 'stable' trap site would often oscillate between the membrane and the nucleus. We then tried to tweeze the large SiHa cells and found it was only possible to tweeze the cells in the plane parallel to the coverslip for a time before they attached to the glass slide. Although we were able to tweeze these cells to an extent, the high power density at the focus of the single beam tweezer poses a serious risk of photodamage. Using the dual beam trap we can ensure trapping

---

---

stability over long periods of time and keep the cells away from any surfaces denying the cell any opportunity to form attachments thus making long term studies on a single cell viable.

For the localized Raman experiment on PHK cells, 40mW of power from each singlemode fibre (irradiance of  $4.6 \times 10^9 \text{ W/m}^2$ ) with a fibre face separation of  $85 \mu\text{m}$  was used to trap the PHK cell. A 20 mW Raman probe beam (irradiance of  $2.5 \times 10^{10} \text{ Wm}^{-2}$ ) was passed through a Nikon x100 NA 1.25 EPLAN oil immersion objective to the sample. The higher power objective was selected in this case to give a tightly focused beam hence a small examination area. In order to avoid interference from surrounding areas a 100 micron diameter pinhole was placed in the image plane to form a confocal arrangement that corresponds to a 1 micron aperture in the sample plane. The signal was then integrated for two minutes. By using this method we recorded separate spectra from the membrane, cytoplasm and the nucleus. Five spectra were taken at each point, summed together and smoothed, using the method of adjacent averaging, to produce the data shown in figure 9(q). Figure 9(q) also contains an image of the cell in the fibre trap displaying the exact locations of the spectral acquisitions and a figure displaying a Raman spectrum of a cell taken in the fibre trap and sitting on the coverslip to demonstrate just what an advantage it is to have the cell optically trapped above the coverslip. The spectrum of the cell on the coverslip has a large amount of auto fluorescence, from the coverslip, masking the detail of the Raman peaks. Accompanying figure 9(q) we also present a tentative band assignment [2, 23 & 24] for the observed Raman peaks as shown in figure 9(r). We should also note that in order to ensure our Raman probe laser, the beam with the highest irradiance, was not adversely affecting the cells we carried out a trypan blue exclusion test. Trypan blue is a membrane impermeable dye that is only able to ingress into the

---

---

cell upon cell death. When viewed under the microscope healthy cells appear normal but dying cells appear blue. We grew SiHa cells onto marked Petri dishes and exposed 40 individual cells to two minutes of 20mW 785nm laser beam and subsequently exposed them to the trypan blue dye. The results were then compared to a non-irradiated control set and no increased rate of cell death was observed.

Observing the spectra in figure 9(q) it is immediately noticeable that the three spectra are visually quite different. If we first consider the spectra pertaining to the nucleus and cytoplasm we can see that strong peaks corresponding to DNA sugar-phosphate backbone and bases A,T,G and C ( $785,830,895,1048$  and  $1093\text{ cm}^{-1}$ ) are markedly reduced in the cytoplasm spectra. This is to be expected as the nucleus contains DNA in highest densities. However these peaks do remain visible in the cytoplasm spectra as the bases A, C and G, but excluding thymine, which form DNA also form RNA which we would expect to be present in significant quantities in the cytoplasm. Perhaps one of the most interesting aspects of this comparison is the study of the peaks attributed solely to thymine and deoxyribose. Thymine is a DNA base that is replaced by uracil when RNA is formed and transferred to the cytoplasm, in a similar manner deoxyribose has a hydroxyl group added to it to form the sugar backbone section in RNA. If we examine the peak at  $751\text{ cm}^{-1}$ , attributed solely to thymine, we see that it almost completely disappears in the cytoplasm spectra when compared with that of the nucleus; it is likely that the remaining small peak, in the cytoplasm spectra, is due to the small amount of DNA present in the cytoplasm. Similarly the two peaks attributed solely to deoxyribose, at  $895$  and  $1048\text{ cm}^{-1}$ , are affected in the same manner with comparatively large depletions in their intensities. It is also interesting to note that, as expected, peaks pertaining to proteins and amino acids ( $643, 852, 939$  and  $1660\text{ cm}^{-1}$ ) remain prevalent in the cytoplasm spectra and, in the

---

---

case of the  $1609\text{ cm}^{-1}$  peak, display a small enhancement. Finally, in this comparison we also may not have expected the large lipid peak at  $1451\text{ cm}^{-1}$  in the cytoplasm spectra. However the geometry of the Raman system means that in order to access the cytoplasm region, despite the small confocal aperture of  $1\mu\text{m}$  in the examination plane, the laser will also pass through the membrane which will contribute to the total spectra collected. It is also possible that the laser beam, used for Raman excitation, may act as a single beam optical trap opening up the possibility of trapping vesicles in the probe during the excitation and collection of the Raman spectra. If we look at the spectra for the membrane we can again see that, in comparison to the other two spectra, the Raman peaks are much reduced. However, we may have expected that the spectra would only contain the large lipid peak at  $1451\text{ cm}^{-1}$  along with a few peaks relevant to proteins and amino acids that may be embedded in the membrane. Although this is generally the case we cannot fail to notice contributions to the spectra from peaks pertaining to DNA/RNA. This is likely to be due to interference from the surrounding cytoplasm.

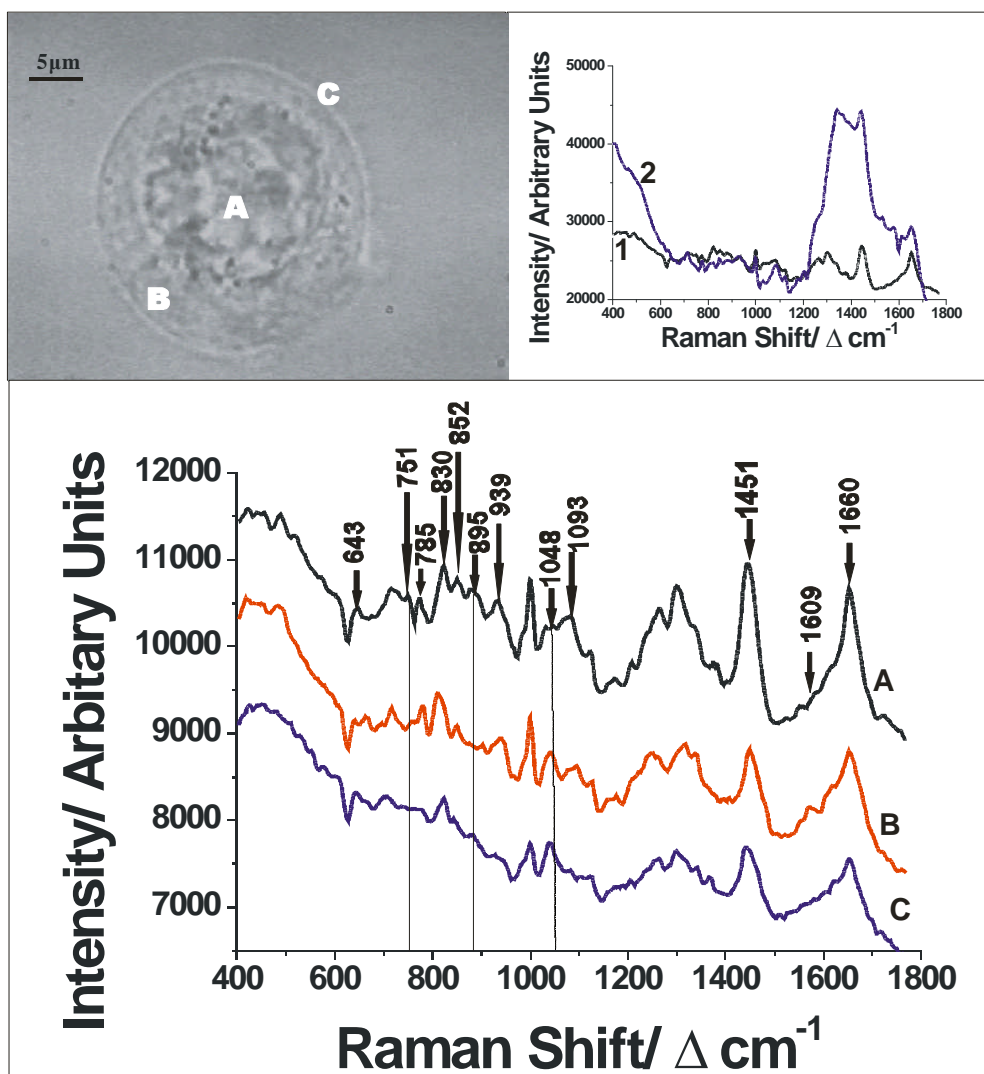


Figure 9(q). Raman Spectra obtained from 3 different positions within a PHK cell: Nucleus (A), Cytoplasm (B) and Membrane (C). The actual laser position during the excitation is also shown by the letters in the top left diagram. The top right hand diagram shows spectra taken from the nucleus of a cell in the fibre optical trap (1) and absorbed onto a glass coverslip (2). The use of the fibre optical trap reduces the background allowing us to discern the Raman features in more detail.

Bands (1/cm)	Assignment	Molecule Type	Expected Location
643	p: C-C twist/ Tyr	Protein/ amino acid	CY&NC
676	T/ G	DNA/ DNA&RNA Base	NC/NC&CY
725	A	DNA& RNA Base	NC&CY
751	T	DNA Base	NC
785	T/C/DNA: O-P-O <sup>(-1)</sup>	DNA/ DNA&RNA Base/DNA Backbone	NC/NC&CY/NC
830	DNA: O-P-O <sup>(-1)</sup> /Tyr	DNA Backbone/ amino acid	NC/NC&CY
852	Tyr	Amino acid	CY&NC
895	DNA bk,deoxyribose	DNA	NC
939	p: C-C bk	Proteins	CY&NC
1004	Phenylalanine	Amino acid	CY&NC
1033	Phenylalanine	Amino acid	CY&NC
1048	C-O str. In deoxyribose	DNA	NC
1093	DNA: O-P-O <sup>(-1)</sup>	DNA Backbone	NC
1126	C-N stretch	Poly Peptide bonds	CY&NC
1178	T/G	DNA/ DNA&RNA Base	NC/NC&CY
1212	T/C,A/Tyr, Phenylalanine	DNA/ DNA&RNA Base/Amino acid	NC/NC&CY/NC&CY
1259	Amide III, $\beta$ sheet/ T/C	Proteins/DNA Base/DNA&RNA Base	CY&NC/NC/NC&CY
1312	A def	DNA&RNA Base	NC&CY
1338	A, G def	DNA&RNA Base	NC&CY
1376	T/A,G	DNA Base/ DNA&RNA Base	NC/NC&CY
1451	Lipids/p: CH def	Membranes	M&NC&CY
1512	A	DNA&RNA Base	NC&CY
1581	A, G	DNA&RNA Base	NC&CY
1618	Trp,Phenylalanine,Tyr	Amino acid	CY&NC
1660	Amide I, $\alpha$ helix	Protein	CY&NC

Figure 9(r). Band Assignment for Raman Spectra of PHK. Abbreviations:P-Protein, Tyr-Tyrosine, T-Thymine, G-Guanine, A-Adenine, C-Cytosine, bk-DNA sugar-phosphate Back Bone, Trp-Tryptophan , CY-Cytoplasm, NC-Nucleus, M-Membrane.

Previous studies investigating localized Raman signals within cellular structures have required the cell to be fixed or adhered to a surface [4] or the use of exceptionally low Raman excitation powers to avoid interference with the trapping mechanism [12]. These results, however, demonstrate the ability of this system to obtain localized sensitive chemical information from cells stably trapped, in the fibre trap, away from interfering surfaces. We did however previously mention two key disadvantages of the fibre optical trap: the lack of an enclosed sample cell and difficulty loading large samples into the trap. In the next section we shall see how

---

these problems may be circumvented whilst tackling an extremely promising area of Raman tweezers, microfluidic Raman systems.

## 9.4 Microfluidic Raman Tweezers spectroscopy

### 9.4.1 Introduction and motivations

The creation of a flow cytometric type system based on Raman spectroscopy as the analyzing method, instead of fluorescence, is an exciting prospect as it would require no molecular labeling of the cells to be analysed and open up the possibility of rapidly studying many more medical conditions and biological species in an unsupervised manner. In the broader area of microfluidics, fibre optical traps are showing great promise as the non contact large trapping area characteristic of fibre traps coupled with their ability to easily trap large biological cells makes them ideal for integration with microfluidic flow channels. Notably this has been realised using the cell stretcher where cell elasticity has been exploited to distinguish normal cells from malignant cells [17]. The incorporation of Raman micro spectroscopy into microfluidic systems has been previously demonstrated by Ramser *et al* and involved a red blood cell held in a single beam trap and monitored whilst fluid was flowed through the system [25] allowing the study of one single cell and its response to it changing environments.

In our microfluidic Raman system we aimed to construct a cell flow system where the fibre trap could be used to trap and hold particles inside a microfluidic channel whilst a Raman probe beam, orthogonal to the fibre trap, could be used to examine the trapped particles in the flow channel.

---

### 9.4.2 Construction and operation of the microfluidic Raman system

The rudimentary microfluidic Raman system that we demonstrate uses exactly the same apparatus as that used throughout this chapter and is one of the main advantages of our system requiring little or no additional complexity in the Raman tweezers system itself. The only difference is the creation of the microfluidic channel; this is simply a square glass capillary tube, of outer dimension  $160\mu\text{m}$  and inner diameter of  $80\mu\text{m}$ , placed between the two optical fibres forming the fibre trap. This is done very simply during the construction phase of the optical trap, as described in section 9.2.1. When the coverslip and fixed fibre have been taped down onto the microscope stage the capillary tube, which is cut to a length of around two centimetres with a razor blade, is placed on the coverslip with a pair of tweezers and pushed up to the fibre face by eye. When this is done the fibre mounted on the translation stage can be brought towards the fixed fibre; as it approaches the capillary tube and fixed fibre it will push the capillary tube up against the face of the fixed fibre and trap it between the two fibres, this immediately lines the capillary tube up orthogonal to the fibres and a trap is formed in the capillary between the two fibres.

We are now able to flow particles through the flow channel, formed by the capillary, and trap them with the fibre trap. We flowed two solutions through our trap; a mono disperse sample of  $10\mu\text{m}$  polymer spheres and a dilute sample of HL60 cells. To set up a flow through the capillary tube two reservoirs were placed at each end of the tube, one larger than the other to drive a flow based on simple capillary action. Unfortunately this means we have no control over the flow speed but a working system could use a micro pump to stably flow particles through the system at a preset speed. A  $1\text{ ml}$  drop of sample was placed on the left hand side of the tube and a  $500\mu\text{l}$  drop was placed at the right hand side that resulted in a left to right flow through the

---

---

tube. As we mentioned, we have no control over the flow speed that starts very fast using the above settings. However as the volume in the reservoirs even out the flow speed reduces to a 'useable' level.

With our sample flowing through we are ready to trap a particle, this is simply done by turning on the laser and waiting for a particle to become trapped. However we are now not relying on a particle in a sample randomly dropping through the trap rather we have forced the particles, via the flow channel, to flow through the trapping region thus a particle becomes rapidly trapped between the fibres. The use of a microfluidic channel overcomes one of the primary disadvantages of the fibre trap, loading the trap; by forcing the particles to pass through the trapping region it makes the trap much easier to load.

At this point it is also useful to note that if we require a sterile system the capillaries can be sterilised and, by the mechanism of capillary action, draw up sterile cellular samples. The tube can then be sealed, keeping it sterile, and transferred to apparatus for examination. This sealed system gives us a sterile environment for our samples and avoids evaporation of the sample addressing two of the major problems in fibre optical trapping.

Although this is a rudimentary flow system, microfluidics is a relatively well known technology and the flow could be driven in a more controllable manner with a micro pump through the capillary tube. Using this system we were able to flow particles through a microfluidic channel trap them and examine them with the Raman probe. This allowed us to perform the experiments described in the following section.

---

**9.4.3 Raman examination of particles in a microfluidic flow system**

Initially, we flowed a solution of 10 $\mu$ m polymer particles through the capillary tube at a volume flow rate of 1.2 nl/s. Against the outside wall of the capillary tube, the two single mode fibers were placed opposing each other, resulting in a fibre face separation of 160 $\mu$ m, as can be seen in figure 9(s). The power from the fibers was set to 80mW emanating from each fibre (irradiance of 4.6x10<sup>9</sup>W/m<sup>2</sup>), the increase in optical power required from the fibres is due to the capillary walls scattering some of the incident light and to hold the particles stably against the flow. A 50mW Raman probe beam (irradiance of 6.3x10<sup>10</sup>W/m<sup>2</sup>) was then introduced from below using a Nikon x50 NA 0.9 oil immersion with an excitation time of 5 seconds. We should also note that a 200 $\mu$ m confocal aperture was used to reduce interference from the glass capillary; the fibre trap however, by holding the sample away from the capillary walls, allows the use of a generous confocal volume. The spectra obtained from a polymer microsphere trapped inside the capillary can also be seen in figure 9(s). We were additionally able to implement cell flow through the system at a volume flow rate of 40 pl/s. Again, a Raman probe beam was introduced, as for the polymer, and an acquisition time of 60 seconds was used for cell studies. Despite the higher laser power from the fibre trap the cells did not exhibit any damage during the trapping. The spectra from HL60 cells, a human promyelocytic leukaemia cell line, are shown in figure 9(t). The Raman peaks can be assigned according to figure 9(q).

This result confirms both the practicality and potential for dual beam fibre traps coupled with Raman spectroscopy for use in microfluidic and lab-on-a-chip environments. Furthermore by using a capillary, to hold the sample, between the two fibres we address a few of the major issues in fibre optical trapping; that of sterility, trap loading and evaporation. Also useful is the fact that the fibres do not have to

---

continually cleaned and cleaved every time we change sample as they no longer sit in the sample but act on the particles through the capillary tube walls. The use of this system in a flow cytometric style system is highly promising but there does remain one major obstacle, and an obstacle for many Raman applications, that of the acquisition time. For the HL60 cells this was 60s, compared to a few milliseconds in fluorescence based flow cytometry, although we shall see in chapter 11 how this may potentially be addressed.

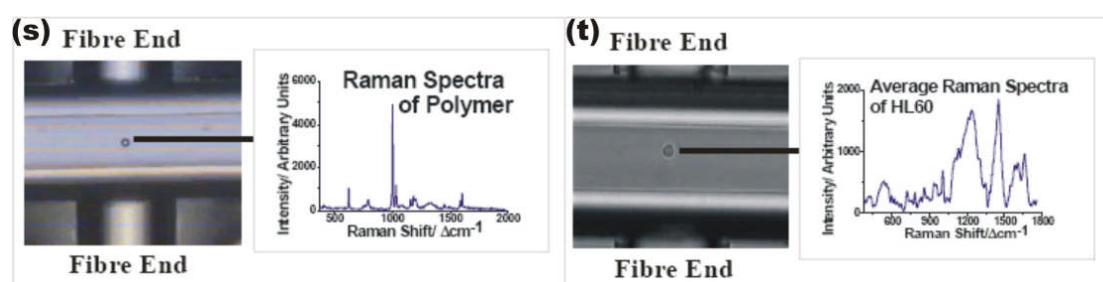


Figure 9(s & t). Figures 9(s) and 9(t) show the fibre optical trapping and Raman examination of a 10 micron sphere and a HL60 cell respectively in a microfluidic flow system constructed from a square capillary tube, the horizontal object in the figure, with two fibers placed orthogonally against the capillary walls forming a dual beam trap with the Raman probe introduced from below the trap.

## 9.5 Conclusions

Single beam Raman tweezers has become an exciting and useful tool in the study of biological samples, in particular the study of single cells. Although Raman tweezers has made the study of single cells feasible the technique does have some drawbacks; single beam tweezers have difficulty trapping, three dimensionally, large cells and the cells do not remain stable in the trap. The required small trapping volume of the single beam tweezer can not engage large areas of the cell so the signal retrieved is not truly representative of the state of the whole cell. Although conversely this small trapping beam should be useful for subcellular mapping and analysis, the movement of the cell in the trap stops the acquisition of a spectrum from only one small area and is compounded by the combined trapping Raman probe system that

---

does not enable us to select at will an area for examination. In order to combat these shortfalls many groups have proposed decoupled Raman tweezers setups to separate the Raman and tweezing functions, however these advanced setups have not been able to effectively control and probe large cells at will.

To address the shortfalls in the Raman tweezers technique we developed a decoupled Raman tweezers system based on the use of a fibre optical light force trap as the primary trapping mechanism, this allows us to effectively control and study large samples. The fibre optical trap is ideal as it can trap very large objects; we have seen in our study how we may use a fibre trap to capture and manipulate objects up to 100 $\mu\text{m}$  in size with reduced power densities in comparison to a single beam tweezers. Although it is rare to find cells 100 $\mu\text{m}$  in size, cellular trapping being the key application of this technique, most cells are in the 20-50  $\mu\text{m}$  size range and the fibre trap allows us to trap these stably. The low power density experienced by particles in a fibre trap is key in the reduced probability of two photon damage in the cells allowing us to study them effectively for longer whilst maintaining strong stable trapping. The stable trapping is most likely the result of a much larger area of the cell being involved in the trapping process, due to the divergent nature of the trapping beams; thus the non uniformity of the cells refractive index profile is less important than in conventional single beam tweezers. As well as the these important properties of the fibre trap, the large fibre face separations, whilst maintaining strong trapping, allows us to incorporate the Raman tweezers probe to study the trapped objects. As the fibre trap merely sits on the microscope stage of the conventional Raman tweezers no alteration of the existing system is required. As we seen we then were able to use this system to study large polystyrene particles, chemically identify mixed species forming a conglomerate in the fibre trap and acquire sensitive localised biochemical

---

information from an optically trapped PHK. It would also be possible to extend this technique and make biochemical maps of entire trapped cells.

The fibre optical Raman tweezers system brings many advantages, in the study of large cells, but as we have discovered there is some significant drawbacks in the use of this technique. Firstly we do not have an enclosed sample chamber leading to a lack of sterility and evaporation causing currents within the sample. Secondly we have little control over the loading of the fibre trap with large particles and we must wait for a particle to pass between the fibres and become trapped. Cells can be optically levitated using the Raman probe beam but this is not ideal and a slow process. These are very serious drawbacks in the use of this system but when we implemented a microfluidic flow into this system we seen how these problems could be addressed.

Finally we implemented a microfluidic flow to evaluate the ability of the system to stop and trap particles in a flow whilst acquiring a Raman signal from them; this allowed us to appraise the possibility of using this technique in a flow cytometry style system. We were able to stop and acquire Raman signals from 10  $\mu\text{m}$  polystyrene particles and HL60 cells in the flow demonstrating the feasibility of using this technique in a possible high throughput technology. The only drawback of this type of system, for studying cells, is the very long acquisition times, although we shall see later in this thesis how this could potentially be addressed. The use of the capillary tube as the microfluidic channel also addressed our two major concerns in the use of the fibre optical trap. By flowing particles through a channel we force them through the trapping region between the two fibres thus we no longer have to wait for a particle to randomly pass between the fibres and become trapped. Furthermore it is also possible to prepare a cellular sample in the capillary tube and seal the ends,

---

before transferring the sample to the fibre optical Raman tweezers system, keeping the sample sterile and avoiding evaporation.

The use of a fibre optical Raman tweezers system allows us to effectively study large cellular samples whilst maintaining the advantages of conventional single beam Raman tweezers that has made it such an attractive technique in the study of single biological cells.

## 9.6 References

- [1] Singh GP, Volpe G, Creely CM, Grotsch H, Geli IM and Petrov D. **The lag phase and G1 phase of a single yeast cell monitored by Raman microspectroscopy.** *Journal of Raman Spectroscopy* 2006; **37**: 858-864
  - [2] Mannie MD, McConnell TJ, Xie C and Li YQ. **Activation-dependant phases of T cells distinguished by use of optical tweezers and near infrared Raman spectroscopy.** *Journal of Immunological Methods* 2005; **297**: 53-60
  - [3] Chan JW, Taylor DS, Zwerdling T, Lane SM, Ihara K and Huser T. **Micro-Raman spectroscopy detects individual neoplastic and normal haematopoietic cells.** *Biophysical Journal* 2006; **90**: 648-656
  - [4] Krafft C, Knetschke T, Siegner A, Funk RHW and Salzer R. **Mapping of single cells by near infrared Raman microspectroscopy.** *Vibrational Spectroscopy* 2003; **32**: 75-83
  - [5] Feofanov AV, Grichine AI, Shitova LA, Karmakova TA, Yakubovskaya RI, Egret-Charlier M and Vigny P. **Confocal Raman Microspectroscopy and Imaging Study of Theraphthal in Living Cancer Cells.** *Biophysical Journal* 2000; **78**: 499-512
  - [6] Xie C, Goodman C, Dinno M and Li YQ. **Real-time Raman spectroscopy of**
-

- 
- optically trapped living cells and organelles.** *Optics Express* 2004; **12**: 6208-6214
- [7] Volpe G, Singh GP and Petrov D. **Dynamics of a growing cell in an optical trap.** *Applied Physics Letters* 2006; **88**: 231106-231108
- [8] Xie C, Dinno MA and Li YQ. **Near-infrared Raman spectroscopy of single optically trapped biological cells.** *Optics Letters* 2002; **27**: 249-251
- [9] Ramser K, Logg K, Goksor M, Enger J, Kall M and Hanstorp D. **Resonance Raman spectroscopy of optically trapped functional erythrocytes.** *Journal of Biomedical Optics* 2004; **9**: 593-600
- [10] Gessner R, Winter C, Rosch P, Schmitt M, Petry R, Kiefer W, Lankers M and Popp J. **Identification of Biotic and Abiotic Particles by Using a Combination of Optical Tweezers and In Situ Raman Spectroscopy.** *ChemPhysChem* 2004; **5**: 1159-1170
- [11] Creely CM, Singh GP and Petrov D. **Dual wavelength optical tweezers for confocal Raman spectroscopy.** *Optics Communications* 2005; **245**: 465-470
- [12] Creely CM, Volpe G, Singh GP, Soler M and Petrov D. **Raman imaging of floating cells.** *Optics Express* 2005; **12**: 6105-6110
- [13] Ashkin A, Dziedzic JM, Bjorkholm JE and Chu S. **Observation of a single-beam gradient force optical trap for dielectric particles.** *Optics Letters* 1986; **11**: 288-290
- [14] Ashkin A. **Acceleration and trapping of particles by Radiation Pressure.** *Physical Review Letters* 1970; **24**: 156-159
- [15] Constable A, Kim J, Mervis J, Zarinetchi F and Prentiss M. **Demonstration of a fibre-optical light-force trap.** *Optics Letters* 1993; **18**: 1867-1869
- [16] Koenig K, Liang H, Berns MW and Tromberg BJ. **Cell damage in near**
-

---

**infrared multimode optical traps as a result of multiphoton absorption.**

Optics Letters 1996; **21**: 1090-1092

- [17] Guck J, Schinker S, Lincoln B, Wottowah F, Ebert S, Romeyke M, Lenz D, Erickson HM, Ananthakrishnan R, Mitchell D, Kas J, Ulvick S and Bilby C.

**Optical deformability as an inherent cell marker for testing malignant transformation and metastatic competence.** Biophysical Journal 2005; **88**: 3689-3698

- [18] Wilson J and Hawkes J. **Optoelectronics: an introduction 3<sup>rd</sup> edition.** 1998; Prentice Hall Europe: 373-392

- [19] Neuman KC, Chadd EH, Liou GF, Bergman K and Block SM. **Characterisation of Photodamage to Escherichia Coli in Optical Taps.** Biophysical Journal 1999; **77**: 2856-2863

- [20] Southern SA, Lewis MH and Herrington CS. **Induction of tetrasomy by human Papillomavirus type 16 E7 protein is independent of pRb binding and disruption of differentiation.** British Journal of Cancer 2004; **90**: 1949-1954

- [21] Collins SJ, Galb RC and Gallagher RE. **Continuous growth and differentiation of human myeloid leukaemic cells in suspension culture.** Nature 1977; **270**: 247-249

- [22] Friedl F, Kimura I, Osato T and Ito Y. **Studies on a new human cell line (SiHa) derived from carcinoma of Uterus I. It's establishment and morphology.** Proceedings of the Society of Experimental Biology and Medicine 1970; **135**: 543-545

- [23] Hamden KE, Bryan BA, Ford PW, Xie C, Li YQ and Akula SM. **Spectroscopic analysis of Kaposi's sarcoma-associated herpesvirus infected cells by Raman tweezers.** Journal of Virological Methods 2005; **129**: 145-151
-

- 
- [24] Puppels GJ, De Mul FFM, Otto C, Greve J, Robert-Nicoud M, Arndt-Jovin DJ  
and Jovin TM. **Studying single living cells and chromosomes by confocal  
Raman microspectroscopy.** Nature 1990; **347**: 301-303
- [25] Ramser K, Enger J, Goksor M, Hanstorp D, Logg K and Kall M. **A microfluidic  
system enabling Raman measurements of the oxygenation cycle in single  
optically trapped red blood cells.** Lab on a chip 2005; **5**: 431-436

---

# 10. Wavelength Modulated Raman Spectroscopy

---

*The prospects for Raman spectroscopy to become a widespread tool in medical diagnostics and for use in monitoring biological processes are extremely good. As we have seen throughout this thesis the technique is excellent for probing the biochemical states of single cells, and indeed tissues, in a range of applications. There is still however one barrier stopping Raman spectroscopy finding more widespread use; the long integration times required to acquire quality Raman spectra. In this chapter we will explore the possible use of wavelength modulated Raman spectroscopy to increase signal to noise ratios and subsequently reduce acquisitions times and discuss what future developments must take place for this technique to become a regular addition to Raman tweezers microscopy.*

---

## 10.1 Introduction and Motivations

Raman spectroscopy, as we have seen, is proving a very powerful tool for monitoring biological cells and for disease diagnosis. It is no surprise therefore that interest is increasing in the use of Raman spectroscopy as a medical diagnostic tool, particularly but not exclusively in cancer medicine. Raman spectroscopy has also been used in the detection of the malaria causing parasites in red blood cells [1], detection of the early onset of dental caries [2], strain typing of the hospital super bug acinetobacter [3] and the diagnosis of heart atherosclerosis [4]. Two of the most probable vehicles for the application of Raman spectroscopy, in medical diagnostics, are fibre optic probes, most likely endoscope based, or incorporated into flow cytometry type systems. This would allow Raman based technologies to sit easily along side current medical practice. The main issue preventing the incorporation of

---

---

Raman spectroscopy into these biomedical systems is the relatively long integration times required to acquire good quality Raman spectra. Typical times to acquire Raman spectra of biological tissue or cells, using a confidently non-destructive laser power, are often on the order of a few tens of seconds to minutes. Compare this to the tens of microseconds to seconds required to excite and analyse the fluorescence signals in flow cytometry. This essentially means that the use of Raman spectroscopy, in its current form, is not practical for the analysis of cells in a flow cytometry style system. Furthermore the use of Raman spectroscopy *in vivo* with the use of a fibre optic probe, to examine patients, will result in acquisition times of such length, to gain useful data, that it would be extremely uncomfortable for the patient. We should mention that fibre optic probes have been demonstrated for *in vivo* studies [5] but their use has not progressed beyond the proof of concept phase. Acquisition time considerations are also extremely important for the monitoring of biological systems in the lab. Although Raman is often touted as a real time monitoring system for cells, it can only monitor events that are much longer than the acquisition times. To exploit the full potential of Raman, as a technique that can engage many biochemical species simultaneously without the need for markers, the acquisition times must be lowered to allow the true real time monitoring of cell function and behaviour.

The ability to acquire good quality Raman spectra in a short time would open up many new avenues of study for Raman spectroscopy and allow this powerful analysis technique to sit easily alongside current medical practices.

## 10.2 Experimental Aims

In this chapter we aim to investigate and develop a technique that will allow us to reduce the integration times required to acquire good quality Raman spectra from

---

---

biological cells with our Raman tweezers system. In developing a technique to reduce the integration times we must keep in mind the end application which is studying single biological cells, although the technique could probably be easily extended to the study of other samples. It would also be advantages to keep any additions to the experimental setup as simple as possible to reduce experimental complexity.

### **10.3 Current approaches to reducing Raman signal acquisition times**

With Raman spectroscopy offering so many advantages in the study of biological, and in fact many other samples, it is no surprise that much effort has gone into reducing signal acquisition times. In this section we will see how these techniques have been implemented and assess their suitability for studying single biological cells.

Decreasing the excitation time essentially means increasing the signal to noise ratio; this can obviously be achieved in two ways, either by increasing the signal strength or reducing or circumventing the noise somehow. Increasing the signal strength is normally based around some form of enhancement mechanism such as resonance Raman spectroscopy. Resonance Raman spectroscopy uses an excitation wavelength close to an electronic transition and is capable of giving an enhancement of around  $10^2$ . Another enhancement mechanism is surface enhanced Raman spectroscopy, which uses aggregated metallic particles or metallic surfaces to provide the enhancement and is capable of providing enhancement factors of up to  $10^{14}$ . Resonance Raman spectroscopy has been demonstrated in a microfluidic system to study red blood cells [6] but as this technique requires a suitable molecule with an electronic transition matching the laser energy it is not widely applicable to all biomedical samples. Furthermore the visible wavelength lasers required to match an

---

---

electronic transition in a molecule may induce photodamage in the cell being studied. Surface enhanced Raman spectroscopy has also been used in the biomedical sciences chiefly in the detection and probing of single biomolecules such as DNA [7]. However the technique has also been used to interrogate cells [8, 9]. By incubating the cells with metal colloid some of it is up taken by the cells and will aggregate inside the cell, a laser can then be used to excite the surface enhanced Raman signal from the aggregate. This technique produces very strong signals from the aggregate inside the cells but the extremely short range of the enhancement, on the order of a few nanometres, means that only a small amount of the cell is probed thus any pertinent information from the rest of the cell is lost. Enhancement techniques are very useful and powerful tools but are less able to engage entire cells simultaneously from virtually any biomedical sample which is one of the major advantages of the use of Raman spectroscopy as a biomedical diagnostic or monitoring tool.

As well as enhancing the signal much effort over the last few decades has gone into reducing the noise or circumventing it. Many of these techniques were developed at a time when spectroscopic instruments were less sensitive in the near infrared and noise, mainly from fluorescent sources, was an extremely large problem in obtaining any Raman signal at all never mind a clear and rapid one. Many of these techniques were developed for traditional forms of Raman spectroscopy rather than Raman microspectroscopy where fluorescence is less of a problem as the high photon density at the laser focus partially quenches fluorescence. However, using the noise reducing techniques in a microspectroscopy system could potentially reduce the noise further and hence reduce the signal integration times required to acquire good quality useable Raman signals. The most notable of these techniques include Kerr gated Raman spectroscopy [10], polarised Raman spectroscopy [2], Phase resolved Raman

---

---

spectroscopy [11] and shifted excitation Raman difference spectroscopy (SERDS) [12].

Kerr gated Raman spectroscopy is a recently developed technique that utilises ultrafast laser pulses. This technique exploits the fact that the Raman process is fast, on the order of tens to hundreds of picoseconds, in comparison to time taken for a fluorescence event which is on the order of tens to hundreds of nanoseconds. The laser pulse is split in two and one section is sent to the sample to excite the Raman scatter, the Raman scatter is then collected and sent to the spectrometer. The time difference between the Raman scatter and fluorescence events is exploited with the use of a Kerr gate, placed at the entrance to the spectrograph, and the second portion of the split laser pulse. A Kerr gate is simply a medium that is opaque until illuminated with a laser pulse whereupon it becomes transparent for the duration of the laser medium interaction. The arrival of the second part of the split laser pulse at the Kerr gate is timed to coincide with the arrival of the Raman scatter from the probed sample; this allows the Raman scatter to pass through the Kerr medium into the spectrograph. The duration of the pulse, interacting with the Kerr gate, is set to such a length as to allow the gate to remain open for only a few picoseconds allowing the Raman scatter to pass and then 'close' the gate before the arrival of the fluorescence signal at the spectrograph. This technique is extremely successful but requires very precise alignment and a complicated experimental arrangement. Furthermore the pulsed nature of the exciting beam increases the risk of causing two photon damage in biological samples.

Polarised Raman spectroscopy [2] in its most elementary form can be very useful for reducing fluorescence; this technique finds its basis in the fact that the polarisation of the scattered radiation has a close relationship with the input laser

---

---

polarisation. Fluorescence emission tends to be more randomly polarised thus the use of a piece of polaroid in front of the spectrograph, aligned with polarisation axis of the Raman scatter, will block much of the fluorescence whilst allowing the majority of the Raman scatter to pass to the spectrograph. This technique is very simple to implement but is less effective in suppressing interfering fluorescence in comparison to the other techniques mentioned here. Rather polarised Raman spectroscopy has found its niche in probing the structure of molecules; by measuring how effective the sample under study is at depolarising the Raman scatter, this can give information on the molecular structure particularly the chirality of molecules.

Phase resolved Raman spectroscopy again exploits the difference in Raman scatter and fluorescence emission. This technique uses two electrooptic modulators, one acting on the laser beam and the other on the collected Raman scatter. The laser is then intensity modulated with the electrooptic modulator driven by an rf oscillator. The same rf modulator, with a phase delay instrument, also drives the electrooptic modulator in the Raman beam path thus, as the Raman scattering is so fast, it is in phase with the laser modulation allowing it to pass through the electrooptic modulator in the Raman beam path. As the fluorescence is slower it is not in phase with the laser beam so is rejected. This technique is successful and has been demonstrated to give a twenty fold increase in signal to noise ratio. This technique is readily incorporated into Raman systems but does require expensive phase modulators and associated equipment and careful synchronisation of the phases of the two electrooptic modulators.

Shifted excitation Raman difference spectroscopy is probably one of the most effective techniques that can be used to remove fluorescence from Raman spectra and is based around the wavelength independence of the Raman effect. As we have

---

---

mentioned previously, a change in the frequency of the exciting laser will result in a change in the frequency of the Raman peaks as they always remain a fixed distance, in wavenumbers, from the exciting laser line. In the SERDS technique an initial Raman spectrum is acquired from the sample, the laser frequency is then tuned slightly and a second spectrum is acquired from the same sample. There is no direct consensus in the literature as to the magnitude of the wavelength shift but it normally tends to be around  $10\text{cm}^{-1}$ , enough to produce a pseudo differential signal when the two signals are subtracted from each other. This can then be integrated to reproduce the original Raman signal. The advantage of this technique is that, although the Raman peaks will move, the fluorescence background remains unchanged thus when the spectra are subtracted it is removed. This technique has the advantage that it requires little or no alteration to existing Raman setups and has in fact been demonstrated in Raman tweezers. In 2004 Xie *et al* were able to acquire SERDS signals from biological cells simply by temperature tuning the laser diode used to power their Raman tweezers system [12]. This technique is easily incorporated into Raman tweezers system but does require careful shifting of the wavelength to create the pseudo differential signal.

These techniques are all successful in improving signal to noise ratios but the technique we chose to investigate and develop is that of wavelength modulated spectroscopy.

## **10.4 Wavelength modulation spectroscopy and its incorporation with Raman spectroscopy**

Wavelength modulation spectroscopy is a technique used widely in spectroscopy and involves the continual sweeping of the laser frequency [13]. This

---

---

technique is often used in absorption spectroscopy where the continual modulation of the frequency causes an amplitude modulation in the beam intensity picked up by the detector. This is fed into a lock in amplifier and essentially produces an amplified differential signal which can be integrated to give the amount of the absorption and width of the absorption peak. This technique picks out the signal from noisy environments as the intensity of the noise is unaffected by the frequency modulation of the laser. Furthermore this technique is ideal for implementation with diode lasers as they are easily frequency modulated by current injection alone giving rapid modulation and requiring no extra special optic devices. This is an extremely powerful technique for identifying spectral features in noisy environments which has led to its widespread implementation.

Indeed the potential application of this technique to draw Raman peaks out of extremely noisy spectra was quickly recognised and in 1976 Funfschilling and Williams demonstrated a wavelength modulated Raman system [14]. This technique was based on the modulation of the dye laser, with the use of an etalon, which was used to excite the Raman scatter. The collected Raman scatter was fed into a monochromator. As we have mentioned before the scanning of the laser frequency will result in the scanning of the Raman peaks themselves thus the Raman peaks, separated out by the monochromator grating, are physically scanned across the exit slit of the monochromator. This results in an amplitude modulation in the output signal picked up by a photomultiplier tube, a single channel detector. This fulfils the requirement of wavelength modulation spectroscopy, converting a frequency modulation into an amplitude modulation which can be fed into a phase lock in amplifier to extract the Raman signal. The grating must then be scanned to examine the entire Raman spectrum. Furthermore, as the fluorescence and noise is not affected

---

---

by the modulation it is not picked up as a signal and is rejected. This is an extremely powerful technique for extracting Raman signals from fluorescent samples. In 1978 Levin and Tang also successfully demonstrated a very similar system for the study of chemical dyes [15]. In 1984 Van de Ven et al, using an almost identical system to Funfschilling and Williams, applied wavelength modulation spectroscopy to biomembranes constructed from lipids demonstrating how this technique could be applied to biological samples [16]. At this point interest in the technique fell away most likely due to improvements in detector technology and infrared laser sources, which are a much simpler way of reducing fluorescence interference. Although these publications demonstrate the effectiveness of wavelength modulated Raman spectroscopy the technique does have a major drawback in its use of single channel detectors. The use of single channel detectors means the grating must be scanned to acquire a full Raman spectrum dramatically increasing the acquisition time.

In our study we want to apply wavelength modulation Raman spectroscopy, as the technique should be easily incorporated into Raman tweezers with little modification to the current experimental setup, to improve signal to noise ratios and hence reduce the time to acquire a quality Raman spectrum. However we also want to continue using our multichannel detector retaining the advantages it brings of low dark noise and being able to acquire a complete spectrum in a single shot. This will almost certainly mean we will not be able to use a phase lockin amplifier but we may be able to mimic its effect with a mathematical algorithm in our data processing.

---

## 10.5 Experimental setup and procedures

### 10.5.1 Experimental setup

The great advantage of using a diode laser in our setup is that it can be very easily frequency modulated by current injection. The laser diode driver, Newport model 505B used to control the power output of the laser diode, has a built in current modulation facility. Thus the only addition to the Raman tweezers setup was the inclusion of a frequency generator that was connected to the diode driver via a BNC cable. The current can be modulated at a rate of 20 mA/V input into the diode driver by the frequency generator.

The Raman tweezers system remains unaltered, except for the addition of the frequency generator, and is the evolved Raman tweezers system based on the commercial microscope as discussed thoroughly in section 6.4, the experimental parameters were then as follows. A Nikon x50 NA 0.9 oil immersion microscope objective was used to focus the laser onto the sample, optically trap it and collect the back scattered Raman signal. The spectrograph and camera were set up, using the Synergy software programme, to make a series of multiple short acquisitions. This was done so we could capture spectra at a faster rate than the modulation rate of the laser frequency to allow us to chart the movement of the Raman peaks across the pixels of the CCD camera. The individual acquisition parameters will be noted before each experiment as they varied depending on the particular acquisition. We should also note that the 300 lines/mm grating was used for all acquisitions to allow us to capture the whole spectra in one shot. The laser power used is variable due to the current injection being used to frequency modulate the laser. The laser was modulated heavily, as we will see later, to move the frequency of the laser substantially. This is a result of the resolution of the spectrograph and the large spectral band that the Raman

---

---

signal covers. In acquiring the whole Raman spectrum in one shot, to reduce acquisition time, we have a single pixel resolution of 74 GHz meaning a substantial modulation of the laser frequency is required to move the Raman peaks over a couple of pixels. This results in the laser power varying from a couple of mW up to a maximum of 30mW at the sample. We shall see the effects of this later and discuss its implications further. A confocal aperture of 200 $\mu$ m was used to help reject any background fluorescence.

These parameters were used in all the following acquisitions.

### 10.5.2 Experimental samples

In this set of experiments we used two samples: polystyrene microspheres and SiHa cells, which are cells derived from a cervical carcinoma, and were used to test the applicability of this technique to biological samples. These samples were prepared as follows.

Polystyrene microspheres of 5 $\mu$ m diameter, sourced from Duke scientific, were suspended in deionised water to form a dilute monodisperse sample.

The SiHa cells were grown in Dulbecco's modified Eagle's medium containing 10% fetal calf serum (FCS) and 1% penicillin, streptomycin and glutamine (PSG) as described in reference 17. Before use the cells must be put into suspension, thus they are exposed to 2ml of trypsin EDTA, an enzyme that releases the cells from the growth flask. After a few minutes, when the cells lift off the flask as seen under the microscope, 8ml of growth medium is added to neutralise the trypsin and form a suspension of cells.

When a sample is required 20 $\mu$ l of the sample is pipetted into a glass sample chamber for the polystyrene spheres and a quartz sample chamber for the cells. A

---

quartz sample chamber had to be used for the cells as they could not be tweezed away from the surface due to their size, thus the fluorescence of the glass would swamp the signal. Although this seems counter intuitive as we are developing a technique to negate fluorescence we want to be able to view the peaks allowing us to maximise the parameters, thus the quartz makes it easier to do this in an informed manner. The construction of the sample chamber is described in section 6.3.1.

### **10.5.3 Experimental procedures**

The big advantage of this technique is not only the minor alteration of the experimental setup but also the little alteration in experimental procedure. We have already discussed the setting of the spectrograph to acquire spectra faster than the modulation rate which is a straight forward procedure utilising the instrument software. Whenever we want to acquire data we must set the frequency generator to the desired parameters, which will be covered with the analysis of each experiment. This creates the modulation and we just acquire Raman data as normal.

### **10.5.4 Spectral analysis**

The spectral analysis of the acquired data is obviously an extremely important part of this analysis and various methods were developed by Michael Mazilu to analyse the data. As such we will discuss the analysis methods with their relevant spectra in the results section.

---

## 10.6 Results

### 10.6.1 Assessment of the inherent noise of the CCD camera

Before we applied the wavelength modulation technique to our samples we began a short series of experiments to evaluate the inherent noise in the CCD camera. This noise is a result of thermally released electrons in the CCD chip, as opposed to photon released electrons, resulting in what is commonly known as a dark count. We wanted to examine if this could be easily subtracted away from our acquired spectra to avoid it playing any part in subsequent analysis of the data. Furthermore we want to know how this noise behaves with signal integration time; for different samples we will likely vary the time of acquisition so a working knowledge of how the noise behaves in time is also extremely useful.

To evaluate the noise and its temporal behaviour we acquired spectra of different time intervals with the entrance slit to the spectrograph closed so no external signal could enter the camera ensuring we were only evaluating the dark count. In total: 100 spectra of 10ms, 100 spectra of 100ms, 100 spectra of 1s, 100 spectra of 5s, 10 spectra of 60s and 2 spectra of 150s were collected. Obviously the statistics will not be quite as accurate for the 60s and 150s acquisitions as they are based on fewer spectra but should give us a guide in this exploratory experiment.

A chart displaying the noise on the spectra at each time interval can be seen in figure 10(a).

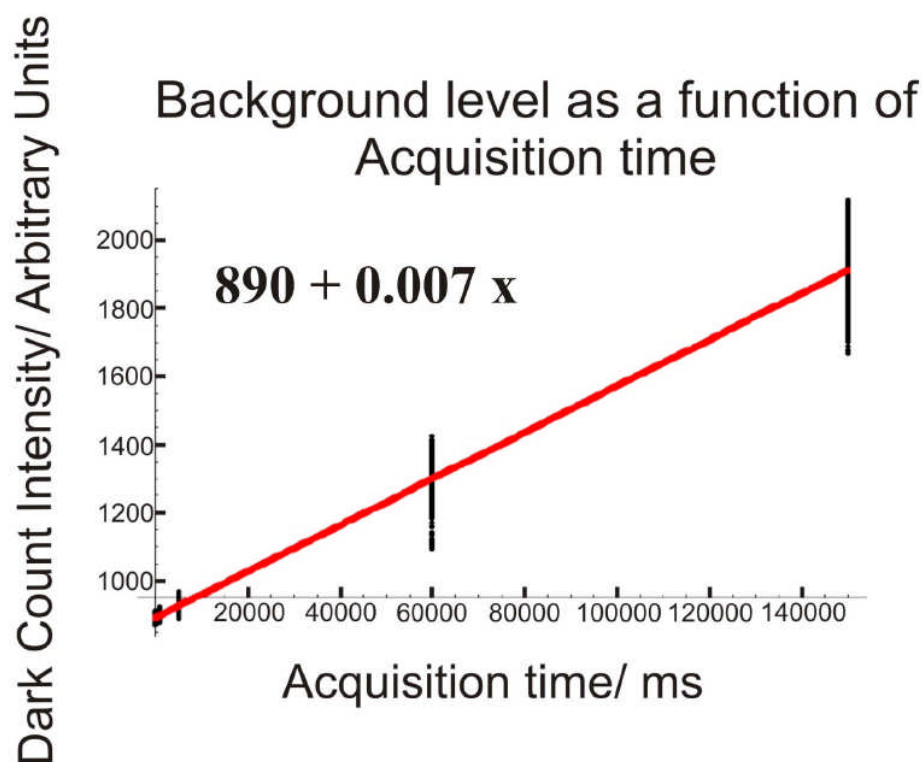


Figure 10(a). Chart displaying the dark noise as a function of acquisition time. Also included on the chart are the spread of the actual values at each acquisition time, shown in black, and an equation to the line allowing us to calculate the noise at a particular acquisition time.

This chart shows, as we expected, that the dark noise increases linearly with time and using the calculated equation, shown in figure 10(a), we can calculate the dark noise at a variety of acquisition times. However we must also ask the question; how repeatable is the noise that registers on the camera? After all this is a random thermal process and we have to know if we can reliably do a straight subtract the dark noise without further analysis. To evaluate this, figure 10(b) shows a chart of the relative standard deviation within the data set acquired at each time interval.

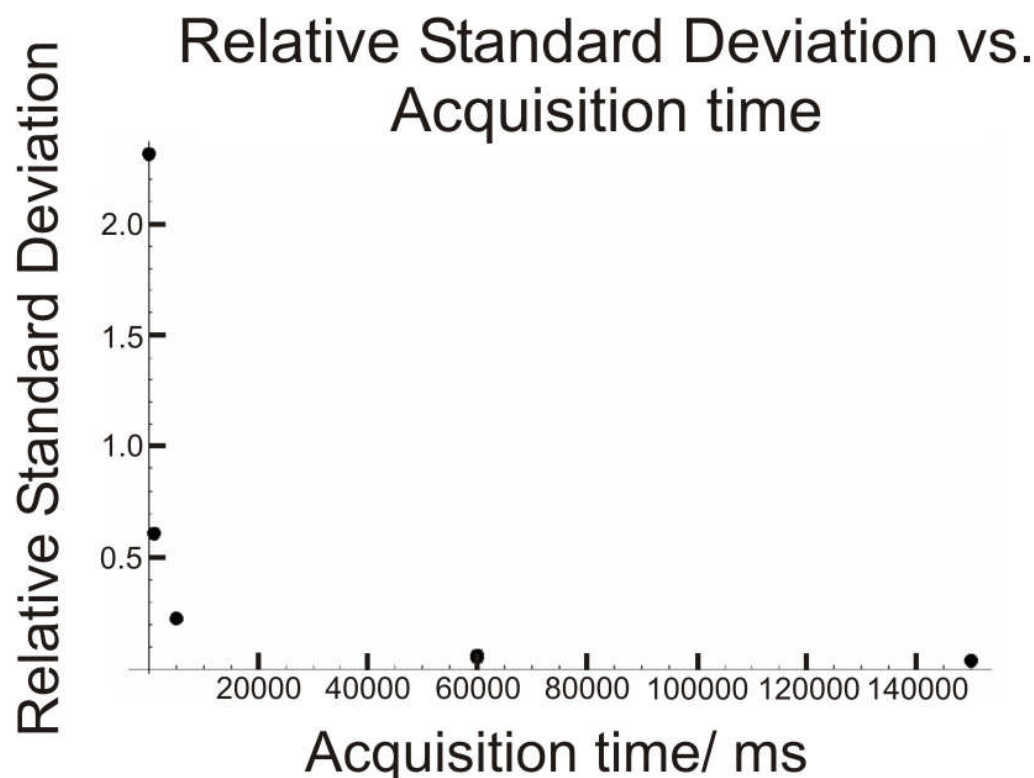


Figure 10(b). Chart displaying the relative standard deviation of the dark noise recorded at each acquisition time.

From figure 10(b) we can see that the relative standard deviation in the noise starts quite high but dramatically reduces as we increase in acquisition time. Although the last two data points are only based on a small data set they fit the pattern and the effect that we would expect to observe. Increasing the acquisition time tends to cancel out the fluctuations in thermal noise thus it can be more reliably subtracted at longer acquisition times.

This study of the dark noise in the camera shows us that, as we expected, it does increase and will add a significant component of noise to signals acquired over long period of time and as such it is routine in Raman spectroscopy to subtract this component. This can be done in a reliable manner as the relative standard deviation in the noise, during long acquisitions, is relatively low. When considering short acquisitions, of the type that we will use in this chapter to chart the wavelength modulated Raman spectra, the dark noise component is small but has a high relative

---

standard deviation. This means we must be careful if we subtract the dark noise away as it may vary significantly, although this may not be such an issue if the signal is comparatively strong. This noise will not respond to the modulation of the laser frequency thus should hopefully be negated by our analysis.

### **10.6.2 Wavelength modulation Raman spectroscopy applied to polystyrene microspheres**

To evaluate the ability of wavelength Raman spectroscopy to increase signal to noise ratios, whilst maintaining the advantages of multichannel detectors, we applied the technique polystyrene microspheres. A sample of 5 $\mu\text{m}$  polystyrene spheres was placed on the microscope stage and the Raman probe laser was used to optically trap one of the spheres. The laser current was set to 80mA and a modulation voltage of +/- 3V was applied at a rate of 0.66Hz. The spectrograph was then set to acquire 100 consecutive scans of 50ms each to allowing us to track the modulation over a few periods.

A chart displaying the intensity according to each horizontal camera pixel for each spectrum is shown in figure 10(c). This essentially tracks the Raman peaks as they are modulated. The white modulated lines represent the intensity of the polystyrene Raman peaks. Although to plot the x axis in  $\text{cm}^{-1}$ , in the charts current form, is not possible we can, after the analysis, identify the peaks according to wavenumber.

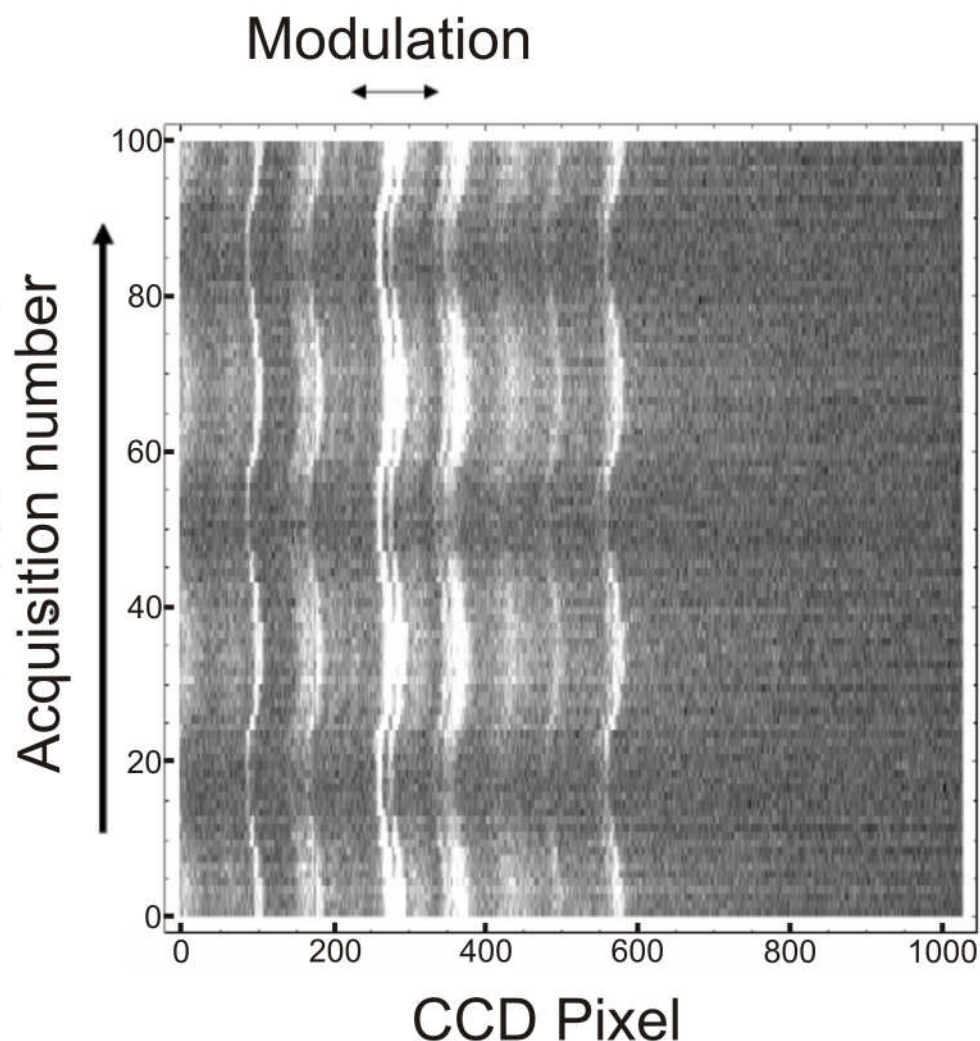


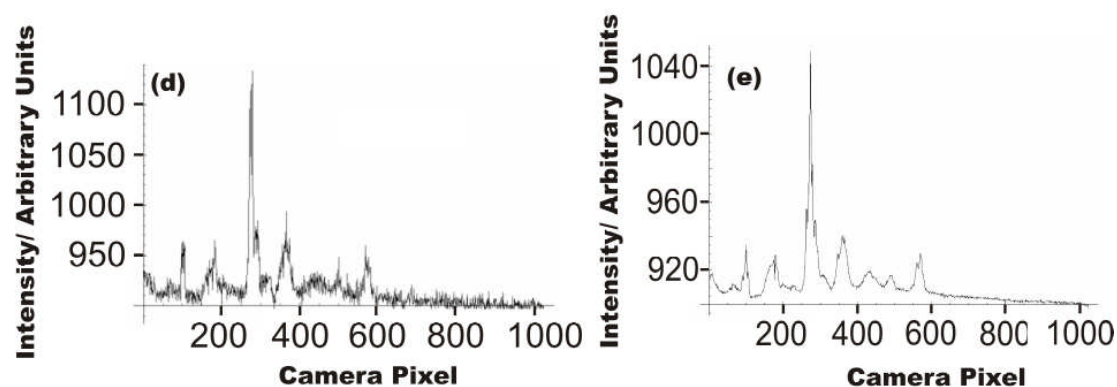
Figure 10(c). Plot of the temporal behaviour of the Raman spectra as the exciting laser line is modulated. We can clearly see the frequency modulation of the Raman peaks with increasing acquisitions.

From figure 10(c) we can see the modulation behaviour of the Raman peaks as the frequency of the laser is modulated by current injection. What is also apparent in this analysis is the intensity dips of the Raman peaks as they are modulated. This is the result of the method used to modulate the laser frequency. By varying the laser current we also vary the laser intensity thus the intensity of the collected Raman spectra. The lower Raman signal will obviously have a negative effect on the signal to noise ratio reducing the efficiency of this technique.

---

To analyse the data Michael Mazilu developed a mathematical algorithm that monitors the intensity at each horizontal pixel. The movement of the Raman peaks essentially appear as noise fluctuations on each pixel; thus the algorithm locks onto pixels displaying the characteristic periodic fluctuation in intensity and records it. Any pixels giving a stable intensity or an intensity not varying at the correct modulation rate have their signal rejected as being noise and not Raman signal. Thus theoretically only the Raman signal is recorded and any noise and fluorescence is rejected as neither of these will vary with the laser frequency modulation. This mathematical algorithm mimics the function of a lockin amplifier that was used in similar experiments with single channel detectors [16, 17 & 18].

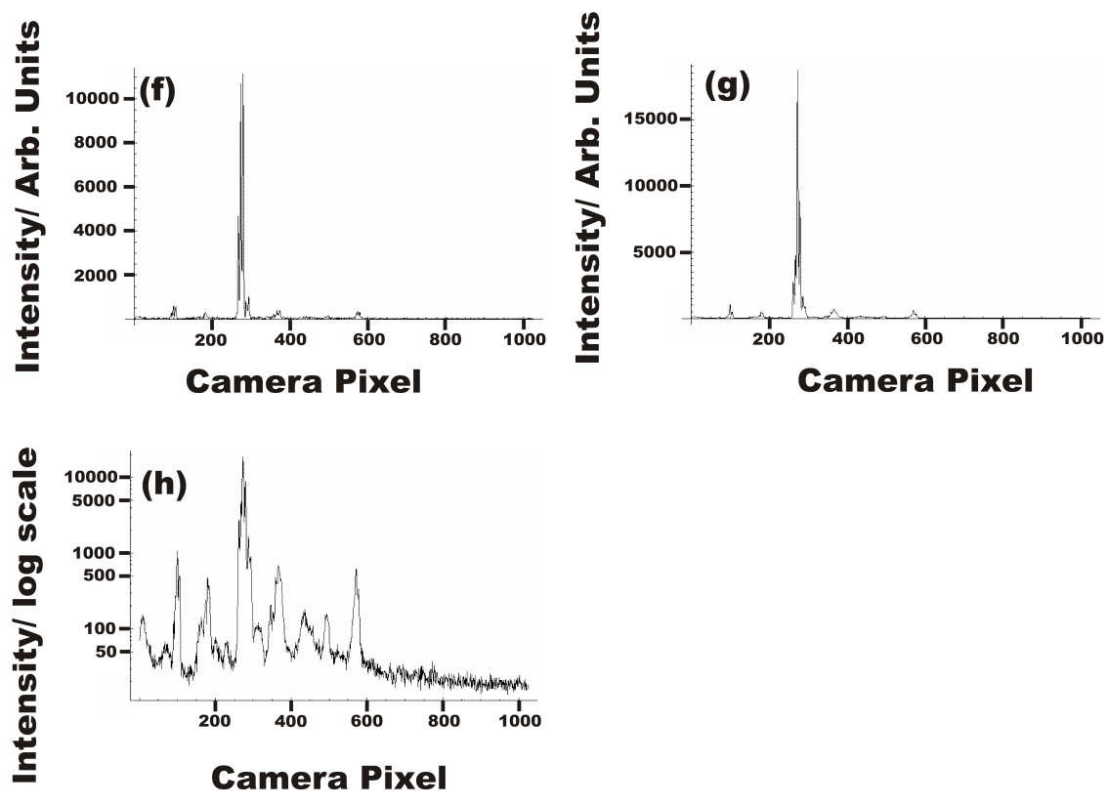
Figure 10(d) shows one of the 50ms spectra and figure 10(e) shows the average of all the one hundred 50 ms spectra. The average spectrum in figure 10(e) contains the peaks recognisable as the polystyrene Raman spectra that we have become familiar with throughout this thesis. We can see the peaks are sitting on a fluorescence background that is a result of the glass coverslips forming the sample chamber. This average spectrum has a calculated signal to noise ratio of approximately 1.16 using the  $1000\text{cm}^{-1}$  polystyrene Raman peak, which appears as the tallest peak on figures 10(d & e). We note this now and will compare it later to the signal to noise ratio resulting from the wavelength modulation analysis.



Figures 10(d & e). Figure 10(d) shows a single 50ms Raman spectrum from the trapped polystyrene sphere. Figure 10(e) shows the average of all one hundred 50ms Raman spectra acquired from the polystyrene sphere.

By implementing the wavelength modulation we were able to produce the spectra shown in figures 10(f), 10(g) and 10(h). From figure 10(f) we can see that using just ten of the 50ms spectra we can extract an extremely strong signal with a minimal background. This is possible as when we sum together the signals from the individual acquisitions we are only summing the signal as the noise has been rejected by the data processing algorithm. Figure 10(g) shows the polystyrene spectrum recorded with the wavelength modulation technique using all one hundred scans; we can see visually the massive improvement in signal to noise ratio. Figure 10(h) shows the same spectrum plotted in log scale showing how the technique still allows for the extraction of all the detailed Raman information and not just the strongest peaks. If we use this chart to calculate the signal to noise ratio, using again the  $1000\text{cm}^{-1}$  peak that appears as the tallest peak on figures 10(f), 10(g) and 10(h), we find it to be approximately 380. Comparing this to our earlier value, of signal to noise from the spectra recorded without the modulation, we can make a conservative estimate of the improvement in signal to noise ratio to be 320 just by implementing the wavelength modulation

technique. This should ultimately help us extract Raman signals much faster from difficult samples.



Figures 10(f, g & h). Figure 10(f) shows the Raman spectrum of polystyrene extracted using only ten of the 50ms spectra. Figure 10(g) shows the Raman spectrum of polystyrene extracted using all one hundred of the 50ms spectra. Figure 10(h) shows the same spectra as displayed in figure 10(h) only plotted in log scale.

This improvement in signal to noise ratio is extremely promising but there are some problems we cannot fail to notice and are centred on the modulation method. The beauty of this technique is its simplicity in implementation; all that we require is a frequency generator to modulate the current of the diode laser thus modulating the frequency. The resolution of each pixel on the spectrograph is 74GHz thus the laser has to be heavily current modulated to move the laser frequency, and hence frequency of the Raman peaks, across a few pixels to reap the benefits of the modulation technique. This however results in the simultaneous modulation of the laser intensity

---

to a large extent. The effect on the Raman signal can be seen in figure 10(c); we can see that as we progress through the acquisition, as well as the 'sideways' frequency modulation, there is an intensity modulation with the peaks becoming very bright and then nearly disappearing in some cases as the laser intensity drops to a very low level. This means that a significant proportion of the spectra recorded are of little use, although the analysis method should still exclude any noise we are not maximising the potential of this method. Slightly more worrying is that the fluorescence noise will also have a modulation on it, not as a result of the frequency modulation but as a result of the intensity modulation of the laser. Although fluorescence is a slow event and will not rapidly follow the laser intensity modulation it may appear on the CCD camera as a modulated signal thus it may slip through the analysis and contribute a noise component to our Raman spectra. The final and probably most significant issue arising from the modulation of laser intensity is the effect on the peak ratios. If we compare figure 10(e) with 10(g) it is clear that the analysis has altered the peak ratios. In Raman spectroscopy this is normally construed as a chemical change in the substance we are studying, this could massively affect any diagnostic analysis based on peak intensities and ratios, such as those used in our cervical cancer diagnostic study in chapter 9. If we look again at figure 10(c) we can see that during the dip in laser intensity most of the peaks disappear except for one that remains strong which is the familiar  $1000\text{cm}^{-1}$  peak and on figure 10(c) is the very bright peak oscillating around camera pixel 275. This peak remains visible due to the strong scattering nature of the originating chemical bond. As a result, whilst all the other peaks are not contributing to the final spectra, this peak continues to contribute a significant intensity to the final spectra thus the signal to noise ratio increases at a greater rate for this peak in comparison to the others. The oscillation in the laser intensity is a

---

---

significant problem that we must overcome either by modulating the laser frequency in a different fashion or by normalising each spectra before the analysis.

This method is extremely promising giving a massive increase in signal to noise ratio of over three hundred that should allow us to reduce our integration time. However there are problems that we must overcome with respect to the fluctuation in laser intensity, as we modulate the frequency, which is currently causing a change in peak ratios that could be falsely construed as a chemical change and affect diagnostic algorithms. This analysis on polystyrene has given us an insight into the capabilities of the technique but this is a compound whose spectrum can be acquired quickly with a normal Raman tweezers setup; the real potential application for this technique is in the study of biological cells which normally require minutes to acquire a quality Raman spectra.

### **10.6.3 Wavelength modulation Raman spectroscopy applied to biological cells**

In order to evaluate the performance of wavelength modulated Raman spectroscopy when applied to biological cells we placed SiHa cells on the microscope stage of the Raman tweezers system and analysed them with the modulated Raman probe beam.

In order to avoid the problems with the largely varying laser intensity the modulation was reduced by applying only +/- 1V modulation to the laser diode driver. The laser diode driver current was set to 100mA thus will vary between 80mA and 120mA. The modulation rate was 0.05 Hz to allow us to capture the laser position several times whilst still acquiring a useful Raman signal from the weakly scattering cells. We then proceeded to acquire 180 scans of 500ms each in duration; also included on the scans was the laser line to allow us to track the modulation and use

---

---

it's intensity to normalise the individual spectra during the analysis to try and avoid the problems associated with the fluctuating laser intensity.

A chart displaying the intensity according to each horizontal camera pixel for each spectrum is shown in figure 10(i). This chart shows the smaller modulation of the laser line and to the right of the chart the modulated Raman peaks. There is an extremely bright band next to the laser, this was initially thought to be fluorescence but it is also being frequency modulated pointing to its origin being a Raman peak. Quartz, and in fact most glasses, is known to have an extremely strong Raman peak at this point so this is most likely due to the Raman spectra of quartz. Knowing its origin means we can simply subtract if required. Initially we performed the same pixel intensity modulation analysis as was performed on the polystyrene spheres. The results can be seen in figures 10(j), 10(k), 10(l) and 10(m).

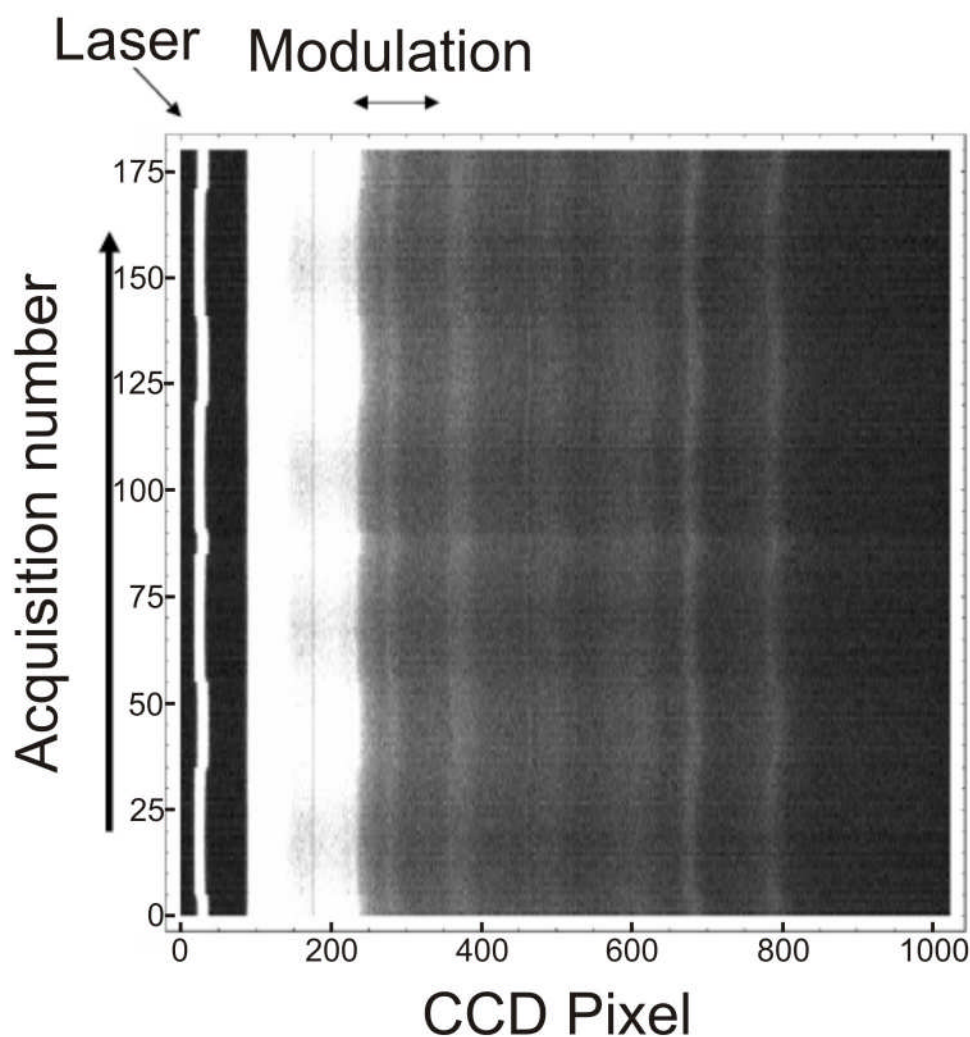
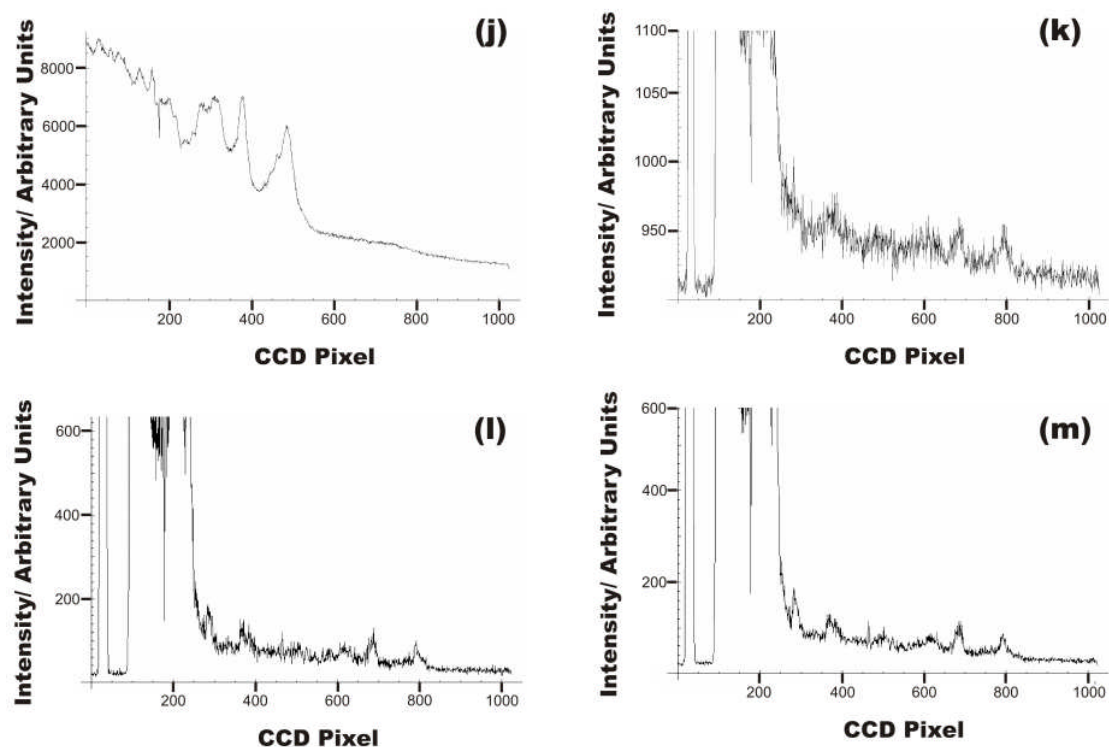


Figure 10(i). Plot of the temporal behaviour of the Raman spectra as the exciting laser line is modulated. We can clearly see the frequency modulation of the Raman peaks with increasing acquisitions.

Looking at figure 10(j) we can see a Raman spectrum of 90s acquisition time; this is obviously the base standard against which we must compare our results, it has clear detailed peaks but does sit on a large fluorescence background. Figure 10(k) shows one single 500ms acquisition with weak and noisy peaks. Figure 10(l) shows the result of the wavelength modulation analysis using ninety of the 500ms acquisitions; as we can see the peaks are beginning to emerge but they are extremely weak and noisy. Figure 10(m) shows the result of the wavelength modulation analysis using all one hundred and eighty of the 500ms acquisitions; we can see the peaks are emerging but are still extremely noisy and lack detail. In this situation the wavelength

---

modulation technique has performed extremely poorly and the reason for this lies again in the modulation of the laser. To try and avoid the negative effects of deep current modulation we have reduced modulation depth to only  $\pm 20$  mA. Whilst this has reduced the effects of the intensity modulation it has dramatically reduced the amount of frequency modulation. In fact, if we look at figure 10(i) and examine the laser line we can see it has two distinct frequencies and unlike the applied modulation the frequency is not varying between these two points in a temporally stable and repetitive manner. This has resulted in a very poor performance of the wavelength modulation analysis algorithm that was designed to work with the stably and widely varying laser frequency seen in the results for the polystyrene spheres. The behaviour of the free running diode laser may have been influenced by an 'accidental' external cavity causing the laser to not vary smoothly but rather hop between two discreet frequencies although further investigation would be required to confirm this. In order to make this analysis for the cells more successful we need to find a way to modulate the laser frequency over a wide range without overly affecting the laser intensity, this may have to be via the use of a grating tuned cavity diode laser or a fabry perot tuned Ti:Sapphire laser.



Figures 10(j, k, l & m). Figure 10(j) shows a single 90s Raman acquisition of a SiHa cell for comparison to our modulated analysis. Figure 10(k) shows a single 500ms Raman acquisition from a SiHa cell. Figure 10(l) shows the results of the modulation analysis after ninety 500ms scans have been analysed. Figure 10(m) shows the results of the modulation analysis after all one hundred and eighty 500ms scans have been analysed.

Although the modulation analysis was not very successful, due to having only two discrete frequencies, we can still perform a SERDS style analysis on the data. This would allow us to evaluate the ability of SERDS to pull cell spectra out of rapid noisy acquisitions.

Initially the laser peak in all the spectra was analysed for its position and intensity, the position was used to assign each spectra to one of two frequency 'bins' and the intensity was used to normalise the Raman spectra. For the SERDS analysis all the spectra in each bin were summed together and then the resulting spectra from the two bins were subtracted and subsequently integrated. The result of this can be seen in figure 10(n). This spectrum is directly comparable to that in figure 10(j) as it uses 90s worth of acquisitions in total. We can see that the peaks have all emerged in

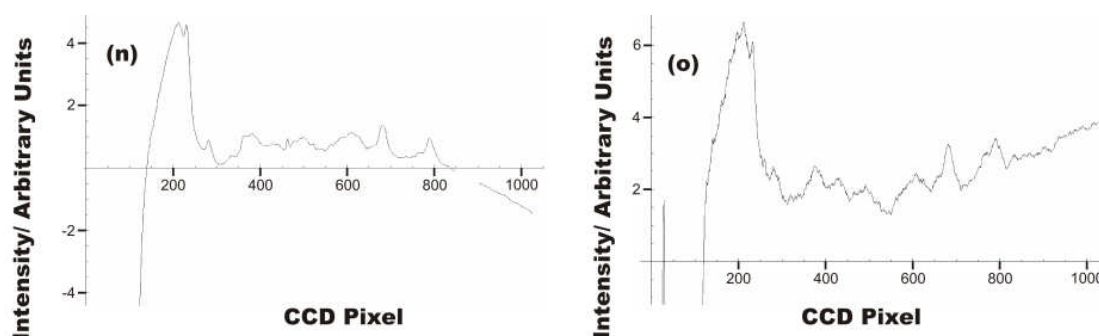
---

detail in this analysis although perhaps not quite to the same extent as in the straight 90s acquisition shown in figure 10(j); also on the spectra we can see the large silica peak that could be removed if required for further analysis. The striking feature of this spectrum however is the removal of the fluorescent background that the peaks sit on in figure 10(j); this could be extremely useful in PCA analysis, such as was performed in chapter 9. In our analysis of cervical neoplasia, the PCA was seriously affected by autofluorescence meaning we lost some valuable Raman information, this technique could be used to effectively remove the fluorescence and improve the results of our analysis. We also analysed if this SERDS style method could be used to bring out the Raman peaks from the noise rapidly. To do this the first five scans from each bin were summed and again the summed spectra were subtracted from each other and subsequently integrated. This corresponds to a total acquisition time of five seconds. The result of this analysis can be seen in figure 10(o). Studying figure 10(o) we can see quite a few of the Raman peaks are emerging and the background is beginning to flatten, however the spectra is probably not yet good enough to be used in any subsequent analysis such as PCA. The variation may be linked into the relative standard deviation in the noise we examined in section 10.5.1; at the short acquisition times used to acquire the spectra the relative standard deviation in the noise is quite high. The SERDS technique relies on the noise remaining consistent, in our case of using just 10 spectra this is unlikely to be the case and is responsible for the unexpected and strange shape of the background seen in figure 10(o).

The SERDS analysis is extremely useful for longer acquisition times and could potentially be used to remove fluorescence and hence improve the results of subsequent analysis techniques such as PCA. However it is not so useful in the

---

analysis of spectra acquired in short times as the increased relative standard deviation in the noise means the SERDS technique is less effective.



Figures 10(n & o). Figure 10(n) shows the SERDS analysis of the Raman spectra acquired from the SiHa cell using all of the 180 acquired spectra. Figure 10(o) shows the SERDS analysis of the Raman spectra acquired from the SiHa cell using only 10 of the acquired spectra.

## 10.7 Conclusions

In this chapter we have examined the possibility of using wavelength modulated Raman spectroscopy to improve the signal to noise ratio of the acquired Raman signal and hence reduce the acquisition time.

Raman spectroscopy is proving an excellent diagnostic tool in the medical and biological sciences. The one aspect of this technique holding back its wide spread use is the length of time to acquire a good quality spectrum. Many techniques have been evaluated to increase the signal to noise ratio including Kerr gated Raman spectroscopy, polarised Raman spectroscopy and phase modulated Raman spectroscopy to name a few. These techniques have been successful to various extents but often require advanced optical setups.

The beauty of wavelength modulated Raman spectroscopy, when the system is based on a diode laser, is that the laser source can be easily frequency modulated by current injection. Thus the only extra piece of equipment we required was a frequency generator which could be used in conjunction with the laser diode driver to modulate the current.

---

Initially we examined the inherent dark noise in the CCD camera to establish whether it could be easily subtracted from our spectra to avoid it interfering in any subsequent analysis. The dark noise is a result of electrons being thermally released in the camera rather than optically released. The noise appeared to increase linearly with acquisition time as we expected but perhaps more interestingly we found that the relative standard deviation in the noise decreased exponentially with acquisition time.

We proceeded to trap and examine a 5 $\mu$ m polystyrene sphere with the laser being heavily frequency modulated. The data was captured with a succession of short 50ms spectra. This allowed us to capture the modulation of the Raman peaks. An algorithm was developed that simulated a lock in amplifier integrating signal from pixels that displayed an intensity modulation according to the frequency modulation of the Raman peaks. This resulted in an excellent increase in signal to noise ratio increase of approximately 300. However there were some serious drawbacks to this technique that were related to the method of modulation of the diode laser. To move the laser frequency across a few pixels the laser had to be heavily current modulated which resulted in the laser intensity varying greatly from a few mW up to 30 mW. This had the effect of varying enhancement for different peaks; this could easily be misconstrued as a chemical change in the substance and affect any diagnostic models based on peak ratios or variations such as the PCA we used in our cervical neoplasia diagnostics. The varying laser intensity will also modulate any fluorescence signals which, although will not be exactly in phase with the laser modulation, may appear as Raman signal on the pixels and be integrated with the signal by the algorithm used to create the final Raman spectra. It became clear that for this technique to be successfully integrated into Raman tweezers for everyday use a better way of modulating the laser will have to be found.

---

---

The analysis of the polystyrene spheres was very successful in demonstrating the power of this technique but the main application for this technique will be in the study of cells and other biomedical samples. To investigate its use with cells we applied the technique to SiHa cells, this time however we reduced the modulation rate to avoid any problems associated with largely varying power. The reduction in current modulation meant a reduction in frequency modulation hence we only recorded spectra at two discrete wavelengths. This unfortunately rendered the wavelength modulation analysis, used so successfully for polystyrene spheres, not suitable and hence the results were poor. However we went on to analyse the data with a SERDS style method and found that SERDS could be extremely useful for removing the fluorescence background, upon which our Raman peaks normally alight, potentially reducing its influence on advanced analysis methods such as the PCA used in our diagnostic tests on cervical neoplasia in chapter 8. We also tried to use SERDS to pull out Raman peaks from noisy rapidly acquired spectra but found that the variability in the noise in such short Raman acquisitions affected the technique producing strangely shaped backgrounds. Some Raman peaks were recovered from the noise but not in great enough detail to be useful for further analysis.

Our study to investigate the possible use of wavelength modulated Raman spectroscopy has proved successful and we have demonstrated the potential of this technique to help reduce acquisition times. However for this technique to go into widespread use we must find a way to modulate the laser in a manner that doesn't overly affect the output intensity. This should be possible with technologies such as extended cavity diode lasers.

---

## 10.8 References

- [1] Wood BR, Langford SJ, Cooke BM, Glenister FK, Lim J and McNaughton D.  
**Raman imaging of hemozoin within the food vacuole of *Plasmodium falciparum* trophozoites.** FEBS Letters 2003; **554**: 247-252
- [2] Ko ACT, Choo-Smith LP, Hewko M, Sowa MG, Dong CCS and Cleghorn B.  
**Detection of early dental caries using polarised Raman spectroscopy.** Optics Express 2006; **14**: 203-215
- [3] Maquelin K, Dijkshoorn L, van der Reijden TJK, Puppels GJ. **Rapid epidemiological analysis of *Ancinetobacter* strains by Raman spectroscopy.** Journal of Microbiological Methods 2006; **64**: 126-131
- [4] Buschman HP, Deinum G, Motz JT, Fitzmaurice M, Kramer JR, van der Laouse A, Brusckhe AV and Feld MS. **Raman microspectroscopy of human coronary atherosclerosis: Biochemical assessment of cellular and extracellular morphologic structures in situ.** Cardiovascular Pathology 2006; **10**: 69-82
- [5] Utzinger U, Heintzelman DL, Mahadevan-Jansen A, Malpica A, Follen M and Richards-Kortum R. **Near infrared Raman spectroscopy for in vivo detection of cervical precancers.** Applied Spectroscopy 2001; **55**: 955-959
- [6] Ramser K, Logg K, Goksor M, Enger J, Kall M and Hanstorp D. **Resonance Raman spectroscopy of optically trapped functional erythrocytes.** Journal of Biomedical Optics 2004; **9**: 593-600
- [7] Kniepp K, Kniepp H, Kartha VB, Manoharan R, Deinum G, Itzkan I, Dasari R and Feld MS. **Detection and identification of a single DNA base molecule using surface enhanced Raman scattering (SERS).** Physical Review E 1998; **57**: R6281-R6284
- [8] Kniepp K, Haka AS, Kniepp H, Badizadegan K, Yoshiwara N, Boone C, Schafer-
-

- 
- Peltier KE, Motz JT, Dasari RR and Feld MS. **Surface-Enhanced Raman Spectroscopy in Single Living Cells Using Gold Nanoparticles.** Applied Spectroscopy 2002; **56**: 150-154
- [9] Singh GP. **Raman Microspectroscopy of Optically Trapped Cells.** 2006 PhD Thesis; Institut de Ciencies Fotoniques: 137-146
- [10] Matousek P, Towrie M, Stanley A and Parker AW. **Efficient Rejection of Fluorescence from Raman Spectra Using Picosecond Kerr Gating.** Applied Spectroscopy 1999; **53**: 1485-1489
- [11] Genack AZ. **Fluorescence Suppression by Phase-Resolved Modulation Raman Scattering.** Analytical Chemistry 1984; **56**: 2957-2960
- [12] Xie C and Li YQ. **Confocal micro-Raman spectroscopy of single biological cells using optical trapping and shifted excitation difference techniques.** Journal of Applied Physics 2003; **93**: 2982-2986
- [13] Carruthers AE, Lake TK, Shah A, Allen JW, Sibbett W and Dholakia K. **Single-scan spectroscopy of mercury at 253.7nm by sum frequency mixing of violet and red microlensed diode lasers.** Optics Communications 2005; **255**: 261-266
- [14] Funfschilling J and Williams DF. **CW Laser Wavelength Modulation in Raman and site selection Fluorescence Spectroscopy.** Applied Spectroscopy 1976; **30**: 443-446
- [15] Levin KH and Tang CL. **Wavelength –modulation Raman spectroscopy.** Applied Physics Letters 1978; **33**: 817-819
- [16] van de Ven M, Meijer J, Verwer W, Levine YK and Sheridan JP. **Derivative Raman Spectroscopy Applied to Biomembrane Systems.** Applied Spectroscopy 1984; **15**: 86-89
- [17] Friedl F, Kimura I, Osato T and Ito Y. **Studies on a new human cell line (SiHa)**
-

---

**derived from carcinoma of Uterus I. It's establishment and morphology.**

Proceedings of the Society of Experimental Biology and Medicine 1970; **135**:

543-545

---

# 11. Thesis Conclusions

---

*In this brief discussion we summarise the work contained within this thesis, discuss the conclusions reached in the experimental chapters of this thesis and pass brief comment on the future potential of Raman tweezers microspectroscopy.*

---

## 11.1 Thesis Conclusions

The demonstration of the single beam optical gradient force trap by Ashkin and co workers in 1986 has had a massive impact on many areas of science opening up new areas of study and creating new techniques. The integration of optical trapping with traditional Raman microspectroscopy, to form the new technique of Raman tweezers microspectroscopy, has offered up the opportunity to study single cells in a way that was not previously possible. Cells can now be readily trapped, isolated from interfering surfaces and subsequently have their biochemical nature probed. The first demonstration of Raman tweezers applied to cells, in 2002 by Xie *et al*, has paved the way for a large portfolio of research covering many aspects of single cell studies and as a technique Raman tweezers continues to attract great interest. In this thesis we have seen how Raman tweezers may be used to study single cells and how advanced experimental geometries can help address the short falls in the standard Raman tweezers geometry.

The interest generated by Raman tweezers microspectroscopy has revolved around the study and monitoring of biological and medical samples in particular single cells. Thus it was pertinent to begin, in chapter 2, by looking at competing

---

---

biological and medical monitoring and investigative technologies to gain a perspective on how Raman tweezers microspectroscopy compares with other methods and where this technique can help to further our understanding of biomedical samples. We discovered that the great strength of Raman spectroscopy, in comparison to other techniques, is its ability to simultaneously engage many biochemicals and monitor their relative concentrations. Its main drawbacks however lie in the weak nature of the Raman effect meaning that acquiring information can take quite some time in comparison to other techniques. Raman tweezers microspectroscopy is ideal for the study of single biological cells as the cells can be trapped, environmentally isolated and have their behaviour probed through the simultaneous engagement of multiple biochemicals. However if we wish to monitor rapid cellular reactions or harness the analytical power of Raman spectroscopy in flow cytometry style systems we must find an approach to reduce the signal integration times.

Raman tweezers spectroscopy encompasses both optical trapping and Raman spectroscopy, thus in order to further the understanding of the technique theory sections on Raman spectroscopy and optical trapping were presented, in chapters 3 and 4 respectively, to aid the interpretation of the experimental results subsequently presented.

With a firm theoretical basis of the techniques involved in Raman spectroscopy chapter 5 presented an introduction to Raman tweezers and gave a research perspective detailing much of the work carried out to date. The work can be split broadly into two categories; the first of these is applications of the Raman tweezers technique where a wide variety of biomedical samples have been studied from neurons to cancer cells demonstrating the flexibility and potential wide spread use of the technique. The second category of research is that of the development of

---

---

the Raman tweezers microspectroscopy technique and experimental setup. Much of this work has focussed on the decoupling of the trapping and Raman probe beams so that the performance of each mechanism may be maximised for a specific application and to address the shortfalls of the basic Raman tweezers technique.

The construction and evolution of our Raman tweezers microspectroscopy system was discussed in chapter 6. The initial Raman system was based upon a previously published design but throughout the course of this thesis continually evolved and incorporated a commercial microscope and a thermal stage to improve cell viability as they were studied.

The first experimental study carried out on our Raman tweezers system, detailed in chapter 7, examined how optical stacking could be used to our advantage in Raman tweezers. Optical stacking occurs when multiple particles align vertically in the focussed laser beam and is often avoided in normal optical traps. We began by studying how the Raman signal behaved as we increased the number of optically stacked spheres in our Raman tweezers system. As we might have expected, the signal increases in a nonlinear fashion and behaves in a Lorentzian manner appearing asymptotically to approach a maximum value. The tail off in signal increase, as we add more and larger spheres to the optical stack, is the result of the collection efficiency profile of the microscope profile tailing off rapidly as we move from the focal plane and the decreasing laser power density, as we move away from the beam focus, which is directly proportional to the intensity of the Raman signal. We applied the stacking technique in the study of red blood cells and yeast cells. The stacking technique provides a pseudo average signal over all the cells trapped. If we have a small population of cells we wish to study, the stacking technique can negate the effects of intra population variation, due to the cells being in different stages of the

---

---

cell cycle, to give a truer biochemical picture of the behaviour of the cell population. This negates the need to acquire signals from individual cells and average the resultant spectra meaning we can acquire a rapid representative Raman spectrum detailing the behaviour of the cell population. One aspect that came out of this study was the extra power required to stack three of the heavier yeast cells, with these larger cells the basic Raman tweezers system began to struggle to maintain stable trapping. The great advantage of using the stacking technique is that it requires no additional experimental complexity and is simply implemented by moving the sample stage to pick up several samples simultaneously allowing us to study them in an isolated environment.

After examining further the performance of our Raman tweezers system in chapter 7 we proceeded to evaluate the potential of Raman tweezers microspectroscopy to identify and diagnose cervical neoplasia in chapter 8. Cancer diagnostics is one of the most promising areas for the application of Raman spectroscopy and recently Raman tweezers microspectroscopy has been applied to study colorectal cancer and neoplastic lymphocytes. Cervical neoplasia is ideal for study with Raman tweezers due to the ability of this technique to study single cells which is similar to the material collected via Pap smear. To evaluate the potential of Raman tweezers spectroscopy to study the development of cervical neoplasia we acquired spectra from CasKi cells, a cervical carcinoma derived cell line, PHKs, which are healthy epithelial cells, and also from PHK E7, which are PHKs manually infected with the HPV-16 virus that is expressing the E7 viral protein only. HPV is known to cause cervical cancer and detecting its effect in the PHK E7 cells would represent detecting cervical cancer at the earliest possible stage. Furthermore we also investigated the possibility of discriminating between these cell types after they had

---

---

been fixed in order to demonstrate the compatibility of Raman tweezers microspectroscopy with current clinical practice. We found that we were able to discriminate effectively between the cell types with sensitivities of up to 96% for the comparison between fixed PHK and PHK E7. These results demonstrated that Raman tweezers microspectroscopy could be used to discriminate between various stages in the progression of cervical neoplasia and the high sensitivities recorded for the fixed samples demonstrate the compatibility of this technique with current clinical practice. There were some issues arising from this study; the first of these was the inability of tweezers portion of the setup to stably 3d trap the large PHK cells thus we had to resort to specialist coverslips to minimise fluorescence interference. Secondly the PCA statistical analysis routine used to examine the cells suffered from fluorescence interference and the discrimination could in fact have been improved if this were somehow negated thus in the future we may have to look to more advanced analysis techniques. Raman tweezers microspectroscopy is an extremely promising technique for the analysis and monitoring of the development of cervical neoplasia, furthermore it appears to be compatible with current clinical practice, however to turn it into a true clinical technique we need to address the issues of stable trapping and long integration times.

As we found in chapters 7 & 8 the study of large cells with Raman tweezers based on the single beam gradient trap is difficult. The single beam gradient trap can trap smaller cells but these often pivot and rotate in the beam as various high index components in the cell strive to move into the beam focus, this negates the ability of Raman tweezers to perform localised measurements in the cell. This is further compounded by the fact that the trapping and Raman probe functions are fulfilled by the same beam thus we have no real control over where in the cell we acquire our

---

---

Raman information from. When it comes to trapping large cells the single beam gradient trap struggles as the trapping volume is so much smaller than the cell thus tweezer can not lift the cell way from the coverslip and be stably 3d trapped. It was the ability to manipulate our samples that made Raman tweezers spectroscopy such an attractive technique but in the study of large cells we loose all these advantages. In order to restore the advantages that made Raman tweezers such an attractive prospect, in the study of large cells, we proposed a decoupled system, described in chapter 9, where the trapping function was performed by a dual beam fibre trap and the Raman probe was provided by the existing single beam gradient Raman tweezers system. The advantage of this system was that the fibre trap could be placed directly onto the microscope stage and be used to trap large cells with its large trapping volume. Furthermore the divergent nature of the trapping beams means the cells experience a reduced power density hence have a lower risk of any two photon damage. This system allowed us to trap and acquire Raman information from very large objects up to 100 $\mu\text{m}$  in size. Furthermore we were able to trap a large PHK cell and acquire localised Raman information demonstrating the potential of this technique to acquire Raman maps of optically trapped cells. This technique worked very well but there were some issues; the sample chamber had to remain open, to get the fibres in, which caused evaporation of the sample and the cellular samples could not be kept sterile. The loading of the trap was also an issue as we had to wait for a particle to float between the fibres and become trapped. However we were able to address these issues when we considered the possibility of implementing a sample flow through our trapping and hence Raman probe region. Raman spectroscopy is attracting attention for possible use in a flow cytometry style system, due to its ability to engage multiple biochemicals simultaneously, to analyse and provide detailed information on multiple

---

---

particles rapidly. In order to evaluate the possibility of Raman tweezers to be used in such a situation we implemented a rudimentary particle and cell flow through a capillary tube. The fibres were then placed against the outside walls of the tube opposite each other to form an optical trap inside the capillary. We were then able to capture the particles or cells flowing through the tube and then, with the Raman probe, examine them. This system proved successful and addressed some of the issues involved in the implementation of the fibre trap; by flowing particles through the trapping region we no longer have to wait for one to float past the fibres and become trapped. Furthermore it is possible to create a sealed capillary to stop evaporation and keep any samples inside sterile. The decoupled Raman tweezers system, utilising a fibre optical trap, allows us to study large cells whilst retaining all the original advantages of Raman tweezers that made it such an attractive technique in the first place. Furthermore this experimental geometry could be used to create a flow cytometry style system based on Raman spectroscopy but for this to become a reality a reduction in the acquisition times is critical.

We have seen throughout this thesis the analytical power of Raman spectroscopy and have often made reference to the need to reduce the signal integration times to allow us to monitor fast biochemical events and increase the clinical compatibility of Raman tweezers microspectroscopy. To try and reduce the time required to obtain a quality Raman signal we investigated the possibility of using wavelength modulated Raman spectroscopy with modern detectors and instrumentation. Wavelength modulation spectroscopy is a commonly used technique in other branches of spectroscopy to draw signals out of noisy backgrounds and revolves around the frequency modulation of exciting laser causing and amplitude modulation of the received signal. As the noise is unaffected by the frequency

---

---

modulation only varying signals are recorded giving us a massive increase in signal to noise ratio. The beauty of this technique, when diode lasers are used as the excitation source, is that the only additional piece of equipment required is a signal generator. This is used to modulate the diode laser injection current which in turn modulates the laser frequency. The modulated signal is captured on the CCD camera with short rapid acquisitions that are then interpreted by a mathematical algorithm to output an improved spectrum. This technique was applied to a trapped polystyrene sphere and an enhancement of over three hundred in the signal to noise ratio was observed. However there were some issues with this technique; the modulation method also caused a large modulation in laser intensity that caused the signal to noise ratio to vary for different peaks. This is a serious problem as this could be construed as a false chemical change in the sample under study and affect the results of any subsequent statistical analysis such as PCA. In order for this very promising technique to work effectively a method must be found to frequency modulate the laser without affecting the laser intensity. We also applied the technique to cells as it is in the analysis of biological samples that this technique would most likely be used. In order to reduce the effects of intensity modulation, the frequency modulation of the laser was reduced. This resulted however in only two distinct laser positions, and hence Raman peak positions, rather than a continuously varying spectrum. This meant the analysis that worked so well for the polystyrene spheres was not effective and gave poor results. We were however able to perform a SERDS style analysis that removed the cells autofluorescence background, upon which the Raman peaks sit, showing the potential of this technique to improve subsequent analysis, such as PCA, by removing any influence of the fluorescent background. Wavelength modulation Raman spectroscopy is an extremely promising technique but in order for it to perform

---

---

reliably we must find a way to controllably modulate the frequency of the exciting laser without overly modulating the laser intensity.

This thesis demonstrates the analytical power and flexibility of Raman tweezers microspectroscopy to study a variety of biomedical samples. With continuous improvements in the technique and demonstrations of ever varying applications the interest in Raman tweezers microspectroscopy is only likely to increase.

## **11.2 The outlook for Raman tweezers microspectroscopy**

Raman tweezers microspectroscopy has a potentially bright future as it can simultaneously engage many biochemicals in an environmentally isolated cell, there are few other techniques that can make as bold a claim as this. However if Raman spectroscopy is to find more widespread use the problem of long integration times must be overcome whether through signal processing techniques, such as wavelength modulated Raman tweezers microspectroscopy, or through possible advanced techniques such as coherent anti-Stokes Raman tweezers spectroscopy (CARTS). We may therefore expect a great deal of effort in the field to address this problem.

Raman/ tweezers spectroscopy has a real chance of becoming an important clinical diagnostic technique and as time progresses it is likely to reveal a great deal of effort in increasing the compatibility of Raman tweezers spectroscopy with current clinical practices, not only for cancer but many other diseases such as Alzheimer's or heart disease. We may also see a large drive towards the development of a Raman based flow cytometry type system based on Raman tweezers that would allow the rapid study of a large number of biomedical and clinical samples without the need for chemical markers.

---

The outlook for Raman tweezers microspectroscopy is promising but its future in the study of biological, medical and clinical samples hinges on the reduction of integration times and effective trapping and analysis methods.

# Appendix A

---

# Appendix A.

# Optical and Quasi Optical Techniques in the Biomedical Sciences

---

*In this appendix we examine some widely used biomedical imaging techniques that have had a major impact on medicine and transformed our knowledge of the biological sciences. These techniques are not entirely suitable for studying cells and thus do not compete directly with Raman tweezers spectroscopy but an understanding of their capabilities allows to gain further insight into the potential applications for Raman tweezers spectroscopy and where it may be most usefully applied.*

---

## **A.1 Introduction**

There are of course many techniques that have been developed to study biomedical samples. Whilst many of these techniques are not in direct competition with Raman spectroscopy we cannot not ignore the important optical and quasi optical techniques that have had such an impact on the biomedical sciences. In this section we will look at a few established and emerging imaging technologies that have had a large impact on the study of biomedical samples.

---

### **A.1.1 Optical Coherence Tomography (OCT)**

Optical coherence tomography [1] is an emerging technique based on interference between a reference beam and another beam that is back scattered from the substance under investigation. Changes in the interference pattern, between the reference beam and the backscattered light the substance being tested, can be used to gain information about the substance. OCT is a sensitive technique that essentially builds up a picture of refractive index variation within the sample studied. The axial resolution of OCT is dependant on the source and is inversely proportional to bandwidth of the source; state of the art systems at the time of writing this thesis have resolutions of approximately two to three microns. This makes OCT very useful for studying biological systems down to a single layer of cells, but is not currently capable of studying sub cellular structures. OCT is mainly used in the study of ophthalmic diseases [2] and shows great promise for use in optical biopsy to detect changes in tissue associated with the onset of neoplasia [3].

OCT is attracting much interest for optical biopsy as it is able to detect cancerous tissues, is compatible with endoscope techniques and can be used for near real time dynamic imaging. It is also very appealing as its low coherence sources are much less destructive to tissue than the often used UV light in fluorescence. However the method by which OCT gleans its information may not be able detect the very earliest biochemical changes associated with the onset of neoplasia as it only investigates changes in refractive index.

---

### **A.1.2 Nuclear Magnetic Resonance (NMR), Magnetic Resonance Imaging (MRI) and Electron Spin Resonance (ESR)**

Although NMR, MRI and ESR are quasi optical techniques, in that they rely on an applied magnetic field and radio or microwave radiation, no discussion on medical and biological imaging techniques could ignore perhaps the most important imaging technique of recent times in the medical and biological sciences. Initially it should be stated that we are dealing with two techniques as opposed to three as alluded to in the title. MRI and NMR are the same technique but the term MRI is used in medical applications to avoid use of the word 'nuclear' that patients may find unsettling.

Magnetic resonance techniques exploit the spin, or intrinsic angular momentum, of particles in atoms. The techniques require a nucleus with non zero spin for NMR, or for ESR, an electron configuration in the atom that has an unpaired electron such as a free radical. The application of a strong magnetic field causes a splitting in the quantum spin energy level. For a simple system such as Hydrogen with spin  $\frac{1}{2}$  the number of levels formed is,  $2 \times \text{spin quantum number} + 1$ , two levels. This can be thought of as a spin aligned with the magnetic field and the higher energy level of spin aligned against the magnetic field. For more involved systems the magnetic splitting can cause multiple levels. The split levels will have an energy gap between them  $\Delta E$ , which is directly proportional to the strength of the applied magnetic field, that corresponds to photon frequencies, in the case of NMR, of approximately 500-650 MHz, and, in the case of ESR, have frequencies of approximately 10-12 GHz depending on the magnetic field applied. It is the energy of this splitting the NMR and ESR probes to gain information on the samples.

---

The normal method of conducting magnetic resonance experiments is to employ a fixed wavelength source close to the resonance of the atoms under study, which is normally hydrogen. The magnetic field is then swept, which causes a variation in the energy gap, until a large absorption occurs i.e. the resonance point is reached and the source begins to drive nuclear spin transitions between the split energy levels. In NMR the resonance of the nucleus is very sensitive to the surroundings due to electron shielding of the nucleus by surrounding atoms. This shielding is well characterised so information on the chemical composition of the surroundings is readily obtained. Furthermore, due to spin coupling between nuclei, the resonance is split and doublet peak is observed yielding further information on the molecular surroundings. The relaxation times of the nuclei can also be observed to yield further information about location and surroundings. The same principles apply for ESR but it is the electrons that yield the information on surrounding chemical compositions and locations [4].

This is an extremely powerful technique and is extensively used throughout the biological and medical sciences. NMR in the form of MRI is used in hospitals to provide detailed in vivo images and is being explored as a technique to grade cancerous growths [5] and in the study of DNA transcription factor interactions [6] to name only a few. ESR is less widely used but is also very important in the study of biological systems, often with the aid of spin labels, and is used to study events such as protein interactions and can also often be used as a molecular ruler in a similar fashion to FRET [7].

Magnetic resonance techniques are extremely powerful and are used extensively in the biological and medical sciences they are capable of giving precise information on molecular structure and environments providing there is a suitable

---

---

atom with non zero spin to study. Their main drawbacks for diagnostic use is their cost as they are extremely expensive instruments, they are often very bulky and ESR can often be dependant on tagging of subjects with suitable spin labels.

### **A.1.3 X-ray scattering**

X-ray scattering is a form of very high energy elastic light scattering. In X-ray scattering a normally crystalline sample is irradiated with high energy X-rays and the resultant diffraction pattern is recorded. The scattering occurs from interactions with electrons, and via conservation of momentum, the X-ray gets scattered off at an angle. Using computer analysis of the diffraction pattern the molecular structure of the substance under study can be revealed with a resolution of approximately 5-25 nm. The short wavelength of X-rays allows very high resolution as resolution is directly proportional to the wavelength of the radiation be scattered.

X-ray scattering is, as is well known, used in hospitals for imaging bone structure and to look for tumours, although the technique is unable to pick up the early biochemical changes associated with cancer and can not easily resolve the difference between benign and malignant tumours. X-ray scattering is a commonly used tool, in the biological sciences, in the determination of protein structure [8] and accounts for over eighty percent of proteins studies to date, although the protein has to be precipitated into a crystalline structure for study due to the high absorption in water.

X-ray scattering is a powerful technique in the study of protein structure yielding high resolution information. However it is not suitable for the continued study of live cells and tissues due to its highly destructive nature and the complex optics required for its use. Whilst X-ray scattering is powerful for revealing structure

---

it is not a good tool for monitoring real time events and reactions either as it can not be used in water.

## A.2 Summary

These techniques are in widespread daily use in hospitals and research labs and have in many ways transformed our understanding of many biomedical processes. However they are not entirely suitable for studying the biomolecular functions of single cells thus do not compete directly with Raman tweezers spectroscopy. It is useful to understand their capabilities however to allow us to gain insight into the areas and samples that are difficult to study and how Raman tweezers may be able to contribute towards the study of these areas.

## A.3 References

- [1] Brezinski M. **Optical Coherence Tomography: principles and applications.** 2006; Academic Press: pp 97-141
- [2] Fujimoto JG. **Optical Coherence Tomography for ultra high resolution in vivo imaging.** Nature Biotechnology 2003; **21**: 1361-1367
- [3] Sergeev A, Gelinkonov V, Gelinkonov G, Feldchlein F, Kuranov R, Gladkova N, Shakhova N, Snopova L, Shakhov A, Kuznetzova I, Denisenko A, Pochinko V, Chunakov Y and Sheltzova. **In vivo endoscopic OCT imaging of precancer and cancer states of human mucosa.** Optics Express 1997; **1**: 432-440
- [4] Bludell S. **Magnetism in Condensed Matter.** 2001; Oxford University Press: pp 52-65
- [5] Padhani AR, Gapinski CJ, MacVicar DA, Parker GJ, Suckling J, Revell PB, Leach MO, Dearnaley DP and Husband JE. **Dynamic contrast enhanced MRI**

- 
- of prostate cancer: correlation with morphology and tumour stage,  
Histological grade and PSA.** Clinical Radiology 2000; **55**: 99-109
- [6] Omichinski JG, Clore GM, Schaad O, Felsenfeld G, Trainor C, Appella E, Stahl SJ and Gronenborn AM. **NMR structure of a specific DNA complex of zn-containing DNA binding domain of GATA-1.** Science 1993; **261**: 438-446
- [7] Marsh D, Watts A, Pales RB, Uhl R, Knowles PF and Esmann M. **ESR spin-label studies of lipid-protein interactions in membranes.** Biophysical Journal 1982; **37**: 265-274
- [8] Deisenhofer J, Epp O, Huber R and Michel H. **X-Ray structure analysis of a membrane protein complex. Electron density map at 3 Å resolution and a model of the chromophores of the photosynthetic reaction centre from Rhodospseudomonas viridis.** Journal of Molecular Biology 1984; **180**: 385-398

# Appendix B

---

# B. The Quantum Theory of Raman Spectroscopy

---

*The classical theory of Raman spectroscopy gives a good conceptual understanding of the fundamental processes that contribute to the inelastic scattering of light, however it struggles to explain some observed phenomena in Raman spectra such as the quantised nature of the observed vibrations and the links between molecular properties and those of the Raman scattered light. To fully understand all the properties of the inelastically scattered light and their relationship with the molecular properties of the scatterer a quantum mechanical approach is necessary. In this chapter an overview of the Quantum theory of Raman spectroscopy is presented allowing further insight into the relationship between the observed Raman spectra and the properties of the scattering molecule.*

---

## B.1 The Quantum Theory of Raman Spectroscopy

The quantum theory of Raman spectroscopy [1] has been extremely successful in describing the inelastic scattering observed from molecules. This theory describes the transitions described in Figures 3(a-c) where a photon interacts with the electron cloud to form a transitory unstable complex of the molecular states that is rejected and the molecule returns to a different vibrational state thus ejecting a photon with a changed frequency. In line with the studies conducted in this thesis we will only consider the situation where the transitory complex has an energy well below the first excited electronic energy level, although the expression can be generalised for more complex situations. In this discussion we will not become entrenched in the

---

complicated mathematical derivations that are the basis of this theory rather we will look at some of the key equations to further out understanding.

The intensity of the Raman scatter can be written as:

$$I = Kl\alpha^2\omega^4 \quad (\text{B.1})$$

Where:  $I$  = Intensity of the Raman scattering

$K$  = Constant of proportionality

$l$  = Incident laser power

$\alpha$  = Polarisability of the molecule

$\omega$  = Angular frequency of the incident radiation

This equation, from the theory of light scattering, contains most of the terms familiar to us from the classical theory; however in the quantum theory the polarisability is represented, not by a harmonic function, but rather by the Kramer Heisenberg Dirac (KHD) expression shown in equation B.2. This expression calculates the polarisability of all the possible states of the molecule as it transits from the initial vibrational state through the transitory complex and lastly to its final vibrational state.

$$(\alpha_{\rho\sigma})_{AB} = \sum_T \left( \frac{\langle B | \mu_\rho | T \rangle \langle T | \mu_\sigma | A \rangle}{\hbar\omega_{AT} - \hbar\omega_0 - i\Gamma_T} + \frac{\langle T | \mu_\rho | A \rangle \langle B | \mu_\sigma | T \rangle}{\hbar\omega_{TB} + \hbar\omega_0 - i\Gamma_T} \right) \quad (\text{B.2})$$

Where:  $\alpha$  = the polarisability

$\rho$  = the polarisation of the input photon

$\sigma$  = the polarisation of the scattered photon

$A$  = Wavefunction representing the initial vibrational state

$B$  = Wavefunction representing the final excited vibrational state

$T$  = Wavefunction representing the superposition of all the electronic and vibronic states that form the short lived transitory complex

$\mu$  = The quantum dipole operator

$\hbar\omega_{AT}$  = Energy of the transitory complex

$\hbar\omega_{TB}$  = Energy of the transitory complex where the molecule was initially in an excited state when the photon interaction began

$\Gamma$  = A damping energy related to the lifetime of the transitory complex

As mentioned previously, in the quantum picture, the transient complex is an unstable mix of all the electronic and vibronic states. In the scattering process the nuclei do not have time to respond to the new electron configuration thus the complex is no real state of the stable molecule hence when evaluating the polarisability of the molecule

in the transient complex we must sum over all the possible states in the ‘mix’ hence the summation sign in equation B.2.

To consider the implications of this equation we must first understand the notation in which it is presented. If we consider the term in equation B.3 which comes from the numerator of the first term in equation B.2 it is presented in what is referred to as the ‘bra’ and ‘ket’ notation.

$$\langle T | \mu_{\sigma} | A \rangle \quad (\text{B.3})$$

This notation is short hand and avoids writing out the traditional integrals in full. The term is read from right to left;  $|A\rangle$  is a wavefunction representing the initial state of the molecule, which in most cases is the ground vibronic state of the ground electronic state. The term in the middle,  $\mu$ , is the quantum dipole operator that is applied to the ground state wavefunction. The final term  $\langle T |$  is the wavefunction of the transient complex that is multiplied with the product, of the application of the dipole operator to the wavefunction A, to effectively ‘mix’ the two states. When this is summed over all the possible states of the molecule it describes, in part, the excitation of the molecule to the transient complex. The first term in the first numerator in equation B.2 describes, in a similar fashion, the de-excitation from the transient complex to the excited vibronic state described by the wavefunction B. The numerator in the second term of equation B.2, takes account for the fact that the molecule does not necessarily have to begin in the ground state rather there is the possibility the molecule may begin in an excited state and return to a lower vibronic state.

Next we will consider the denominators in the terms of equation B.2. The symbols here are familiar, describing the energy of the complex and the energy contained in the laser photon, except for the term  $i\Gamma$ ; this term is also describes an

---

energy that is related to the lifetime of the complex and affects the linewidth of the observed Raman bands. The energy of  $i\Gamma$  is very small in comparison to the other energy terms but plays a vitally important role in determining the molecular polarisability. The denominator in the first term shows how vitally important this term is, if the energy of the transient complex coincides with the energy of the laser photon then, without the energy term  $i\Gamma$ , the term would approach infinity and thus the scattering would tend to infinity, this actually becomes much more important when considering a more general case where the complex can be very close to an electronic level. In term one of equation B.2, as the complex energy is dependant on the input photon energy, the denominator is normally very small making the first term very large. In the denominator of the second term, in equation B.2, the energy of the photon and the complex are added meaning the second term will normally be very small thus can conveniently be disregarded from here on in.

In order to continue our analysis we must now employ the Born-Oppenheimer approximation. Equation B.2 will depend upon the exact nature of each of the states involved; the Born-Oppenheimer approach allows us to split the wavefunction representing the state into its individual electronic, vibrational and rotational components. The wavefunction, of a particular state, can then be written as:

$$\Psi = \theta \cdot \Phi \cdot r \quad (\text{B.4})$$

Where:  $\Psi$  = the wavefunction representing a specific state  
 $\theta$  = the electronic component of the wavefunction  
 $\Phi$  = the vibrational component of the wavefunction  
 $r$  = the rotational part of the wavefunction

The components of the wavefunction can be separated out in this manner due to the varying timescales that is required for each process. At this point we should state that the rotational part of the wavefunction will be neglected in this basic study as this thesis is concerned with molecules in solid or solution thus rotational effects are

---

normally drowned out by the effects of collisions. The term  $\theta$ , representing the electronic part of the state, will depend upon the nuclear co-ordinates,  $N$ , and the electronic co-ordinates,  $e$ , whereas the vibrational component of the wavefunction will depend only upon the nuclear co-ordinates. The separation of the components of the wavefunction allows the separation of the terms in the KHD expression. Only the electronic states are influenced by the dipole operator thus we may write the terms in the KHD expression in the following form:

$$\langle T | \mu_\sigma | A \rangle = \langle \theta_T \cdot \Phi_T | \mu_\sigma | \theta_A \cdot \Phi_A \rangle = \underbrace{\langle \theta_T | \mu_\sigma | \theta_A \rangle}_{\text{Electronic}} \underbrace{\langle \Phi_T | \Phi_A \rangle}_{\text{Vibrational}} \quad (\text{B.5})$$

We may now consider the influence, on the polarisability, of the electronic and vibrational elements separately. As the Raman process is so rapid no appreciable movement of the nuclei can occur thus we may consider the effect of the electronic component of the wavefunction at the equilibrium position of the molecule. This means we can evaluate the effect of the electronic states when the nuclei are at rest and subsequently add a correction to account for change in the electronic structure when the nuclei do move. To make the equations slightly more manageable the electronic form of the expression in B.5 is written as:

$$\langle \theta_T | \mu_\sigma | \theta_A \rangle = M_{TA}(N) \quad (\text{B.6})$$

The influence of the electronic levels can then be written as a Taylor expansion:

$$\begin{aligned} M_{TA}(N) &= \underbrace{M_{TA}(N_0)}_{\text{Term 1}} + \underbrace{\left[ \frac{\delta M_{TA}}{\delta N_x} \right]_{N_0}}_{\text{Term 2}} N_x + \underbrace{\dots}_{\text{Higher order terms}} \\ &= M_{TA}(N_0) + M'_{TA}(N_0) \end{aligned} \quad (\text{B.7})$$

In the Taylor expansion *term 1* is the evaluation of the influence, on the molecule polarisability, of the electronic states at the equilibrium nuclear position. *Term 2* is the correction term where the influence of the nuclear movement, in some direction  $x$ , on

the electronic states is accounted for. The higher order terms are part of this correction but as even *term 2* is very small we need only consider the effects of the first two terms in the Taylor expansion. As we can see this expansion is only for nuclear movement in the x direction, in order to build up a full interpretation of the effects of the nuclear movements we must add correction factors for all the possible vibrational nuclear motions. Furthermore this Taylor expansion is for the excitation to the transitory complex but the de-excitation process, to the excited vibronic state can be described in an identical fashion.

Using the Born-Openheimer approximation the Kramer Heisenberg Dirac expression can be solved [2] and results in the following expression:

$$\begin{aligned}
 (\alpha_{\rho\sigma})_{AB} = & \underbrace{M_{TA}^2(N_0) \sum_T \frac{\langle \Phi_{N_B} | \Phi_{N_T} \rangle \langle \Phi_{N_T} | \Phi_{N_A} \rangle}{\hbar\omega_{AT} - \hbar\omega_0 - i\Gamma_T}}_{\text{Term 1}} \\
 & + \underbrace{M_{TA}(N_0)M'_{TA}(N_0) \sum_T \frac{\langle \Phi_{N_B} | N_x | \Phi_{N_T} \rangle \langle \Phi_{N_T} | \Phi_{N_A} \rangle + \langle \Phi_{N_B} | \Phi_{N_T} \rangle \langle \Phi_{N_T} | N_x | \Phi_{N_A} \rangle}{\hbar\omega_{AT} - \hbar\omega_0 - i\Gamma_T}}_{\text{Term 2}}
 \end{aligned}$$

This is an extremely complex looking equation but once again we may understand its implications without becoming engrossed in the mathematics. Considering first the symbols outwith the summation signs we can see that *term 1* is prefaced by  $M_{TA}^2$  whereas *term 2* is prefaced by  $M_{TA}M'_{TA}$ . As  $M_{TA}$  is much larger than  $M'_{TA}$  *term 1* will be substantially larger than *term 2*, this as we shall see later contributes to the weak nature of Raman scattering. Again as stated before the summation signs ensure that the polarisability accounts for all states involved in formation of the transient complex. The integrals, inside the summation signs, account for the mixing of all the vibrational states involved in the scattering process.

In *term 1* the numerator contains merely the multiplication of all the possible vibrational wavefunctions. There is a theory in quantum mechanics called the closure

---

theorem that demonstrates the multiplication of all the vibrational wavefunctions are multiplied together the final contribution will collapse to zero thus term 1 does not contribute any Raman scattering.

*Term 2*, unlike *term 1*, is not a straight forward multiplication of all the vibrational wavefunctions rather it contains the co-ordinate operator  $N_x$ . This operator describes the effect, on the polarisability, of nuclear movement along the molecular x axis and appears in *term 2* because of the influence of the correction factor  $M'_{TA}$ . When evaluated this term has a small but finite value that is the origin of Raman scattering in the quantum theory of Raman spectroscopy. There is a very interesting condition attached to this result, *term 2* will only have a finite value when the change in vibrational energy is one single quanta or a change of only one energy level, this theory thus accounts, unlike the classical theory, for the absence of overtones in most spectra. It should be noted that overtones can appear in Raman spectra but require a further perturbation in the polarisability. The selection rule that requires symmetrical vibrations for Raman scattering is also described in *term 2* but is tied up in the nature of the operators. When the vibrational wavefunctions are multiplied together only those that describe symmetrical vibrations produce allowed solutions of the co-ordinate operator.

The quantum theory of Raman spectroscopy, although less intuitive and conceptual, is the most successful theory describing the inelastic scattering process enabling us to understand fully the features observed in collected Raman spectra.

## B.2 References

[1] Smith E and Dent G. **Modern Raman Spectroscopy: A practical approach.**

2005; John Wiley & Sons: pp. 86-90

---

---

[2] Rousseau DL, Friedman JM & Williams PF. **The Resonance Raman Effect.**

Topics in current Physics 1979; **2**: 203

# Appendix C

---

# C. A Brief Introduction to the Eukaryotic Cell

---

*The cell is the basic unit of life that contains the genetic code for life and is the building block for larger organisms such as humans. In this thesis different types of eukaryotic cells are probed with Raman tweezers and in order to interpret the results a basic understanding of the cell and its functions as well as the cell cycle is useful. In this chapter the basic components of the cell and their functions is discussed and it concludes with a look at the cell cycle and how it is controlled.*

---

## **C.1 Introduction to Eukaryotic cells**

The cell is the basic unit of life and is the simplest collection of matter that can live. It contains the code for life, wrapped up in molecules known as Deoxyribonucleic acid (DNA) within the nucleus, the ability to metabolise energy, in the mitochondria in the cytoplasm, the ability to control its boundaries and the molecules that come into and leave the cell, via lipid membranes, and the ability to reproduce to ensure the continuation of life. More complex organisms, such as human beings, are constructed from cells of many different kinds each with their own specialised functions. Although the cell is often referred to as the ‘basic’ unit of life it is a highly complex organism with each individual sub-cellular process demanding its own dedicated research field. For a cell to function correctly it requires tens of thousands of individual molecules that enable, monitor and carry out individual processes to work together. It is when these processes go wrong that individual diseases and conditions, such as cancer, arise and affect both the cell and organism of

---

---

which it is part. This thesis is concerned with the probing and interrogating of individual cells, and although the cell is an extremely complex entity that entire books are dedicated to, a basic working knowledge is useful and indeed necessary in the interpretation of the results and studies presented within this study. We will not attempt to understand all the biochemical pathways involved in a cells operation rather we will embark on a brief overview of the main components and their functions. Where a working knowledge of a specific process or biochemical pathway, being probed by the Raman Tweezers technique, is required to understand the results, this will be discussed in more detail in the appropriate chapter.

In our discussion we will be considering eukaryotic cells, these are a broad category of cells where the chromosomes, containing the DNA, are located in a membrane enclosed organelle called the nucleus and is the cell type that is probed throughout this thesis with the exception of the human red blood cell which has no nucleus. We will begin by looking at the main components of the cell and their functions and will finish with a brief overview of the cell cycle which will be pertinent in our study of cervical cancer in chapter 8 of this thesis.

## **C.2 A Tour of the Cell**

Although there are many different types of eukaryotic cells from single yeast cells to those often specialised cells that make up larger organisms such as the human body, most have many common features and functions. In our brief tour of the cell we shall examine the main components, or organelles, and their functions within the cell. A schematic of a eukaryotic cell, taken from reference 1, can be seen in figure C(a). Despite the great variety of eukaryotic cells they all have some basic common features. All cells are bound by a membrane, known as a plasma membrane, within

---

the membrane is a semi-fluid substance, cytosol, in which the organelles are located. In the cytosol there is an organelle that is present in all eukaryotic cells in which the DNA is concentrated in a membrane enclosed organelle called the nucleus and finally all cells contain ribosomes, in the cytosol, that are responsible for the manufacturing of proteins. It should also be noted that the region between the nucleus and the plasma membrane is more commonly referred to as the cytoplasm. As we have mentioned it is useful to understand the individual functions of the organelles and their importance in cellular function and is thus addressed in the following discussion.

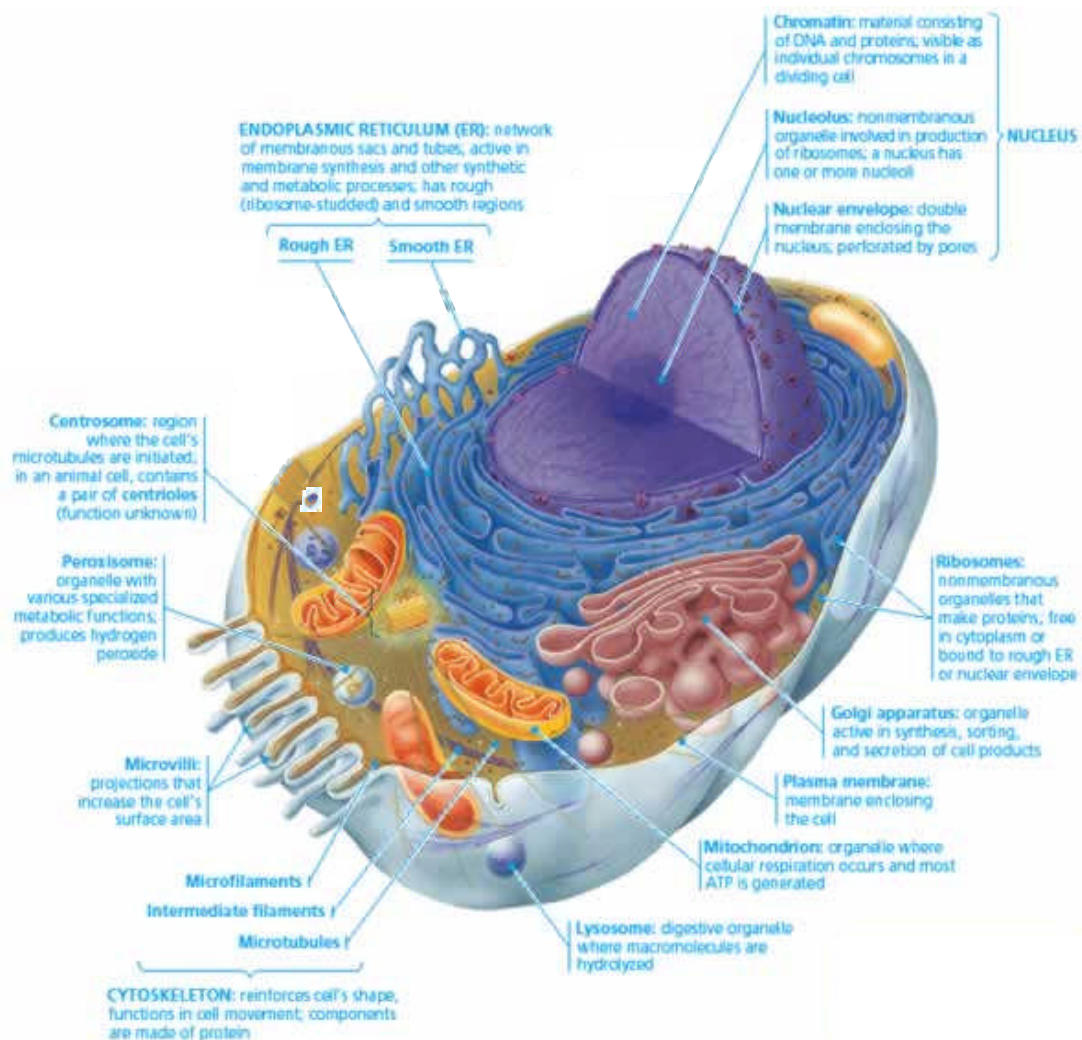


Figure C(a). A schematic of a eukaryotic cell displaying the major organelles and their individual functions [1].

---

### **C.2.1 The Cellular Plasma Membrane**

At the boundary of every cell there is a plasma membrane that encloses the cell and acts as a selective barrier that allows the passage of nutrients into the cell and waste to be removed over the volume of the entire cell. The plasma membrane, and the internal organelle membranes, are constructed from a dual layer, or bilayer, of phospholipids with proteins embedded within it. A phospholipid is a molecule with a hydrophilic head and a hydrophobic tail constructed from fatty acids. Due to the hydrophobic nature of the tails, it is these parts of the molecule that form the internal structure of the membrane along with any hydrophobic sections of the imbedded proteins. It is then the hydrophilic heads of the phospholipids and embedded proteins that form the outer surface of the membrane that is in contact with aqueous solution both inside and outside the cell. A schematic of the structure of the lipid bilayer can be seen in figure C(b). If the phospholipids form the cell wall, it is the proteins that are the gatekeepers of the cell that allow and facilitate the passing of materials through the membrane into the cell itself. As well as the proteins there are also carbohydrate chains on the outside of the bilayer that facilitate cell and membrane function. The precise nature of the embedded proteins and carbohydrate chains will depend on the function of the membrane and ultimately the cells specific function.

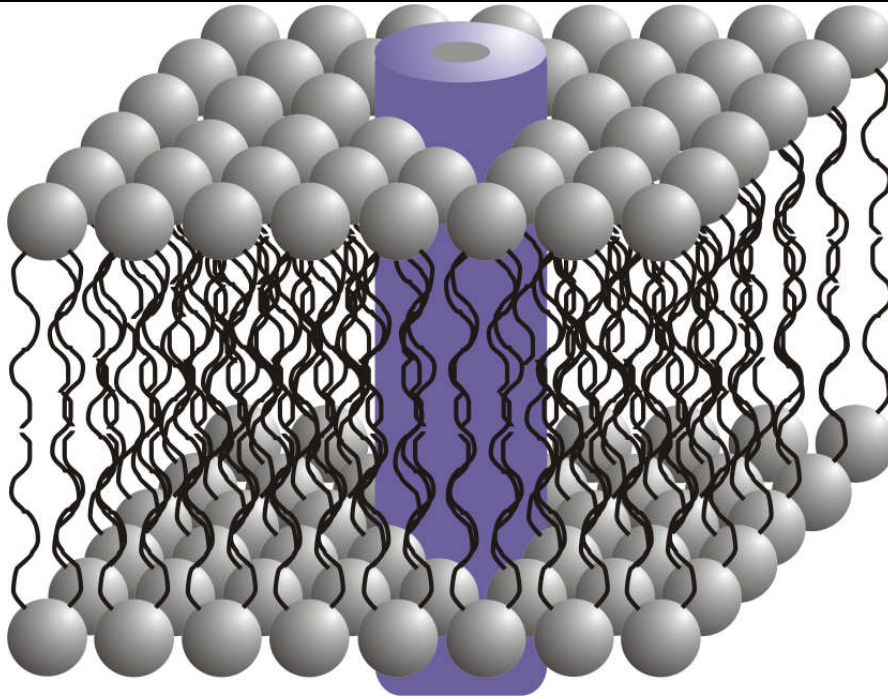


Figure C(b). A depiction of the protein studded phospholipid bilayer that forms the plasma membrane. The hydrophobic tails of the phospholipid molecule, in black, form the internal structure of the membrane while the outer and inner surfaces of the membrane are constructed from the hydrophilic heads, in grey, of the phospholipid molecule. The membrane is studded with proteins, depicted in purple, that facilitate the transport of materials across the membrane.

We should also note at this point that lipid bilayers not only form the outer cell membrane but compartmentalise many of the cells individual organelles and functions.

### **C.2.2 The Nucleus**

The nucleus contains the genes of the eukaryotic cell and viewed through a microscope it appears as the most easily recognised organelle. A bright field microscope image of a primary human keratinocyte cell can be seen in figure C(c). The nucleus is a membrane enclosed organelle; again the membrane is constructed from a phospholipid bilayer studded with protein ringed pores that allow the flow of proteins and RNA in and out of the nucleus. There is also a net like structure, consisting of protein filaments, surrounding the nucleus called the nuclear lamina that

---

---

maintains its shape. Within the nucleus the DNA, the molecular code for life and cell function, is organised along with proteins, histones and non-histones, into a fibrous material called chromatin. As the cells prepare to reproduce the chromatin is super coiled into chromosomes in preparation for cell division.



Figure C(c). Brightfield microscope image of a primary human keratinocyte cell. Clearly visible are the nucleus and the nucleolus as well as the membrane and cytoplasm regions.

A basic understanding of the process by which the code and instructions contained in DNA is turned into proteins for cell function is useful at this point in our discussion. The cell requires over eight thousand proteins to function correctly and it is in the DNA that the instruction for the building and function of these proteins is contained. DNA is a long molecule supported by sugar phosphate backbone which contains a long sequence of molecules known as DNA bases, although there are only four of these bases, adenine guanine thymine and cytosine, it is the order in which are constructed that is important and thus gives the coding. As well as the DNA in the nucleus there is also a number of proteins and enzymes fulfilling individual tasks. A small group of enzymes called RNA polymerases are responsible for unwinding the DNA double helix and ‘reading the code’ that is used to transcribe Ribonucleic acid, a single strand nucleic acid which serves as the template for the translation of the genetic code into proteins. RNA is a molecule consisting of a nucleotide of the

---

monomers; it is supported by an oxygenated sugar phosphate backbone and monomers are three of the four original DNA bases, adenine guanine and cytosine, however thymine is replaced by another molecule called uracil. Before leaving the nucleus the RNA is processed further into messenger RNA (mRNA), this is then dispatched to the cytoplasm where particles called ribosomes transcribe the code contained in mRNA into specific primary structure sequences of amino acids that will eventually be folded into functional proteins. This is a very basic explanation of this process required for the understanding of the results presented in this thesis but a more detailed explanation of this complicated process can be found in reference 2.

The discussion on the transcription of DNA and the subsequent translation into proteins brings us back to our original consideration of the nucleus. One of the most prominent features in a nucleus viewed through a bright field microscope is the presence of a dark spot, which can be seen in figure C(c), and is known as the nucleolus. Here a special type of RNA, called ribosomal RNA is synthesised and assembled with proteins, imported from the cytoplasm, into ribosomal subunits that are then passed to the cytoplasm where they combine to form the ribosomes used in mRNA translation. Ribosomes are found in two main locations in the cell, the cytoplasm (free ribosomes) and in the endoplasmic reticulum (bound ribosomes). Free ribosomes usually manufacture proteins that are used in the cytosol and bound ribosomes normally manufacture proteins for secretion outside the cell or for insertion into membranes, bound and free ribosomes are identical and can switch between roles.

The nucleus contains a cells genetic library but also contains many proteins involved in DNA storage and in the reading and manufacture of proteins essential for the cells function and survival.

---

---

### **C.2.3 The Endomembrane system**

The endomembrane system is a set of membranous organelles that are related through either direct physical contact or via communication by the transfer of vesicles, small membrane sacs used in the transport of materials throughout the cell. Although these organelles are closely related they have varying structures and fulfil diverse functions. The endomembrane system includes the nuclear envelope, which we have already discussed, the endoplasmic reticulum, the Golgi apparatus, lysosomes and various vacuoles.

The endoplasmic reticulum is an extensive membranous labyrinth continuous with the nuclear envelope that performs many biosynthetic functions and manufactures membranes. It is a network of tubules and sacs called cisterna whose contents are separate from the cytoplasm. Despite being such an extensive organelle it has two distinct structural sections known as the smooth ER and the rough ER. The smooth ER, so known as it does not contain any bound ribosomes, is responsible for diverse metabolic processes including the detoxification of drugs and poisons, synthesis of lipids and the metabolism of carbohydrates. It is the enzymes contained within the smooth ER that are also important in the synthesis of phospholipids, essential oils and in the manufacture of various steroid hormones such as the sex hormones or those secreted by the adrenal glands in humans. Those cells which are responsible for detoxification and expression of sex hormones such as liver cells and ovaries respectively have extensive smooth ER to fulfil their functions effectively. The rough ER, so named as it is studded with bound ribosomes, is also involved in the secretion of proteins that are formed by the bound ribosomes. As the proteins are synthesized, by the ribosomes, they are threaded into the cisternal space where they then fold into their native conformation, at this point we should note that the eight

---

thousand or so proteins involved in cell function are constructed from various orders of just twenty amino acids but it is their conformation, or secondary structure, that defines their function. Again cells involved in the secretion of proteins, such as pancreatic cells that secrete insulin, are rich in rough ER. As well as being involved in the manufacture of proteins the rough ER is the centre for the manufacture of membrane itself. It manufactures membrane to enable itself to continually grow and replenish and make transport vesicles to move proteins, steroids and enzymes around the cell. The phospholipids for the membrane are constructed by the ribosomes and ordered by enzymes built into the rough ER. The endoplasmic reticulum is essentially the manufacturing floor of the cell where the steroids and proteins are made for use throughout the cell and for secretion.

If the ER is the manufacturing floor of the cell then the Golgi apparatus is the finishing, labelling and shipping warehouse. The Golgi apparatus consists of flattened membranous stacks and its two flattened faces are known as the cis and trans face. The cis face is normally located near the ER and it is here that the Golgi apparatus receives materials for final processing. The Golgi apparatus is not directly connected to the ER thus proteins and steroids etc. created in the ER are contained in vesicles that bud from it and move to the Golgi apparatus where the membrane of the vesicle fuses with that of the Golgi apparatus and thus the contents of the vesicle are transferred into it. As the ER products transfer through the Golgi apparatus, via vesicle transport, special teams of enzymes modify them into finished macromolecules. It should also be noted that the Golgi apparatus produces its own products such as polysaccharides. Before the Golgi apparatus stack dispatches its products, in vesicles, from the trans face it sorts them, with the aid of phosphate molecular tags added by enzymes, and may label their transport vesicle membrane

---

depending upon their final destination so that they may be recognised by binding sites on destination organelles or the membrane if the products are intended for secretion. Again, cells specialised in secretion have extended Golgi apparatus.

The next part of the endomembrane system we will consider is lysosomes. Lysosomes are the cells digestive compartments; they allow digestive enzymes to breakdown many macromolecules safely within the cell without causing widespread destruction that would occur if the enzymes were free in the cytoplasm. A further motivation for enclosing the enzymes is their enhanced performances at lower pH levels thus the lysosomes lower their internal pH, in comparison to the neutral cytoplasm, by pumping hydrogen ions across their membranes. Lysosomes are manufactured in the ER, both membrane and enzymes, and finished by the Golgi apparatus. Lysosomes perform digestion in a variety of circumstances such as fusing to food vacuoles and digesting the macromolecules and releasing the amino acids and simple sugars as nutrients for the cell. Lysosomes also recycle the cells own material by engulfing another organelle or small amount of cytoplasm and then returning the broken down products to the cytosol for reuse, this allows a cell to continually renew itself and some prolific cells, such as human liver cells, recycle half their macromolecules every week. Perhaps a very important role for lysosomes is in human white blood cells that engulf foreign invaders with their membrane and the internal lysosomes set about their destruction, this allows the human body to destroy any infecting bacteria or viruses. Lysosomes are also involved in programmed cell death that prevents the potential development of diseases and the continued growth and development of the host organism.

---

The final part of the endomembrane system is vacuoles, these have many functions but they act mainly as a container. In human cells this is mostly for food to be digested and used as nutrients for the cell.

#### **C.2.4 Mitochondria**

Mitochondria are the powerhouse of the cell and sites of cellular respiration, they extract energy from sugars and fats in the cells, with the use of oxygen, to form adenosine triphosphate (ATP) that acts as a chemical battery in the cell. These organelles are constructed from membranes but are not part of the endomembrane system as they make their own membrane and proteins using free ribosomes in the cytoplasm. Not only do mitochondria contain their own ribosomes but they contain a small amount of DNA that directs the ribosomes synthesis of the proteins required in the mitochondria. The mitochondria are approximately 1-10  $\mu\text{m}$  in size and are not fixed in the cell but rather are free to move in the cytoplasm; a cell may contain hundreds and even thousands of mitochondria depending on the cells metabolic activity.

#### **C.2.5 The Cytoskeleton**

Initially it was thought that the organelles in the cytoplasm floated freely but improvements in electron microscopy have shown a network of fibres extending throughout the cytoplasm known as the cytoskeleton that play a major role in cell structure and function.

The first major role for the cytoskeleton is in the support of the cell shape, this is important in human cells, or any animal cell, as they do not have a cell wall. The remarkable strength of the cytoskeleton is a direct result of its geodesic dome

---

---

structure. The cytoskeleton is made microtubules, microfilaments and intermediate filaments. Microtubules are constructed from a globular protein called tubulin and are initiated in a region near the nucleus called the centrosome, the microtubules are used to resist compression forces on the cell and are also involved in the maintaining of the cell membrane and in maintaining its shape. Microfilaments are constructed from the globular protein actin and, in contrast to microtubules, are used to bear tension. Intermediate filaments are also involved in the bearing of tension forces but unlike microtubules and microfilaments, which are often disassembled and reassembled elsewhere in the cell, intermediate filaments are a more permanent structure. These filaments are extremely important in maintaining the cell shape and for anchoring organelles such as the nucleus which sits in an intermediate filament cage.

As well as being involved in the maintaining of cell shape and the anchoring of organelles the cytoskeleton is also involved in cell transport, the different tubules and filaments act as guides or ‘highways’ for motor proteins and vesicles that can ‘walk’ along them. Microfilaments are also extremely important in muscle cells forming a guide for myosin motor that can walk along the filaments contracting the cell and allowing the muscle to move. Other important applications of microtubules include their role in vesicle formation at the plasma membrane boundary and in the division of the chromosomes during cell mitosis.

### **C.2.6 The Extracellular Matrix**

The extracellular matrix comprises a series of proteins and carbohydrates that are used in support, adhesion, movement and integration into higher structures. The extracellular matrix composes mostly of proteins secreted by the cell, such as collagen, and polysaccharides on the plasma membrane surface. These fibres allow

---

---

the binding of cells to each other to form tissues and are used in cell communication to help regulate the internal cellular functions. Figure C(d) shows a cell on a microscope slide, viewed in bright field, which has put down collagen fibres in order to bind to the slide surface.

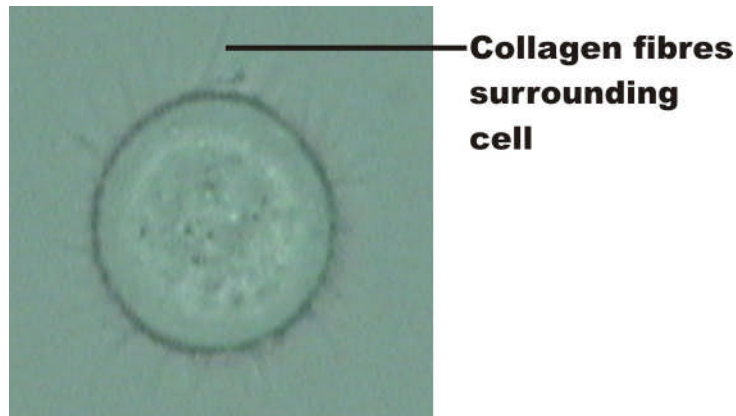


Figure C(d). Cell, viewed in bright field, which has put down collagen fibres, as part of the extracellular matrix, to bind to the microscope slide

We have examined the main organelles and components of a cell. Different and in particular specialised cells will have organelles in different abundance but most share these common features. As mentioned before the cell is an extraordinarily complex environment and more detail on these organelles and biochemical processes can be found in reference 3.

### **C.3 The cell cycle**

The cell cycle is an important process in the reproduction of cells and in the growth and maintenance of larger organisms such as humans. When we think of the cell cycle we think immediately of the division of cells, however this is only a small part of the cycle that involves growth and replication and finishes with division. As with the cell itself the process of growth replication and division is extremely complicated and requires the coordination of a great many proteins controlling the biochemical pathways that make this process possible, for the purposes of

---

understanding the results presented in this thesis we will take a brief look at the basics of the cell cycle but a further more advanced discussion on the subject may be found in reference 4. A graphical representation of the cell cycle can be seen in figure C(e) taken from reference 5.

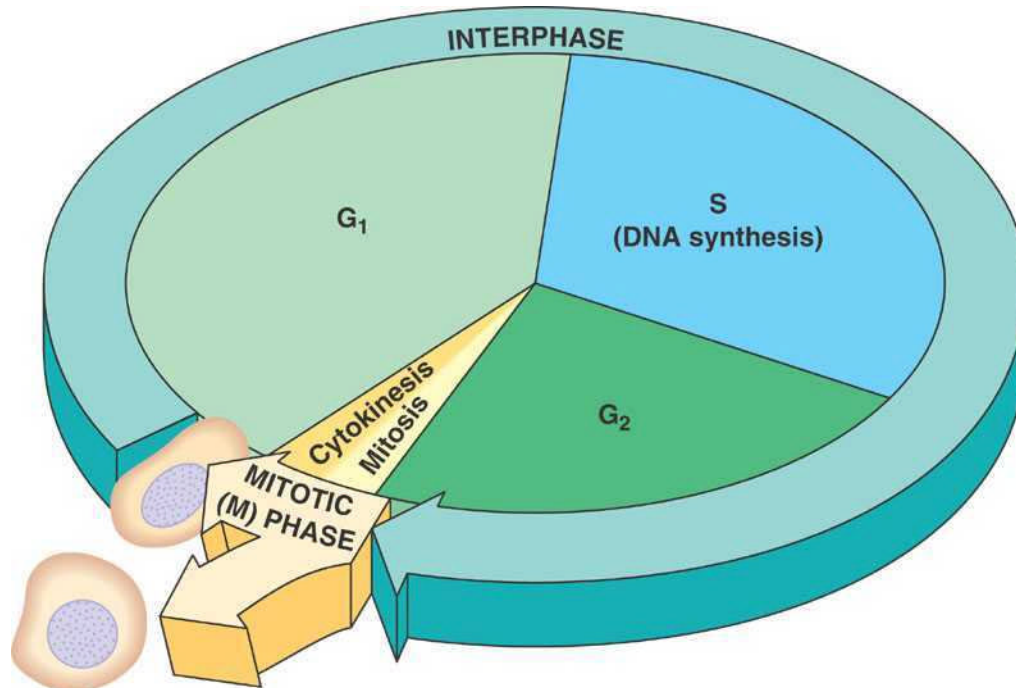


Figure C(e). A diagrammatic representation of the cell cycle; which is split between the mitotic phase, where actual cell division takes place, and the interphase that can be further split into three sections,  $G_1$  the initial growth phase, S the synthesis phase when the DNA is replicated and  $G_2$  the second growth phase [5].

The cell cycle can be divided into two clear phases, the mitotic phase and the interphase. During the interphase, which generally lasts between twelve and twenty four hours in human cells, the cell is constantly synthesising RNA, producing proteins and membranes and growing in physical size. In the first step  $G_1$ , which stands for Gap 1, the cells increase in size, synthesise RNA and proteins and prepare for DNA synthesis. This is followed by the S phase, which stands for synthesis phase, the complete DNA library is duplicated in order to form two identical sets of chromosomes for the daughter cells. The final step in the interphase portion of the cell cycle is the  $G_2$  phase, which stands for Gap 2, in this phase the cell continues to grow

---

and produce proteins in preparation for mitosis. At the end of the interphase the mitotic, or M, phase begins that typically only lasts a couple of hours for human cells. Here the M phase is broken down into two main parts mitosis and cytokinesis, the mitosis stage can be further broken down into events that see the coiling of the chromatin into tightly wound chromosomes and the dissolution of the nuclear membrane. This is followed by the formation of the mitotic spindle, a set of microtubules stretching between the two centrosomes that capture and separate the two sets of identical chromosomes. The mitotic spindle is then employed in the cytokinesis stage where the membrane is cleaved along the centre, to form two daughter cells, and the reformation of the nuclear membrane around chromosomes in the new cells. In our brief explanation of the cell cycle we omitted one step in the interphase process that can occur and is not strictly speaking part of the process but rather a halt in the process, this is known as the G<sub>0</sub>, or Gap 0, phase where the cell exits the cell cycle and ceases replication activity, it is this event that leads us on to our next discussion, that of cell cycle control.

The cell cycle is not a process running wild, rather it is tightly controlled and monitored by proteins that give stop and go signals at each point throughout the cell cycle, known as checkpoints. At the end of the G<sub>1</sub> phase the cell checks it is ready for DNA synthesis and presence of a protein, known as cyclin dependant kinase (Cdk), instructs the cell to proceed into the S phase, Cdks are, along with cyclins, known as maturation promoting factors (MPF) that push the cell through the cycle. At the end of G<sub>2</sub> the cell reaches another checkpoint where the cell again checks it is ready to begin the division process and again, if everything is in order, Cdks instruct the cell to begin the division process. The final checkpoint in the cycle is reached just before cytokineases and the cell checks the chromosomes have been separated correctly and

---

---

the actual division of the membrane can begin, again directed to do so by Cdks. As well as the Cdks there are some other important proteins involved in the cell cycle, and perhaps more importantly in a cells exit from the cell cycle should something go wrong in order to avoid diseases like cancer. The main protein involved in blocking the cell cycle is p53 and, if the damage to the cell is severe enough induce apoptosis (cell death). The main use of p53 in the cell is to block the cell cycle and send it into the G<sub>0</sub> phase to allow the cell time to repair itself. A mutation in the p53 protein is a very common event in many cancers and would allow damaged cells to proliferate freely. The other main protein involved in cell cycle regulation is p27, which binds to cyclin and cdk blocking entry into the S phase. Again a mutation in this protein can also cause cancer and is particularly important in breast cancer [6].

The cell cycle allows the effective reproduction and repair of organisms that is tightly regulated to avoid damage and ensure healthy reproduction.

## C.4 Conclusion

This concludes our brief tour of the eukaryotic cell and its reproductive cycle, although cells vary widely in form and purpose the basic introduction given here should assist in the understanding of the subsequent results obtained using Raman tweezers spectroscopy.

## C.5 References

- [1] Campbell NA and Reece JB. **Biology 6<sup>th</sup> edition, International edition.** 2002;  
Benjamin Cummings publications: pp. 114
- [2] Campbell NA and Reece JB. **Biology 6<sup>th</sup> edition, International edition.** 2002;  
Benjamin Cummings publications: pp. 303-325

- 
- [3] Campbell NA and Reece JB. **Biology 6<sup>th</sup> edition, International edition.** 2002;  
Benjamin Cummings publications: pp. 112-134
- [4] Campbell NA and Reece JB. **Biology 6<sup>th</sup> edition, International edition.** 2002;  
Benjamin Cummings publications: pp. 215-231
- [5] Campbell NA and Reece JB. **Biology 6<sup>th</sup> edition, International edition.** 2002;  
Benjamin Cummings publications: pp. 217
- [6] Steeg PA and Abrams JS. **Cancer prognostics: Past, present and p27.** Nature  
Medicine 1997; **3**: 152-154

# Appendix D

---

# D. Principle Component Analysis

---

*This appendix describes in greater detail the operation of the principle component analysis technique that was used in chapter 8 to discriminate between Raman spectra acquired from different cell types. In this chapter we consider a basic example and see how the technique operates to separate out varying sample sets.*

---

## D.1 Introduction to principle component analysis

Principle component analysis (PCA) is a type of multivariate analysis that was developed in 1901 by Pearson and also independently by Hotelling in 1933. PCA allows the compression of a large amount of data into a few important variations. Whenever we acquire a single Raman spectrum it contains 1024 data points. Now if we have acquired many spectra for comparison, as we did in chapter 8, we have an extremely large bank of information. The PCA process then allows us to discard most of the information that doesn't vary and only retain the variation between data sets that we can subsequently use to discriminate between them. The easiest way to consider the operation of PCA is to examine an example; in the next section we will consider a worked example kindly provided by Michael Mazilu.

---

## **D.2 Demonstration of the operation of Principle component analysis**

In our example to demonstrate the operation of PCA we will consider three groups of five identical spectra that we will attempt to discriminate between with PCA. PCA can pick up three types of variation in spectral peaks: shifts in peak position, changes in peak height and changes in peak width. Examples of our three types of fabricated spectra can be seen in figure D(a), colour coded as red, blue and green along with other components that frequently make up typical Raman spectra: background and noise. We can see that our fabricated spectra contain four peaks of which three are varying in a different manner as we move from red to green. The peak on the left is decreasing in height, the central peak is moving spectral position to the right and the peak on the right is increasing in width. These spectra are then put together with the background and noise, which we would commonly find in Raman spectra, to form the spectra shown in figure D(b). PCA is however a blind technique so we do not keep a record of the origin of the spectra. These spectra are then used to form an intensity map with one spectrum forming a row of the map. This allows us to see how the peaks are varying at each spectral position as we move through all the acquired spectra. The blind spectra and intensity map can be seen in figure D(c); the intensity map in this figure allows us to see clearly how each peak is varying.

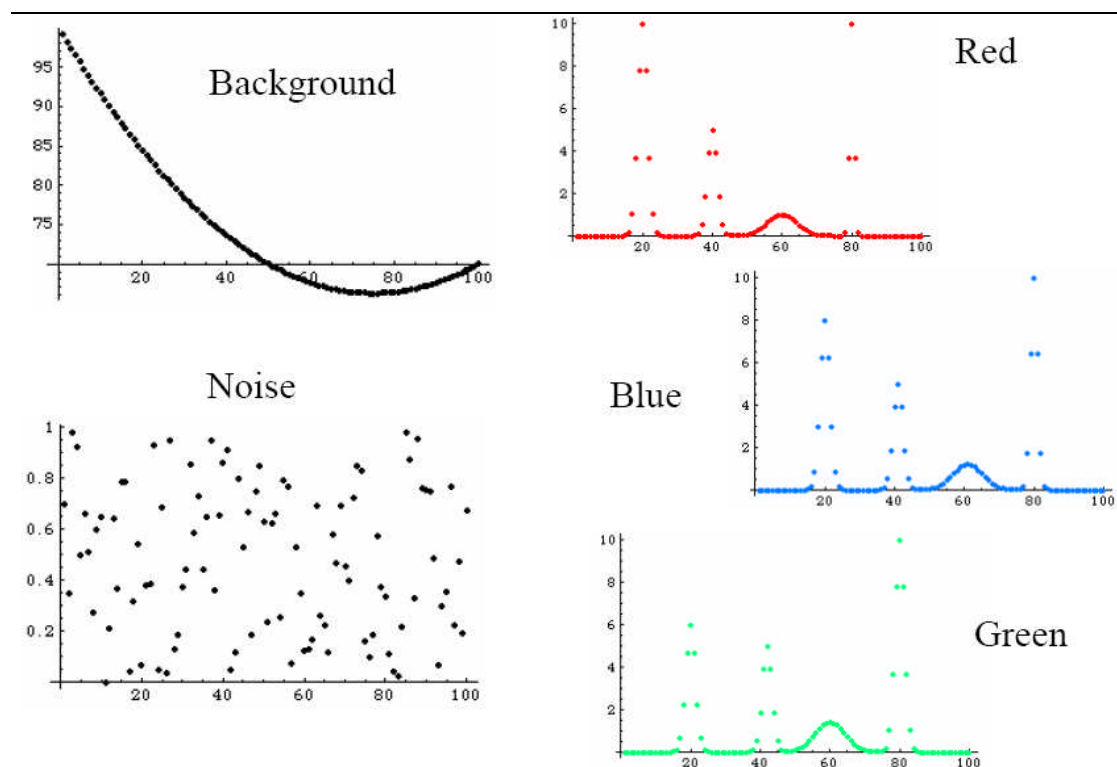
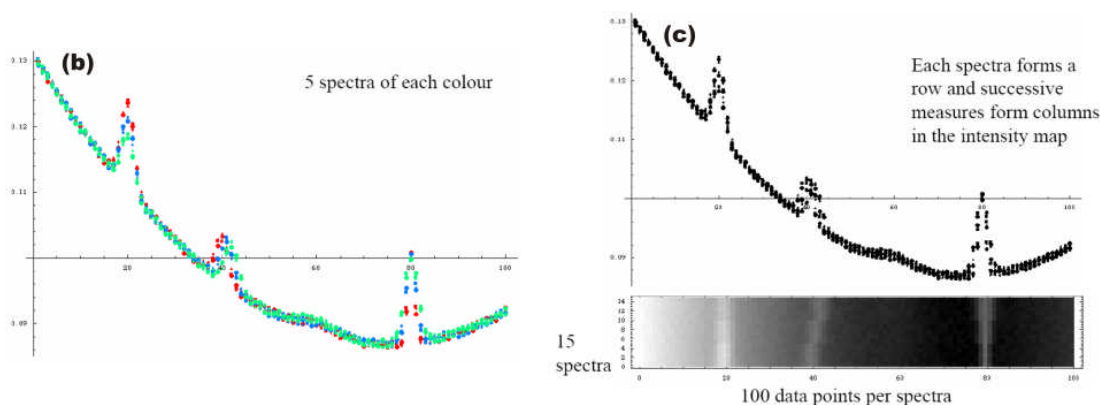


Figure D(a). Examples of our three types of fabricated spectra labelled red, blue and green. Also included are the other components of noise and background that are often found in Raman spectra.



Figures D(b & c). Figure D(b) shows the combined spectra of the signals background and noise for all five spectra of the three different spectral types. Figure D(c) shows the blind spectra and the subsequently formed intensity map that allows us to see easily how the spectra are varying.

Once we have formed this intensity map we then calculate the mean of all the spectra and subtract it from all the individual spectra. This data is then used to form a new intensity map of the deviation of each spectrum from the mean spectrum. A diagram of this procedure showing the intensity map, the mean of the data and the

subsequently formed intensity map of the deviation from the mean can be seen in figure D(d).

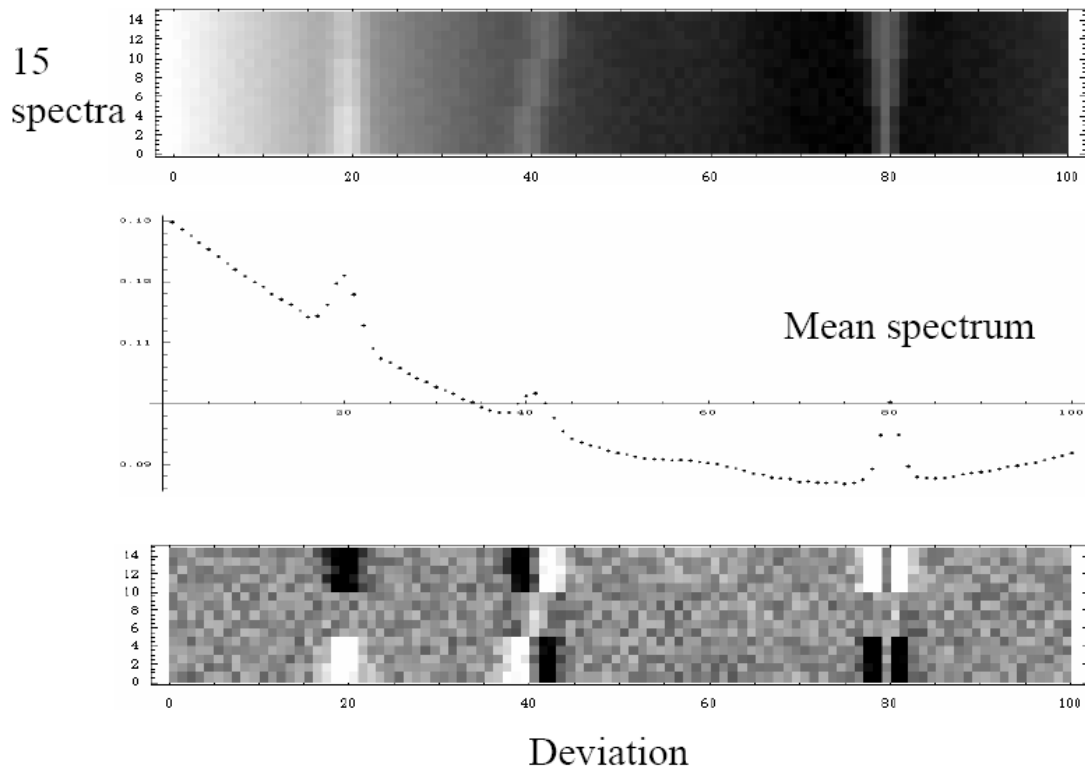
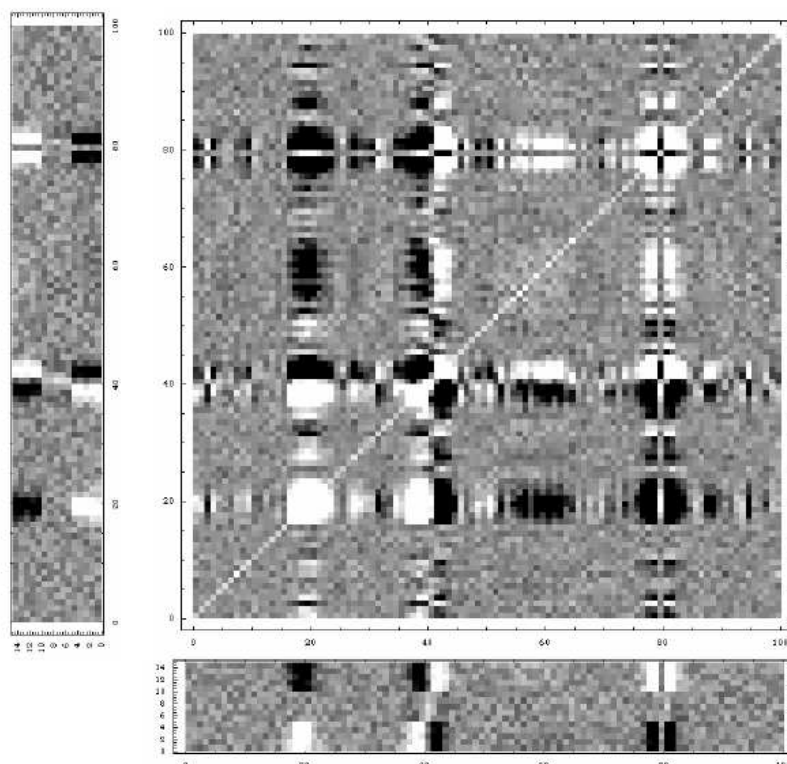


Figure D(d). Once the intensity map of the spectra has been formed the mean of all the spectra is calculated. The mean is then subtracted from each spectra to form the deviation from the mean intensity map.

This intensity map of the deviation is then multiplied by itself to form the covariance matrix. The covariance matrix, which can be seen in figure D(e), allows us to measure how any two points on any of the spectra vary together. This can be thought of as one of those distance charts between cities we are familiar with where all the cities are placed along both axes so we can find the distance between any two cities. The covariance matrix can tell us how any two points on any two spectra vary together.

---

## Covariance matrix



Covariance is the measure of how much two data-points vary together.

Figure D(e). The covariance matrix allows us to measure how any two points on any two spectra vary together.

From the covariance matrix we can construct the eigenspectra or principle components. These are spectra that chart the maximum variation at each spectral point and carry a weighting value known as the eigenvalue. The eigenvalue is a measure of the energy content of each eigenspectra, this means it is a measure of how much of the total variation each eigenspectrum, or principle component, carries. The first eigenspectrum carries the most information followed by the second eigenspectrum that contains the second most important information and so on. The first three eigenspectra generated from our analysis of our fabricated spectra can be seen in figure D(f). We can see from figure D(f) that the first eigenspectrum carries most of information about the variation between our three fabricated spectral types, the second eigenspectrum carries only a small amount of information about the variation and the third carries very little information about the variation. This is quite obvious from the

---

inspection of the spectra, the first carries lots of strong peaks, the second has only a couple of strong spikes consistent with the lower variation content and finally the third appears to only describing variations in the noise. We can now use these eigenspectra to discriminate between our three spectral groups.

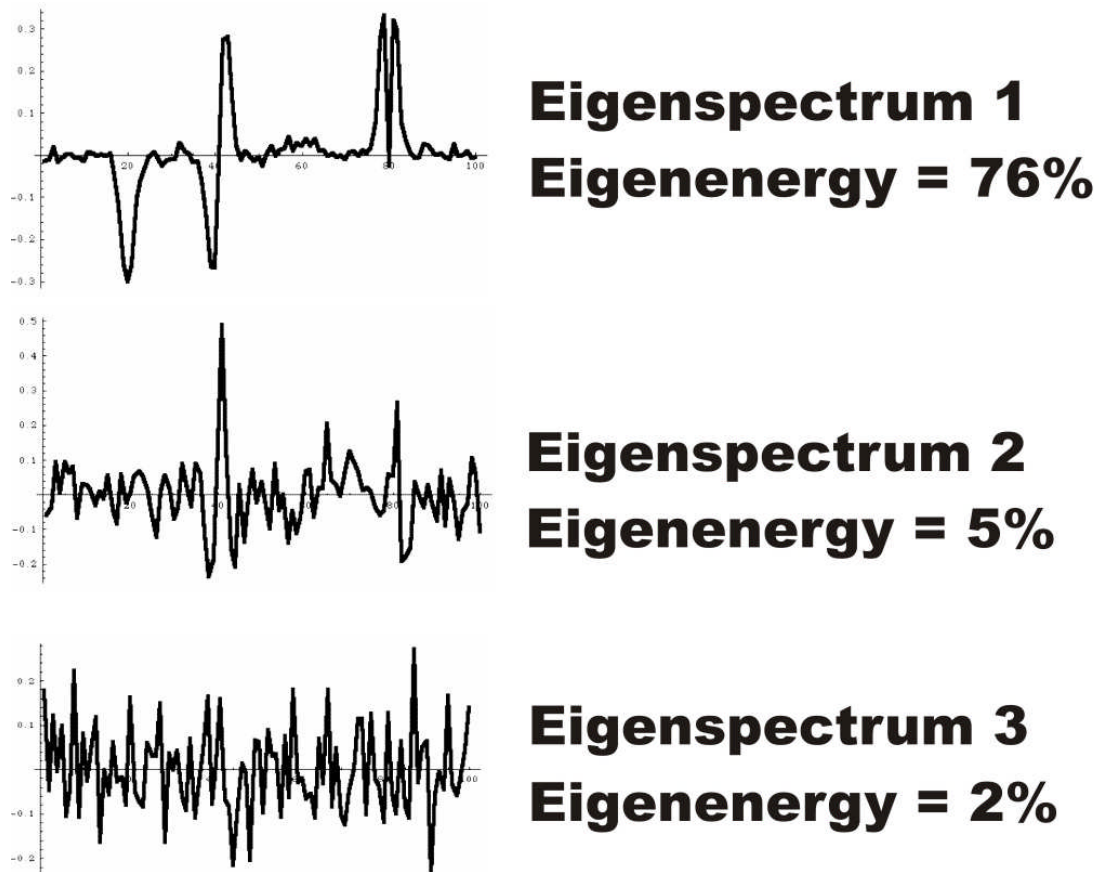


Figure D(f). Diagram showing the first three eigenspectra generated from the covariance matrix for our analysis on our fabricated spectra.

We now use the eigenspectra to create a score for each of our input spectra that we can use to plot a chart that should see the spectral types separate out. For each spectrum the deviation from the mean is found and plotted, this is then projected onto the eigenspectrum. The difference between the eigenspectrum and deviation from the mean spectrum is summed to give a score. The same spectrum can be compared to the second eigenspectrum to gain a second score which in combination with the score from the first eigenspectrum can be used as a coordinate to be plotted on a chart. A schematic of this process can be seen in figure D(g). Once we have compared all our

spectra to the first two principle components we will have a set of scores for each spectrum and can plot them, as we have compared our original data to the eigenspectra we obviously know which spectral group each spectrum came from so can include the colour on the chart to see if they actually separated out. A schematic of the whole process including the resulting chart can be seen in figure D(h). Looking at the chart in figure D(h) we can see that PCA successfully separated the spectra from the three spectral groups we started with. An interesting question however remains; we input three groups of five identical spectra, so why did they not generate three sets of identical scores? The answer lies in the noise we added to each spectrum, real spectra have a random noise components so sets of spectra tend to cluster rather than sit on top of each other.

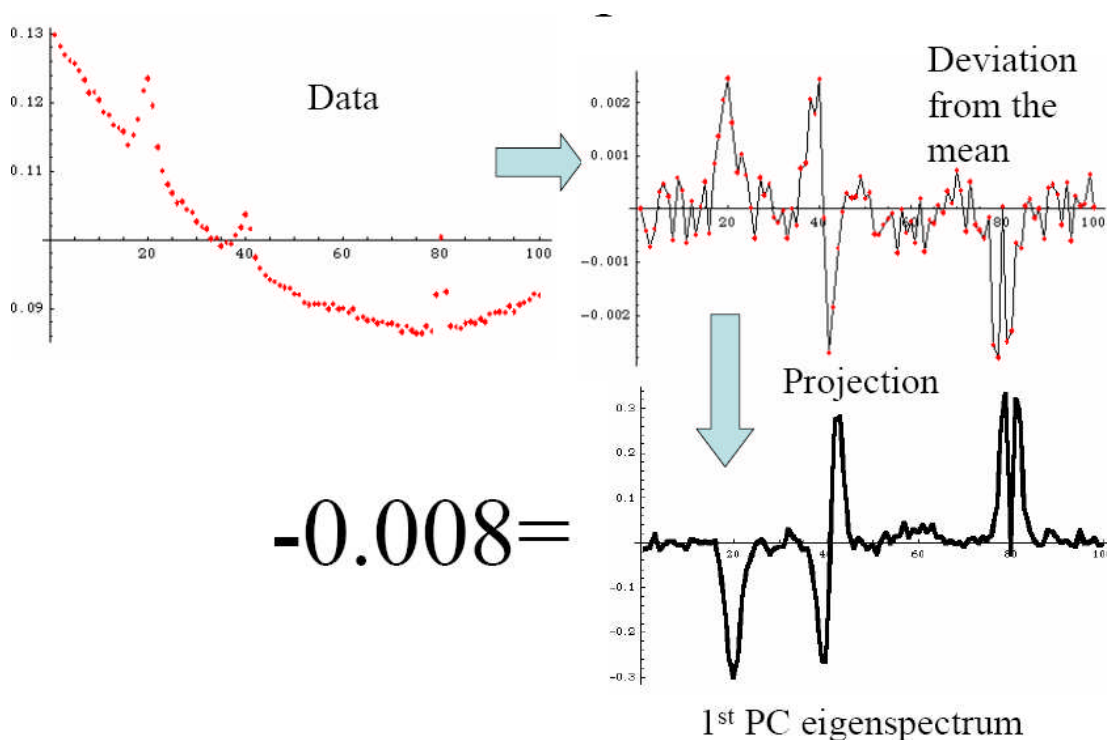


Figure D(g). A schematic of the process of gaining a score for a spectrum from the eigenspectra. An original spectrum has the mean spectrum subtracted from it to give the deviation from the mean. This then projected onto the eigenspectrum and the variation between them is summed together to give a score that can be used to plot a chart.

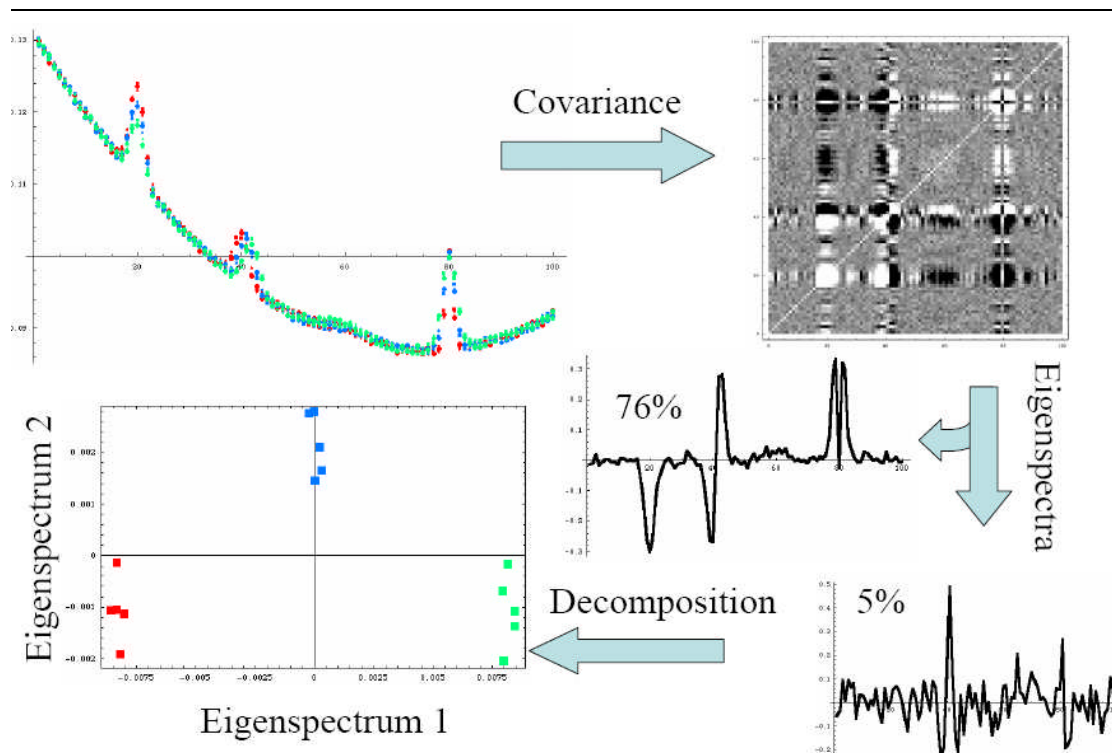


Figure D(h). Schematic of the complete PCA process including the final chart showing how PCA was able to separate out the three types of spectral input.

### D.3 Conclusions

PCA is an extremely powerful tool used in many applications and as we seen in chapter 8 could successfully discriminate between different cell types. Obviously real Raman spectra are much more complicated than the simple example we have considered here but the principles remain exactly the same and the technique can be applied successfully to separate spectral sets objectively and rapidly.